

Long-lasting epigenetic microglial memory  
of peripheral inflammation modulates  
hallmarks of Alzheimer's disease pathology

Dissertation

zur Erlangung des Grades  
eines Doktors der Naturwissenschaften

der Mathematisch-Naturwissenschaftlichen Fakultät  
und  
der Medizinischen Fakultät  
der Eberhard-Karls-Universität Tübingen

vorgelegt

von

Ann-Christin Wendeln  
aus Friesoythe, Deutschland

September 2018

Tag der mündlichen Prüfung:	26.09.2018
Dekan der Math.-Nat. Fakultät:	Prof. Dr. W. Rosenstiel
Dekan der Medizinischen Fakultät:	Prof. Dr. I. B. Autenrieth
1. Berichterstatter:	Dr. Jonas Neher
2. Berichterstatter:	Prof. Dr. Olga Garaschuk
Prüfungskommission:	Dr. Jonas Neher Prof. Dr. Olga Garschuk Prof. Dr. Peter Heutink Prof. Dr. Hansjürgen Volkmer

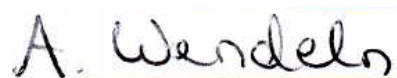
## **Erklärung**

Ich erkläre, dass ich die zur Promotion eingereichte Arbeit mit dem Titel:

**“Long-lasting epigenetic microglial memory of peripheral inflammation modulates hallmarks of Alzheimer’s disease pathology”**

selbständig verfasst, nur die angegebenen Quellen und Hilfsmittel benutzt und wörtlich oder inhaltlich übernommene Stellen als solche gekennzeichnet habe. Ich versichere an Eides statt, dass diese Angaben wahr sind und dass ich nichts verschwiegen habe. Mir ist bekannt, dass die falsche Angabe einer Versicherung des Eides statt mit Freiheitsstrafe bis zu drei Jahren oder mit Geldstrafe bestraft wird.

Tübingen, 04.09.2018

A handwritten signature in black ink that reads "A. Wendeln". The signature is written in a cursive style and is positioned above a horizontal dotted line.

Unterschrift

*Für meine Eltern*

## Acknowledgements

First of all I want to thank Jonas, who has supervised me in the best possible way during the three years of my PhD. Your enthusiastic introduction to your research ideas brought me to Tübingen, and I have not once regretted it. Thank you for granting me freedom, when I needed it, and guidance, when I asked for it. I always felt supported in every possible way. I would also like to thank Mathias for taking me as a PhD student and supporting me in my projects. Furthermore, I want to express my gratitude to my Advisory Board members, Peter Heutink and Michael Heneka, for their time and helpful comments, and to Olga Garaschuk for examining my thesis.

I had the great privilege to spend my PhD in a lab full of helpful, enthusiastic and friendly people. I want to express my deep gratitude to Jörg, Carina, Eva, and the other animal caretakers. Their great work every day is absolutely elemental for our success as PhD students and without them I would have had no time to perform any experiments. I want to thank Angelos for the introduction to microscopy, fixing all computer-related issues, helpful (and entertaining) scientific discussions, and for being a great person. I would like to thank Kati for her help and for the fun conversations during many microglia isolations. Furthermore, I want to thank Lisa, Marius, and Ulli for their help and support, and all the other members of AG Jucker. A big thank you goes to my initial office mates – Timo, Jay, Manuel, Juliane, and Mehtap (who still half-lived there even though I took her space). You are amazing friends and I will never forget the fun times we had in Tübingen! Thank you, Timo, for always making me laugh about your (really not very funny) jokes. Thank you, Jay, for talking to me despite your grumpy mood in the morning and for your helpful insights on any topic I asked you about. Thank you, Mehtap, for all the gym hours we spent together and the way to the bus station afterwards. The biggest thank you goes to Juliane, who is an absolutely selfless amazing friend, and who I will always admire for her big heart. I also want to thank my friends Sophie and Nadine, who are part of my life since boarding school. Another big thank you goes to Florian, for all the fun times, for making me forget everything about the lab when I am with you, and mostly for your never-fading support. But the final and biggest thank you goes to my family: my grandparents, brothers, and in particular my parents. My parents have sacrificed a lot to support me and help me along my way, and for that I will always be deeply grateful.

# Table of Contents

<b>1 SUMMARY</b>	<b>1</b>
<b>2 SYNOPSIS</b>	<b>3</b>
2.1 INNATE IMMUNE MEMORY	3
2.2 MICROGLIA AT A GLANCE	7
2.3 CHARACTERISTICS OF ALZHEIMER'S DISEASE	9
2.4 INFLAMMATION IN ALZHEIMER'S DISEASE	12
2.5 LONG-LASTING EPIGENETIC MICROGLIAL MEMORY OF PERIPHERAL INFLAMMATION MODULATES HALLMARKS OF ALZHEIMER'S DISEASE PATHOLOGY	14
2.5.1 MICROGLIAL LONGEVITY AND ITS CONSEQUENCES	14
2.5.2 MODULATION OF CEREBRAL B-AMYLOIDOSIS BY EPIGENETICALLY ENCODED MICROGLIAL MEMORY AFTER SYSTEMIC INFLAMMATION	17
2.5.3 MODULATION OF AMYLOID PLAQUE STRUCTURE AND NEURONAL DAMAGE THROUGH LONG- TERM MICROGLIAL CHANGES AFTER SYSTEMIC INFLAMMATION	27
2.6 CONCLUDING REMARKS AND OUTLOOK	32
2.7 REFERENCES	39
<b>3 PUBLICATIONS</b>	<b>57</b>
3.1 STATEMENT OF PERSONAL CONTRIBUTIONS	57
3.2 MICROGLIA TURNOVER WITH AGING AND IN AN ALZHEIMER'S MODEL VIA LONG-TERM <i>IN VIVO</i> SINGLE-CELL IMAGING	59
3.3 INNATE IMMUNE MEMORY IN THE BRAIN SHAPES NEUROLOGICAL DISEASE HALLMARKS	72
3.4 SYSTEMIC INFLAMMATION INDUCES LONG-TERM MODULATION OF AMYLOID PLAQUE MORPHOLOGY AND NEURONAL DAMAGE IN A MOUSE MODEL OF ALZHEIMER'S DISEASE	112
<b>4 APPENDIX</b>	<b>143</b>
4.1 ABBREVIATIONS	143
4.2 BIBLIOGRAPHY	144

# 1 Summary

Microglia comprise the resident tissue macrophage population in the brain parenchyma. They acquire a variety of functions in health and disease and are thus one of the most studied cell types regarding their contribution to neurological disease. In Alzheimer's disease, deposition of amyloid- $\beta$  occurs in senile plaques and leads to alterations of the microglial phenotype. This feature is mimicked in transgenic mouse models developing cerebral  $\beta$ -amyloidosis. How microglia influence onset and progression of Alzheimer's disease remains incompletely understood despite many studies.

Microglia are developmentally distinct from tissue macrophages in other organs and invade the brain early in embryogenesis. A long lifetime has been attributed to microglia; however, this has only scarcely been studied. Today, technological advances in the development of transgenic mouse models and *in vivo* microscopy allow for the in depth analysis of microglial turnover. In the first study presented here, we used genetic tools to label individual microglia and followed them *in vivo* by two-photon imaging. Long-term imaging over many months revealed that microglia are a long-lived cell population with low turnover rates. Furthermore, the rates of microglial proliferation and death were equal, matching previous reports that microglial cell numbers stay stable over time. In line with previous studies, higher proliferation rates were found in a mouse model of cerebral  $\beta$ -amyloidosis. Nevertheless, both in health and disease conditions, microglia lived many months and a proportion of microglia persisted throughout the entire lifespan of mice.

The long lifetime of microglia renders them suitable for the characterization of innate immune memory, a recently emerged concept, in the brain. While it was previously believed that only adaptive immune cells depict memory characteristics, recent reports have demonstrated immune memory also in cells of the innate immune system. Herein, a priming immune stimulus leads to a long-lasting change in the activation state of the innate immune cell, thereby modifying its response towards a secondary stimulus. In particular, two paradigms can be distinguished: a heightened response has been termed training, while a reduced response is called tolerance.

Our second study aimed to reveal whether training and tolerance are inducible in the brain and could be long-lasting modifiers of later occurring neurological disease pathology. We demonstrate that following peripheral immune stimulation with lipopolysaccharides or certain cytokines acute training and tolerance effects were evident in the brain. Furthermore, training and tolerance had opposing effects on much later occurring neuropathology of stroke and early stages of cerebral  $\beta$ -amyloidosis. Microglial enhancer landscape, gene expression, and function differed in response to peripheral immune stimulation with lipopolysaccharides, indicating long-term microglial reprogramming. Therefore, our study provides evidence for long-lasting innate immune memory in microglia that is epigenetically encoded and is sufficient to alter later developing neuropathology.

In the third study, we investigated whether training and tolerance modify amyloid plaque structure and neurotoxicity in mice with more advanced cerebral  $\beta$ -amyloidosis. Strikingly, modifications of amyloid plaque structure were evident 9 months after induction of training and tolerance, and occurred concomitantly with alterations in microglial function. In particular, peripheral training and tolerance stimuli altered the phenotype of plaque-associated microglia or reduced their number, respectively. Both impaired microglial barrier function, a recently described feature of microglia around amyloid plaques in Alzheimer's disease mouse models and patients. Importantly, modulation of microglial function, as induced by peripheral immune stimulation, altered amyloid plaque structure and thereby increased plaque-associated neurotoxicity. These results indicate that changes in microglial function contribute to neuronal damage by modulating amyloid structure and that such changes may occur in response to peripheral inflammatory events.

In summary, this thesis demonstrates that microglia are exceptionally long-lived cells with the capability to form persisting immune memory. Peripheral immune stimulation epigenetically reprograms microglia to acquire distinct phenotypes that subsequently modify pathological features of cerebral  $\beta$ -amyloidosis. Therefore, we identified epigenetic microglial memory of peripheral inflammation as an essential modifier of neurological diseases.



## 2 Synopsis

### 2.1 Innate immune memory

Every organism lives in constant interaction with microorganisms – some form symbiotic relationships with the host, while others are pathogenic and cause serious disease. The immune system evolved as a defense mechanism against harmful pathogens and relies on a complex interplay between immune cells and humoral factors. Two main branches of immunity, termed innate and adaptive immunity, exist in mammals (Parkin & Cohen, 2001).

The innate immune system is present in all metazoans and provides the first line of defense against infection and tissue damage. The innate immune system relies on sensing structures common to broad classes of microorganisms, so called pathogen-associated molecular patterns (PAMPs). These are recognized by pattern recognition receptors (PRRs) on innate immune cells including macrophages, granulocytes, and natural killer cells (Akira *et al.*, 2006). As a result, soluble mediators such as cytokines, chemokines, and complement proteins, are locally produced, initiate phagocytosis, recruit other immune cells, and exert multiple effects on the body.

In higher organisms such as mammals, adaptive immunity evolved as a second arm of the immune system to provide an additional layer of defense. While the main task of innate immunity is to produce a fast protective response and limit damage to the host, adaptive immunity provides a slower but more specific immune response that will protect the host against reinfection with the same pathogen (Dempsey *et al.*, 2003). Innate immunity plays a key role in initiating the adaptive immune response through the action of antigen-presenting cells that in turn activate adaptive immune cells, the lymphocytes (Iwasaki & Medzhitov, 2015). The adaptive immune response is mediated by clonal expansion and differentiation of antigen-specific B- and T-lymphocytes into effector and memory cells. Antibody-producing B-lymphocytes, cytotoxic T-lymphocytes, and activated innate immune cells then cooperate to clear pathogens. After resolution of infection, memory lymphocytes reside in the body and initiate a faster and enhanced immune response upon reinfection with the same pathogen (Dempsey *et al.*, 2003).

Despite playing different roles during the course of an immune reaction, innate and adaptive immunity cooperate intimately and cannot be viewed as distinct entities. Several immune cells contribute to both arms of immunity and are not readily classifiable into one of the two systems. Furthermore, the distinctions between innate and adaptive immunity have started to fade regarding memory formation (Hamon & Quintin, 2016).

Immunological memory refers to the immune system's ability to respond with an adapted immune response, which differs from the naïve response, to a secondary infection. For innate immune cells, memory characteristics have only recently been described and attributed to lasting epigenetic and transcriptional changes after stimulus cessation (Netea *et al.*, 2016; Ostuni *et al.*, 2013). These changes occur as a result of the first immunological insult (termed priming stimulus) and lead to persistent alterations in the cell's functional state, thereby mediating a differential response towards a secondary immune stimulus (Figure 1). This differential response can be heightened (termed trained immunity or training) or suppressed (termed tolerance) compared to the naïve immune response (Quintin *et al.*, 2014).

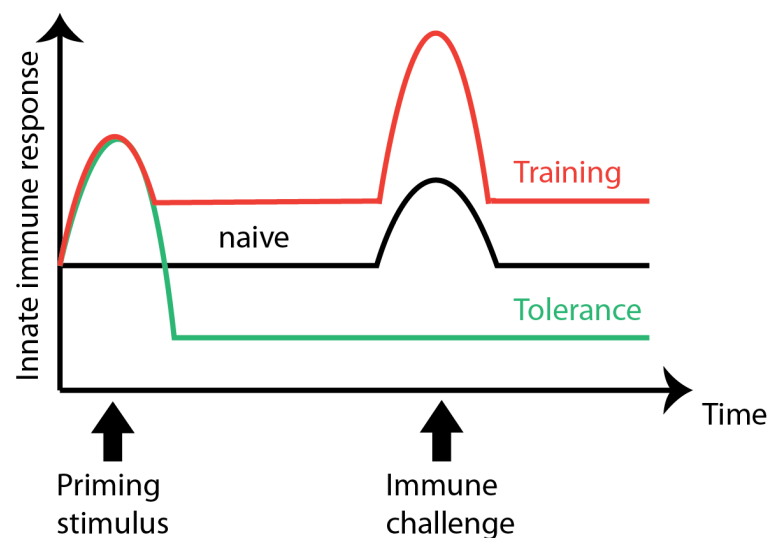


**Figure 1: Innate immune memory.** Following a priming stimulus, the cellular activity state is altered long-term. Upon a secondary immune stimulus, cells respond with an adapted immune response, which can be heightened (training) or suppressed (tolerance). Adapted from Quintin *et al.*, 2014.

While immune memory in adaptive immune cells is very specific to the encountered antigen, innate immune memory is in most cases non-specific (Hamon & Quintin, 2016; Song & Colonna, 2018). Since innate immune memory is mediated by long-lasting alterations of the cellular homeostatic state, the reaction to a broader range of subsequent stimuli is altered and thereby confers cross-protection to some up to now unresolved extent (Moret & Siva-Jothy, 2003; Netea *et al.*, 2011; Pham *et al.*, 2007).

So far, innate immune memory has been described for NK cells, monocytes, and macrophages in response to a range of pathogens, including bacteria, fungi, viruses, and parasites (Hamon & Quintin, 2016; Netea *et al.*, 2016). The most well known example of innate immune memory is endotoxin tolerance, which describes a refractory immune state induced by repeated or high-dose administration of lipopolysaccharide (LPS), a membrane component of Gram-negative bacteria. Endotoxin tolerance occurred in septic patients after the initial acute systemic hyperinflammatory response and persisted for at least 2 weeks (Monneret *et al.*, 2004). Epigenetic and transcriptional reprogramming underlie the refractory state of endotoxin-tolerant innate immune cells (Biswas & Lopez-Collazo, 2009; Foster *et al.*, 2007; Schaafsma *et al.*, 2015; Shalova *et al.*, 2015). However, the effects of LPS on the immune system are extremely diverse and depend largely on its dose and administration frequency. For example, low doses of LPS can have opposing effects and prime macrophages, subsequently inducing trained immunity (Deng *et al.*, 2013; Zhang & Morrison, 1993).

Other observations, such as the cross-protection of Bacillus Calmette-Guérin (BCG) vaccination against other non-mycobacterial diseases, have been known for a long time and only recently been studied in more detail (Netea & van Crevel, 2014; Arts *et al.*, 2018). The beneficial non-specific effects of the BCG vaccine were now attributed to heightened cytokine production and altered functional states of peripheral monocytes (Arts *et al.*, 2018; Kleinnijenhuis *et al.*, 2012). Interestingly, the BCG vaccine and other inflammatory stimuli exert effects also on hematopoietic progenitor cells, resulting in their myeloid-biased proliferation (Christ *et al.*, 2018; Kaufmann *et al.*, 2018; Mitroulis *et al.*, 2018). Thus, recent studies indicate that not only differentiated cells, but also certain progenitor and stem cell types, possess capacity for immune memory formation (Christ *et al.*, 2018; Kaufmann *et al.*, 2018; Mitroulis *et al.*, 2018; Naik *et al.*, 2017).

One of the best examples for trained immunity occurs following priming with  $\beta$ -glucan, a component of the fungal cell wall. Stimulation of monocytes with  $\beta$ -glucan led to stable epigenetic histone modifications and transcriptional reprogramming, resulting in a metabolic shift towards glycolysis (Cheng *et al.*, 2014; Quintin *et al.*, 2012; Saeed *et al.*, 2014). Interestingly,  $\beta$ -glucan treatment partially reversed epigenetic and transcriptional alterations occurring after LPS-induced tolerance *in vitro*, indicating that training and tolerance confer modifiable epigenetic alterations on to some extent overlapping signaling pathways (Novakovic *et al.*, 2016). The role of epigenetic and metabolic reprogramming in innate immune memory will be further discussed in chapter 2.5.2.

## 2.2 Microglia at a glance

Microglia are the resident parenchymal macrophages of the central nervous system (CNS). They have been described and named by del Rio-Hortega in 1919 (Rio-Hortega, 1919; Sierra *et al.*, 2016) and comprise 5-12% of glial cells in the brain (Lawson *et al.*, 1990). Due to their wide array of functions they play a role in CNS development, circuit and synapse rewiring (Graeber, 2010; Parkhurst *et al.*, 2013; Schafer *et al.*, 2012), innate immune response, and have been implicated in neurological disease states (Gomez-Nicola & Perry, 2015).

Under homeostatic conditions, microglia exhibit a ramified morphology and are constantly surveying the tissue environment by movement of their numerous processes (Davalos *et al.*, 2005; Nimmerjahn *et al.*, 2005). As innate immune cells, they participate in host defense and are equipped to respond to any alteration of the tissue environment. Microglia express a variety of PRRs to detect pathogen entry or injury to the brain (Kettenmann *et al.*, 2011). Activation of PRRs can result in the release of inflammatory cytokines, chemokines, and induction of phagocytosis (Hanisch, 2002; Ransohoff & Cardona, 2010; Ransohoff & Perry, 2009). Under certain conditions, other cells – such as astrocytes, neurons, and invading peripheral immune cells – contribute to inflammatory processes in the brain (Heneka & O’Banion, 2007). However, inflammation in the brain has to be tightly controlled, as many pro-inflammatory cytokines are potent inducers of neuronal dysfunction and cell death (Ransohoff & Cardona, 2010).

Changes from the surveying microglial morphology and function to different phenotypes were originally termed “microglial activation”. Up until recently, scientists categorized microglial and macrophage phenotypes into opposing activation states (previously termed M1 and M2), but it has become evident that this simplistic view cannot capture the full picture of their phenotypic diversity (Xue *et al.*, 2014). Since the alterations that can occur in the brain environment are extremely pleiotropic and versatile, such are the microglial adaptive responses (Hanisch & Kettenmann, 2007; Ransohoff & Perry, 2009). Therefore, an accurate description of microglial phenotypes in health and disease states can solely be achieved by in depth ‘omics’, e.g. transcriptomic or epigenomic, approaches. Recently, genome-wide approaches have been used to study macrophage and microglial phenotypes and led to the characterization of the microglial transcriptome and epigenome under different

conditions (Gosselin *et al.*, 2014; Lavin *et al.*, 2014; Orre *et al.*, 2014). Analysis of the microglial transcriptome on a single-cell level has proven the substantial heterogeneity of microglial phenotypes and resulted in the description of molecular microglial profiles under different conditions (Keren-Shaul *et al.*, 2017; Korin *et al.*, 2017; Mathys *et al.*, 2017). This will be further discussed in chapter 2.5.2.

Microglia originate from primitive hematopoiesis in the yolk sac of the early embryo and invade the brain during early embryonic development (Ginhoux *et al.*, 2010; Hoeffel *et al.*, 2015). Hence, microglial identity is established by a combination of developmentally determined and environment-dependent transcriptional networks (Gosselin *et al.*, 2014; Mass *et al.*, 2016; Matcovitch-Natan *et al.*, 2016). Microglia reside in the brain throughout their life and are maintained by local self-renewal with no appreciable contribution from the peripheral hematopoietic system under homeostatic conditions (Ajami *et al.*, 2007; Hashimoto *et al.*, 2013). However, until recently, mechanisms of microglial network maintenance and turnover of microglia *in vivo* have only been scarcely studied and remained poorly understood. This topic will be discussed in depth in chapter 2.5.1.

Understanding the turnover and lifetime of microglia *in vivo* is of particular importance for the study of long-term changes in these cell types, which might influence aging and neurodegenerative diseases. A concept reminiscent of trained immunity termed priming has been described to occur in microglia under certain circumstances (Haley *et al.*, 2017). Priming has first been demonstrated in macrophages *in vitro*, wherein a primary stimulation heightened the cellular response towards a secondary stimulus (Henricson *et al.*, 1993; Hirohashi & Morrison, 1996; Zhang & Morrison, 1993). Microglial priming is believed to be elicited by diverse stimuli such as aging, neurodegenerative disease, and acute or chronic systemic inflammation (Cunningham, 2013; Perry & Teeling, 2013). Applying priming stimuli such as systemic inflammation during particularly susceptible periods, i.e. pre- or neonatally, led to life-long alterations of the microglial phenotype that predisposed the brain to the development of neurodegenerative-like conditions (Krstic *et al.*, 2012). Evidence for immune memory in microglia, its mechanisms, and its consequences for neurological disease will be further discussed in chapter 2.5.2.

### 2.3 Characteristics of Alzheimer's disease

Alzheimer's disease (AD) is the most common cause of dementia in the elderly and has become increasingly epidemic with rising life expectancies (Dartigues, 2009; Holtzman *et al.*, 2011). AD is a complex neurological disorder, in which a multitude of cellular processes go awry. However, on a molecular level AD is characterized by the presence of two aggregated hallmark proteins: amyloid-beta ( $A\beta$ ) and tau, as first described by Alois Alzheimer in 1907. In every AD patient,  $A\beta$  is deposited in the brain parenchyma in the form of aggregated, insoluble, fibrillar structures called senile plaques (Glenner & Wong, 1984; Masters *et al.*, 1985). The second disease hallmark is the presence of neurofibrillary tangles (NFT's), intraneuronal inclusions mainly consisting of the hyperphosphorylated, aggregated microtubule-associated protein tau (Grundke-Iqbal *et al.*, 1986; Kosik *et al.*, 1986).

Tragically, the molecular aggregation processes underlying disease development already start decades before onset of symptoms in patients (Jack *et al.*, 2010). The  $A\beta$  peptide has been of immense interest to the scientific community because its misfolding and aggregation in amyloid structures is believed to mark the beginning of the disease process. In fact, the deposition of  $A\beta$  and resulting neuronal damage precedes symptom onset by about 15 years (Bateman *et al.*, 2012). Once  $A\beta$  deposits form in the brain parenchyma due to a misbalance in its production and clearance rate, a series of reactions takes place that ultimately leads to symptoms of AD. Multimeric  $A\beta$  aggregates activate the immune system in the brain (see chapter 2.4 for details), leading to an inflammatory reaction, the induction of neurofibrillary tangles, and ultimately synaptic and neuronal loss resulting in dementia. This series of events initiated by the aggregation of the  $A\beta$  peptide has been described as the amyloid cascade hypothesis (Hardy & Selkoe, 2002; Selkoe & Hardy, 2016).

The  $A\beta$  peptide is generated by proteolytic cleavage of the transmembrane protein amyloid-precursor protein (APP) (Haass & Selkoe, 1993), a process occurring continuously throughout an individual's life span (Haass *et al.*, 1992). APP is cleaved first by  $\beta$ -secretase, resulting in the generation of a C-terminal fragment (CTF- $\beta$ ) (Vassar *et al.*, 1999), which is subsequently processed by the  $\gamma$ -secretase complex. The  $\gamma$ -secretase complex cleaves CTF- $\beta$  progressively between residues 37 and 43, leading to the liberation of  $A\beta$  isoforms with variable lengths into the extracellular space (Haass *et al.*, 2012; Vassar *et al.*, 1999). The most common isoform of  $A\beta$  in

healthy individuals is A $\beta$ <sub>1-40</sub>, while AD patients often exhibit increased amounts of the more aggregation prone isoform A $\beta$ <sub>1-42</sub> (Hellström-Lindh *et al.*, 2009). The mechanism by which natively unfolded monomeric A $\beta$  peptides are converted into aggregated structures with the distinct structural and histochemical properties of amyloids (e.g. cross  $\beta$ -structure, Congo red binding and concomitant birefringence) is still under debate. For aggregation prone amyloidogenic proteins such as A $\beta$ , *in vitro* and *in vivo* evidence suggests a self-propagating nucleation-dependent polymerization process (Jucker & Walker, 2013), comparable to the templated protein misfolding occurring in prion disease. In a first step, A $\beta$  misfolds into a  $\beta$ -sheet rich structure that subsequently forms a multimeric nucleus (also termed seed), which converts and incorporates other A $\beta$  molecules into growing aggregates (Harper & Lansbury, 1997; Jarrett & Lansbury, 1993). The formation of the initial misfolded A $\beta$  seed is a rare event that happens due to its unfavorable kinetics stochastically over a long period of time. The exact nature of the A $\beta$  seed is still unknown and remains to be resolved (Jucker & Walker, 2013). However, once sufficient A $\beta$  seeds have formed, growth of aggregates proceeds quickly and deposition of amyloid plaques starts, ultimately leading to neuron loss and symptoms of AD.

AD can be subdivided into an early-onset familial and a late-onset sporadic form. Familial AD accounts for less than one percent of disease cases and is caused by rare dominantly inherited mutations affecting A $\beta$  homeostasis (Bekris *et al.*, 2010; Scheuner *et al.*, 1996). All known familial mutations causing early-onset AD occur in proteins involved in A $\beta$  generation (Crook *et al.*, 1997; Goate *et al.*, 1991; Mullan *et al.*, 1992), namely APP and presenilin 1 and 2, the latter two being part of the  $\gamma$ -secretase complex (Wolfe *et al.*, 1999).

Knowledge about the genetic causes for AD has been used to generate animal models to mimic the disease process. Many of the widely studied transgenic mouse models overexpress mutated human APP, sometimes in combination with presenilin mutations. In contrast to wildtype animals, these mice show age-dependent deposition of A $\beta$  in parenchymal plaques and/or cerebral blood vessels (cerebral  $\beta$ -amyloidosis), accompanied by glial and neuronal alterations (Ashe & Zahs, 2010; Jucker, 2010). However, global neuron loss and NFT's are lacking in mouse models with cerebral  $\beta$ -amyloidosis (Bornemann & Staufenbiel, 2000; Howlett & Richardson, 2009), although early stages of tau pathology (i.e. hyperphosphorylation of tau) are evident



around amyloid plaques in some models (Kurt *et al.*, 2003; Sturchler-Pierrat *et al.*, 1997). Despite these animal models not recapitulating all features of the disease process, they comprise useful tools for the study of the molecular aggregation process of A $\beta$  and concomitant cellular changes in the brain.

The vast majority of AD cases occurs sporadically, i.e. in the absence of a known disease-causing mutation, with symptom onset much later in life compared to familial AD patients (Bekris *et al.*, 2010). However, the molecular cascade leading to disease pathogenesis is believed to be similar in sporadic and familial forms of AD. The risk of developing sporadic AD is determined by a combination of genetic (see chapter 2.4 for details) and environmental risk factors (Reitz *et al.*, 2011; Tosto & Reitz, 2013). Importantly, by far the biggest risk factor for the development of sporadic AD is aging (Reitz *et al.*, 2011). Since A $\beta$  is continuously produced throughout life, the chance for the stochastic formation of sufficient amounts of disease-initiating A $\beta$  seeds increases with time. Moreover, cell regeneration is limited within the brain, resulting in gene expression changes with aging particularly in glial cells, which have A $\beta$  clearance capability (Soreq *et al.*, 2017). Low-grade chronic inflammation in the brain occurs with age as a result of alterations in cellular phenotypes; microglia are skewed towards adopting a more pro-inflammatory phenotype (microglial priming, see chapter 2.2) and simultaneously lose features implicated in ensuring brain homeostasis (Hefendehl *et al.*, 2014; Lynch *et al.*, 2010; Yu *et al.*, 2002). Thereby, alterations of cellular functions with aging may predispose to the development of neurodegenerative processes and act in concert with the life-long continuous production of A $\beta$  in the initiation of AD.

## 2.4 Inflammation in Alzheimer's disease

Historically, due to the view of the brain as an immunologically privileged organ, inflammation was not believed to contribute to AD and other neurological diseases. This concept has dramatically changed in the last two decades and led to a new field of research concentrating on the interaction between the immune and the nervous system in health and disease. Today, we know that a variety of immune cell subtypes exist in the brain (Korin *et al.*, 2017) and drive inflammation in many neurological diseases (Heneka *et al.*, 2014). Especially in AD, inflammation occurs and contributes to disease progression and neuronal loss (Heneka & O'Banion, 2007).

The first hints about the contribution of immunology to neurological disease appeared upon discovery of inflammatory molecules such as complement, cytokines, and acute phase proteins, in AD brains (Akiyama *et al.*, 2000). Since then, it has become evident that multimeric A $\beta$  itself activates the immune system in several ways (Bate *et al.*, 2004; Paresce *et al.*, 1996; Rogers *et al.*, 1992; Wang *et al.*, 2004; Yan *et al.*, 1998). Microglia and astrocytes proliferate and accumulate around A $\beta$  plaques (gliosis), a process accompanied by alterations in cellular function (Akiyama *et al.*, 2000; Itagaki *et al.*, 1989). Furthermore, A $\beta$  deposition in the brain alters the production of pro- and anti-inflammatory cytokines (Butovsky *et al.*, 2005; Floden & Combs, 2006; Lee *et al.*, 2002; Lindberg *et al.*, 2005; Lue *et al.*, 2001; Szczepanik *et al.*, 2001). This altered inflammatory environment may propagate further amyloid deposition, the formation of NFT's, and neuronal damage (Guo *et al.*, 2002; Kitazawa *et al.*, 2005; Kitazawa *et al.*, 2011; Li *et al.*, 2003; Sheng *et al.*, 2000). Damaged neurons release danger-associated molecular patterns (DAMPs), which in turn activate PRR on microglia, thereby creating a feed-forward loop between inflammation and neurotoxicity (Block *et al.*, 2007).

Although A $\beta$  is regarded as the disease-initiating cause of AD pathology, A $\beta$  burden itself does not correlate with cognitive decline in patients (Edison *et al.*, 2008; Lue *et al.*, 1996). In contrast, increased inflammatory markers are significantly correlated with the occurrence and severity of dementia (Edison *et al.*, 2008; Lue *et al.*, 1996), implicating inflammation as a main contributor to memory impairment in AD. Interestingly, many risk factors for the development of AD are related to inflammation (Heneka *et al.*, 2015). Local inflammatory insults to the brain, such as traumatic brain injury, as well as systemic infections and peripheral diseases with an

immune component, such as diabetes mellitus, increase the risk for AD (Heneka *et al.*, 2014; Sims-Robinson *et al.*, 2010). Acute peripheral infections in AD patients dramatically worsen disease symptoms and lead to irreversible long-term cognitive decline (Cunningham, 2013; Dunn *et al.*; Holmes *et al.*, 2009). On the other hand, the long-term use of non-steroidal anti-inflammatory drugs (NSAIDs) lowers the risk of developing dementia (Hoozemans *et al.*, 2011), although therapeutic use of NSAIDs did not show beneficial effects in clinical trials. Nevertheless, these clinical observations and epidemiological studies connect local and systemic inflammation to the development and progression of AD.

The impact of inflammation on neurological disorders has been further highlighted by genome-wide association studies (GWAS) that have linked variants in several immune-related genes to neurological disease (Gagliano *et al.*, 2016; Guerreiro *et al.*, 2013; Hollingworth *et al.*, 2011; Huang *et al.*, 2017; Lambert *et al.*, 2013; Naj *et al.*, 2011; Sims *et al.*, 2017; Zhang *et al.*, 2013). Many of the disease-linked immune-related gene products, such as Pu.1, Trem2, CD33, and complement receptor 1, are expressed by microglia. In addition, recent studies identified epigenetic changes in a number of genes, some of them immune-related, in sporadic AD cases (De Jager *et al.*, 2014; Gjoneska *et al.*, 2015; Lunnon *et al.*, 2014), highlighting the importance of epigenetic regulatory mechanisms in driving cellular dysfunction in disease.

Since the immune system is tightly involved in the progression of neurodegenerative diseases, alterations of immune cells or molecules in turn change disease progression. This has been demonstrated by a multitude of experimental studies, in which the knockout or overexpression of an immune molecule modulated disease severity in mouse models of AD (Chakrabarty *et al.*, 2015; Heneka *et al.*, 2013; Jay *et al.*, 2017; Masashi Kitazawa *et al.*, 2011; Shi *et al.*, 2011; Vom Berg *et al.*, 2012). In summary, data from animal models and epidemiological and genetic data in humans implicate inflammation as a disease contributing component rather than a mere bystander effect of AD pathology. However, despite the many studies on this subject, it remains unclear how microglia are involved and which microglial activation states are beneficial or detrimental for disease progression. Our studies on the impact of microglial immune memory on features of cerebral  $\beta$ -amyloidosis will be discussed in chapters 2.5.2 and 2.5.3.

## 2.5 Long-lasting epigenetic microglial memory of peripheral inflammation modulates hallmarks of Alzheimer's disease pathology

### 2.5.1 Microglial longevity and its consequences

---

In reference to:

#### **Microglia turnover with aging and in an Alzheimer's model via long-term *in vivo* single-cell imaging**

Petra Füger, Jasmin K. Hefendehl, Karthik Veeraraghavalu, Ann-Christin Wendeln, Christine Schlosser, Ulrike Obermüller, Bettina M. Wegenast-Braun, Jonas J. Neher, Peter Martus, Shinichi Kohsaka, Martin Thunemann, Robert Feil, Sangram S. Sisodia, Angelos Skodras, Mathias Jucker (2017). *Nature Neuroscience*

---

Under homeostatic conditions, microglia are uniformly distributed in the cortex, forming a dense, non-overlapping territorial network with their constantly moving ramified processes (Davalos *et al.*, 2005; Lawson *et al.*, 1990; Nimmerjahn *et al.*, 2005). Upon encountering tissue damage, microglia rapidly react with phenotypic changes and proliferation (Hanisch & Kettenmann, 2007). Microgliosis occurs in various neurological conditions (Gomez-Nicola *et al.*, 2013; Streit *et al.*, 1999); despite this, there is a paucity of knowledge on microglial turnover under homeostatic and disease conditions.

Deciphering microglial maintenance is instrumental for understanding microglial function and dysfunction in aging, neurodegenerative disease, and following early-life priming. An early study using labeling with <sup>3</sup>H-thymidine reported very low proliferation rates of microglia and shaped the view of microglia as very long-lived tissue macrophages (Lawson *et al.*, 1992). However, estimation of the microglial lifetime was done indirectly by labeling DNA synthesis rather than cellular division (Duque & Rakic, 2011; Maurer, 1981).

In our study, we aimed to directly observe microglial turnover by long-term *in vivo* imaging of individual microglia. To this end, we fluorescently labeled a small subpopulation of microglia using tamoxifen-inducible Cre-mediated recombination. In contrast to ectopic labeling of all microglia, where individual cells are hardly

distinguishable from each other, tamoxifen-inducible labeling allows fine-tuning the amount of recombined cells by adjusting tamoxifen dose and injection paradigm. In our study, we chose a tamoxifen injection paradigm that led to random recombination in about 2% of all microglia, thereby allowing repeated identification of the same cell with great certainty. Using two-photon imaging of the living mouse brain, the fate of individual labeled microglia was followed over longitudinally up to 16 months. While most microglia remained stable over time, rare events of proliferation and cellular death occurred. Over the course of 6 months, roughly 13% of microglia died. Strikingly, the same percentage of microglia appeared as newly born cells. In line with previous reports (Hefendehl *et al.*, 2014), these data indicate that microglial numbers are largely stable during the lifespan of a mouse.

A recent paper described spatially and temporally coupled apoptosis and proliferation as a mechanism for microglial network maintenance (Askew *et al.*, 2017). However, in their study, newly appearing microglia were more prone to apoptotic cell death than the remaining microglial population; an effect we did not observe. Askew *et al.* also reported markedly higher microglial proliferation rates than previously described (Lawson *et al.*, 1992) and attributed cortical microglia a lifetime of roughly 3 months. However, estimating the microglial turnover rate was done indirectly using bromodeoxyuridine (BrdU) incorporation or following labeling with viral vectors, which could alter the homeostatic microglial proliferation rate. In contrast, our study revealed low microglial proliferation rates and stable insertion of newly generated cells into the microglial network. From our long-term *in vivo* imaging data, the microglial lifetime in the cortex was estimated to around 29 months. A recent study, which was based on a genetically modified mouse model to label individual microglia followed by analysis of brain sections, assigned microglia a lifetime of 24 months in the cortex (Tay *et al.*, 2017), comparable to our results.

While some studies have suggested the existence of a microglial progenitor cell type in the brain (Bruttger *et al.*, 2015; Elmore *et al.*, 2014), neither our study nor the other recent reports (Askew *et al.*, 2017; Tay *et al.*, 2017) found evidence for this. Our long-term *in vivo* imaging data revealed that newly appearing microglia initially appeared at a distance smaller than the average inter-microglial distance to already existing microglial cells, and this observation was sometimes preceded by an increase in cell-body volume of a stable microglial cell. This indicates that new cells arise by

division of existing microglia. However, it remains unclear whether the newly born microglial cell is phenotypically similar to its chronologically older parent cell or acquires a different phenotype.

Recent studies described brain region-dependent variety in microglial proliferation rates (Askew *et al.*, 2017; Tay *et al.*, 2017). In addition, region-dependent heterogeneity in microglial transcriptomes has been demonstrated (Grabert *et al.*, 2016), indicating that microglial function and turnover vary depending on local environment. Alterations of the brain environment in disease have been shown to induce marked microgliosis (Gomez-Nicola *et al.*, 2013; Streit *et al.*, 1999). In line with these findings, following the fate of individual microglia in a mouse model with early onset and fast progression of A $\beta$  deposition (APPPS1 mice) revealed a 3-fold increase in microglial proliferation, but unaltered microglial death rates in comparison to imaged mice without cerebral  $\beta$ -amyloidosis. Surprisingly, plaque-associated microglia showed equivalent proliferation and death rates. In fact, increased microglial proliferation was solely observed in plaque-distant microglia and was followed by migration of the newly born cells to amyloid plaques. These data point to marked heterogeneity among plaque-associated microglia in APP transgenic mice above a certain age.

Furthermore, our study indicates that both in health and disease the microglial population in an aged brain consists of microglia with varying ages. Our data reveal that about 50% of the microglial population persist throughout the life span of a healthy mouse, while the remaining microglia are of varying age and have arisen by cellular division. This provides an explanation for age-associated heterogeneity in microglial responses (Grabert *et al.*, 2016; Hefendehl *et al.*, 2014; Streit *et al.*, 2004) and highlights the importance of single-cell profiling studies. Furthermore, their long lifetime explains the previously described long-lasting alterations of microglial function after early-life priming (Krstic *et al.*, 2012; Perry & Holmes, 2014). Of note, other macrophage populations (perivascular and meningeal) in the CNS have recently been shown to resemble microglia in their development from embryonic hematopoietic precursors, a very limited turnover from peripheral monocytes, and an extremely long lifetime (Goldmann *et al.*, 2016; Prinz *et al.*, 2017). It remains to be determined whether these other long-lived resident macrophage populations also contribute to aging- or priming-related changes in the brain.

## 2.5.2 Modulation of cerebral $\beta$ -amyloidosis by epigenetically encoded microglial memory after systemic inflammation

---

In reference to:

### **Innate immune memory in the brain shapes neurological disease hallmarks**

Ann-Christin Wendeln<sup>\*</sup>, Karoline Degenhardt<sup>\*</sup>, Lalit Kaurani, Michael Gertig, Thomas Ulas, Gaurav Jain, Jessica Wagner, Lisa M. Häsler, Katleen Wild, Angelos Skodras, Thomas Blank, Ori Staszewski, Moumita Datta, Tonatiuh Pena Centeno, Vincenzo Capece, Md. Rezaul Islam, Cemil Kerimoglu, Matthias Staufenbiel, Joachim L. Schultze, Marc Beyer, Marco Prinz, Mathias Jucker, André Fischer, and Jonas J. Neher (2018). <sup>\*</sup>contributed equally.

---

With all cells possessing the same genetic information, epigenetic regulation of transcriptional programs is required for adaptation of specific cell fates. Epigenetics refers to all modifications of DNA or histones that occur without altering the genetic sequence. Instead, epigenetic modifications alter chromatin packaging and control accessibility of DNA-binding factors to regulatory elements (Jenuwein & Allis, 2001). Thereby, specific histone modifications in promoter regions or in distant cis-regulatory elements, so called enhancers, critically control gene expression (Ivashkiv, 2013), with chromatin modifications at enhancers reflecting cellular transcriptional profiles better than epigenetic modifications at promoter regions (Heintzman *et al.*, 2009). In any given cell, only a small subset of all genome-wide enhancers is active at a given time and subsequently determines gene expression profiles. During development, lineage-determining transcription factors (LDTFs) prime a subset of enhancers. In turn, signal-dependent transcription factors (SDTFs) activated in response to cues of the local environment bind to primed enhancers to initiate cell-type specific gene expression. Thereby, lineage- and tissue-specific regulatory networks are integrated to epigenetically determine cellular identity and function (Glass & Natoli, 2015; Heinz *et al.*, 2015).

While microglia have a distinct ontogeny from tissue-resident macrophage populations in other organs, they share common functions and developmental features, such as the dependency on the LDTF Pu.1 (Kierdorf *et al.*, 2013; Smith *et al.*, 2013). However, due to the major influence of the CNS environment, microglial

enhancer landscape and gene expression differ in several hundred genes from other macrophages (Gautier *et al.*, 2012; Gosselin *et al.*, 2014; Lavin *et al.*, 2014). Interestingly, transferring macrophages to another tissue environment reshaped their active enhancer and gene expression profile to a certain extent to resemble the resident macrophage population (Lavin *et al.*, 2014), confirming that external stimuli in the tissue environment exert a major influence on cellular identity via SDTFs.

Epigenetic reprogramming has previously been implied as the basis for innate immune memory, since training and tolerance led to stable epigenetic histone modifications and transcriptional reprogramming in monocytes and macrophages *in vitro* (Saeed *et al.*, 2014). So far, innate immune memory has been described *in vitro* and *in vivo* for up to 3 months in circulating monocytes (Kleinnijenhuis *et al.*, 2012; Saeed *et al.*, 2014), but whether it exists in the brain remains completely unknown. In our study, we therefore tested whether innate immune memory occurs in microglia and influences neurological disease. We found that peripheral immune stimulation epigenetically reprogrammed microglia and was sufficient to alter much later occurring neurological disease hallmarks. Since microglia are long-lived cells (see chapter 2.5.1), it is possible that microglial immune memory persists for their entire lifetime and thereby exerts long-lasting effects on brain homeostasis and pathology.

It is well established that peripheral inflammatory events are transduced to the brain (Cunningham *et al.*, 2009; Perry *et al.*, 2007; Qin *et al.*, 2007). In our study, we therefore used daily peripheral application of LPS for up to four consecutive days to induce systemic inflammation and tested whether acute immune memory effects were evident in the brain. A single peripheral injection of LPS (1xLPS) led to acute cytokine release in the periphery and brain. In the brain, repeated exposure to LPS on the following day (2xLPS) resulted in a much stronger release of several pro-inflammatory cytokines (such as IL-1 $\beta$ , TNF- $\alpha$ , IL-6, and IL-12) compared to the first LPS injection, indicative of training. This massive cytokine release upon training was abrogated in microglia-specific knockout mice (of *Tak1* or *Hdac1/2*), indicating that immune training in the brain is predominantly mediated by microglia. Training was accompanied by morphological changes of microglia, suggesting that microglia are the cells capable of immune memory formation in the brain.

In contrast, training was not detectable in the periphery, since pro-inflammatory cytokine release in the serum was diminished upon the second LPS injection, and was



even further reduced with the following daily LPS injections (3xLPS and 4xLPS). However, the levels of the anti-inflammatory cytokine IL-10 remained high with repeated LPS injections in the serum, indicating induction of tolerance in the periphery. In contrast to immune training observed after 2xLPS in the brain, 3x and 4xLPS led to a strong reduction in pro-inflammatory cytokine release while IL-10 levels remained elevated, demonstrating that repeated LPS exposure (3x and 4xLPS) also caused immune tolerance in the brain.

These results demonstrate that dependent on the number of LPS injections acute immune training and tolerance are inducible in the brain (Figure 3). In line with our results, dose and time-dependency of training and tolerance have previously been described for LPS. While low doses of LPS induced training in macrophages (Deng *et al.*, 2013; Zhang & Morrison, 1993), high doses resulted in endotoxin tolerance *in vitro* and *in vivo* (Beeson & Roberts, 1947; del Fresno *et al.*, 2009). While we used one dose of LPS in our study, our results demonstrate dependency on the number of applications, with the first injection inducing training subsequently, and repeated injections (3x and 4xLPS) on consecutive days leading to tolerance.

In line with results from others (Banks & Robinson, 2010), LPS did not enter the brain of mice, suggesting other ways of signal transduction to the brain, such as cytokine transport across the intact blood-brain barrier (BBB) or cytokine secretion by endothelial cells of the BBB (Quan & Banks, 2007). A study on the protective effects of IL-1 $\beta$  pretreatment on lethal infection in mice suggested that certain cytokines can induce training by themselves (van der Meer *et al.*, 1988). In addition, several recent studies assigned IL-1 $\beta$  a crucial role in mediating trained immunity in the periphery (Arts *et al.*, 2018; Christ *et al.*, 2018; Mitroulis *et al.*, 2018). In our study, we demonstrate that peripheral injection of the cytokines TNF- $\alpha$  and IL-10 also gave rise to innate immune memory effects in the brain in response to LPS stimulation 4 weeks later. Interestingly, while a low dose injection of TNF- $\alpha$  elicited training, application of high dose TNF- $\alpha$  caused tolerance, highlighting the importance of the dose also in shaping innate immune memory in the brain. Furthermore, tolerance was induced after repeated application of the anti-inflammatory cytokine IL-10, suggesting that multiple cytokines are able to induce innate immune memory in the brain.

As acute immune memory effects were evident in the brain after peripheral immune stimulation, we wondered whether immune training and tolerance exert long-lasting

effects on the brain's immune response and thereby influence later occurring neuropathology. Since a single peripheral injection of LPS (1xLPS) induced immune training upon subsequent re-exposure to LPS, and four LPS injections (4xLPS) led to tolerance in the brain, we tested the effects of 1xLPS as a training stimulus or 4xLPS as a tolerizing stimulus on disease pathology. Peripheral immune stimulation of pre-depositing APP23 mice with 1xLPS or 4xLPS modified hallmarks of cerebral  $\beta$ -amyloidosis 6 months later, i.e. at an early stage of disease pathology. In 9 months old APP23 mice, animals that were treated at 3 months of age with 1xLPS had increased plaque load and A $\beta$  levels, while animals treated with 4xLPS showed decreased A $\beta$  pathology. A differential immune state as indicated by changes in cytokine levels (i.e. reduced IL-10 levels in 1xLPS treated APP23 mice and reduced IL-1 $\beta$  levels in 4xLPS treated APP23 mice) was evident in the brain, but not the periphery, of immune stimulated 9 months old APP23 animals (Figure 3). These data highlight that immunological memory in the periphery was by far shorter lived compared to the brain, an effect that can be explained by the differing lifetimes of myeloid cell populations (a period of days for circulating monocytes versus many months for microglia). Since changes in the brain's immune state were absent in 9 months old immune stimulated wildtype animals, a second stimulus (e.g. A $\beta$  deposition in APP23 mice) within a certain time frame of the first immune stimulus seems to be required to observe a differential immune response. In line with this, analysis of the microglial enhancer repertoire revealed differences in enhancer activation in response to peripheral immune stimulation in wildtype compared to APP23 animals.

Previous studies suggested a stepwise model of macrophage enhancer activation in innate immune memory (Netea *et al.*, 2016; Ostuni *et al.*, 2013). An immune stimulus elicits gene expression changes, which are epigenetically encoded in histone modifications on promoters and enhancers. Large scale epigenomic studies revealed that methylation and acetylation of particular histone residues are either constitutive or activity-dependent marks indicative of particular gene elements such as exons, introns, enhancers, and promoters (Jenuwein & Allis, 2001; Zhou *et al.*, 2011). In particular, acetylation at lysine 27 on histone 3 (H3K27ac) occurs in enhancers and promoters that are activated by SDTFs in response to an immune stimulus, changing chromatin structure to an open state and initiating gene transcription. A subset of enhancers, termed latent enhancers, is believed to form the epigenetic basis of innate

immune memory (Netea *et al.*, 2016; Saeed *et al.*, 2014). Latent enhancers are distal regulatory elements that are epigenetically unmarked or marked at low levels in unstimulated cells, but gain histone modifications characteristic of enhancers, such as monomethylation at lysine 4 on histone 3 (H3K4me1), in response to specific stimuli (Netea *et al.*, 2016; Shlyueva *et al.*, 2014). Latent enhancers activated by SDTFs in response to an immune stimulus thereupon gain the epigenetic modifications H3K27ac and H3K4me1 (Figure 2). Once the acute immune reaction has been resolved, which is in the experimental setup in this study less than 24 hours after the last LPS injection, enhancers and promoters are turned off and lose H3K27ac. However, some of the previously active latent enhancers retain H3K4me1 as a sign of their recent activity and thereupon stay in a primed state. These primed enhancers are not yet active but are associated with open chromatin structure and thus can undergo a stronger activation upon restimulation (Netea *et al.*, 2016; Shlyueva *et al.*, 2014). Upon a secondary immune stimulus, such as the deposition of A $\beta$ , a subset of H3K4me1-marked primed enhancers are reactivated and regain H3K27ac, leading to adapted transcriptional changes in comparison to the naïve immune reaction, indicative of innate immune memory (Figure 2).

In line with this concept, peripheral immune stimulation with LPS led to changes in the microglial primed enhancer repertoire (based on differential H3K4me1 levels) 6 months later in wildtype and APP23 animals, while no changes in primed enhancers occurred in response to cerebral  $\beta$ -amyloidosis itself. Both in wildtype and APP mice, H3K4me1 levels of microglial enhancers differed significantly between all treatment groups, demonstrating that primed enhancers are primarily established in response to peripheral immune stimulation. In comparison to 4xLPS treated wildtype mice, the thyroid hormone signaling pathway, including an enhancer of hypoxia-inducible factor (HIF) 1- $\alpha$ , was enriched in microglial primed enhancers after 1xLPS treatment in wildtype mice. These pathways are central regulators of metabolism and activity of innate immune cells (Weichhart *et al.*, 2015). The HIF1- $\alpha$  signaling pathway was also enriched in microglial primed enhancers from 1xLPS versus 4xLPS treated APP mice, in line with the description of HIF1- $\alpha$  as a central regulator of macrophage function (Cramer *et al.*, 2003) and immune training in monocytes (Cheng *et al.*, 2014).

Most changes in microglial primed enhancer repertoire occurred after 4xLPS treatment both in wildtype and APP23 mice, confirming the proposed view of endotoxin tolerance as an alternative activation state of the immune system rather than complete silencing (Foster *et al.*, 2007; Shalova *et al.*, 2015). Primed enhancers from 4xLPS treated mice were enriched in pathways related to phagocytosis. Of note, the vast majority of primed enhancers established by 4xLPS did not gain H3K27ac, possibly due to the presence of additional repressive histone modifications. In support of this hypothesis, tolerance initiating LPS preconditioning of microglia revealed reduced deposition of activating histone marks and increased amounts of repressive histone marks on pro-inflammatory IL-1 $\beta$  gene promoter (Schaafsma *et al.*, 2015).

In line with the idea that primed enhancers gain H327ac only upon secondary stimulation, such as the deposition of A $\beta$  that in turn activates microglia, differential enhancer activation occurred predominantly in APP23 and to a lesser extent in wildtype mice after peripheral immune stimulation. Of note, our analysis revealed changes in microglial active enhancers in response to cerebral  $\beta$ -amyloidosis itself, including enhancer activation of mechanistic target of rapamycin (mTOR), whose dysregulation has been implicated in AD (Wang *et al.*, 2014). Furthermore, active enhancers were enriched in the thyroid hormone signaling pathway, including an active enhancer of HIF1- $\alpha$ , in APP23 animals.

In line with the description of HIF1- $\alpha$  as an essential mediator of training in monocytes (Cheng *et al.*, 2014) and reflecting the establishment of primed enhancers, HIF1- $\alpha$  signaling pathway was enriched after 1xLPS treatment in microglial active enhancers in APP23 mice. Both mTOR and HIF1- $\alpha$  regulate trained immunity by controlling the metabolic state of immune cells, leading to a shift towards aerobic glycolysis upon training of monocytes (Bekkering *et al.*, 2018; Cheng *et al.*, 2014). In contrast, microglial active enhancers of 4xLPS treated mice were enriched for Ras-related protein 1 (Rap1) signaling, a pathway involved in phagocytosis (Chung *et al.*, 2008), again reflecting the established primed enhancers. Microglial active enhancers of 1xLPS treated mice showed enrichment of many inflammatory pathways in comparison to 4xLPS, in line with a previous study on the epigenetic state of endotoxin tolerant macrophages (Foster *et al.*, 2007). In summary, our results imply that differential modulation of neuropathology is at least partly mediated by long-term changes in microglial function based on epigenetic reprogramming, in line with

previous reports on the epigenetic basis of innate immune memory (Saeed *et al.*, 2014).

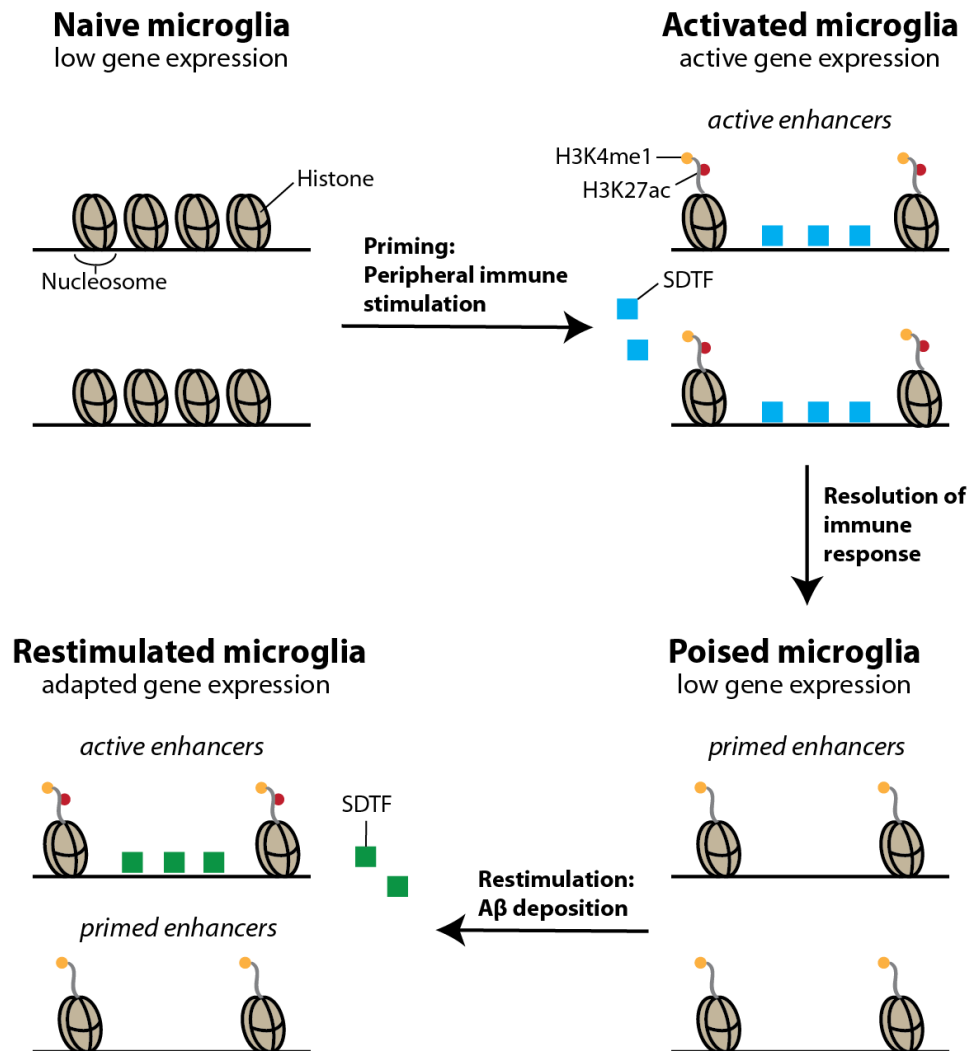


**Figure 2: Epigenetic basis of innate immune memory.** Peripheral immune stimulation activates SDTFs and leads to deposition of H3K27ac at a subset of enhancers, thereby opening chromatin structure and initiating gene transcription. After cessation of the immune stimulus, enhancers are turned off and lose H3K27ac; however, primed enhancers retain H3K4me1 as an epigenetic mark of their previous activity. A secondary immune stimulus, e.g. the deposition of A $\beta$ , activates a subset of primed H3K4me1-marked enhancers and thereby elicits an adapted immune reaction with altered gene expression in comparison to the naïve immune response. Based on Netea *et al.*, 2016.

Since enhancers are critical regulators of transcriptional activity (Heintzman *et al.*, 2009; Ivashkiv, 2013), epigenetic alterations in active enhancers should be reflected in gene expression levels. Indeed, there was a significant concordance between alterations in H3K27ac levels and the direction of change in the expression of the nearest gene in sorted microglia. Furthermore, weighted gene correlation network analysis (WGCNA) revealed striking similarities to epigenetic changes. WGCNA identified a module enriched for HIF1- $\alpha$  signaling, for which gene expression correlated strongly with microglia from 1xLPS treated APP23 mice, but not with microglia from 4xLPS treated APP23 mice. In addition, HIF1- $\alpha$  protein levels were increased in plaque-associated microglia and further upregulated in 1xLPS treated APP23 mice. Interestingly, other genes that have been genetically linked to AD risk appeared in the same module as HIF1- $\alpha$ , indicating that HIF1- $\alpha$  signaling may indeed represent a detrimental event in AD pathology.

Upon immune cell activation, cellular energy and biosynthesis pathways need to be repurposed to meet increased energy demands and provide necessary building blocks. Changes in the contribution of metabolic pathways to energy production and biosynthesis have been linked to immune cell polarization (Galván-Peña & O'Neill, 2014; O'Neill & Pearce, 2016; Pearce & Pearce, 2013) and innate immune memory (Arts *et al.*, 2016a; Bekkering *et al.*, 2018; Cheng *et al.*, 2014; Saeed *et al.*, 2014). In pro-inflammatory activated macrophages *in vitro*, mitochondria shift from adenosine triphosphate (ATP) production to reactive oxygen species (ROS) generation, enabling mitochondria to maintain a high membrane potential (Mills *et al.*, 2016). In turn, ROS stabilize and activate HIF1- $\alpha$ , promoting energy production by glycolysis, leading to increased lactate release, and altering inflammatory gene expression (Hamanaka *et al.*, 2016; Mills *et al.*, 2016). In  $\beta$ -glucan trained monocytes, a mTOR- and HIF1- $\alpha$ -dependent shift towards glycolysis occurred *in vitro* (Cheng *et al.*, 2014), resembling metabolic reprogramming described in LPS activated macrophages *in vitro* (Tannahill *et al.*, 2013).

In our study, WGCNA identified a module enriched in genes of the glycolytic pathway. Indeed, in line with increased HIF1- $\alpha$  activity, microglial gene expression in this module was increased in microglia from APP versus wildtype control mice and showed further upregulation in 1xLPS treated APP animals. Functional analysis of sorted microglia confirmed that microglia from 1xLPS treated mice possessed an

increased mitochondrial membrane potential, which correlated with microglial lactate release as readout of glycolytic activity. In summary, increased HIF1- $\alpha$  activity and a metabolic switch to glycolysis occurred in response to cerebral  $\beta$ -amyloidosis and was enhanced by immune training in microglia (Figure 3), confirming metabolic reprogramming in trained immunity *in vivo*.

In line with enhancer modification, WGCNA revealed increased expression of a module enriched in phagocytic and endocytic pathways and Rap1 signaling in microglia from 4xLPS treated mice. Indeed, tolerized microglia contained higher amounts of A $\beta$ , confirming epigenetic and gene expression data. This, together with the reduced plaque load in 4xLPS treated mice, suggests that microglia change to a beneficial phenotype associated with increased A $\beta$  phagocytosis after induction of tolerance (Figure 3).

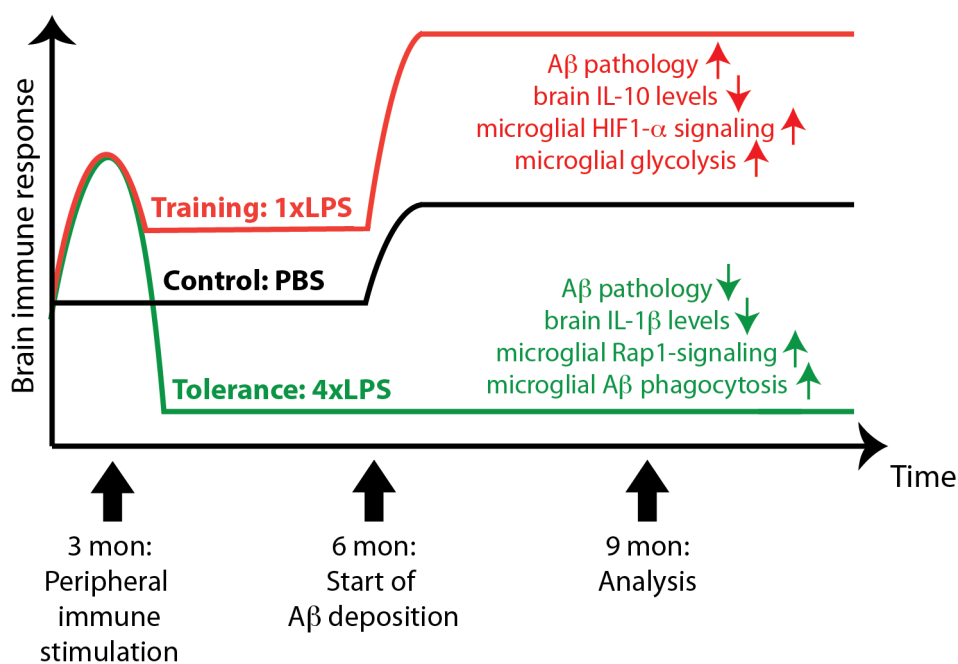


**Figure 3: Acute and long-lasting effects of peripheral immune stimulation in APP23 mice.** A single peripheral LPS injection at 3 months of age (1xLPS) induces immune training subsequently, while repeated peripheral LPS application (4xLPS) causes tolerance in the brain. In immune stimulated APP23 mice, A $\beta$  deposition starts at 6 months of age and acts as a secondary immune stimulus. At 9 months of age, differential modulation of A $\beta$  pathology and the brain's immune response is apparent after 1xLPS and 4xLPS stimulation. Immune memory effects are based on epigenetic reprogramming of microglia, thereby altering their gene expression profile and impacting on microglial function.

The described changes in global microglial enhancer and transcriptional landscape are likely driven by alterations in a subset of microglia, since differences in protein expression, e.g. for HIF1-  $\alpha$ , were mainly restricted to plaque-associated cells. Recently, heterogeneity of microglia was confirmed based on single-cell transcriptional profiling (Keren-Shaul *et al.*, 2017; Korin *et al.*, 2017; Mathys *et al.*, 2017). In addition, subtypes of microglia with pathology-specific distinct molecular signatures (termed disease-associated microglia and microglial neurodegenerative phenotype) have been described (Keren-Shaul *et al.*, 2017; Krasemann *et al.*, 2017). Our work indicates that training and tolerance are able to modulate disease-induced alterations of microglial gene expression and function in a differential fashion. In addition to modulation of cerebral  $\beta$ -amyloidosis after peripheral immune stimulation, 1xLPS and 4xLPS treatment also altered neuropathological features of stroke, indicating that modification of disease pathology after epigenetic microglial reprogramming in response to systemic inflammation is not specific to the context of cerebral  $\beta$ -amyloidosis. Since microglia play a role in virtually all neurological diseases investigated so far, microglial immune memory of previous inflammatory events could be an essential modifier of disease pathogenesis in many other circumstances. It remains to be determined, which stimuli (systemic or local) induce microglial epigenetic reprogramming and how long this persists under different conditions in the tissue environment.



### 2.5.3 Modulation of amyloid plaque structure and neuronal damage through long-term microglial changes after systemic inflammation

---

In reference to:

#### **Systemic inflammation induces long-term modulation of amyloid plaque morphology and neuronal damage in a mouse model of Alzheimer's disease**

Ann-Christin Wendeln, Angelos Skodras, Natalie Beschorner, Peter Nilsson, Mathias Jucker, Jonas Neher

---

Recently, a previously unappreciated role of microglia in amyloid plaque compaction has been described. Microglia strongly accumulate around A $\beta$  plaques and closely interact with them (Itagaki *et al.*, 1989), but how intimate the interaction between microglia and amyloid plaques is has only recently emerged. In AD, microglia are not merely passive bystanders around plaques but can actively clear them by phagocytosis, a process that increases after immunotherapy against A $\beta$  (D'Andrea *et al.*, 2004; Fu *et al.*, 2010; Lai & McLaurin, 2012). In addition, recent studies demonstrated that microglial processes form a tight barrier around amyloid plaques, thereby compacting the toxic A $\beta$  species and reducing their interaction with the brain environment (Condello *et al.*, 2015; Wang *et al.*, 2016; Yuan *et al.*, 2016). In mouse models of cerebral  $\beta$ -amyloidosis, neuronal damage occurs in the form of dystrophic neurites and axonal damage around A $\beta$  plaques (Calhoun *et al.*, 1998; Sturchler-Pierrat & Staufenbiel, 2000). By forming a barrier around amyloid deposits, microglia reduce amyloid-associated neuronal damage and protect surrounding cells by shielding toxic A $\beta$  species.

In AD, there is considerable heterogeneity in plaque structures, ranging from dense core and compact (Thioflavin S positive) to diffuse and filamentous amyloid deposits (D'Andrea *et al.*, 2004; Yuan *et al.*, 2016). Furthermore, microglial interaction with plaques differs, with dense plaques showing strong clustering of microglial processes and diffuse plaques having much less microglial coverage (Condello *et al.*, 2015; Itagaki *et al.*, 1989). Importantly, modulation of the microglial barrier function by genetic deletion of *CX3CR1* or *Trem2* or in response to anti-A $\beta$  immunization resulted in structurally altered amyloid plaques (Condello *et al.*, 2015; Wang *et al.*, 2016; Yuan *et al.*, 2016). In turn, plaque structure influenced the amount of associated

neuritic dystrophy, with recent studies demonstrating an association between reduced compaction of plaques and increased neuronal damage (Condello *et al.*, 2015; Wang *et al.*, 2016; Yuan *et al.*, 2016). These studies imply another previously unappreciated microglial function in the modulation of AD pathology.

As discussed in chapter 2.5.2, we provided evidence for long-lasting alterations in microglial function after systemic inflammation. These microglial changes occurring in response to single (1xLPS) or repeated (4xLPS) peripheral LPS stimulation were sufficient to differentially modulate A $\beta$  plaque load at an early stage of pathology in 9 months old APP23 mice. In this follow-up study, we characterized the long-term effects of systemic inflammation, induced by 1xLPS or 4xLPS treatment at young adult age, on the structure of amyloid deposits and associated neuronal damage. Using staining with luminescent conjugated oligothiophenes (LCOs) followed by spectral imaging, we showed that 1xLPS and 4xLPS treatment at 3 months of age both caused structural changes in much later formed amyloid plaques in APP23 animals.

LCOs are fluorescent dyes showing shifts in their emission spectrum upon binding to different amyloid structures (Aslund *et al.*, 2009; Klingstedt *et al.*, 2011). Costaining with two LCOs, quadro-formyl thiophene acetic acid (qFTAA) and hepta-formyl thiophene acetic acid (hFTAA), has previously been used to discriminate between different plaque structures in human AD cases and demonstrated intra- and inter-individual variability in plaque morphologies (Rasmussen *et al.*, 2017). While qFTAA resembles Thioflavin S in its binding affinity for mature A $\beta$  fibrils in the dense core of plaques, hFTAA stains both immature and mature fibrillar forms (Klingstedt *et al.*, 2011). The ratio of emission intensities at the respective maxima of qFTAA and hFTAA provides a useful readout for the spectral distinction of different amyloid plaque structures (Rasmussen *et al.*, 2017).

In this study, we analyzed 12 months old APP23 animals treated with 1xLPS or 4xLPS to induce training or tolerance in the brain, respectively, at 3 months of age. Peripheral stimulation with both 1xLPS and 4xLPS altered amyloid structure in comparison to control animals: Control animals showed a significantly higher proportion of dense core plaques (qFTAA- and hFTAA-positive), while diffuse amyloid deposits (qFTAA-negative) predominated in LPS treated animals. In line with previous studies (Condello *et al.*, 2015; Wang *et al.*, 2016; Yuan *et al.*, 2016), less compact plaques induced by 1xLPS and 4xLPS were associated with increased

neuronal damage. In fact, neuronal damage around single plaques was not only significantly influenced by plaque size but also by plaque structure (as measured by the core qFTAA/hFTAA binding ratio).

Despite the differences in plaque structure, total plaque load did not differ among treatment groups, indicating that the continuous strong overproduction of A $\beta$  in this mouse model overrides the effects of peripheral immune stimulation on A $\beta$  load with time. Strikingly, alterations of plaque-associated microglia were still present in LPS treated 12 months old APP23 mice, in line with the hypothesis that microglia may be mediating the observed changes in amyloid conformation.

We first analyzed microglial numbers and found no alterations in the overall number of microglia; however, the number of plaque-associated microglia was reduced in 4xLPS treated animals, possibly due to altered migration or turnover of tolerant microglia. No alterations in the amount of plaque-associated astrocytes were found after LPS stimulation in 12 months old APP23 mice. Since microglia can compact amyloid plaques (Condello *et al.*, 2015; Wang *et al.*, 2016; Yuan *et al.*, 2016), a reduction in the number of microglia and concomitantly the amount of microglial processes encompassing the plaque could result in impairment of the microglial barrier function and thereby alter amyloid plaque structure.

We have previously observed increased A $\beta$  phagocytosis in 4xLPS treated microglia at an earlier stage of pathology (see chapter 2.5.2). Since microglial phagocytosis could contribute to the restructuring of amyloid plaques, we assessed CD68 expression, which marks active phagolysosomes (Rabinowitz *et al.*, 1992). Microglial CD68 expression and colocalization with amyloid plaques was reduced in 1xLPS treated animals in comparison to controls, indicating a reduction in phagocytic activity of 1xLPS but not 4xLPS treated microglia.

Trem2 has previously been linked to microglial barrier function and structural compaction of amyloid plaques (Wang *et al.*, 2016; Yuan *et al.*, 2016). Analysis of Trem2 expression revealed, similar to CD68, a reduction in microglial expression and colocalization with amyloid plaques in 1xLPS treated animals. Furthermore, 1xLPS treated animals depicted an altered immune state in the brain with elevated pro-inflammatory cytokine levels (such as IL-6, IL-12, and IFN- $\gamma$ ). Together, these data demonstrate a shift in the phenotype of plaque-associated microglia after 1xLPS

treatment and indicate that alterations in the microglial phenotype can change amyloid plaque structure.

In summary, this study suggests that both number and phenotype of plaque-associated microglia influence amyloid structure. Modulation of amyloid plaque structure after 1xLPS and 4xLPS treatment occurred through different microglia-mediated mechanisms, demonstrating that the differential effects of training and tolerance persisted even longer than we had previously shown (Wendeln & Degenhardt *et al.*, 2018). Furthermore, this study highlights the complex interaction between the immune system and amyloid deposits and its influence on disease progression. While at early stages of pathology, induction of tolerance by peripheral 4xLPS stimulation reduced cerebral  $\beta$ -amyloidosis while training with 1xLPS increased A $\beta$  pathology, these effects on plaque load diminished at a later stage of pathology. Instead, exacerbated neuronal damage was evident around structurally altered amyloid plaques in both treatment groups. Similar to the stage-dependent effects of tolerance, such a biphasic influence on A $\beta$  pathology has previously been described for *Trem2* knockout mice (Jay *et al.*, 2015, 2017).

While at early stages of A $\beta$  pathology (before 10 months in APP23 animals), only immature A $\beta$  fibrils with a binding affinity for hFTAA are present, the amount of plaques with dense cores (qFTAA-positive) increases as A $\beta$  fibrils mature and amyloid plaques grow in size (Nyström *et al.*, 2013). Interestingly, binding of qFTAA reaches a plateau around 18 months of age and decreases afterwards, indicating that structural rearrangement takes place in amyloid plaques in aged animals. In line with this finding, microglial barrier function was impaired in aged mice, resulting in less compact plaques with more associated neuritic dystrophy (Condello *et al.*, 2015). Thus, similar to the diminishment of homeostatic and injury-induced microglial activity with age (Hefendehl *et al.*, 2014; Lynch *et al.*, 2010; Yu *et al.*, 2002), microglial coverage of amyloid plaques seems to be reduced in aged mice and might therefore account for the described differences in qFTAA binding over the course of aging.

In summary, this study confirms that systemic inflammation causes long-lasting alterations in microglial function that subsequently influence amyloid plaque structure. In 12 months old APP23 animals, both 1x and 4xLPS treatment (albeit through different mechanisms) caused impairments of microglial barrier function,

hence leading to altered amyloid plaque structures associated with increased neuronal damage. These results confirm the protective nature of the microglial barrier around amyloid plaques and demonstrate that this function can be permanently impaired by systemic inflammatory events occurring much earlier in life. Thereby, long-lasting alterations of the microglial barrier function represent another mechanism modulating neurological disease progression.

## 2.6 Concluding remarks and outlook

In this thesis, an in-depth analysis of microglial lifetime, immune memory, and its consequences for disease was presented. Knowledge of the microglial turnover is essential for the interpretation of innate immune memory effects, since the transmission of epigenetic modifications during cell division is still under investigation. Inheritance has been described for different epigenetic modifications; however, the mechanisms behind removal and persistence of certain chromatin marks remain elusive. While DNA methylation can be reestablished after DNA replication with high fidelity, it is less clear which histone modifications are inherited during cell division and how they are established (Probst *et al.*, 2009). Therefore, it remains unclear, whether chronologically younger cells are also biologically younger, or whether they retain the epigenetic marks and age-induced changes of their respective parent cell.

We investigated microglial lifetime and turnover under homeostatic conditions and in a mouse model with cerebral  $\beta$ -amyloidosis by imaging individual microglia. Our results demonstrated very limited turnover of the microglial population and assigned cortical microglia a lifetime of many months in mice. At any given age, animals will thus contain a heterogeneous mixture of microglia of varying individual ages. Bulk sequencing studies, especially of aged mice, will therefore profile microglia with variable ages and unclear inheritance of chromatin marks, highlighting the importance for future single-cell studies across different ages under homeostatic and disease conditions. Since about half of the microglial population persists for the entire lifespan of mice, age-related cellular senescence might contribute to the development of neurological diseases. Indeed, homeostatic functions of microglia decline in aged mice (Hefendehl *et al.*, 2014), thereby predisposing to disease onset. Even in a mouse model of cerebral  $\beta$ -amyloidosis, where microglial proliferation was increased, a considerable proportion of microglia persist for the entire lifespan of mice, indicating that microglial senescence could occur even under disease conditions with increased turnover.

Translation of our findings about the microglia lifetime to the human brain remains uncertain. However, other cell types such as neurons and oligodendrocytes have been shown to persist in the brain throughout the human lifespan (Frisén, 2016). Furthermore, a heterogeneous microglial population with senescent cells has also

been described in the aged human brain (Streit *et al.*, 2004; Streit *et al.*, 2009), indicating that microglia in humans might also be of varying ages, with some possibly persisting throughout the entire lifespan. Preliminary studies on two cancer patients suggest (based on IdU labeling and  $^{14}\text{C}$  measurements) that human microglia renew at a median rate of 28% per year (Réu *et al.*, 2017). Of note, human microglia appeared heterogeneous in their individual age, with some being more than two decades old (Réu *et al.*, 2017). Further studies in a higher number of subjects will provide additional evidence on the turnover rate and mechanisms of microglial maintenance in humans compared to mice.

Our data demonstrating a microglial lifetime of many months in mice render microglia suitable candidates for the study of innate immune memory, since they are susceptible to long-lasting alterations in their function after immune stimulation. Using repeated peripheral administration of LPS, we showed acute training and tolerance effects in the brain of mice, dependent on the number of LPS injections. In our study, tolerance was induced with repeated LPS injections subsequent to training; however, with this setup it remained unclear whether a massive immune reaction such as immune training is required for subsequent formation of tolerance. Dependency on mTOR- and HIF1- $\alpha$ -mediated induction of glycolysis has been shown for training in monocytes (Cheng *et al.*, 2014); however, whether this applies to microglia remains unknown. Microglia-specific deletion of mTOR or HIF1- $\alpha$  will specify their role in the induction of acute training and tolerance effects in this cell type. In addition, a metabolic switch from glycolysis towards fatty acid oxidation, which predominates in endotoxin tolerant cells, has been described for the transition from the early phase of an acute immune response to the later phase (T.F. Liu *et al.*, 2012). It remains to be determined whether metabolic reprogramming also accompanies the acute transition from training to tolerance.

Our study provided evidence that TNF- $\alpha$  and IL-10 also elicit immune memory effects in the brain after peripheral application. Interestingly, a low dose of TNF- $\alpha$  resulted in immune training, while a high dose caused tolerance. This suggests, in line with the induction of tolerance after repeated LPS exposure, that a repeated or high dose application of a pro-inflammatory stimulus is sufficient to induce immune tolerance, while a single or low dose stimulus preferentially gives rise to training. Future studies investigating several doses of the same stimulus will reveal details

about the dose-dependency of innate immune memory effects. Interestingly, application of the anti-inflammatory cytokine IL-10 also elicited immune tolerance, demonstrating that tolerance is not solely induced following a strong pro-inflammatory immune response. Future studies involving peripheral application of different pro- and anti-inflammatory cytokines will demonstrate which other cytokines induce training and tolerance in the brain, and whether they converge on similar signaling pathways. Importantly, any infection in the body results in release of a diverse array of cytokines, allowing for the possibility that innate immune memory in the brain could occur in response to a wide range of inflammatory events.

We demonstrated modulation of pathology in stroke and in cerebral  $\beta$ -amyloidosis months after induction of training and tolerance in the brain by peripheral immune stimulation. Changes in pathology were accompanied by differing immune states in the brain and altered epigenetic and transcriptional profiles of microglia. Similar to the previously described epigenetic basis of innate immune memory (Netea *et al.*, 2016), differential enhancer activation in microglia also required two stimuli. In our study, enhancers were activated by peripheral immune stimulation and stayed in a primed state until reactivated upon deposition of A $\beta$ . So far, it is unclear how long enhancers stay primed in response to an immune stimulus; therefore the maximal latency between the first and second stimulus to elicit differential enhancer activation in comparison to the naïve reaction remains to be determined. In addition, it is unclear whether newly generated microglia retain epigenetic marks of immune memory, potentially resulting in fading of memory of the priming stimulus over time. Long-term studies employing peripheral immune stimulation at young ages with subsequent analysis of aged mice will determine how long-lasting microglial immune memory is, and whether it also influences age-related physiological changes.

Priming of innate immune cells has been described to confer cross-protection against a range of pathogens (Moret & Siva-Jothy, 2003; Netea *et al.*, 2011; Pham *et al.*, 2007); however, the mechanisms and extent of this cross-protection remain unknown. At the present time, the nature of the secondary stimuli that elicit immune memory effects and the extent of their overlap in signaling pathways with the priming stimulus are unknown. In our study, immune memory of peripheral immune stimulation elicited differential effects on more than one disease process (chronic A $\beta$  deposition



and stroke), but it remains to be resolved which particular circumstances elicit immune memory effects.

Analysis of the microglial enhancer and transcriptional landscape in immune-stimulated mice with cerebral  $\beta$ -amyloidosis revealed differential expression of metabolic pathways, which have previously been implicated in innate immune memory (Bekkering *et al.*, 2018; Cheng *et al.*, 2014; Saeed *et al.*, 2014), after training and tolerance. Increased HIF1- $\alpha$  activity and a metabolic switch to glycolysis occurred in microglia in response to cerebral  $\beta$ -amyloidosis and were enhanced by immune training, in line with previous studies (Ip *et al.*, 2017; Mills *et al.*, 2016). However, the exact nature of the metabolic pathways involved in the response of tolerized microglia remains unknown. Metabolic rewiring upon immune cell activation is dependent on several factors such as stimulus and tissue environment, thereby creating unique metabolic signatures in different inflammatory conditions (Stienstra *et al.*, 2017). Whereas LPS stimulation of myeloid cells *in vitro* induced a switch from oxidative phosphorylation towards aerobic glycolysis (Palsson-McDermott & O'Neill, 2013; Rodriguez-Prados *et al.*, 2010; Stienstra *et al.*, 2017), stimulation with other TLR ligands promoted both glycolysis and oxidative phosphorylation in monocytes *in vitro* (Lachmandas *et al.*, 2016). While many pro-inflammatory stimuli enhanced the glycolytic rate of myeloid cells (Everts *et al.*, 2014; Mills *et al.*, 2016; Stienstra *et al.*, 2017), anti-inflammatory effects of IL-10 were shown to be mediated by downregulation of mTOR and a metabolic shift towards oxidative phosphorylation in macrophages (Ip *et al.*, 2017). In addition, a metabolic profile with predominating oxidative phosphorylation has been linked to phagocytic activity (Reiss & Roos, 1978), which was increased in tolerized microglia, implicating metabolic rewiring possibly also in other immune cell functions. While the acute hyperinflammatory phase in sepsis was associated with increased glycolytic rates in blood leukocytes (Haimovich *et al.*, 2010), mTOR signaling and glycolysis were downregulated in the subsequent immune tolerant state (Cheng *et al.*, 2016). Furthermore, a metabolically altered profile with predominating fatty acid oxidation has been described in endotoxin tolerant blood cells of septic patients (Liu *et al.*, 2012), implicating metabolic reprogramming in immune tolerance in peripheral cells. Further studies will reveal whether the metabolic profile of microglia is changed in

similar ways after induction of immune tolerance in the context of neurological disease.

Interestingly, macrophage function can be directly modulated by addition or depletion of metabolic factors that impact the balance between glycolysis and mitochondrial oxidative phosphorylation (Mills *et al.*, 2016; Mills & O'Neill, 2016). Importantly, a causal link between certain metabolites and epigenetic alterations in immune training and tolerance has been described *in vitro*. The Krebs cycle metabolite fumarate accumulated in  $\beta$ -glucan trained monocytes and inhibited a family of histone demethylases, thereby contributing to the maintenance of open chromatin in trained immunity (Arts *et al.*, 2016b). Strikingly, fumarate addition by itself induced epigenetic changes resembling immune training in monocytes. In addition, nicotinamide adenine dinucleotide (NAD)<sup>+</sup>-dependent activation of sirtuins, a family of histone deacetylases, altered histone acetylation and thereby inhibited gene transcription in endotoxin tolerant cells (Liu *et al.*, 2012). These studies highlight the close interplay between epigenetic, metabolic, and immune alterations in innate immune memory. Our data are in line with this concept and demonstrate changes in the epigenetic regulation of gene expression, metabolic state, and immune function of microglia after induction of immune training and tolerance.

Of note, other long-lived cell types in the brain could in theory also possess immune memory characteristics and contribute to the described differential modulation of brain pathology after training and tolerance. Perivascular and meningeal macrophages are, similar to microglia, long-lived cells (Goldmann *et al.*, 2016; Prinz *et al.*, 2017), and thus might also be capable of immune memory formation. Astrocytes, which contribute to immune reactions in the brain (DeWitt *et al.*, 1998; Liddelow *et al.*, 2017; Schubert *et al.*, 2000), have – similar to microglia – low turnover rates under homeostatic conditions and likely persist for a long time in the brain (Colodner *et al.*, 2005; Sofroniew & Vinters, 2010). Future studies will reveal whether these cell types form immune memory under certain circumstances as described here for microglia.

This work demonstrates diverse and long-lasting effects of peripheral immune stimulation on brain cytokine levels, microglial phagocytosis, and microglial barrier function. Microglial barrier function has recently been implicated in AD pathogenesis and has been assigned a beneficial role (Condello *et al.*, 2015; Yuan *et al.*, 2016). Our study corroborates the described neuroprotective role of the microglial barrier in

compacting amyloid plaques, thereby shielding surrounding cells from toxic A $\beta$  species. Previous studies showed that the amount of microglial immunoreactivity differed between plaque structures (Condello *et al.*, 2015). Whether alterations in microglial barrier are cause or consequence of differing plaque structures remains to be determined. While we show long-term alterations in microglial function following systemic inflammation, no alterations in A $\beta$  processing or onset of A $\beta$  deposition were evident, thereby implying alterations in microglial function as the cause of changes to amyloid plaque structure. Of note, structurally altered plaques might subsequently alter microglial function, rendering it difficult to determine microglial phenotype as purely cause or consequence of differences in amyloid plaque structure.

Our study demonstrates that the long-term effects of training and tolerance persisted even at advanced stages of neuropathology, since alterations in amyloid plaque structure occurred through different microglia-mediated mechanisms (i.e. reduced number of plaque-associated microglia or an altered microglial phenotype). However, while training was detrimental and tolerance beneficial in early stages of cerebral  $\beta$ -amyloidosis, both programs showed detrimental effects on amyloid-associated neurotoxicity at a later stage. Such stage-dependent effects of inflammation might contribute to the many controversial descriptions of either pro- or anti-inflammatory modulation of the immune system as beneficial for pathology in mouse models with cerebral  $\beta$ -amyloidosis (Chakrabarty *et al.*, 2015; Heneka *et al.*, 2013; Jay *et al.*, 2017; Masashi Kitazawa *et al.*, 2011; Shi *et al.*, 2011; Vom Berg *et al.*, 2012).

Whether microglial immune memory exists in humans and contributes to neurological disease remains to be determined. The enhancer and transcriptional landscape of human microglia have recently been assessed and showed similarities but also differences in several hundred genes, especially genes induced with aging, between human and mouse microglia (Galatro *et al.*, 2017; Gosselin *et al.*, 2017). Importantly, genetic and epigenetic studies have clearly implicated immunity as a central component of AD pathogenesis (Gagliano *et al.*, 2016; Gjoneska *et al.*, 2015; Guerreiro *et al.*, 2013; Hollingworth *et al.*, 2011; Huang *et al.*, 2017; Lambert *et al.*, 2013; Naj *et al.*, 2011; Sims *et al.*, 2017; Zhang *et al.*, 2013). If our study were transferable to humans, it would suggest that peripheral infections or any inflammatory event in the body might lead to long-lasting alterations in a diverse array of microglial functions, which in turn could influence disease onset and

pathology progression. Indeed, epidemiological studies suggest that inflammatory burden correlates positively with AD (Bu *et al.*, 2014), and conversely long-term use of NSAIDs lowers AD risk (Hoozemans *et al.*, 2011). Interestingly, a recent study linked increased systemic inflammatory markers in midlife to episodic memory loss and reduced brain volume, especially in AD associated regions, more than 20 years later (Walker *et al.*, 2017), in line with the idea that systemic inflammation might influence much later occurring neurodegenerative processes through long-term alterations in microglial functions.

Our work demonstrates effects of microglial immune memory on pathology in stroke and cerebral  $\beta$ -amyloidosis, indicating that modulation of neuropathology is not specific to one disease context. Therefore, microglial immune memory could be an essential modifier of disease pathogenesis in many other circumstances. Some evidence suggests that long-term immune memory also occurs in tissue macrophages in other organs, e.g. in lung alveolar macrophages (Chen *et al.*, 2014). Thus, innate immune memory of tissue macrophages might be a global mechanism for regulating immune activity with yet unresolved consequences for disease. Of note, molecules known to induce immune training in macrophages have clinically been used in cancer treatment (Kawai *et al.*, 2013; Liu *et al.*, 2015), indicating that innate immune memory can aid in fighting diseases with inflammatory components. This work demonstrates epigenetically encoded innate immune memory of peripheral inflammation in long-lived microglia and highlights its role as an essential modifier of neurological diseases. In the future, innate immune memory might emerge as a previously unappreciated modifier of many other inflammatory diseases, and applying this concept clinically might aid conventional disease therapies.

## 2.7 References

- Ajami, B., Bennett, J.L., Krieger, C., Tetzlaff, W. & Rossi, F.M. V. (2007). Local self-renewal can sustain CNS microglia maintenance and function throughout adult life. *Nature neuroscience* 10(12): 1538–1543.
- Akira, S., Uematsu, S. & Takeuchi, O. (2006). Pathogen recognition and innate immunity. *Cell* 124(4): 783-801.
- Akiyama, H., Barger, S., Barnum, S., Bradt, B., Bauer, J., Cole, G.M., ... Wyss-Coray, T. (2000). Inflammation and Alzheimer's disease. *Neurobiology of aging* 21(3): 383–421.
- Arts, R.J.W., Joosten, L.A.B. & Netea, M.G. (2016a). Immunometabolic circuits in trained immunity. *Seminars in Immunology* 28(5): 425–430.
- Arts, R.J.W., Moorlag, S.J.C.F.M., Novakovic, B., Li, Y., Wang, S.-Y., ... Netea, M.G. (2018). BCG vaccination protects against experimental viral infection in humans through the induction of cytokines associated with trained immunity. *Cell Host Microbe* 23(1): 89-100.
- Arts, R.J.W., Novakovic, B., Ter Horst, R., Carvalho, A., Bekkering, S., Lachmandas, E., ... Netea, M.G. (2016b). Glutaminolysis and Fumarate Accumulation Integrate Immunometabolic and Epigenetic Programs in Trained Immunity. *Cell metabolism* 24(6): 807–819.
- Ashe, K.H. & Zahs, K.R. (2010). Probing the Biology of Alzheimer's Disease in Mice. *Neuron* 66(5): 631–645.
- Askew, K., Li, K., Olmos-Alonso, A., Garcia-Moreno, F., Liang, Y., Richardson, P., ... Gomez-Nicola, D. (2017). Coupled Proliferation and Apoptosis Maintain the Rapid Turnover of Microglia in the Adult Brain. *Cell Reports* 18(2): 391–405.
- Aslund, A., Sigurdson, C.J., Klingstedt, T., Grathwohl, S., Bolmont, T., Dickstein, D.L., ... Nilsson, K.P.R. (2009). Novel pentameric thiophene derivatives for in vitro and in vivo optical imaging of a plethora of protein aggregates in cerebral amyloidoses. *ACS chemical biology* 4(8): 673–684.
- Banks, W.A. & Robinson, S.M. (2010). Minimal penetration of lipopolysaccharide across the murine blood-brain barrier. *Brain, behavior, and immunity* 24(1): 102–109.
- Bate, C., Veerhuis, R., Eikelenboom, P. & Williams, A. (2004). Microglia kill amyloid-beta1-42 damaged neurons by a CD14-dependent process. *Neuroreport* 15(9): 1427–1430.
- Bateman, R.J., Xiong, C., Benzinger, T.L.S., Fagan, A.M., Goate, A., Fox, N.C., ... Dominantly Inherited Alzheimer Network. (2012). Clinical and Biomarker Changes in Dominantly Inherited Alzheimer's Disease. *New England Journal of Medicine* 367(9): 795–804.
- Beeson, P.B. & Roberts, E. (1947). Tolerance to bacterial pyrogens : I. Factors influencing its development. *The Journal of Experimental Medicine* 86(1): 29–38.

- Bekkering, S., Arts, R.J.W., Novakovic, B., Kourtzelis, I., van der Heijden, C.D.C.C., Li, Y., ... Netea, M.G. (2018). Metabolic induction of trained immunity through the mevalonate pathway. *Cell* 172(1-2): 135-146.
- Bekris, L.M., Yu, C.-E., Bird, T.D. & Tsuang, D.W. (2010). Genetics of Alzheimer Disease. *Journal of Geriatric Psychiatry and Neurology* 23(4): 213–227.
- Biswas, S.K. & Lopez-Collazo, E. (2009). Endotoxin tolerance: new mechanisms, molecules and clinical significance. *Trends in Immunology* 30(10): 475–487.
- Block, M.L., Zecca, L. & Hong, J.-S. (2007). Microglia-mediated neurotoxicity: uncovering the molecular mechanisms. *Nature Reviews Neuroscience* 8: 57–69.
- Bornemann, K.D. & Staufenbiel, M. (2000). Transgenic mouse models of Alzheimer's disease. *Annals of the New York Academy of Sciences* 908: 260–6.
- Bruttger, J., Karram, K., Wörtge, S., Regen, T., Marini, F., Hoppmann, N., ... Waisman, A. (2015). Genetic Cell Ablation Reveals Clusters of Local Self-Renewing Microglia in the Mammalian Central Nervous System. *Immunity* 43(1): 92–107.
- Bu, X.-L., Yao, X.-Q., Jiao, S.-S., Zeng, F., Liu, Y.-H., Xiang, Y., ... Wang, Y.-J. (2014). A study on the association between infectious burden and Alzheimer's disease. *European Journal of Neurology* 22(12): 1519-25.
- Butovsky, O., Talpalar, A.E., Ben-Yaakov, K. & Schwartz, M. (2005). Activation of microglia by aggregated beta-amyloid or lipopolysaccharide impairs MHC-II expression and renders them cytotoxic whereas IFN-gamma and IL-4 render them protective. *Molecular and Cellular Neurosciences* 29(3): 381–393.
- Calhoun, M.E., Wiederhold, K.-H., Abramowski, D., Phinney, A.L., Probst, A., Sturchler-Pierrat, C., ... Jucker, M. (1998). Neuron loss in APP transgenic mice. *Nature* 395(6704): 755–756.
- Cattaneo, A., Cattane, N., Galluzzi, S., Provasi, S., Lopizzo, N., Festari, C., ... INDIA-FBP Group. (2017). Association of brain amyloidosis with pro-inflammatory gut bacterial taxa and peripheral inflammation markers in cognitively impaired elderly. *Neurobiology of Aging* 49: 60–68.
- Chakrabarty, P., Li, A., Ceballos-Diaz, C., Eddy, J.A., Funk, C.C., Moore, B., ... Golde, T.E. (2015). IL-10 alters immunoproteostasis in APP mice, increasing plaque burden and worsening cognitive behavior. *Neuron* 85(3): 519–33.
- Chen, F., Wu, W., Millman, A., Craft, J.F., Chen, E., Patel, N., ... Gause, W.C. (2014). Neutrophils prime a long-lived effector macrophage phenotype that mediates accelerated helminth expulsion. *Nature Immunology* 15(10): 938–46.
- Cheng, S.-C., Quintin, J., Cramer, R.A., Shepardson, K.M., Saeed, S., Kumar, V., ... Netea, M.G. (2014). mTOR- and HIF-1 -mediated aerobic glycolysis as metabolic basis for trained immunity. *Science* 345(6204): 1250684.
- Cheng, S.-C., Scicluna, B.P., Arts, R.J.W., Gresnigt, M.S., Lachmandas, E., Giamarellos-Bourboulis, E.J., ... Netea, M.G. (2016). Broad defects in the energy metabolism of leukocytes underlie immunoparalysis in sepsis. *Nature*

- Immunology* 17(4): 406–413.
- Christ, A., Günther, P., Lauterbach, M., Pelka, K., Scholz, C., Duewell, P., ... Latz, E. (2018). Western diet triggers NLRP3-dependent innate immune reprogramming. *Cell* 172(1-2): 162-175.
- Chung, J., Serezani, C.H., Huang, S.K., Stern, J.N.H., Keskin, D.B., Jagirdar, R., ... Peters-Golden, M. (2008). Rap1 activation is required for Fc gamma receptor-dependent phagocytosis. *Journal of Immunology* 181(8): 5501–9.
- Colodner, K.J., Montana, R.A., Anthony, D.C., Folkerth, R.D., De Girolami, U. & Feany, M.B. (2005). Proliferative potential of human astrocytes. *Journal of Neuropathology and Experimental Neurology* 64(2): 163–9.
- Condello, C., Yuan, P., Schain, A. & Grutzendler, J. (2015). Microglia constitute a barrier that prevents neurotoxic protofibrillar A $\beta$ 42 hotspots around plaques. *Nature Communications* 6: 6176.
- Cramer, T., Yamanishi, Y., Clausen, B.E., Förster, I., Pawlinski, R., Mackman, N., ... Johnson, R.S. (2003). HIF-1 $\alpha$  is essential for myeloid cell-mediated inflammation. *Cell* 112(5): 645–57.
- Crook, R., Ellis, R., Shanks, M., Thal, L.J., Perez-Tur, J., Baker, M., ... Galasko, D. (1997). Early-onset Alzheimer's disease with a presenilin-1 mutation at the site corresponding to the volga German presenilin-2 mutation. *Annals of Neurology* 42(1): 124–128.
- Cunningham, C. (2013). Microglia and neurodegeneration: the role of systemic inflammation. *Glia* 61(1): 71–90.
- Cunningham, C., Champion, S., Lunnon, K., Murray, C.L., Woods, J.F.C., Deacon, R.M.J., ... Perry, V.H. (2009). Systemic inflammation induces acute behavioral and cognitive changes and accelerates neurodegenerative disease. *Biological Psychiatry* 65(4): 304–312.
- D'Andrea, M.R., Cole, G.M. & Ard, M.D. (2004). The microglial phagocytic role with specific plaque types in the Alzheimer disease brain. *Neurobiology of Aging* 25(5): 675-83.
- Dartigues, J.F. (2009). Alzheimer's disease: a global challenge for the 21st century. *The Lancet Neurology* 8(12): 1082–1083.
- Davalos, D., Grutzendler, J., Yang, G., Kim, J. V, Zuo, Y., Jung, S., ... Gan, W.-B. (2005). ATP mediates rapid microglial response to local brain injury in vivo. *Nature Neuroscience* 8(6): 752–758.
- De Jager, P.L., Srivastava, G., Lunnon, K., Burgess, J., Schalkwyk, L.C., Yu, L., ... Bennett, D.A. (2014). Alzheimer's disease: early alterations in brain DNA methylation at ANK1, BIN1, RHBDF2 and other loci. *Nature Neuroscience* 17(9): 1156–1163.
- del Fresno, C., García-Río, F., Gómez-Piña, V., Soares-Schanoski, A., Fernández-Ruiz, I., Jurado, T., ... López-Collazo, E. (2009). Potent Phagocytic Activity with Impaired Antigen Presentation Identifying Lipopolysaccharide-Tolerant

- Human Monocytes: Demonstration in Isolated Monocytes from Cystic Fibrosis Patients. *The Journal of Immunology* 182(10): 6494-507.
- Dempsey, P.W., Vaidya, S.A. & Cheng, G. (2003). The Art of War: Innate and adaptive immune responses. *Cellular and Molecular Life Sciences* 60(12): 2604–2621.
- Deng, H., Maitra, U., Morris, M. & Li, L. (2013). Molecular mechanism responsible for the priming of macrophage activation. *The Journal of Biological Chemistry* 288(6): 3897–3906.
- DeWitt, D.A., Perry, G., Cohen, M., Doller, C. & Silver, J. (1998). Astrocytes regulate microglial phagocytosis of senile plaque cores of Alzheimer’s disease. *Experimental Neurology* 149(2): 329–340.
- Dunn, N., Mullee, M., Perry, V.H. & Holmes, C. (2005). Association between dementia and infectious disease: evidence from a case-control study. *Alzheimer disease and associated disorders* 19(2): 91–94.
- Duque, A. & Rakic, P. (2011). Different effects of bromodeoxyuridine and [3H]thymidine incorporation into DNA on cell proliferation, position, and fate. *The Journal of Neuroscience* 31(42): 15205–17.
- Edison, P., Archer, H.A., Gerhard, A., Hinz, R., Pavese, N., Turkheimer, F.E., ... Brooks, D.J. (2008). Microglia, amyloid, and cognition in Alzheimer’s disease: An [11C](R)PK11195-PET and [11C]PIB-PET study. *Neurobiology of Disease* 32(3): 412–419.
- Elmore, M.R.P., Najafi, A.R., Koike, M.A., Dagher, N.N., Spangenberg, E.E., Rice, R.A., ... Green, K.N. (2014). Colony-stimulating factor 1 receptor signaling is necessary for microglia viability, unmasking a microglia progenitor cell in the adult brain. *Neuron* 82(2): 380–397.
- Everts, B., Amiel, E., Huang, S.C.-C., Smith, A.M., Chang, C.-H., Lam, W.Y., ... Pearce, E.J. (2014). TLR-driven early glycolytic reprogramming via the kinases TBK1-IKK $\epsilon$  supports the anabolic demands of dendritic cell activation. *Nature Immunology* 15(4): 323–332.
- Floden, A.M. & Combs, C.K. (2006). Beta-amyloid stimulates murine postnatal and adult microglia cultures in a unique manner. *The Journal of Neuroscience* 26(17): 4644–4648.
- Foster, S.L., Hargreaves, D.C. & Medzhitov, R. (2007). Gene-specific control of inflammation by TLR-induced chromatin modifications. *Nature* 447(7147): 972–978.
- Frisén, J. (2016). Neurogenesis and Gliogenesis in Nervous System Plasticity and Repair. *Annual Review of Cell and Developmental Biology* 32(1): 127–141.
- Fu, H.J., Liu, B., Frost, J.L. & Lemere, C.A. (2010). Amyloid-beta immunotherapy for Alzheimer’s disease. *CNS & neurological disorders drug targets* 9(2): 197–206.
- Gagliano, S.A., Pouget, J.G., Hardy, J., Knight, J., Barnes, M.R., Ryten, M. & Weale,



- M.E. (2016). Genomics implicates adaptive and innate immunity in Alzheimer's and Parkinson's diseases. *Annals of Clinical and Translational Neurology* 3(12): 924–933.
- Galatro, T.F., Holtman, I.R., Lerario, A.M., Vainchtein, I.D., Brouwer, N., Sola, P.R., ... Eggen, B.J.L. (2017). Transcriptomic analysis of purified human cortical microglia reveals age-associated changes. *Nature Neuroscience* 20(8): 1162–1171.
- Galván-Peña, S. & O'Neill, L.A.J. (2014). Metabolic reprogramming in macrophage polarization. *Frontiers in Immunology* 5: 420.
- Gautier, E.L., Shay, T., Miller, J., Greter, M., Jakubzick, C., Ivanov, S., ... Immunological Genome Consortium. (2012). Gene-expression profiles and transcriptional regulatory pathways that underlie the identity and diversity of mouse tissue macrophages. *Nature Immunology* 13(11): 1118–1128.
- Ginhoux, F., Greter, M., Leboeuf, M., Nandi, S., See, P., Gokhan, S., ... Merad, M. (2010). Fate mapping analysis reveals that adult microglia derive from primitive macrophages. *Science* 330(6005): 841–845.
- Gjoneska, E., Pfenning, A.R., Mathys, H., Quon, G., Kundaje, A., Tsai, L.-H. & Kellis, M. (2015). Conserved epigenomic signals in mice and humans reveal immune basis of Alzheimer's disease. *Nature* 518(7539): 365–369.
- Glass, C.K. & Natoli, G. (2015). Molecular control of activation and priming in macrophages. *Nature Immunology* 17(1): 26–33.
- Glenner, G.G. & Wong, C.W. (1984). Alzheimer's disease: initial report of the purification and characterization of a novel cerebrovascular amyloid protein. *Biochemical and biophysical research communications* 120(3): 885–890.
- Goate, A., Chartier-Harlin, M.-C., Mullan, M., Brown, J., Crawford, F., Fidani, L., ... Hardy, J. (1991). Segregation of a missense mutation in the amyloid precursor protein gene with familial Alzheimer's disease. *Nature* 349(6311): 704–706.
- Goldmann, T., Wieghofer, P., Jordão, M.J.C., Prutek, F., Hagemeyer, N., Frenzel, K., ... Prinz, M. (2016). Origin, fate and dynamics of macrophages at central nervous system interfaces. *Nature Immunology* 17(7): 797–805.
- Gomez-Nicola, D., Fransen, N.L., Suzzi, S. & Perry, V.H. (2013). Regulation of Microglial Proliferation during Chronic Neurodegeneration. *Journal of Neuroscience* 33(6): 2481–2493.
- Gomez-Nicola, D. & Perry, V.H. (2015). Microglial Dynamics and Role in the Healthy and Diseased Brain. *The Neuroscientist* 21(2): 169–184.
- Gosselin, D., Link, V.M., Romanoski, C.E., Fonseca, G.J., Eichenfield, D.Z., Spann, N.J., ... Glass, C.K. (2014). Environment Drives Selection and Function of Enhancers Controlling Tissue-Specific Macrophage Identities. *Cell* 159(6): 1327–1340.
- Gosselin, D., Skola, D., Coufal, N.G., Holtman, I.R., Schlachetzki, J.C.M., Sajti, E., ... Glass, C.K. (2017). An environment-dependent transcriptional network

- specifies human microglia identity. *Science* 356(6344).
- Grabert, K., Michoel, T., Karavolos, M.H., Clohisey, S., Baillie, J.K., Stevens, M.P., ... McColl, B.W. (2016). Microglial brain region-dependent diversity and selective regional sensitivities to aging. *Nature Neuroscience* 19(3): 504-16.
- Graeber, M.B. (2010). Changing Face of Microglia. *Science* 330(6005): 783–788.
- Grammas, P. & Ovase, R. Inflammatory factors are elevated in brain microvessels in Alzheimer's disease. *Neurobiology of Aging* 22(6): 837–842.
- Grundke-Iqbal, I., Iqbal, K., Tung, Y.C., Quinlan, M., Wisniewski, H.M. & Binder, L.I. (1986). Abnormal phosphorylation of the microtubule-associated protein tau (tau) in Alzheimer cytoskeletal pathology. *Proceedings of the National Academy of Sciences of the United States of America* 83(13): 4913–4917.
- Guerreiro, R., Wojtas, A., Bras, J., Carrasquillo, M., Rogaeva, E., Majounie, E., ... Hardy, J. (2013). *TREM2* Variants in Alzheimer's Disease. *New England Journal of Medicine* 368(2): 117–127.
- Guo, J.-T., Yu, J., Grass, D., de Beer, F.C. & Kindy, M.S. (2002). Inflammation-dependent cerebral deposition of serum amyloid a protein in a mouse model of amyloidosis. *The Journal of Neuroscience* 22(14): 5900–5909.
- Haass, C., Kaether, C., Thinakaran, G. & Sisodia, S. (2012). Trafficking and Proteolytic Processing of APP. *Cold Spring Harbor Perspectives in Medicine* 2(5).
- Haass, C., Schlossmacher, M.G., Hung, A.Y., Vigo-Pelfrey, C., Mellon, A., Ostaszewski, B.L., ... Selkoe, D.J. (1992). Amyloid- $\beta$  peptide is produced by cultured cells during normal metabolism. *Nature* 359(6393): 322–325.
- Haass, C. & Selkoe, D.J. (1993). Cellular processing of beta-amyloid precursor protein and the genesis of amyloid beta-peptide. *Cell* 75(6): 1039–42.
- Haimovich, B., Reddell, M.T., Calvano, J.E., Calvano, S.E., Macor, M.A., Coyle, S.M. & Lowry, S.F. (2010). A novel model of common Toll-like receptor 4- and injury-induced transcriptional themes in human leukocytes. *Critical care* 14(5): R177.
- Haley, M.J., Brough, D., Quintin, J., Allan, S.M. (2017). Microglial priming as trained immunity in the brain. *Neuroscience*. S0306-4522(17)30929-6
- Hamanaka, R.B., Weinberg, S.E., Reczek, C.R. & Chandel, N.S. (2016). The Mitochondrial Respiratory Chain Is Required for Organismal Adaptation to Hypoxia. *Cell Reports* 15(3): 451–459.
- Hamon, M.A. & Quintin, J. (2016). Innate immune memory in mammals. *Seminars in Immunology* 28(4): 351–358.
- Hanisch, U.-K. (2002). Microglia as a source and target of cytokines. *Glia* 40(2): 140–155.
- Hanisch, U.-K. & Kettenmann, H. (2007). Microglia: active sensor and versatile effector cells in the normal and pathologic brain. *Nature Neuroscience* 10(11): 1387–1394.

- Hardy, J. & Selkoe, D.J. (2002). The amyloid hypothesis of Alzheimer's disease: progress and problems on the road to therapeutics. *Science* 297(5580): 353–356.
- Harper, J.D. & Lansbury, P.T. (1997). Models of amyloid seeing in Alzheimer's disease and scrapie: Mechanistic Truths and Physiological Consequences of the Time-Dependent Solubility of Amyloid Proteins. *Annual Review of Biochemistry* 66(1): 385–407.
- Hashimoto, D., Chow, A., Noizat, C., Teo, P., Beasley, M., Leboeuf, M., ... Merad, M. (2013). Tissue-Resident Macrophages Self-Maintain Locally throughout Adult Life with Minimal Contribution from Circulating Monocytes. *Immunity* 38(4): 792–804.
- Hefendehl, J.K., Neher, J.J., Sühs, R.B., Kohsaka, S., Skodras, A. & Jucker, M. (2014). Homeostatic and injury-induced microglia behavior in the aging brain. *Aging cell* 13(1): 60–69.
- Heintzman, N.D., Hon, G.C., Hawkins, R.D., Kheradpour, P., Stark, A., Harp, L.F., ... Ren, B. (2009). Histone modifications at human enhancers reflect global cell-type-specific gene expression. *Nature* 459(7243): 108–112.
- Heinz, S., Romanoski, C.E., Benner, C. & Glass, C.K. (2015). The selection and function of cell type-specific enhancers. *Nature Reviews Molecular Cell Biology* 16(3): 144–154.
- Hellström-Lindahl, E., Viitanen, M. & Marutle, A. (2009). Comparison of A $\beta$  levels in the brain of familial and sporadic Alzheimer's disease. *Neurochemistry International* 55(4): 243–252.
- Heneka, M.T., Golenbock, D.T. & Latz, E. (2015). Innate immunity in Alzheimer's disease. *Nature Immunology* 16(3): 229–236.
- Heneka, M.T., Kummer, M.P. & Latz, E. (2014). Innate immune activation in neurodegenerative disease. *Nature Reviews Immunology* 14(7): 463–477.
- Heneka, M.T., Kummer, M.P., Stutz, A., Delekate, A., Schwartz, S., Vieira-Saecker, A., ... Golenbock, D.T. (2013). NLRP3 is activated in Alzheimer's disease and contributes to pathology in APP/PS1 mice. *Nature* 493(7434): 674–678.
- Heneka, M.T. & O'Banion, M.K. (2007). Inflammatory processes in Alzheimer's disease. *Journal of Neuroimmunology* 184(1–2): 69–91.
- Henricson, B.E., Manthey, C.L., Perera, P.Y., Hamilton, T.A. & Vogel, S.N. (1993). Dissociation of lipopolysaccharide (LPS)-inducible gene expression in murine macrophages pretreated with smooth LPS versus monophosphoryl lipid A. *Infection and Immunity* 61(6): 2325–33.
- Hirohashi, N. & Morrison, D.C. (1996). Low-dose lipopolysaccharide (LPS) pretreatment of mouse macrophages modulates LPS-dependent interleukin-6 production in vitro. *Infection and Immunity* 64(3): 1011–5.
- Hoeffel, G., Chen, J., Lavin, Y., Low, D., Almeida, F.F., See, P., ... Ginhoux, F. (2015). C-myb(+) erythro-myeloid progenitor-derived fetal monocytes give rise to adult tissue-resident macrophages. *Immunity* 42(4): 665–678.

- Hollingworth, P., Harold, D., Sims, R., Gerrish, A., Lambert, J.-C., Carrasquillo, M.M., ... Williams, J. (2011). Common variants at ABCA7, MS4A6A/MS4A4E, EPHA1, CD33 and CD2AP are associated with Alzheimer's disease. *Nature Genetics* 43(5): 429–435.
- Holmes, C., Cunningham, C., Zotova, E., Woolford, J., Dean, C., Kerr, S., ... Perry, V.H. (2009). Systemic inflammation and disease progression in Alzheimer disease. *Neurology* 73(10): 768–774.
- Holtzman, D.M., Morris, J.C. & Goate, A.M. (2011). Alzheimer's Disease: The Challenge of the Second Century. *Science Translational Medicine* 3(77).
- Hoozemans, J.J.M., Veerhuis, R., Rozemuller, J.M. & Eikelenboom, P. (2011). Soothing the inflamed brain: effect of non-steroidal anti-inflammatory drugs on Alzheimer's disease pathology. *CNS & neurological disorders drug targets* 10(1): 57–67.
- Howlett, D.R. & Richardson, J.C. (2009). The pathology of APP transgenic mice: a model of Alzheimer's disease or simply overexpression of APP? *Histology and histopathology* 24(1): 83–100.
- Huang, K.-L., Marcora, E., Pimenova, A.A., Di Narzo, A.F., Kapoor, M., Jin, S.C., ... Goate, A.M. (2017). A common haplotype lowers PU.1 expression in myeloid cells and delays onset of Alzheimer's disease. *Nature Neuroscience* 20(8): 1052–1061.
- Ip, W.K.E., Hoshi, N., Shouval, D.S., Snapper, S. & Medzhitov, R. (2017). Anti-inflammatory effect of IL-10 mediated by metabolic reprogramming of macrophages. *Science* 356(6337): 513–519.
- Itagaki, S., McGeer, P.L., Akiyama, H., Zhu, S. & Selkoe, D. (1989). Relationship of microglia and astrocytes to amyloid deposits of Alzheimer disease. *Journal of Neuroimmunology* 24(3): 173–182.
- Ivashkiv, L.B. (2013). Epigenetic regulation of macrophage polarization and function. *Trends in Immunology* 34(5): 216–223.
- Iwasaki, A. & Medzhitov, R. (2015). Control of adaptive immunity by the innate immune system. *Nature Immunology* 16(4): 343–353.
- Jack, C.R., Knopman, D.S., Jagust, W.J., Shaw, L.M., Aisen, P.S., Weiner, M.W., ... Trojanowski, J.Q. (2010). Hypothetical model of dynamic biomarkers of the Alzheimer's pathological cascade. *The Lancet Neurology* 9(1): 119–128.
- Jarrett, J.T. & Lansbury, P.T. (1993). Seeding "one-dimensional crystallization" of amyloid: a pathogenic mechanism in Alzheimer's disease and scrapie? *Cell* 73(6): 1055–8.
- Jay, T.R., Hirsch, A.M., Broihier, M.L., Miller, C.M., Neilson, L.E., Ransohoff, R.M., ... Landreth, G.E. (2017). Disease Progression-Dependent Effects of TREM2 Deficiency in a Mouse Model of Alzheimer's Disease. *The Journal of Neuroscience* 37(3): 637–647.
- Jay, T.R., Miller, C.M., Cheng, P.J., Graham, L.C., Bemiller, S., Broihier, M.L., ...

- Lamb, B.T. (2015). TREM2 deficiency eliminates TREM2+ inflammatory macrophages and ameliorates pathology in Alzheimer's disease mouse models. *Journal of Experimental Medicine* 212(3): 287-95.
- Jenuwein, T. & Allis, C.D. (2001). Translating the Histone Code. *Science* 293(5532): 1074–1080.
- Jucker, M. (2010). The benefits and limitations of animal models for translational research in neurodegenerative diseases. *Nature Medicine* 16(11): 1210–1214.
- Jucker, M. & Walker, L.C. (2013). Self-propagation of pathogenic protein aggregates in neurodegenerative diseases. *Nature* 501(7465): 45–51.
- Kaufmann, E., Sanz, J., Dunn, J.L., Khan, N., Mendonca, L.E., Pacis, A., ... Divangahi, M. (2018). BCG educates hematopoietic stem cells to generate protective innate immunity against tuberculosis. *Cell* 172(1-2): 176-190.
- Kawai, K., Miyazaki, J., Joraku, A., Nishiyama, H. & Akaza, H. (2013). Bacillus Calmette-Guerin (BCG) immunotherapy for bladder cancer: Current understanding and perspectives on engineered BCG vaccine. *Cancer Science* 104(1): 22–27.
- Keren-Shaul, H., Spinrad, A., Weiner, A., Matcovitch-Natan, O., Dvir-Szternfeld, R., Ulland, T.K., ... Amit, I. (2017). A Unique Microglia Type Associated with Restricting Development of Alzheimer's Disease. *Cell* 169(7): 1276-1290.
- Kettenmann, H., Hanisch, U.-K., Noda, M. & Verkhratsky, A. (2011). Physiology of microglia. *Physiological reviews* 91: 461–553.
- Kierdorf, K., Erny, D., Goldmann, T., Sander, V., Schulz, C., Perdiguero, E.G., ... Prinz, M. (2013). Microglia emerge from erythromyeloid precursors via Pu.1- and Irf8-dependent pathways. *Nature Neuroscience* 16(3): 273–280.
- Kitazawa, M. (2005). Lipopolysaccharide-Induced Inflammation Exacerbates Tau Pathology by a Cyclin-Dependent Kinase 5-Mediated Pathway in a Transgenic Model of Alzheimer's Disease. *Journal of Neuroscience* 25(39): 8843–8853.
- Kitazawa, M., Cheng, D., Tsukamoto, M.R., Koike, M.A., Wes, P.D., Vasilevko, V., ... LaFerla, F.M. (2011). Blocking IL-1 signaling rescues cognition, attenuates tau pathology, and restores neuronal  $\beta$ -catenin pathway function in an Alzheimer's disease model. *Journal of Immunology* 187(12): 6539–49.
- Kleinnijenhuis, J., Quintin, J., Preijers, F., Joosten, L.A.B., Ifrim, D.C., Saeed, S., ... Netea, M.G. (2012). Bacille Calmette-Guerin induces NOD2-dependent nonspecific protection from reinfection via epigenetic reprogramming of monocytes. *Proceedings of the National Academy of Sciences of the United States of America* 109(43): 17537–42.
- Klingstedt, T., Aslund, A., Simon, R.A., Johansson, L.B.G., Mason, J.J., Nyström, S., ... Nilsson, K.P.R. (2011). Synthesis of a library of oligothiophenes and their utilization as fluorescent ligands for spectral assignment of protein aggregates. *Organic & biomolecular chemistry* 9(24): 8356–8370.
- Korin, B., Ben-Shaan, T.L., Schiller, M., Dubovik, T., Azulay-Debby, H., Boshnak,

- N.T., ... Rolls, A. (2017). High-dimensional, single-cell characterization of the brain's immune compartment. *Nature Neuroscience* 20(9): 1300-1309.
- Kosik, K.S., Joachim, C.L. & Selkoe, D.J. (1986). Microtubule-associated protein tau (tau) is a major antigenic component of paired helical filaments in Alzheimer disease. *Proceedings of the National Academy of Sciences of the United States of America* 83(11): 4044–8.
- Krasemann, S., Madore, C., Cialic, R., Baufeld, C., Calcagno, N., El Fatimy, R., ... Butovsky, O. (2017). The TREM2-APOE Pathway Drives the Transcriptional Phenotype of Dysfunctional Microglia in Neurodegenerative Diseases. *Immunity* 47(3): 566–581.
- Krstic, D., Madhusudan, A., Doehner, J., Vogel, P., Notter, T., Imhof, C., ... Knuesel, I. (2012). Systemic immune challenges trigger and drive Alzheimer-like neuropathology in mice. *Journal of Neuroinflammation* 9(1).
- Kurt, M.A., Davies, D.C., Kidd, M., Duff, K. & Howlett, D.R. (2003). Hyperphosphorylated tau and paired helical filament-like structures in the brains of mice carrying mutant amyloid precursor protein and mutant presenilin-1 transgenes. *Neurobiology of disease* 14(1): 89–97.
- Lachmandas, E., Boutens, L., Ratter, J.M., Hijmans, A., Hooiveld, G.J., Joosten, L.A.B., ... Stienstra, R. (2016). Microbial stimulation of different Toll-like receptor signalling pathways induces diverse metabolic programmes in human monocytes. *Nature Microbiology* 2: 16246.
- Lai, A.Y. & McLaurin, J. (2012). Clearance of amyloid- $\beta$  peptides by microglia and macrophages: the issue of what, when and where. *Future Neurology* 7(2): 165–176.
- Lambert, J.C., Ibrahim-Verbaas, C.A., Harold, D., Naj, A.C., Sims, R., Bellenguez, C., ... Amouyel, P. (2013). Meta-analysis of 74,046 individuals identifies 11 new susceptibility loci for Alzheimer's disease. *Nature Genetics* 45(12): 1452–1458.
- Lavin, Y., Winter, D., Blecher-Gonen, R., David, E., Keren-Shaul, H., Merad, M., ... Amit, I. (2014). Tissue-Resident Macrophage Enhancer Landscapes Are Shaped by the Local Microenvironment. *Cell* 159(6): 1312–1326.
- Lawson, L.J., Perry, V.H., Dri, P. & Gordon, S. (1990). Heterogeneity in the distribution and morphology of microglia in the normal adult mouse brain. *Neuroscience* 39(1): 151–170.
- Lawson, L.J., Perry, V.H. & Gordon, S. (1992). Turnover of resident microglia in the normal adult mouse brain. *Neuroscience* 48(2): 405–415.
- Lee, Y.B., Nagai, A. & Kim, S.U. (2002). Cytokines, chemokines, and cytokine receptors in human microglia. *Journal of Neuroscience Research* 69(1): 94–103.
- Li, Y., Liu, L., Barger, S.W. & Griffin, W.S.T. (2003). Interleukin-1 mediates pathological effects of microglia on tau phosphorylation and on synaptophysin synthesis in cortical neurons through a p38-MAPK pathway. *The Journal of Neuroscience* 23(5): 1605–1611.

- Liddel, S.A., Guttenplan, K.A., Clarke, L.E., Bennett, F.C., Bohlen, C.J., Schirmer, L., ... Barres, B.A. (2017). Neurotoxic reactive astrocytes are induced by activated microglia. *Nature* 541(7638): 481-487.
- Lindberg, C., Selenica, M.-L.B., Westlind-Danielsson, A. & Schultzberg, M. (2005). Beta-amyloid protein structure determines the nature of cytokine release from rat microglia. *Journal of Molecular Neuroscience* 27(1): 1-12.
- Liu, M., Luo, F., Ding, C., Albeituni, S., Hu, X., Ma, Y., ... Yan, J. (2015). Dectin-1 Activation by a Natural Product  $\beta$ -Glucan Converts Immunosuppressive Macrophages into an M1-like Phenotype. *The Journal of Immunology* 195(10): 5055-5065.
- Liu, T.F., Vachharajani, V.T., Yoza, B.K. & McCall, C.E. (2012). NAD<sup>+</sup>-dependent Sirtuin 1 and 6 Proteins Coordinate a Switch from Glucose to Fatty Acid Oxidation during the Acute Inflammatory Response. *Journal of Biological Chemistry* 287(31): 25758-25769.
- Lue, L.F., Brachova, L., Civin, W.H. & Rogers, J. (1996). Inflammation, A beta deposition, and neurofibrillary tangle formation as correlates of Alzheimer's disease neurodegeneration. *Journal of Neuropathology and Experimental Neurology* 55(10): 1083-1088.
- Lue, L.F., Rydel, R., Brigham, E.F., Yang, L.B., Hampel, H., Murphy, G.M., ... Rogers, J. (2001). Inflammatory repertoire of Alzheimer's disease and nondemented elderly microglia in vitro. *Glia* 35(1): 72-79.
- Lunnon, K., Smith, R., Hannon, E., De Jager, P.L., Srivastava, G., Volta, M., ... Mill, J. (2014). Methyloomic profiling implicates cortical deregulation of ANK1 in Alzheimer's disease. *Nature Neuroscience* 17(9): 1164-1170.
- Lynch, A.M., Murphy, K.J., Deighan, B.F., O'Reilly, J.-A., Gun'ko, Y.K., Cowley, T.R., ... Lynch, M.A. (2010). The impact of glial activation in the aging brain. *Aging and Disease* 1(3): 262-278.
- Mass, E., Ballesteros, I., Farlik, M., Halbritter, F., Günther, P., Crozet, L., ... Geissmann, F. (2016). Specification of tissue-resident macrophages during organogenesis. *Science* 353(6304).
- Masters, C.L., Simms, G., Weinman, N.A., Multhaup, G., McDonald, B.L. & Beyreuther, K. (1985). Amyloid plaque core protein in Alzheimer disease and Down syndrome. *Proceedings of the National Academy of Sciences of the United States of America* 82(12): 4245-4249.
- Matcovitch-Natan, O., Winter, D.R., Giladi, A., Vargas Aguilar, S., Spinrad, A., Sarrazin, S., ... Amit, I. (2016). Microglia development follows a stepwise program to regulate brain homeostasis. *Science* 353(6301).
- Mathys, H., Adai, C., Gao, F., Young, J.Z., Manet, E., Hemberg, M., ... Tsai, L.-H. (2017). Temporal Tracking of Microglia Activation in Neurodegeneration at Single-Cell Resolution. *Cell reports* 21(2): 366-380.
- Maurer, H.R. (1981). Potential Pitfalls of [<sup>3</sup>H]Thymidine Techniques to Measure Cell Proliferation. *Cell Proliferation* 14(2): 111-120.

- Mills, E.L., Kelly, B., Logan, A., Costa, A.S.H., Varma, M., Bryant, C.E., ... O'Neill, L.A. (2016). Succinate Dehydrogenase Supports Metabolic Repurposing of Mitochondria to Drive Inflammatory Macrophages. *Cell* 167(2): 457-470.
- Mills, E.L. & O'Neill, L.A. (2016). Reprogramming mitochondrial metabolism in macrophages as an anti-inflammatory signal. *European Journal of Immunology* 46(1): 13–21.
- Mitroulis, I., Ruppova, K., Wang, B., Chen, L.S., Grzybek, M., Grinenko, T., ... Chavakis, T. (2018). Modulation of Myelopoiesis Progenitors Is an Integral Component of Trained Immunity. *Cell* 172(1-2): 147-161.
- Monneret, G., Finck, M.-E., Venet, F., Debard, A.-L., Bohé, J., Bienvenu, J. & Lepape, A. (2004). The anti-inflammatory response dominates after septic shock: association of low monocyte HLA-DR expression and high interleukin-10 concentration. *Immunology Letters* 95(2): 193–198.
- Moret, Y. & Siva-Jothy, M.T. (2003). Adaptive innate immunity? Responsive-mode prophylaxis in the mealworm beetle, *Tenebrio molitor*. *Proceedings Biological Sciences* 270(1532): 2475–80.
- Mullan, M., Crawford, F., Axelman, K., Houlden, H., Lilius, L., Winblad, B. & Lannfelt, L. (1992). A pathogenic mutation for probable Alzheimer's disease in the APP gene at the N-terminus of beta-amyloid. *Nature Genetics* 1(5): 345–347.
- Naik, S., Larsen, S.B., Gomez, N.C., Alaverdyan, K., Sandoel, A., Yuan, S., ... Fuchs, E. (2017). Inflammatory memory sensitizes skin epithelial stem cells to tissue damage. *Nature* 550(7677): 475-480.
- Naj, A.C., Jun, G., Beecham, G.W., Wang, L.-S., Vardarajan, B.N., Buross, J., ... Schellenberg, G.D. (2011). Common variants at MS4A4/MS4A6E, CD2AP, CD33 and EPHA1 are associated with late-onset Alzheimer's disease. *Nature Genetics* 43(5): 436–441.
- Netea, M.G., Joosten, L.A.B., Latz, E., Mills, K.H.G., Natoli, G., Stunnenberg, H.G., ... Xavier, R.J. (2016). Trained immunity: A program of innate immune memory in health and disease. *Science* 352(6284).
- Netea, M.G., Quintin, J. & van der Meer, J.W.M. (2011). Trained immunity: a memory for innate host defense. *Cell host & microbe* 9(5): 355–361.
- Netea, M.G. & van Crevel, R. (2014). BCG-induced protection: effects on innate immune memory. *Seminars in immunology* 26(6): 512–517.
- Nimmerjahn, A., Kirchhoff, F. & Helmchen, F. (2005). Resting microglial cells are highly dynamic surveillants of brain parenchyma in vivo. *Science* 308(5726): 1314–1318.
- Novakovic, B., Habibi, E., Wang, S.-Y., Arts, R.J.W., Davar, R., Megchelenbrink, W., ... Stunnenberg, H.G. (2016).  $\beta$ -Glucan Reverses the Epigenetic State of LPS-Induced Immunological Tolerance. *Cell* 167(5): 1354–1368.
- Nyström, S., Psonka-Antonczyk, K.M., Ellingsen, P.G., Johansson, L.B.G., Reitan, N., Handrick, S., ... Nilsson, K.P.R. (2013). Evidence for Age-Dependent in



- Vivo Conformational Rearrangement within A $\beta$  Amyloid Deposits. *ACS Chemical Biology* 8(6): 1128–1133.
- O'Neill, L.A.J. & Pearce, E.J. (2016). Immunometabolism governs dendritic cell and macrophage function. *The Journal of Experimental Medicine* 213(1): 15–23.
- Orre, M., Kamphuis, W., Osborn, L.M., Melief, J., Kooijman, L., Huitinga, I., ... Hol, E.M. (2014). Acute isolation and transcriptome characterization of cortical astrocytes and microglia from young and aged mice. *Neurobiology of aging* 35(1): 1–14.
- Ostuni, R., Piccolo, V., Barozzi, I., Polletti, S., Termanini, A., Bonifacio, S., ... Natoli, G. (2013). Latent Enhancers Activated by Stimulation in Differentiated Cells. *Cell* 152(1–2): 157–171.
- Palsson-McDermott, E.M. & O'Neill, L.A.J. (2013). The Warburg effect then and now: from cancer to inflammatory diseases. *BioEssays : news and reviews in molecular, cellular and developmental biology* 35(11): 965–973.
- Paresce, D.M., Ghosh, R.N. & Maxfield, F.R. (1996). Microglial cells internalize aggregates of the Alzheimer's disease amyloid beta-protein via a scavenger receptor. *Neuron* 17(3): 553–565.
- Parkhurst, C.N., Yang, G., Ninan, I., Savas, J.N., Yates, J.R., Lafaille, J.J., ... Gan, W.-B. (2013). Microglia promote learning-dependent synapse formation through brain-derived neurotrophic factor. *Cell* 155(7): 1596–1609.
- Parkin, J. & Cohen, B. (2001). An overview of the immune system. *The Lancet* 357(9270): 1777–1789.
- Pearce, E.L. & Pearce, E.J. (2013). Metabolic Pathways in Immune Cell Activation and Quiescence. *Immunity* 38(4): 633–643.
- Perry, V.H., Cunningham, C. & Holmes, C. (2007). Systemic infections and inflammation affect chronic neurodegeneration. *Nature Reviews Immunology* 7(2): 161–167.
- Perry, V.H. & Holmes, C. (2014). Microglial priming in neurodegenerative disease. *Nature Reviews Neurology* 10(4): 217–224.
- Perry, V.H. & Teeling, J. (2013). Microglia and macrophages of the central nervous system: the contribution of microglia priming and systemic inflammation to chronic neurodegeneration. *Seminars in Immunopathology* 35(5): 601–612.
- Pham, L.N., Dionne, M.S., Shirasu-Hiza, M. & Schneider, D.S. (2007). A specific primed immune response in *Drosophila* is dependent on phagocytes. *PLoS pathogens* 3(3).
- Prinz, M., Erny, D. & Hagemeyer, N. (2017). Ontogeny and homeostasis of CNS myeloid cells. *Nature Immunology* 18(4): 385–392.
- Probst, A. V., Dunleavy, E. & Almouzni, G. (2009). Epigenetic inheritance during the cell cycle. *Nature reviews. Molecular cell biology* 10(3): 192–206.
- Qin, L., Wu, X., Block, M.L., Liu, Y., Breese, G.R., Hong, J.-S., ... Crews, F.T. (2007). Systemic LPS causes chronic neuroinflammation and progressive

- neurodegeneration. *Glia* 55(5): 453–462.
- Quan, N. & Banks, W.A. (2007). Brain-immune communication pathways. *Brain, Behavior, and Immunity* 21(6): 727–735.
- Quintin, J., Cheng, S.-C., van der Meer, J.W. & Netea, M.G. (2014). Innate immune memory: towards a better understanding of host defense mechanisms. *Current Opinion in Immunology* 29: 1–7.
- Quintin, J., Saeed, S., Martens, J.H.A., Giamarellos-Bourboulis, E.J., Ifrim, D.C., Logie, C., ... Netea, M.G. (2012). *Candida albicans* infection affords protection against reinfection via functional reprogramming of monocytes. *Cell host & microbe* 12(2): 223–232.
- Rabinowitz, S., Horstmann, H., Gordon, S. & Griffiths, G. (1992). Immunocytochemical characterization of the endocytic and phagolysosomal compartments in peritoneal macrophages. *The Journal of Cell Biology* 116(1): 95–112.
- Ransohoff, R.M. & Cardona, A.E. (2010). The myeloid cells of the central nervous system parenchyma. *Nature* 468(7321): 253–262.
- Ransohoff, R.M. & Perry, V.H. (2009). Microglial physiology: unique stimuli, specialized responses. *Annual Review of Immunology* 27: 119–145.
- Rasmussen, J., Mahler, J., Beschoner, N., Kaeser, S.A., Häslér, M.L., Baumann, F., ... Jucker, M. (2017). Amyloid polymorphisms constitute distinct clouds of conformational variants in different etiological subtypes of Alzheimer's disease. *Proceedings of the National Academy of Sciences of the United States of America* 114(49): 13018-13023.
- Reiss, M. & Roos, D. (1978). Differences in Oxygen Metabolism of Phagocytosing Monocytes and Neutrophils. *Journal of Clinical Investigation* 61(2): 480–488.
- Reitz, C., Brayne, C. & Mayeux, R. (2011). Epidemiology of Alzheimer disease. *Nature Reviews Neurology* 7(3): 137–52.
- Réu, P., Khosravi, A., Bernard, S., Mold, J.E., Salehpour, M., Alkass, K., ... Frisé, J. (2017). The Lifespan and Turnover of Microglia in the Human Brain. *Cell Reports* 20(4): 779–784.
- Rio-Hortega, P. (1919). El 'tercer elemento' de los centros nerviosos. I. La microglia en estado normal. *Bol Soc Esp Biol VIII*: 67-82.
- Rodriguez-Prados, J.-C., Traves, P.G., Cuenca, J., Rico, D., Aragonés, J., Martín-Sanz, P., ... Bosca, L. (2010). Substrate Fate in Activated Macrophages: A Comparison between Innate, Classic, and Alternative Activation. *The Journal of Immunology* 185(1): 605–614.
- Rogers, J., Cooper, N.R., Webster, S., Schultz, J., McGeer, P.L., Styren, S.D., ... Ward, P. (1992). Complement activation by beta-amyloid in Alzheimer disease. *Proceedings of the National Academy of Sciences of the United States of America* 89(21): 10016–10020.
- Saeed, S., Quintin, J., Kerstens, H.H.D., Rao, N.A., Aghajani-Refah, A., Matarese, F.,

- ... Stunnenberg, H.G. (2014). Epigenetic programming of monocyte-to-macrophage differentiation and trained innate immunity. *Science* 345(6204).
- Schaafsma, W., Zhang, X., van Zomeren, K.C., Jacobs, S., Georgieva, P.B., Wolf, S.A., ... Eggen, B.J.L. (2015). Long-lasting pro-inflammatory suppression of microglia by LPS-preconditioning is mediated by RelB-dependent epigenetic silencing. *Brain, behavior, and immunity* 48: 205-21.
- Schafer, D.P., Lehrman, E.K., Kautzman, A.G., Koyama, R., Mardinly, A.R., Yamasaki, R., ... Stevens, B. (2012). Microglia Sculpt Postnatal Neural Circuits in an Activity and Complement-Dependent Manner. *Neuron* 74(4): 691–705.
- Scheuner, D., Eckman, C., Jensen, M., Song, X., Citron, M., Suzuki, N., ... Younkin, S. (1996). Secreted amyloid beta-protein similar to that in the senile plaques of Alzheimer's disease is increased in vivo by the presenilin 1 and 2 and APP mutations linked to familial Alzheimer's disease. *Nature Medicine* 2(8): 864–70.
- Schubert, P., Morino, T., Miyazaki, H., Ogata, T., Nakamura, Y., Marchini, C. & Ferroni, S. (2000). Cascading glia reactions: a common pathomechanism and its differentiated control by cyclic nucleotide signaling. *Annals of the New York Academy of Sciences* 903: 24–33.
- Selkoe, D.J. & Hardy, J. (2016). The amyloid hypothesis of Alzheimer's disease at 25 years. *EMBO Molecular Medicine* 8(6): 595–608.
- Shalova, I.N., Lim, J.Y., Chittiezath, M., Zinkernagel, A.S., Beasley, F., Hernández-Jiménez, E., ... Biswas, S.K. (2015). Human Monocytes Undergo Functional Re-programming during Sepsis Mediated by Hypoxia-Inducible Factor-1 $\alpha$ . *Immunity* 42(3): 484–498.
- Sheng, J.G., Zhu, S.G., Jones, R.A., Griffin, W.S. & Mrak, R.E. (2000). Interleukin-1 promotes expression and phosphorylation of neurofilament and tau proteins in vivo. *Experimental Neurology* 163(2): 388–391.
- Shi, J.-Q., Shen, W., Chen, J., Wang, B.-R., Zhong, L.-L., Zhu, Y.-W., ... Xu, J. (2011). Anti-TNF- $\alpha$  reduces amyloid plaques and tau phosphorylation and induces CD11c-positive dendritic-like cell in the APP/PS1 transgenic mouse brains. *Brain research* 1368: 239–47.
- Shlyueva, D., Stampfel, G. & Stark, A. (2014). Transcriptional enhancers: from properties to genome-wide predictions. *Nature Reviews Genetics* 15(4): 272–286.
- Sierra, A., de Castro, F., del Río-Hortega, J., Rafael Iglesias-Rozas, J., Garrosa, M. & Kettenmann, H. (2016). The 'Big-Bang' for modern glial biology: Translation and comments on Pío del Río-Hortega 1919 series of papers on microglia. *Glia* 64(11): 1801–1840.
- Sims-Robinson, C., Kim, B., Rosko, A. & Feldman, E.L. (2010). How does diabetes accelerate Alzheimer disease pathology? *Nature Reviews Neurology* 6(10): 551–559.
- Sims, R., van der Lee, S.J., Naj, A.C., Bellenguez, C., Badarinarayan, N., Jakobsdottir, J., ... Schellenberg, G.D. (2017). Rare coding variants in PLCG2,

- ABI3, and TREM2 implicate microglial-mediated innate immunity in Alzheimer's disease. *Nature Genetics* 49(9): 1373-1384.
- Smith, A.M., Gibbons, H.M., Oldfield, R.L., Bergin, P.M., Mee, E.W., Faull, R.L.M. & Dragunow, M. (2013). The transcription factor PU.1 is critical for viability and function of human brain microglia. *Glia* 61(6): 929-942.
- Sofroniew, M. V & Vinters, H. V. (2010). Astrocytes: biology and pathology. *Acta neuropathologica* 119(1): 7-35.
- Song, W.M., Colonna, M. (2018). Immune Training Unlocks Innate Potential. *Cell* 172(1-2): 3-5.
- Soreq, L., Rose, J., Soreq, E., Hardy, J., Trabzuni, D., Cookson, M.R., ... Ule, J. (2017). Major Shifts in Glial Regional Identity Are a Transcriptional Hallmark of Human Brain Aging. *Cell Reports* 18(2): 557-570.
- Stienstra, R., Netea-Maier, R.T., Riksen, N.P., Joosten, L.A.B. & Netea, M.G. (2017). Specific and Complex Reprogramming of Cellular Metabolism in Myeloid Cells during Innate Immune Responses. *Cell metabolism* 26(1): 142-156.
- Streit, W.J., Braak, H., Xue, Q.-S. & Bechmann, I. (2009). Dystrophic (senescent) rather than activated microglial cells are associated with tau pathology and likely precede neurodegeneration in Alzheimer's disease. *Acta neuropathologica* 118(4): 475-485.
- Streit, W.J., Sammons, N.W., Kuhns, A.J. & Sparks, D.L. (2004). Dystrophic microglia in the aging human brain. *Glia* 45(2): 208-212.
- Streit, W.J., Walter, S.A. & Pennell, N.A. (1999). Reactive microgliosis. *Progress in neurobiology* 57(6): 563-81.
- Sturchler-Pierrat, C., Abramowski, D., Duke, M., Wiederhold, K.H., Mistl, C., Rothacher, S., ... Sommer, B. (1997). Two amyloid precursor protein transgenic mouse models with Alzheimer disease-like pathology. *Proceedings of the National Academy of Sciences of the United States of America* 94(24): 13287-13292.
- Sturchler-Pierrat, C. & Staufenbiel, M. (2000). Pathogenic mechanisms of Alzheimer's disease analyzed in the APP23 transgenic mouse model. *Annals of the New York Academy of Sciences* 920: 134-139.
- Szczepanik, A.M., Rampe, D. & Ringheim, G.E. (2001). Amyloid-beta peptide fragments p3 and p4 induce pro-inflammatory cytokine and chemokine production in vitro and in vivo. *Journal of Neurochemistry* 77(1): 304-317.
- Tannahill, G.M., Curtis, A.M., Adamik, J., Palsson-McDermott, E.M., McGettrick, A.F., Goel, G., ... O'Neill, L.A.J. (2013). Succinate is an inflammatory signal that induces IL-1 $\beta$  through HIF-1 $\alpha$ . *Nature* 496(7444): 238-42.
- Tay, T.L., Mai, D., Dautzenberg, J., Fernández-Klett, F., Lin, G., Sagar, ... Prinz, M. (2017). A new fate mapping system reveals context-dependent random or clonal expansion of microglia. *Nature Neuroscience* 20(6): 793-803.
- Tosto, G. & Reitz, C. (2013). Genome-wide association studies in Alzheimer's

- disease: a review. *Current Neurology and Neuroscience Reports* 13(10): 381.
- van der Meer, J.W., Barza, M., Wolff, S.M. & Dinarello, C.A. (1988). A low dose of recombinant interleukin 1 protects granulocytopenic mice from lethal gram-negative infection. *Proceedings of the National Academy of Sciences of the United States of America* 85(5): 1620–3.
- Vassar, R., Bennett, B.D., Babu-Khan, S., Kahn, S., Mendiaz, E.A., Denis, P., ... Citron, M. (1999). Beta-secretase cleavage of Alzheimer's amyloid precursor protein by the transmembrane aspartic protease BACE. *Science* 286(5440): 735–41.
- Vom Berg, J., Prokop, S., Miller, K.R., Obst, J., Kälin, R.E., Lopategui-Cabezas, I., ... Heppner, F.L. (2012). Inhibition of IL-12/IL-23 signaling reduces Alzheimer's disease-like pathology and cognitive decline. *Nature Medicine* 18(12): 1812–1819.
- Walker, K.A., Hoogeveen, R.C., Folsom, A.R., Ballantyne, C.M., Knopman, D.S., Windham, B.G., ... Gottesman, R.F. (2017). Midlife systemic inflammatory markers are associated with late-life brain volume. *Neurology* 89(22): 2262–2270.
- Wang, C., Yu, J.-T., Miao, D., Wu, Z.-C., Tan, M.-S. & Tan, L. (2014). Targeting the mTOR Signaling Network for Alzheimer's Disease Therapy. *Molecular Neurobiology* 49(1): 120–135.
- Wang, Q., Rowan, M.J. & Anwyl, R. (2004). Beta-amyloid-mediated inhibition of NMDA receptor-dependent long-term potentiation induction involves activation of microglia and stimulation of inducible nitric oxide synthase and superoxide. *The Journal of Neuroscience* 24(27): 6049–6056.
- Wang, Y., Ulland, T.K., Ulrich, J.D., Song, W., Tzaferis, J.A., Hole, J.T., ... Colonna, M. (2016). TREM2-mediated early microglial response limits diffusion and toxicity of amyloid plaques. *The Journal of Experimental Medicine* 213(5).
- Weichhart, T., Hengstschläger, M. & Linke, M. (2015). Regulation of innate immune cell function by mTOR. *Nature Reviews Immunology* 15(10): 599–614.
- Wendeln, A.C., Degenhardt, K., Kaurani, L., Gertig, M., Ulas, T., Jain, G., ... Neher, J.J. (2018). Innate immune memory in the brain shapes neurological disease hallmarks. *Nature*. Accepted
- Wolfe, M.S., Selkoe, D.J., Xia, W., Ostaszewski, B.L., Diehl, T.S. & Kimberly, W.T. (1999). Two transmembrane aspartates in presenilin-1 required for presenilin endoproteolysis and gamma-secretase activity. *Nature* 398(6727): 513–517.
- Xue, J., Schmidt, S. V., Sander, J., Draffehn, A., Krebs, W., Quester, I., ... Schultze, J.L. (2014). Transcriptome-based network analysis reveals a spectrum model of human macrophage activation. *Immunity* 40(2): 274–288.
- Yan, S.D., Stern, D., Kane, M.D., Kuo, Y.M., Lampert, H.C. & Roher, A.E. (1998). RAGE-Abeta interactions in the pathophysiology of Alzheimer's disease. *Restorative Neurology and Neuroscience* 12(2–3): 167–173.

- Yu, W.H., Go, L., Guinn, B.A., Fraser, P.E., Westaway, D. & McLaurin, J. (2002). Phenotypic and functional changes in glial cells as a function of age. *Neurobiology of Aging* 23(1): 105–115.
- Yuan, P., Condello, C., Keene, C.D., Wang, Y., Bird, T.D., Paul, S.M., ... Grutzendler, J. (2016). TREM2 Haplodeficiency in Mice and Humans Impairs the Microglia Barrier Function Leading to Decreased Amyloid Compaction and Severe Axonal Dystrophy. *Neuron* 90(4): 724–739.
- Zhang, B., Gaiteri, C., Bodea, L.-G., Wang, Z., McElwee, J., Podtelezhnikov, A.A., ... Emilsson, V. (2013). Integrated systems approach identifies genetic nodes and networks in late-onset Alzheimer's disease. *Cell* 153(3): 707–720.
- Zhang, X. & Morrison, D.C. (1993). Lipopolysaccharide-induced selective priming effects on tumor necrosis factor alpha and nitric oxide production in mouse peritoneal macrophages. *The Journal of Experimental Medicine* 177(2): 511–516.
- Zhou, V.W., Goren, A. & Bernstein, B.E. (2011). Charting histone modifications and the functional organization of mammalian genomes. *Nature Reviews Genetics* 12(1): 7–18.

## 3 Publications

### 3.1 Statement of personal contributions

- I. Petra Füger, Jasmin K. Hefendehl, Karthik Veeraraghavalu, Ann-Christin Wendeln, Christine Schlosser, Ulrike Obermüller, Bettina M. Wegenast-Braun, Jonas J. Neher, Peter Martus, Shinichi Kohsaka, Martin Thunemann, Robert Feil, Sangram S. Sisodia, Angelos Skodras, Mathias Jucker: Microglia turnover with aging and in an Alzheimer's model via long-term *in vivo* single-cell imaging

**Personal contribution:** stereological assessment of microglial numbers; Tamoxifen injection, preparation, flow cytometric and histological analysis of recombined cells of animals for dose-response curve; editing of the manuscript

Others: PF, CS, UO, BW, and AS performed the experimental work. KV, SK, MT, RF, and SSS generated the mouse models. AS and PM performed the statistical analysis. PF, JKH, JJN, AS, and MJ designed the study. PF, JJN, AS, and MJ wrote the manuscript with contributions from all authors.

- II. Ann-Christin Wendeln<sup>\*</sup>, Karoline Degenhardt<sup>\*</sup>, Lalit Kaurani, Michael Gertig, Thomas Ulas, Gaurav Jain, Jessica Wagner, Lisa M. Häsler, Katleen Wild, Angelos Skodras, Thomas Blank, Ori Staszewski, Moumita Datta, Tonatiuh Pena Centeno, Vincenzo Capece, Md. Rezaul Islam, Cemil Kerimoglu, Matthias Staufienbiel, Joachim L. Schultze, Marc Beyer, Marco Prinz, Mathias Jucker, André Fischer, Jonas J. Neher: Innate immune memory in the brain shapes neurological disease hallmarks

<sup>\*</sup>contributed equally

**Personal contribution:** injection of wildtype/APP23 mice with LPS and preparation of animals (together with K.D., Figure 1, Figure 2); injection of CX3CR1-CreER mice with LPS and preparation of animals (Figure 1); injection of cytokines and preparation of animals (Extended Data Figure 9); stereological quantification of A $\beta$ , Pu.1 (together with K.D., Figure 2), and GFAP (Extended Data Figure 3); microglial isolation and FAC sorting for ChIP-seq (together with K.D., Figure 4), RNA-seq (Figure 5); microglial isolation followed by flow cytometric analysis (DiOC), cultivation for analysis of lactate release, and quantification of A $\beta$  content (Figure 5); immunostainings for A $\beta$ , Pu.1 (together with K.D.), Iba-1, GFAP, APP, and HIF1- $\alpha$ ; image acquisition and image analysis for HIF1- $\alpha$  expression (Figure 5), APP quantification (Extended Data Figure 3), and microglial morphology

(Extended Data Figure 1); data analysis (together with K.D. and J.N.); editing of the manuscript

Others: MG, LK, GJ, TP, VC, RI, CK, AF, MB, TU, JLS, and JJN performed ChIP-Seq/RNA-Seq analyses. KD, JW, PR, LMH, KW, AS, TB, OS, MD, and JJN performed all other experimental work. JJN, MJ, AF, MP, MB, JLS, and MS designed the study. JJN wrote the manuscript with contributions from all authors.

- III. Ann-Christin Wendeln, Angelos Skodras, Natalie Beschorner, Peter Nilsson, Mathias Jucker, Jonas J. Neher: Systemic inflammation induces long-term modulation of amyloid plaque morphology and neuronal damage in a mouse model of Alzheimer's disease

**Personal contribution:** Experimental design of the study (together with J.N. and M.J.); preparation of animals; Western Blotting; LCO staining and spectral analysis; immunostainings; image acquisition and analysis (with help from A.S.); data analysis and figure preparation; manuscript preparation (with J.N.)

Others: NB performed stainings of human sections. AS developed tools for image and data analysis, PN developed LCO dyes. JJN and MJ designed the study.




### **3.2 Microglia turnover with aging and in an Alzheimer's model via long-term *in vivo* single-cell imaging**

Petra Föger, Jasmin K. Hefendehl, Karthik Veeraraghavalu, Ann-Christin Wendeln, Christine Schlosser, Ulrike Obermüller, Bettina M. Wegenast-Braun, Jonas J. Neher, Peter Martus, Shinichi Kohsaka, Martin Thunemann, Robert Feil, Sangram S. Sisodia, Angelos Skodras, Mathias Jucker

*Nature Neuroscience (2017)*

# Microglia turnover with aging and in an Alzheimer's model via long-term *in vivo* single-cell imaging

Petra Föger<sup>1,2</sup>, Jasmin K Hefendehl<sup>1,2</sup>, Karthik Veeraraghavalu<sup>3</sup>, Ann-Christin Wendeln<sup>1,2,4</sup>, Christine Schlosser<sup>1</sup>, Ulrike Obermüller<sup>1,2</sup>, Bettina M Wegenast-Braun<sup>1,2</sup>, Jonas J Neher<sup>1,2</sup> , Peter Martus<sup>5</sup>, Shinichi Kohsaka<sup>6</sup>, Martin Thunemann<sup>7</sup>, Robert Feil<sup>7</sup>, Sangram S Sisodia<sup>3</sup>, Angelos Skodras<sup>1,2</sup> & Mathias Jucker<sup>1,2</sup>

To clarify the role of microglia in brain homeostasis and disease, an understanding of their maintenance, proliferation and turnover is essential. The lifespan of brain microglia, however, remains uncertain, and reflects confounding factors in earlier assessments that were largely indirect. We genetically labeled single resident microglia in living mice and then used multiphoton microscopy to monitor these cells over time. Under homeostatic conditions, we found that neocortical resident microglia were long-lived, with a median lifetime of well over 15 months; thus, approximately half of these cells survive the entire mouse lifespan. While proliferation of resident neocortical microglia under homeostatic conditions was low, microglial proliferation in a mouse model of Alzheimer's  $\beta$ -amyloidosis was increased threefold. The persistence of individual microglia throughout the mouse lifespan provides an explanation for how microglial priming early in life can induce lasting functional changes and how microglial senescence may contribute to age-related neurodegenerative diseases.

Microglia are the brain-resident macrophages<sup>1</sup>. They are developmentally distinct from other tissue-resident macrophage populations<sup>2,3</sup> and are maintained with no appreciable contribution of peripheral myeloid cells under normal, healthy conditions<sup>4,5</sup>. In the human neocortex microglia account for an estimated 5% of all cells<sup>6</sup>.

Microglia are uniformly distributed throughout the CNS parenchyma, and they form a cellular grid with their ramified and highly motile processes<sup>7,8</sup>. It is now well appreciated that microglia are essential for proper brain function due to their crucial role in neural circuit remodeling and synaptic function, but these cells also contribute to the pathogenesis of neurological diseases<sup>1,9,10</sup>. This increasingly recognized function of microglia during development, aging and neurological disease has garnered significant interest since the first description of these cells more than 100 years ago (see ref. 11). Although it is known that microglia can rapidly proliferate in response to CNS insults<sup>12,13</sup>, microglial proliferation and turnover under homeostatic conditions has not been accurately characterized. Previous studies provided conflicting results<sup>14–16</sup>, reporting very low and very high microglial turnover rates in mice, but the estimations were mainly done indirectly using [<sup>3</sup>H]thymidine and bromodeoxyuridine (BrdU) pulse-labeling combined with postmortem histology, arguably a technique with limited validity<sup>17,18</sup>.

How the microglial population is maintained in the brain is crucial to understanding microglial function. For example, stimulation of the brain's immune system during development can induce long-lasting changes in microglial immune responses<sup>19,20</sup>, while aging and senescence

of microglia are thought to contribute to neurodegenerative disorders<sup>21,22</sup>. However, whether these effects are due to a change in the brain environment or to the longevity of microglia remains unclear, as the lifespan of individual microglia has not been determined. To directly address this question, we have genetically marked and repeatedly imaged single microglial cells over their lifetime in the mouse neocortex, both under homeostatic conditions and in a mouse model of cerebral  $\beta$ -amyloidosis.

## RESULTS

### Genetic labeling and imaging of individual microglial cells

To label individual microglia, we generated double-transgenic CD11b-CreERT2;R26-tdTomato mice or triple-transgenic mice that also carried an Iba1-eGFP transgene (Fig. 1). Expression of the fluorescent protein tdTomato was induced by tamoxifen injection, with the dose adjusted to induce the tdTomato fluorophore stochastically in only a small population (less than 2%) of neocortical microglial cells, identified as CD11b<sup>high</sup>CD45<sup>low</sup> cells by flow cytometry and by histological analyses (Supplementary Fig. 1). Moreover, the fraction of Iba1-positive microglia that were tdTomato-positive remained constant after imaging (1.64%  $\pm$  0.8%;  $n = 3$  mice), excluding selective expansion or death of recombined cells.

Young (4 months old,  $n = 27$ ) and adult (10 months old,  $n = 6$ ) mice with induced recombination were imaged. For that purpose a customized titanium ring was attached to the mouse's skull, allowing micrometer-precise, long-term repositioning on the motorized

<sup>1</sup>Department of Cellular Neurology, Hertie Institute for Clinical Brain Research, University of Tübingen, Tübingen, Germany. <sup>2</sup>DZNE—German Center for Neurodegenerative Diseases, Tübingen, Germany. <sup>3</sup>Department of Neurobiology, The University of Chicago, Chicago, Illinois, USA. <sup>4</sup>Graduate School of Cellular and Molecular Neuroscience, University of Tübingen, Tübingen, Germany. <sup>5</sup>Institute of Medical Biometry, University of Tübingen, Tübingen, Germany. <sup>6</sup>Department of Neurochemistry, National Institute of Neuroscience, Kodaira, Tokyo, Japan. <sup>7</sup>Interfaculty Institute of Biochemistry, University of Tübingen, Tübingen, Germany. Correspondence should be addressed to A.S. ([angelos.skodras@medizin.uni-tuebingen.de](mailto:angelos.skodras@medizin.uni-tuebingen.de)) or M.J. ([mathias.jucker@uni-tuebingen.de](mailto:mathias.jucker@uni-tuebingen.de)).

Received 3 February; accepted 2 August; published online 28 August 2017; doi:10.1038/nn.4631

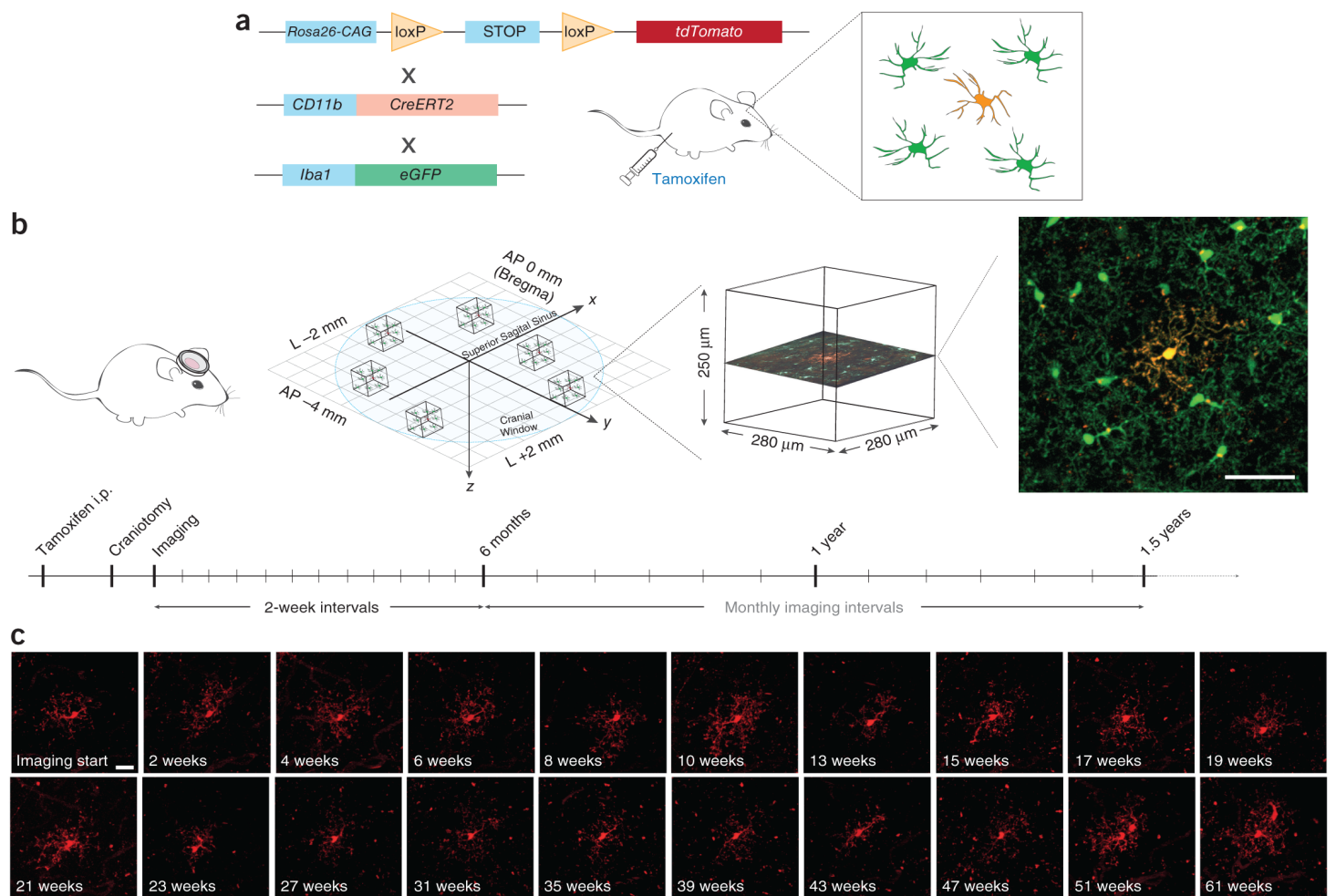


**Figure 1** Visualization and long-term *in vivo* imaging of individual microglia in the mouse brain. **(a)** Transgenic mice expressing the red fluorophore tdTomato with an upstream floxed stop codon (R26-loxP-STOP-loxP-tdTomato) were crossed with mice that express an inducible Cre recombinase in myeloid cells (CD11b-CreERT2). Most of these double transgenic mice were then crossed with mice expressing GFP in microglia (Iba1-eGFP). Double- and triple-transgenic mice were injected intraperitoneally with tamoxifen, resulting in the expression of tdTomato in a subset of microglia (red) that enabled individual tracking of these cells. In triple-transgenic mice, recombined microglia appeared yellow while surrounding microglia were green. **(b)** Four weeks after tamoxifen administration, mice underwent craniotomy (anteroposteriorly 0 mm to –4 mm from bregma, laterally  $\pm 2$  mm) and a ring was attached to the skull, enabling repeated long-term localization (in an *xy* coordinate system) and imaging of specific positions. A stack was acquired on each position, up to a depth of 250  $\mu\text{m}$  from the brain surface, with a field of view of  $280 \times 280 \mu\text{m}^2$ . In each mouse, typically four to six positions were selected so that at least one tdTomato-positive microglial cell was visible within each stack. Positions were imaged biweekly for the first 6 months, followed by imaging at monthly intervals. Scale bar is 40  $\mu\text{m}$ . **(c)** *In vivo* imaging of a tdTomato-positive individual microglia in a double-transgenic CD11b-CreERT2;R26-tdTomato mouse starting at 4 months of age and continuing over 61 weeks, demonstrating that microglia can be very long-lived and persist in certain positions. Note the division of the microglia at week 51. Scale bar is 20  $\mu\text{m}$ .

microscope stage to previously imaged regions of interest<sup>23</sup> (Fig. 1). For each animal, typically four to six neocortical volumes were selected, each containing at least one tdTomato-positive microglial cell. Microglia were longitudinally tracked at biweekly intervals over the first 6 months, followed by monthly imaging for as long as the optical quality of the cranial window allowed (Fig. 1). Careful post-mortem histological analysis was performed to exclude activation of microglia through surgery or laser-induced activation through repeated imaging (Supplementary Fig. 2).

#### Average lifetime of microglia in mouse neocortex

Remarkably, most microglial cells were found in the same position for imaging periods up to 15.5 months in duration. However, a small number of microglia disappeared during imaging. Because we were able to rule out inactivation of tdTomato expression or the migration of the imaged microglia out of the imaging volume (Fig. 2a,b; see

also Online Methods), this observation suggests microglial death. To estimate the lifetime of the cells, each microglial cell that disappeared was marked as a ‘death event’, with subsequent Kaplan–Meier survival analysis. Surprisingly, considering the longest imaging periods (>15 months), a median survival point was not reached, for either the young or the adult mice, indicating that the median microglial lifetime spans well over 15 months (Fig. 2d). However, the lifetime of the cells was found to be somewhat shorter in the adult mice than in the young mice, as a steeper drop in adult microglial survival was observed (although the survival curves were not significantly different; Fig. 2d). To extrapolate the mean age of microglial survival from our observations, we used an exponential probability distribution fit to the survival data. The lifetimes of microglia in the young and adult mouse groups were calculated to be 29 and 22 months, respectively (Fig. 2e). Strikingly, this difference in the estimated microglial lifetime matches approximately the mean age difference of the two

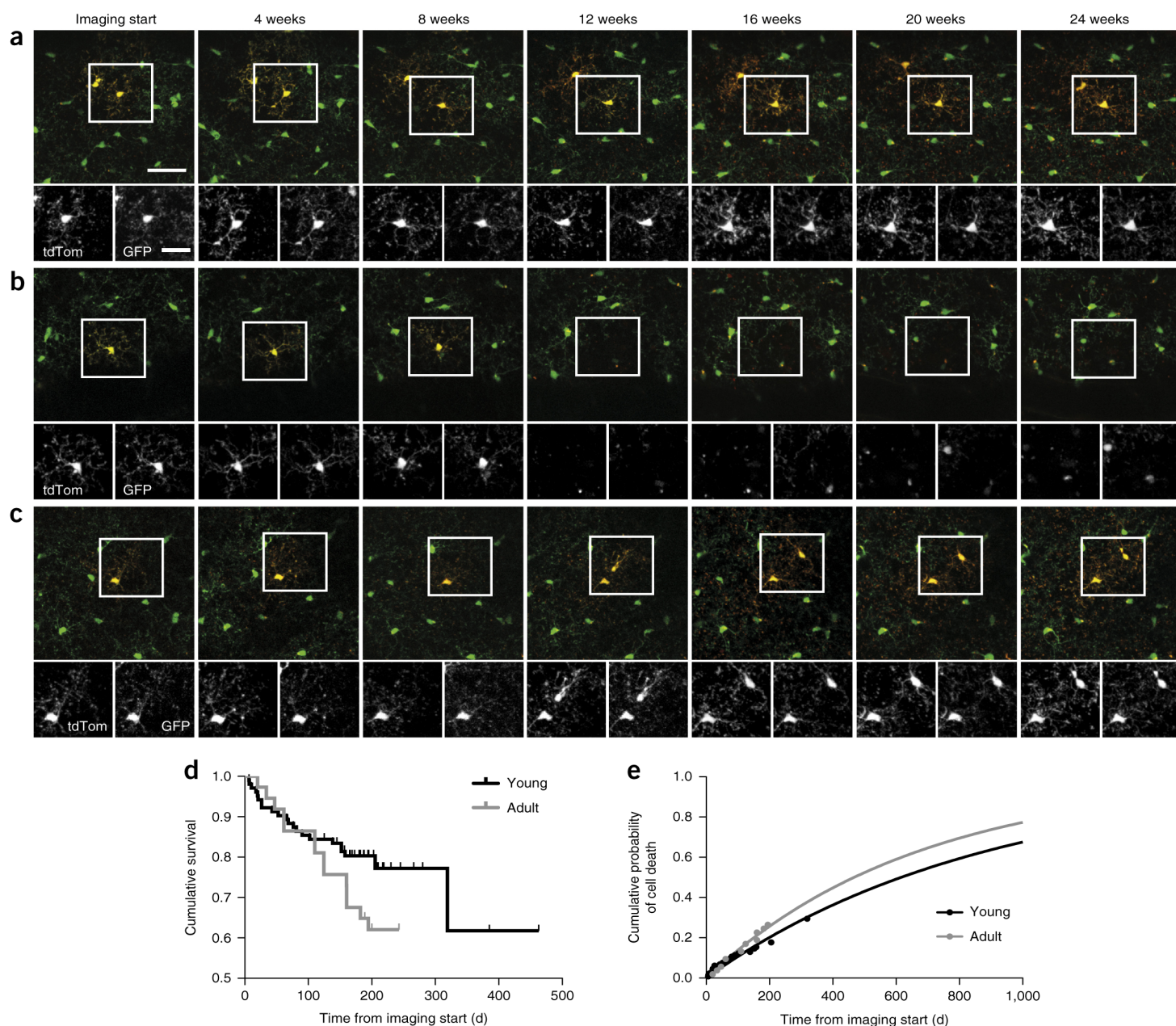


**Figure 2** Estimated average lifetime of a microglial cell in the mouse neocortex. **(a)** An example of a stable microglial cell (yellow). **(b)** A microglial cell that is lost after 8 weeks of imaging. **(c)** A cell that divides after 8 weeks. Insets in **a–c** depict the separate imaging channels for tdTomato and GFP. Note that when a cell is lost **(b)**, both tdTomato and GFP signals are lost, demonstrating that the cell has died (nonspecific ‘switching off’ of the tdTomato expression was never observed). A 50- $\mu\text{m}$  ‘guard area’ excluded misclassification of migrating tdTomato-positive microglia as newly appearing or lost cells (see Online Methods). Monthly time points (z-projections of the imaged volumes) are shown; however, animals were imaged biweekly (see **Fig. 1**). The lower shaded area in **b** is a large blood vessel. Disappearing and appearing (green) cells in the z-projections are located close to the border of the imaged volumes, thus moving in or out of the region of interest. Scale bars are 40  $\mu\text{m}$  for main panels and 20  $\mu\text{m}$  for insets. **(d)** Kaplan–Meier survival analysis of lost microglial cells in the young 4-month-old mice ( $n = 27$  mice, total 132 cells) and adult 10-month-old mice ( $n = 6$  mice; total 53 cells). For details see **Supplementary Table 1**. **(e)** Fitting an exponential distribution to the observed microglial lifetimes revealed an estimated mean lifetime of 29.1 months for the young animals and 22.1 months for the adult animals (see Online Methods). Mouse gender was not found to have an effect in our analysis.

mouse groups imaged. In line with our hypothesis, this suggests that in the older group of animals most individual microglia are older at the time of imaging.

### Newly appearing microglia cells

In addition to microglial cell death, we also observed proliferation of individually labeled cells (**Figs. 2c** and **3**). The quantitative analysis was confined to the young group. Notably, the number of cells that appeared or were lost was almost identical (13%) over the 6-month

biweekly imaging period (**Fig. 3e**), consistent with the total number of neocortical microglia being stable throughout life under normal circumstances<sup>7</sup>. Moreover, new tdTomato-expressing cells always appeared in proximity to an existing tdTomato-expressing microglial cell that typically had been imaged over many weeks. The appearance of new cells was sometimes preceded by a recognizable increase in cell body volume of the presumed originating cell, further indicating cell proliferation (**Fig. 3a–d**). While the originator cells remained stable within the network of Iba1-positive cells and persisted at the imaged

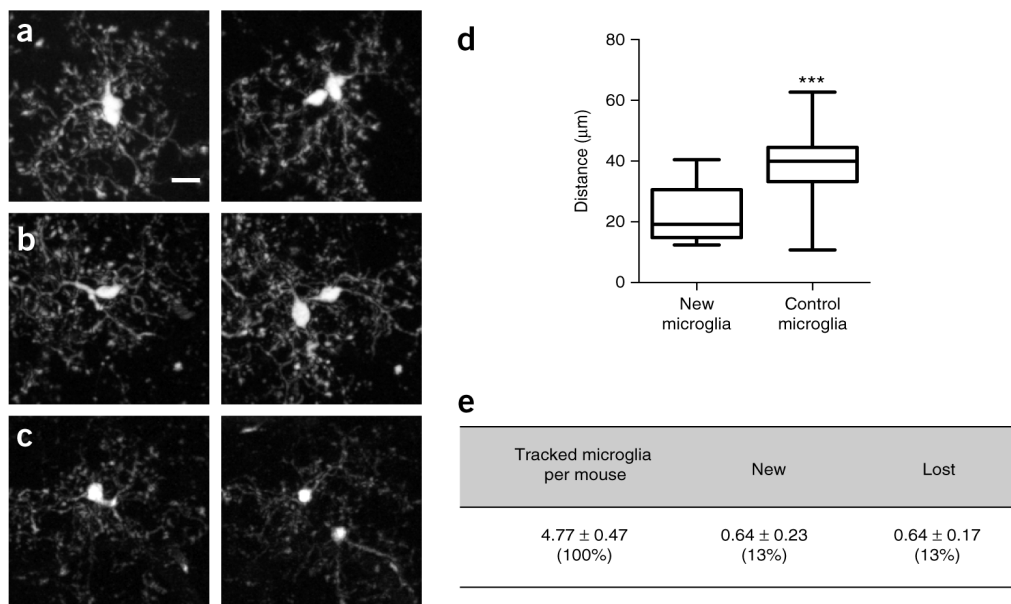


**Figure 3** New microglia appear in close proximity to existing microglial cells. Analysis was done for the young 4-month-old mice and confined to the mice with complete biweekly imaging data set over the first 6 months ( $n = 22$ ). (a–c) Three examples of newly appearing tdTomato-positive cells within two consecutive imaging sessions. In the first column, only a single cell was present; in the following imaging session, a second cell appeared in close proximity. All (100%) of the newly generated microglial cells were still present in the following imaging session; scale bar is 10  $\mu\text{m}$ . (d) Quantitative nearest-neighbor analysis of newly appearing tdTomato-expressing cells revealed a median distance of 20  $\mu\text{m}$  from an already existing tdTomato-positive cell ( $n = 13$  cell pairs; the analysis was done on the stacks from the imaging session when new tdTomato-positive microglia appeared). In comparison, the median distance between resident Iba1-eGFP-positive control microglia (within the same stacks) was 40  $\mu\text{m}$  ( $n = 374$  cell pairs; Mann–Whitney test,  $U = 609$ ,  $***P < 0.001$ ). (e) Average number of tdTomato-positive microglial cells tracked per mouse, the number of newly appearing cells and the number of lost cells during the imaging period. Given is the mean  $\pm$  s.e.m. of  $n = 22$  mice. The similar number of newly appearing and lost cells is consistent with a stable number of Iba1-eGFP-positive microglia per imaged neocortical volume in the CD11b-CreERT2;R26-tdTomato;Iba1-eGFP mice over the 6-month imaging period (mean  $\pm$  s.d. cells per volume:  $73 \pm 9$  vs.  $73 \pm 7$  at the beginning and end of the imaging period, respectively; 14 volumes from 8 animals were analyzed; paired  $t$ -test,  $t(13) = 0.14$ ;  $P > 0.05$ ).

$xyz$  position, the newly generated microglia cells then moved away from the mother cells and took up permanent residence at an average inter-microglial distance of approximately 40  $\mu\text{m}$ , with their typical ramified processes interconnecting with the existing microglial network (Fig. 3d). Notably, 100% of the newly generated microglial cells were still present in the following imaging session, indicating stable integration of newborn cells in the brain microglial network.

Daily imaging of neocortical microglia for 10 d again showed low rates of microglial death and proliferation, making a rapid replacement of these cells within the biweekly imaging interval unlikely, yet impossible to rule out completely (Supplementary Fig. 3). Moreover, the possibility that the microglial turnover rate is different in CD11b-CreERT2;R26-tdTomato or CD11b-CreERT2;R26-tdTomato;Iba1-eGFP mice compared to normal C57BL/6J mice appeared unlikely because there was no difference between neocortical microglial number and BrdU incorporation between the mouse lines (Supplementary Fig. 4).

### Increased microglia turnover in the presence of amyloid lesions

To decipher microglial lifetime and turnover under pathological conditions, we imaged individually labeled microglia in APPPS1 mice, a mouse model that begins to develop  $\beta$ -amyloid plaques at 1.5 months of age<sup>24</sup>. To this end, we generated triple-transgenic CD11b-CreERT2;R26-tdTomato;APPPS1 mice and again imaged individually labeled microglia longitudinally starting at 4 months of age (Fig. 4). Surprisingly, the number of microglia lost in areas without amyloid deposits ('non-plaque-associated microglia') over the 6-month

biweekly imaging period was  $\sim 20\%$  (Fig. 4d). This number is only slightly higher than the number of microglial cells lost in the wild-type mice over the same imaging period ( $\sim 13\%$ , see Fig. 3e). This suggests that even in the neocortex of a 10-month-old APPPS1 mouse, most (non-plaque-associated) microglia are the same cells that populated the brain early during development. However, in contrast to the comparable rates of cell proliferation and loss in wild-type animals, the division of non-plaque-associated microglia was at least three times more frequent than the loss of these cells in APPPS1 animals (Fig. 4d). As in wild-type mice, newly appearing tdTomato-positive microglia first emerged close to an existing tdTomato-positive cell, but in the APPPS1 mice they then moved toward nearby amyloid plaques (Fig. 4a–c). Notably, and in contrast to non-plaque-associated cells, the rates at which plaque-associated microglia disappeared and proliferated were almost identical (Fig. 4d). This indicates that the increase in the numbers of microglia around amyloid deposits<sup>24</sup> results from microglial proliferation in plaque-free areas. While we cannot rule out the possibility that some of the plaque-associated tdTomato-positive cells are derived from peripheral myeloid cells, the threefold increase in newly appearing microglia compared to lost microglia in the imaged volumes corresponds well to the threefold increase in total microglial number in the neocortex of APPPS1 mice at this age<sup>24</sup>.

### DISCUSSION

Our results show that in the absence of disease, the proliferation of microglia in the mouse neocortex appears to be a rather quiescent process, with roughly half of the microglia persisting until the end of the 26- to 28-month mean lifespan of C57BL/6 mice<sup>25</sup>. Microglia

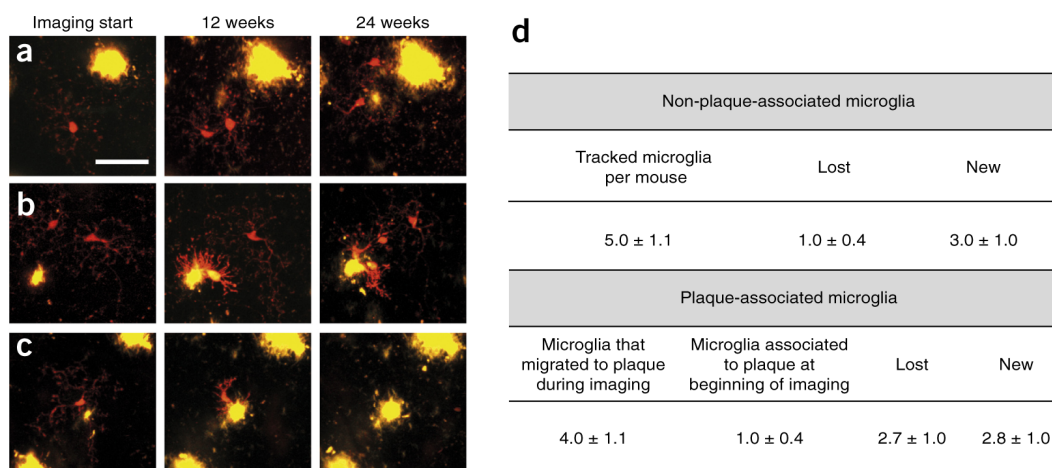


**Figure 4** Microglial turnover rate in the neocortex of a mouse model of cerebral  $\beta$ -amyloidosis. (a–c) Individual microglia (red) were tracked in young 4-month-old triple transgenic CD11b-CreERT2;R26-TdTomato;APP<sup>PS1</sup> mice after intraperitoneal injections with tamoxifen (see Fig. 1). Mice were injected with the dye hFTAA for visualization of amyloid plaques (yellow). Shown are three imaging time points of the biweekly imaging over 6 months. Microglia were classified as non-plaque-associated if their processes were visibly ramified and the cell body was not in contact with a plaque. Division of non-plaque-associated microglia and subsequent movement of the newly appearing microglia to the plaque is shown in a and b. In some instances, the non-plaque-associated microglia divided again at a later time point (b). Non-plaque-associated microglia can passively become associated with plaques by the emergence of a plaque in close vicinity (c). Scale bar is 40  $\mu$ m. (d) For quantification, non-plaque-associated microglia and those contacting the plaque were analyzed separately to determine the average number of tdTomato-positive microglial cells tracked per mouse, the number of lost cells and number of newly appearing cells during the imaging period. Given is the mean  $\pm$  s.e.m. of  $n = 9$  mice. Note that the loss of non-plaque-associated microglia was similar to cell loss in wild-type mice, while these microglia divided three times as often as cells in wild-type mice (Fig. 3e). Moreover, virtually all newly generated microglial cells moved to the plaques during the 6-month imaging period; thereafter they were assessed as plaque-associated microglia. Data of individual mice ( $n = 9$  mice; total 54 cells) are presented in **Supplementary Table 2**.

thus are very long-lived tissue-resident macrophages, and this appears to be true even for some microglia in APP<sup>PS1</sup> mice with profuse age-related  $\beta$ -amyloid deposition. Our data further indicate that newly appearing microglial cells are derived from the division of resident, mature microglia, and not from still undefined microglial precursor cells<sup>26,27</sup>. Brain-region-dependent diversity of microglia has been described<sup>28</sup>, and region-specific differences in microglial turnover are likely (for example, a higher rate has been described in the olfactory bulb)<sup>14–16</sup>.

We do not yet know whether the division of microglia is symmetrical or asymmetrical<sup>29</sup>; that is, whether the chronologically younger cell is also biologically younger. However, the idea that the aged brain contains both senescent and young cells is fully consistent with the finding of heterogeneous decline and increased variability in microglial function in the aged brain<sup>7,30</sup>. The finding that microglia in a given animal show considerable heterogeneity in terms of their individual age will be important for the interpretation of results from genomic and transcriptomic profiling of pooled microglia<sup>1,28</sup>, and even more so for future single-cell analyses.

Overall, our observations show that stability of the microglial population and longevity of individual resident microglia are fundamental features of the mouse neocortex under homeostatic and even some pathological conditions. Because the mice that we analyzed were maintained in a pathogen-free, controlled and stable environment, translation of our findings to humans is uncertain. Nevertheless, a heterogeneous microglial population with senescent cells has also been described in the aging human brain<sup>30</sup>. Furthermore, other cell types in the brain, such as neurons and oligodendrocytes, have been shown to persist for the entire lifespan of humans<sup>31</sup>. If the longevity of microglia is proportional to the lifespan of the species in which they reside (or, as in the case of neurons and oligodendrocytes, greater in humans than in mice), the present findings are consistent with the idea that individual microglia could persist throughout the entire

human lifespan. This extraordinary longevity provides a mechanistic explanation for how stimulation of microglia early in life can induce long-term changes in human brain function and also suggests how the senescence of resident microglia might contribute to the age-related increase in risk for neurodegenerative diseases<sup>19,20,22,32</sup>.

## METHODS

Methods, including statements of data availability and any associated accession codes and references, are available in the [online version of the paper](#).

*Note: Any Supplementary Information and Source Data files are available in the online version of the paper.*

## ACKNOWLEDGMENTS

We thank L. Walker, G. Kempermann and M. Staufenbiel, as well as all other laboratory members, for help and comments on the manuscript, and P. Nilsson (Linköping University) for providing the LCO amyloid dye. This work was supported by internal institutional funds from the Ministry of Science, Research and the Arts, Baden-Wuerttemberg (M.J.), by a Ph.D. fellowship of the Studienstiftung des Deutschen Volkes (A.-C.W.), by National Institute of Health grants AG021494 and AG027854 (S.S.S., K.V.) and by the Cure Alzheimer's Fund (S.S.S.).

## AUTHOR CONTRIBUTIONS

P.F., J.K.H., J.J.N., A.S., M.J. designed the study. P.F., C.S., A.-C.W., U.O., B.M.W.-B. and A.S. performed the experimental imaging work. K.V., S.K., M.T., R.F. and S.S.S. generated the mouse models. A.S. and P.M. did the statistical analysis. The manuscript was prepared by P.F., J.J.N., A.S. and M.J. with the help of all authors.

## COMPETING FINANCIAL INTERESTS

The authors declare no competing financial interests.

Reprints and permissions information is available online at <http://www.nature.com/reprints/index.html>. Publisher's note: Springer Nature remains neutral with regard to jurisdictional claims in published maps and institutional affiliations.

- Crotti, A. & Ransohoff, R.M. Microglial physiology and pathophysiology: insights from genome-wide transcriptional profiling. *Immunity* **44**, 505–515 (2016).
- Ginhoux, F. *et al.* Fate mapping analysis reveals that adult microglia derive from primitive macrophages. *Science* **330**, 841–845 (2010).
- Sheng, J., Ruedl, C. & Karjalainen, K. Most tissue-resident macrophages except microglia are derived from fetal hematopoietic stem cells. *Immunity* **43**, 382–393 (2015).
- Ajami, B., Bennett, J.L., Krieger, C., Tetzlaff, W. & Rossi, F.M. Local self-renewal can sustain CNS microglia maintenance and function throughout adult life. *Nat. Neurosci.* **10**, 1538–1543 (2007).
- Hashimoto, D. *et al.* Tissue-resident macrophages self-maintain locally throughout adult life with minimal contribution from circulating monocytes. *Immunity* **38**, 792–804 (2013).
- Pelvig, D.P., Pakkenberg, H., Stark, A.K. & Pakkenberg, B. Neocortical glial cell numbers in human brains. *Neurobiol. Aging* **29**, 1754–1762 (2008).
- Hefendehl, J.K. *et al.* Homeostatic and injury-induced microglia behavior in the aging brain. *Aging Cell* **13**, 60–69 (2014).
- Nimmerjahn, A., Kirchhoff, F. & Helmchen, F. Resting microglial cells are highly dynamic surveillants of brain parenchyma *in vivo*. *Science* **308**, 1314–1318 (2005).
- Prinz, M. & Priller, J. Microglia and brain macrophages in the molecular age: from origin to neuropsychiatric disease. *Nat. Rev. Neurosci.* **15**, 300–312 (2014).
- Ransohoff, R.M. How neuroinflammation contributes to neurodegeneration. *Science* **353**, 777–783 (2016).
- Sierra, A. *et al.* The “big-bang” for modern glial biology: translation and comments on Pío del Río-Hortega 1919 series of papers on microglia. *Glia* **64**, 1801–1840 (2016).
- Gómez-Nicola, D., Fransen, N.L., Suzzi, S. & Perry, V.H. Regulation of microglial proliferation during chronic neurodegeneration. *J. Neurosci.* **33**, 2481–2493 (2013).
- Graeber, M.B. *et al.* The microglia/macrophage response in the neonatal rat facial nucleus following axotomy. *Brain Res.* **813**, 241–253 (1998).
- Lawson, L.J., Perry, V.H. & Gordon, S. Turnover of resident microglia in the normal adult mouse brain. *Neuroscience* **48**, 405–415 (1992).
- Askew, K. *et al.* Coupled proliferation and apoptosis maintain the rapid turnover of microglia in the adult brain. *Cell Rep.* **18**, 391–405 (2017).
- Tay, T.L. *et al.* A new fate mapping system reveals context-dependent random or clonal expansion of microglia. *Nat. Neurosci.* **20**, 793–803 (2017).
- Nowakowski, R.S. & Hayes, N.L. New neurons: extraordinary evidence or extraordinary conclusion? *Science* **288**, 771 (2000).
- Rakic, P. Neurogenesis in adult primates. *Prog. Brain Res.* **138**, 3–14 (2002).
- Knuesel, I. *et al.* Maternal immune activation and abnormal brain development across CNS disorders. *Nat. Rev. Neurol.* **10**, 643–660 (2014).
- Perry, V.H. & Holmes, C. Microglial priming in neurodegenerative disease. *Nat. Rev. Neurol.* **10**, 217–224 (2014).
- Heppner, F.L., Ransohoff, R.M. & Becher, B. Immune attack: the role of inflammation in Alzheimer disease. *Nat. Rev. Neurosci.* **16**, 358–372 (2015).
- Streit, W.J., Xue, Q.S., Tischer, J. & Bechmann, I. Microglial pathology. *Acta Neuropathol. Commun.* **2**, 142 (2014).
- Hefendehl, J.K. *et al.* Repeatable target localization for long-term *in vivo* imaging of mice with 2-photon microscopy. *J. Neurosci. Methods* **205**, 357–363 (2012).
- Radde, R. *et al.* Aβ42-driven cerebral amyloidosis in transgenic mice reveals early and robust pathology. *EMBO Rep.* **7**, 940–946 (2006).
- Jucker, M. & Ingram, D.K. Murine models of brain aging and age-related neurodegenerative diseases. *Behav. Brain Res.* **85**, 1–26 (1997).
- Bruttger, J. *et al.* Genetic cell ablation reveals clusters of local self-renewing microglia in the mammalian central nervous system. *Immunity* **43**, 92–106 (2015).
- Elmore, M.R. *et al.* Colony-stimulating factor 1 receptor signaling is necessary for microglia viability, unmasking a microglia progenitor cell in the adult brain. *Neuron* **82**, 380–397 (2014).
- Grabert, K. *et al.* Microglial brain region-dependent diversity and selective regional sensitivities to aging. *Nat. Neurosci.* **19**, 504–516 (2016).
- Moore, D.L. & Jessberger, S. Creating age asymmetry: consequences of inheriting damaged goods in mammalian cells. *Trends Cell Biol.* **27**, 82–92 (2017).
- Streit, W.J., Sammons, N.W., Kuhns, A.J. & Sparks, D.L. Dystrophic microglia in the aging human brain. *Glia* **45**, 208–212 (2004).
- Frisén, J. Neurogenesis and gliogenesis in nervous system plasticity and repair. *Annu. Rev. Cell Dev. Biol.* **32**, 127–141 (2016).
- Hoeijmakers, L., Heinen, Y., van Dam, A.M., Lucassen, P.J. & Korosi, A. Microglial priming and Alzheimer's disease: a possible role for (early) immune challenges and epigenetics? *Front. Hum. Neurosci.* **10**, 398 (2016).

## ONLINE METHODS

**Generation of CD11b-CreERT2 mice.** The CD11b-CreERT2 construct was generated in a pSP73 vector background with the following elements ligated in tandem: the 1,723-bp human *CD11b* (*ITGAM*) promoter, a 2,578-bp fragment encoding a rabbit  $\beta$ -globin intron and the *CreERT2* sequence, a 603-bp transcript-stabilizing WPRE sequence and a 170-bp spanning SV-40 poly(A) sequence. To generate transgenic mice, the CD11b-CreERT2 sequence was linearized with restriction enzymes AflII and PacI to remove the vector backbone. The remaining 5,074-bp fragment was purified for pronuclear injections. The cassette was injected into fertilized mouse oocytes from C57BL/6J  $\times$  C3HeJ strains. Potential founders were screened by PCR genotyping and positive founders were crossed to non-transgenic C57BL/6J  $\times$  C3HeJ F<sub>1</sub> strains to obtain an F<sub>1</sub> generation that stably inherited the transgene. To validate the activity of the *CD11b-CreERT2* transgene in microglia, three founder lines were crossed with the reporter strain Gt[ROSA]26Sor<sup>tm4[ACTB-tdTomato,-EGFP]Luo/J</sup> (JAX number 007576)<sup>33</sup>, used to identify cell-type-specific Cre activity. Bigenic mice carrying both *CD11b-CreERT2* and the *ROSA26* reporter transgene were tested for tamoxifen-induced Cre activity in microglia. The founder line with the most robust and microglia-specific recombination was chosen for further breeding (F9 line). Mice were generated at the University of Chicago transgenic facility in accordance with the institutional regulations for animal use, which was approved by the Institutional Animal Care and Use Committee (IACUC).

**Mice used for imaging.** CD11b-CreERT2 mice were crossed to the B6.Cg-Gt[ROSA]26Sor<sup>tm14(CAG-tdTomato)Hze/J</sup> reporter line, harboring a *loxP*-flanked STOP codon followed by the fluorescent protein tdTomato in the *ROSA26* locus (R26-tdTomato; JAX number 007914)<sup>34</sup>. Some of the double transgenic CD11b-CreERT2;R26-tdTomato mice were further crossed to either *Iba1-eGFP* mice that express enhanced GFP under the *Iba1* promoter (generated and maintained on a C57BL/6J (B6) background<sup>7,35</sup>) or APPPS1 mice that express human APP<sub>KM670/671NL</sub> and PS1<sub>L166P</sub> under the control of the *Thy1* promoter (generated and maintained on a B6 background<sup>24</sup>) to generate triple transgenic CD11b-CreERT2;R26-tdTomato;Iba1-eGFP and CD11b-CreERT2;R26-tdTomato;APPPS1 mice, respectively.

**Tamoxifen-induced recombination of tdTomato.** To study the induction and specificity of tdTomato-labeling in microglia, CD11b-CreERT2;R26-tdTomato or CD11b-CreERT2;R26-tdTomato;Iba1-eGFP mice were i.p. injected once, twice or five times with 100  $\mu$ g tamoxifen (TAM, Sigma-Aldrich) per gram body weight dissolved in corn oil (Sigma-Aldrich) containing 5% ethanol. Mice were analyzed 4 weeks later (**Supplementary Fig. 1**). Based on these results, two TAM injections 48 h apart (100  $\mu$ g of TAM per gram of body weight) were selected for the present study and revealed labeling of approximately 2% of neocortical microglia (**Supplementary Fig. 1**). Male and female mice were included in the imaging study and all were treated with TAM at an age of 7 to 8 weeks. Four to 6 weeks after induction of recombination, mice underwent cranial window surgery (see below).

**Flow cytometry and histological analysis of recombination efficiency and specificity.** Mice were deeply anesthetized using sedaxylan and ketamine (64 mg/kg and 472 mg/kg, respectively) and transcardially perfused with ice-cold PBS for 2 min. For flow cytometry, the neocortex from one brain hemisphere was dissected and finely minced in ice-cold HBSS (Invitrogen) containing 15 mM HEPES, 0.54% D-glucose and 1 mg/ml DNase (Sigma). Minced tissue was sequentially processed in glass Dounce and Potter homogenizers and resulting homogenates were filtered through a 70- $\mu$ m cell strainer and centrifuged at 300g for 10 min at 4 °C. The resulting pellet was resuspended in 70% isotonic Percoll solution, overlaid with 37% and 30% isotonic Percoll layers and centrifuged for 30 min at 800g and 4 °C. Cells were recovered from the 70/37% gradient interface and washed in FACS buffer (PBS, 2% FCS, 10 mM EDTA). Cells were resuspended and incubated with Fc-block (BD Bioscience) for 10 min on ice, followed by staining for 15 min at 4 °C with CD11b–brilliant violet 785 (1:200, BioLegend) and CD45–Alexa Fluor 700 (1:100, Biozol). Cells were analyzed on a Sony SH800 device.

The other hemisphere was immersion-fixed in 4% paraformaldehyde (PFA)/PBS for 24 h and placed in 30% sucrose/PBS for another 48 h. Brains were frozen in 2-methylbutane and serially sectioned on a freezing-sliding microtome at 25  $\mu$ m. For each animal the total number of tdTomato-positive

cells in a random set of every 12th section was counted to get an estimate of the total number per neocortex.

**Cranial window surgery.** The surgery has been described in detail previously<sup>23</sup>. In short: under general anesthesia (fentanyl 0.05 mg/kg, midazolam 5 mg/kg, medetomidin 0.50 mg/kg) a circular section of the skull was removed (from the midline  $\pm$ 2 mm and approximately 0.0 to  $-$ 4.0 mm from the bregma) and the opening was covered with a 4-mm-diameter sterile cover slip sealed to the skull with light-curing dental cement. A custom-made titanium ring<sup>23</sup> (14 mm diameter) was attached to the skull above the cranial window using light-curing dental cement to enable head fixation of the mouse during imaging and thereby repeated imaging of identified positions in the cortex. After surgery, mice were singly housed and allowed to recover for at least 2 weeks before imaging was started. All procedures were conducted in accordance with animal protocols approved by the local Animal Care and Use Committees (Baden-Wuerttemberg, Germany).

**Imaging.** Mice were anesthetized with isoflurane vapor mixed in pure O<sub>2</sub> (induction at 3% isoflurane; isoflurane subsequently reduced and held constant at 1.5% during imaging). Some mice were injected i.v. with dextran-fluorescein (70,000 DA molecular weight; 12.5 mg/ml in sterile PBS; Invitrogen) for a fluorescence angiogram to confirm repositioning at identified positions. For visualization of amyloid- $\beta$  plaques, CD11b-CreERT2;R26-tdTomato;APPPS1 mice were i.v. injected once before the first imaging session with 5  $\mu$ g per gram of body weight of the amyloid-staining dye hFTAA<sup>36,37</sup> dissolved in sterile PBS. This amyloid-staining dye binds stably to amyloid plaques for up to 6 months<sup>38</sup>). Before each imaging session, the cranial window was cleaned with ddH<sub>2</sub>O. The anesthetized mouse was affixed to the microscope stage by attaching the titanium ring to the custom-built head fixation apparatus connected to the motorized *xy* stage of the microscope, enabling precise relocation of the previously imaged positions<sup>23</sup>.

Two-photon *in vivo* imaging was performed on a Leica SP2 upright confocal microscope equipped with a tunable Spectra-Physics Mai-Tai laser (710–990 nm) coupled to a pulse compressor (FemtoControl, APE, Berlin) for pulse spectral dispersion compensation, ensuring optimal two-photon excitation using the least possible laser intensity. We used two-photon excitation at 990 nm and a 25 $\times$  HCX IRAPO water-immersion objective (0.95 NA; Leica Microsystems). Fluorescence was detected using the non-descanned port of the microscope; fluorescence emission signal was split between two PMTs by an LP 560 nm beamsplitter, ensuring minimal light loss and reliable spectral separation of tdTomato and GFP or dextran-fluorescein signals. Care was taken to ensure similar fluorescence excitation levels during all imaging sessions by adjusting the laser power using standard fluorescence calibration beads (ImSpeck beads, Invitrogen). For each mouse, typically four to six different *xyz* positions were chosen, with at least one tdTomato-positive microglial cell visible in each. Each position spanned 282  $\times$  282  $\mu$ m<sup>2</sup> in *xy* and 200–250  $\mu$ m in depth (voxel size 0.27  $\times$  0.27  $\times$  1.49  $\mu$ m<sup>3</sup>).

### Quantitative analysis of microglial loss and newly appearing microglia.

A Gaussian filter of 1 pixel (ImageJ, Version 1.51f) was applied to the image stacks to remove grain noise from the detectors, rendering the images smoother and improving the localization of microglia processes. To determine the gain and loss of tdTomato-expressing microglia and to avoid edge effects from cells potentially moving in or out of the imaged volume, only cells that were at least 50  $\mu$ m from the top, bottom and sides of the imaged volumes were considered for the analysis ('guard volume'). The distance of 50  $\mu$ m was selected because we have previously shown<sup>7</sup> that some microglial cells can move up to 25  $\mu$ m within 2 weeks. Using 50  $\mu$ m as a guard area ensures no misclassification of migrating microglia as newly appearing cells in the 2-week imaging interval. Moreover, initial analyses indicated that microglial proliferation was somewhat higher in the uppermost cortical regions—that is, close to the cranial window—potentially resulting from the surgery (although microglial activation in response to surgical and imaging procedures was not detectable; **Supplementary Figure 1**). Therefore, microglia within 50  $\mu$ m of the optical window were excluded from analysis.

**Kaplan–Meier survival and exponential distribution fit.** Survival probabilities were estimated using the Kaplan–Meier method. The disappearance of a tracked tdTomato microglia was marked as a death event. The estimated time of death was taken as the middle point of the interval from the last time-point the cell



was observed to the next point where the cell disappeared. All acquired data points were left-censored; that is, the lifetime of the microglia between mouse birth and before the imaging starting point was ignored (as it cannot be known), thus underestimating the actual lifetimes of the cells. A log-rank test was used to check whether survival curves were statistically different; the resulting *P*-value of 0.203 indicates no statistically significant differences between the young and adult group survival times.

Using the Kaplan–Meier survival data, we fitted the standard exponential CDF ( $p(X \leq x) = 1 - e^{-\lambda x}$ ) to the cumulative probability of cells dying (as the complement to the number of cells surviving at a certain time), using the nonlinear fit algorithm of the Statistics toolbox in Matlab. For the young group, the mean  $x$  of the fitted curve, defined as the inverse of the fitted  $\lambda$ , was calculated as 889 d; for the adult group, the mean was calculated as 674 d.

For sensitivity analysis we used the maximum likelihood (ML) approach as described by Collet<sup>39</sup> to estimate the mean survival times, which led to even longer mean life times (1,107 and 778 d for the young and adult groups, respectively). These larger values were obtained because ML takes into account the censored observations, which include very long-lived cells (the last censored observations visible in the Kaplan–Meier curve). The exponential curve resulting from the ML estimates, however, did not fit well to the cumulative probabilities of cell dying, and thus we instead used the shorter mean lifetimes calculated from the fitted exponential. Note that both approaches use extrapolations to estimate the mean survival, which lies in a time range with no observations.

**Counting microglial numbers in 3D stacks.** To exclude changes in microglial numbers within the imaged 3D stacks, GFP-expressing microglia in imaged triple transgenic CD11b-CreERT2;R26-tdTomato;Iba1-eGFP mice were counted using the software IMARIS (8.3.1; Bitplane). For the analysis, microglial cells detected at the first imaging time point and the imaging time point after 6 months were used. Counting was done automatically using the spot recognition tool in IMARIS. Stacks were further edited manually to delete false positives and include cells missed by the software.

**Nearest neighbor analysis.** Microglia were classified into new vs. old (stable) cells and green vs. red/green cells. To determine the distance of new tdTomato-expressing microglia to neighboring microglia, we used the 3D stack of the time point in which the new cells were detected for the first time in double CD11b-CreERT2;R26-tdTomato and triple CD11b-CreERT2;R26-tdTomato;Iba1-eGFP transgenic animals. Distances of control Iba1-GFP-positive resting microglia were determined in the triple transgenic animals (CD11b-CreERT2;R26-tdTomato;Iba1-eGFP) at the same time point. For calculation of distances, the *xyz* position of each microglia within the imaged area was determined using the IMARIS spot recognition tool fitting a sphere to the microglial cell body. Pairwise Euclidean distances between the sphere centroid *xyz* positions were calculated to determine the nearest neighbor cell to each microglia cell. If microglia were closer to the border of the imaged area than to their nearest calculated neighbor, they were excluded from analysis to account for the possibility of a nearest neighbor outside the imaging field.

**BrdU labeling.** Incorporation of bromodeoxyuridine (BrdU) into microglia was done by i.p. injection of BrdU (150 µg/g body weight, Sigma), dissolved in 0.9% NaCl, for 5 consecutive days. Three days after the last BrdU application, mice were overdosed with ketamine/xylazine and transcardially perfused with PBS. Brains were removed and postfixed in 4% PFA/PBS for 24 h and placed in 30% sucrose/PBS for another 48 h. Brains were frozen in 2-methylbutane and serially sectioned on a freezing-sliding microtome at 25 µm.

**Immunofluorescence double labeling and quantification.** To investigate the number of microglial cells that incorporated BrdU, double immunofluorescence staining was performed using BrdU and the microglial marker Iba1. Sections were pretreated for 2 h at 65 °C in 50% formamide in 2× SSC buffer, followed by two incubations for 10 min each in 2× SSC buffer at room temperature, 30 min in 2 N HCl at 37 °C and 10 min in 0.1 M borate buffer at room temperature and washing of the sections for 3 × 10 min in PBS. Sections then were then blocked in 5% NGS, 0.3% Triton in PBS for 30 min and incubated with primary antibodies in 2% NGS, 0.3% Triton in PBS at 4 °C overnight (anti-BrdU, AB6326, rat monoclonal, 1:2,000, Abcam; anti-Iba1, 019-19741, rabbit polyclonal, 1:1,000, Wako). After washing (three times for 10 min each in PBS), sections were incubated with fluorescent secondary antibodies in 2% NGS, 0.3% Triton in PBS for 90 min at

room temperature (goat-anti rat Alexa568, A11077; goat-anti rabbit Alexa488, A11008, 1:250; Life Technologies). Sections were mounted in Dako fluorescence embedding medium and stored in the dark at 4 °C. For analysis, the number of double-labeled cells of every 24th systematically sampled section in the neocortex of the left brain hemisphere was counted using a fluorescence microscope (Axioplan 2, Zeiss). The rater was blinded with respect to the groups.

**Stereological quantification of microglia.** PFA-fixed brain sections of the BrdU-treated mice were immunohistochemically stained using the Vectastain Elite ABC Kit (Vector Laboratories) and a polyclonal antibody for the microglial marker Iba1 (anti-Iba1, rabbit polyclonal, 1:1,000, Wako, catalog number 019-19741). After primary antibody incubation (4 °C overnight) sections were incubated in biotinylated secondary anti-rabbit IgG (1:250; Vector Laboratories, catalog number PK-6101) for 45 min at room temperature, followed by incubation in the avidin–biotin–peroxidase complex solution (45 min at room temperature). The chromogen was Vector SG (Vector Laboratories). Total microglial numbers were assessed on every 24th systematically sampled section using a motorized *xyz* stage coupled to a videomicroscopy system and the Stereologer software (Stereo Investigator 6). The optical fractionator technique was used with 3D disectors (grid size 500 × 500 µm<sup>2</sup>; height 15 µm; guard height 2 µm; counting frame 100 × 100 µm<sup>2</sup>). Iba1-positive cells with complete somata within the disector volume were counted and the total number of neocortical microglial cells per brain was estimated. The operator was blinded with respect to the groups.

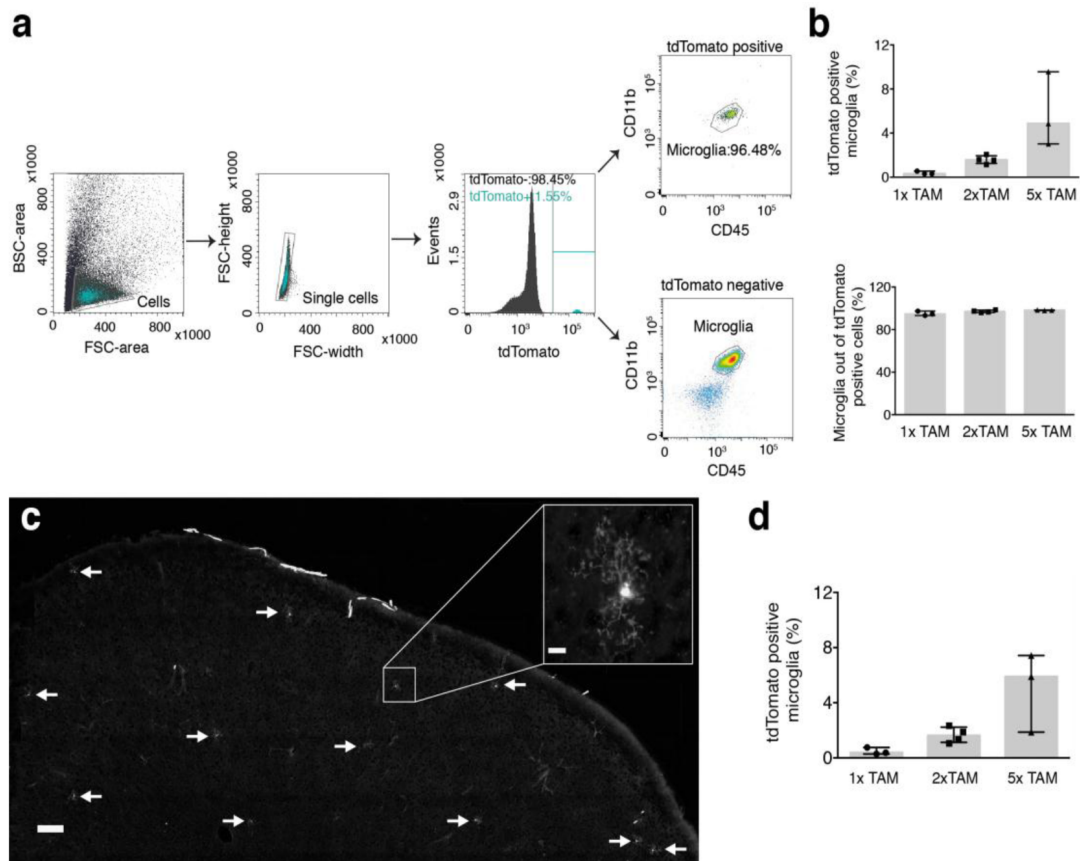
**Horizontal and coronal cutting to assess potential microglial activation after imaging.** PFA-fixed brains of imaged triple transgenic mice (CD11b-CreERT2;R26-tdTomato;Iba1-eGFP) and un-imaged control mice of the same age were sectioned horizontally or coronally at 25 µm on a freezing-sliding microtome and immunohistochemically stained using the Vectastain Elite ABC Kit (Vector Laboratories) and a polyclonal antibody for the microglial marker Iba1 (Wako, catalog number 019-19741). Microglial morphology was assessed within the area of the craniotomy (from the midline ±2 mm and approximately 0.0 to –4.0 mm from the bregma) up to a depth of 500 µm.

**Statistics.** No statistical methods were used to predetermine sample sizes; however, our sample sizes are similar to those reported in recently published similar studies<sup>15,16</sup> and even more animals were used in our long-term study. For the nearest neighbor analysis (Fig. 3d) the Mann–Whitney test was used to compare the medians, as the two data sets did not pass the D’Agostino and Pearson normality test. For the statistical comparison of Iba1-eGFP microglia within imaged volumes (Fig. 3) a paired *t*-test was carried out, as the data passed the D’Agostino and Pearson normality test. Due to the low cell turnover over the course of imaging (new or lost cells in Figs. 3e and 4d), as per our hypothesis, no statistical testing was performed. For the total microglial number and the number of BrdU-labeled microglia (Supplementary Fig. 4), the Kruskal–Wallis test was used to compare the distribution means; data sets were too small to test for normality, and hence non-parametric tests were used, not assuming a normal distribution. All tests were performed using GraphPad Prism Version 6.

A Life Sciences Reporting Summary is available.

**Data availability.** The remaining data that support the findings of this study are available from the corresponding authors upon reasonable request.

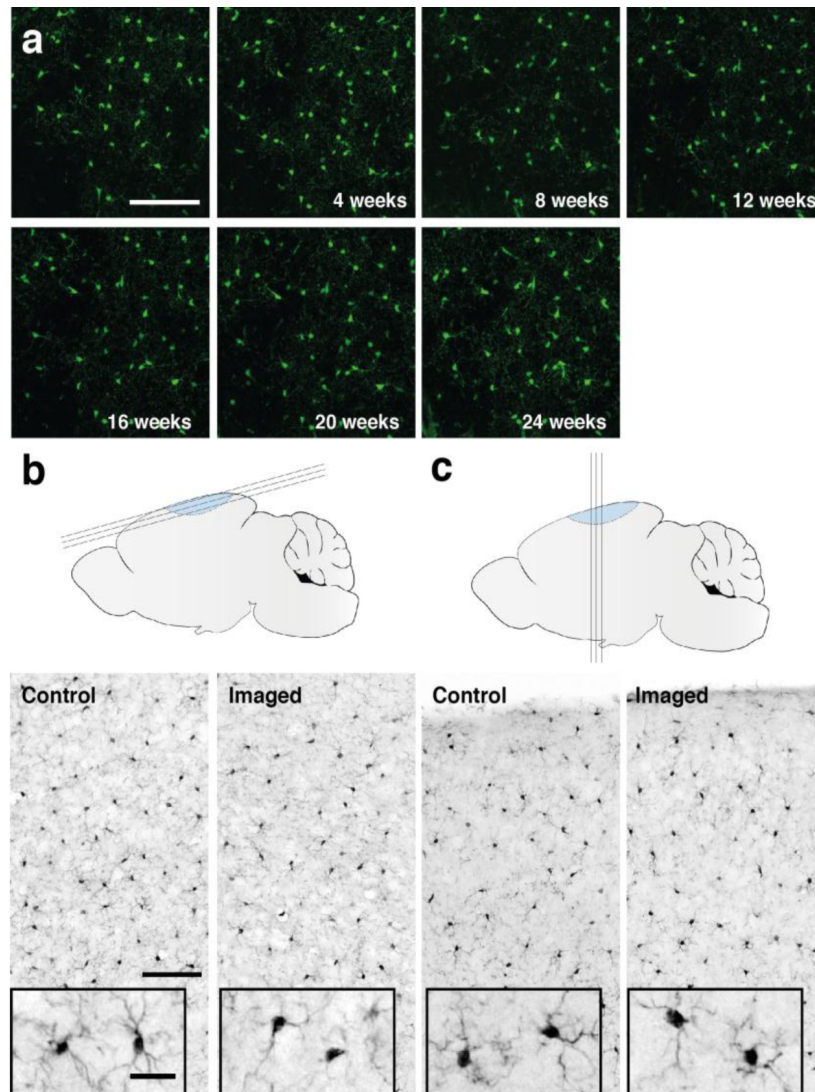
- Muzumdar, M.D., Tasic, B., Miyamichi, K., Li, L. & Luo, L. A global double-fluorescent Cre reporter mouse. *Genesis* **45**, 593–605 (2007).
- Madisen, L. *et al.* A robust and high-throughput Cre reporting and characterization system for the whole mouse brain. *Nat. Neurosci.* **13**, 133–140 (2010).
- Hirasawa, T. *et al.* Visualization of microglia in living tissues using Iba1-EGFP transgenic mice. *J. Neurosci. Res.* **81**, 357–362 (2005).
- Klingstedt, T. *et al.* Synthesis of a library of oligothiophenes and their utilization as fluorescent ligands for spectral assignment of protein aggregates. *Org. Biomol. Chem.* **9**, 8356–8370 (2011).
- Wegenast-Braun, B.M. *et al.* Spectral discrimination of cerebral amyloid lesions after peripheral application of luminescent conjugated oligothiophenes. *Am. J. Pathol.* **181**, 1953–1960 (2012).
- Mahler, J. *Ex vivo* and *in vivo* analysis of protein aggregates in transgenic mouse models of cerebral amyloidosis using luminescent conjugated oligothiophenes. MSc thesis, University of Tübingen (2012).
- Collet, D. *Modelling Survival Data in Medical Research* 2nd edn. (Chapman & Hall, New York, 2003).



## Supplementary Figure 1

### Genetic labeling of microglia

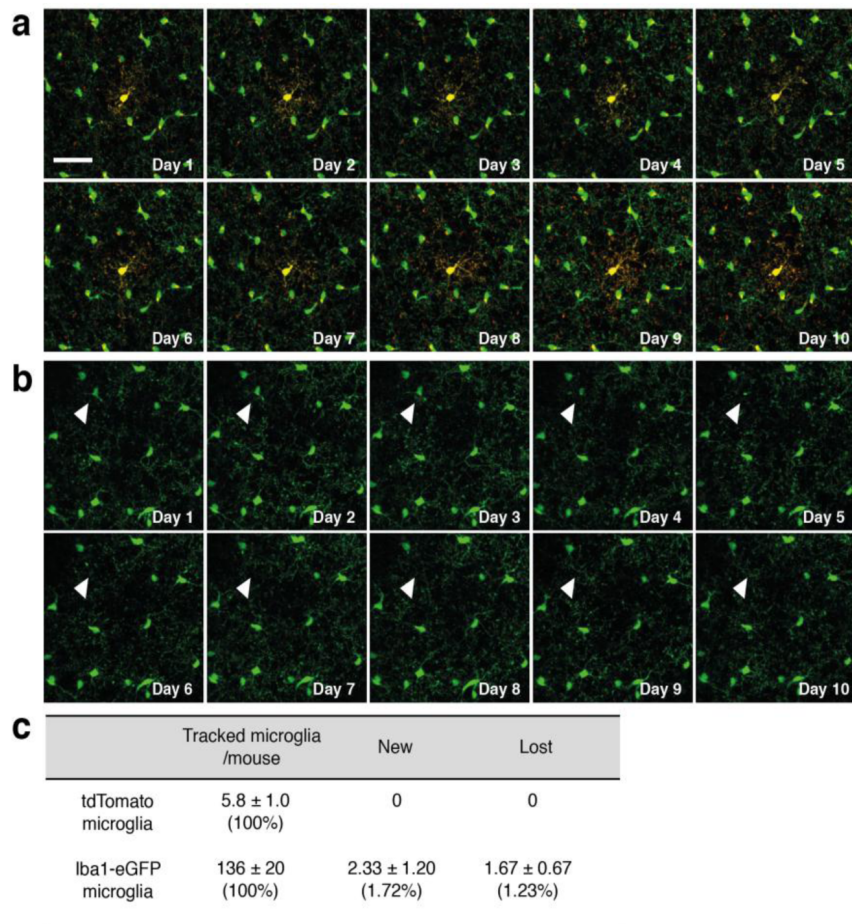
Male and female 2-3 month-old CreERT2;R26-tdTomato mice or CreERT2;R26-tdTomato;Iba1-eGFP transgenic mice were treated with 1x, 2x (48 h apart), or 5x (each 24 h apart) Tamoxifen (TAM; 100  $\mu$ g per gram bodyweight) and analyzed 4 weeks later. One hemisphere was used for flow cytometry (only the neocortex was used, see methods for details), the second hemisphere was used for histology. **(a)** Exemplary gating strategy of an animal injected with 2xTAM. Cells were gated based on forward (FSC) and backward scatter (BSC). FSC-width and height was used to determine single cells. 1.55% of single cells were tdTomato positive, of which the vast majority (approximately 97%) were microglia, identified as the CD11b<sup>high</sup> and CD45<sup>low</sup> cell population by flow cytometry. tdTomato-positive microglia were not distinguishable from tdTomato-negative microglia in size and granularity, as indicated by their similar position in the FSC/BSC blot (tdTomato-positive cells colour-coded in green) and were distributed across the microglial population based on CD11b and CD45 intensity. **(b)** Flow cytometric analysis of the neocortex revealed a dose-dependent increase in the induction of tdTomato-positive cells, of which the vast majority were microglia (n=3, 4, 3 mice per group, for 1x, 2x, and 5x TAM, respectively). **(c)** Histological analysis of tdTomato-positive microglia (arrows) revealed an apparent random distribution throughout the neocortex (shown in the frontal cortex). Morphologically, tdTomato-labeled microglial cells revealed all aspects of mature microglia (insert). Scale bars 100  $\mu$ m and 10  $\mu$ m for the insert. Some perivascular macrophages also showed recombination, but were clearly distinguishable from microglia due to their elongated shape and lack of processes. **(d)** The total number of tdTomato-positive cells per neocortex was estimated and related to the total number of Iba-1-positive microglia in the neocortex (the latter was assessed in **Supplementary Figure 4** and the mean number of 880,000 was used for the calculation). In accordance with the flow cytometry analysis, a dose-dependent and comparable increase was found (n=3, 4, 3 mice per group, for 1x, 2x, and 5x TAM, respectively).



## Supplementary Figure 2

Long-term repetitive *in vivo* imaging does not cause microglial activation

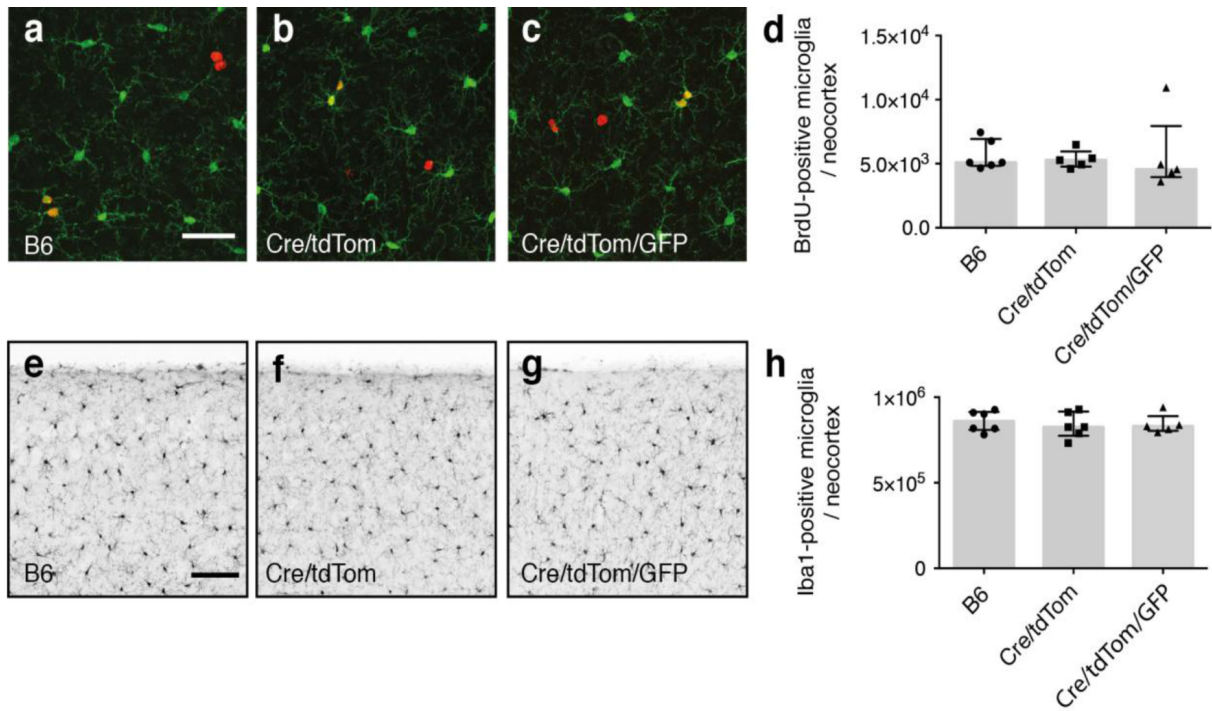
(a) There was no noticeable activation of microglial cells in any of the *in vivo* imaged areas. Shown are *in vivo* images (z-projections of imaged volumes) of a triple-transgenic CD11b-CreERT2;R26-tdTomato;Iba1-eGFP mouse after an imaging period of 24 weeks (6 months). Scale bar is 100  $\mu\text{m}$ . (b, c) Consistently, postmortem immunohistochemical analysis of the triple-transgenic CD11b-CreERT2;R26-tdTomato;Iba1-eGFP animals after the 24 week-imaging period using an Iba1-antibody did not reveal any signs of microglial activation, regardless of whether the cortical tissue was cut horizontally (b) or coronally (c), when compared to a non-imaged control animal of the same age. Blue area indicates the location of the cranial window. Three imaged and three control mice were analysed. Scale bars are 100  $\mu\text{m}$  and 20  $\mu\text{m}$  for the insert.



### Supplementary Figure 3

#### Daily imaging of neocortical microglial cells rules out rapid cell turnover

To study potential rapid replacement of microglial cells that would have been unrecognized in our long-term biweekly imaging protocol (see Fig. 1 and 2), three CD11b-CreERT2;R26-tdTomato;Iba1-eGFP mice (13 months of age; one male, two females) and two CD11b-CreERT2;R26-tdTomato mice (13 months of age; two males) were imaged daily for 10 consecutive days. (a, b) Shown are z-projections of imaged volumes of CD11b-CreERT2;R26-tdTomato;Iba1-eGFP mice where recombined microglia appeared yellow while surrounding microglia were green. An example of a recombined yellow microglial cell with surrounding green cells that are all stable over the imaging period of ten days is shown in (a). An example with a lost green microglial cell on day 5 is shown in (b). Scale bar is 40  $\mu$ m. Note that in contrast to the long-term biweekly imaging (Fig. 2), the daily imaging also allowed us to track the Iba1-eGFP positive cells (green) since movement from day-to-day was minimal. (c) Average number of tdTomato-positive and Iba1-eGFP-positive cells tracked per mouse, the number of newly appearing cells (New) and the number of lost cells (Lost) during the imaging period. Given is the mean  $\pm$  SEM of n=5 mice. The analysis and tracking was done as described for the long-term analysis in Figure 3. Occasionally, additional structures, which were connected to microglial processes, were observed. In two cases, these resembled a cell body in shape and size, but were identified as being formed by distinct microglial processes reminiscent of recently described extruded exophers albeit in *C. elegans* (Melentijevic, I. *et al.* *C. elegans* neurons jettison protein aggregates and mitochondria under neurotoxic stress. *Nature* **542**, 367–371, 2017), whereas in three other instances, their composition was ambiguous. Though rapid splitting and consecutive death of the daughter cell in these cases cannot be ruled out, these observations were excluded from the analysis. Moreover, they do not change the lifetime estimate of the microglia.



#### Supplementary Figure 4

No difference was observed in total microglial numbers or the number of BrdU-labeled microglia in the different mouse lines used in this study

To exclude differences in microglial number or microglial proliferation based on BrdU incorporation, 7-month-old C57BL/6J mice, CD11b-CreERT2;R26-tdTomato;Iba1-eGFP (Cre/tdTom/GFP) mice and CD11b-CreERT2;R26-tdTomato (Cre/tdTom) mice of mixed gender were selected (n=5-6 per group). The selected age corresponds to the mid-time of the biweekly imaging period (4 months to 10 months) that was used for quantification in Figure 3. Mice were intraperitoneally injected on five consecutive days with BrdU and then analysed three days later. **(a-c)** Immunofluorescence double staining for Iba1 (green) and BrdU (red). Scale bar is 50  $\mu\text{m}$ . **(d)** Quantification of double-labeled (yellow) cells (Iba1/BrdU) in the neocortex revealed no differences in BrdU-labeled microglia among the three groups (Kruskal-Wallis,  $\chi^2_{(2)} = 2.19$ ,  $p > 0.05$ ); dataset was checked for outliers using Graphpad Prism's ROUT method and an outlier value was excluded from the Cre/tdTom dataset. **(e-g)** Immunohistochemical staining of the neocortex using an Iba1 antibody for the three genotypes. Scale bar is 100  $\mu\text{m}$ . **(h)** Stereological analysis of total neocortical microglia revealed no difference in microglial number between C57BL/6J control mice and the double- and triple-transgenic animals used in this study (Kruskal-Wallis,  $\chi^2_{(2)} = 0.10$ ,  $p > 0.05$ ).

### **3.3 Innate immune memory in the brain shapes neurological disease hallmarks**

Ann-Christin Wendeln\*, Karoline Degenhardt\*, Lalit Kaurani, Michael Gertig, Thomas Ulas, Gaurav Jain, Jessica Wagner, Lisa M. Häsler, Katleen Wild, Angelos Skodras, Thomas Blank, Ori Staszewski, Moumita Datta, Tonatiuh Pena Centeno, Vincenzo Capece, Md. Rezaul Islam, Cemil Kerimoglu, Matthias Staufenbiel, Joachim L. Schultze, Marc Beyer, Marco Prinz, Mathias Jucker, André Fischer, and Jonas J. Neher

*Accepted*

*Nature (2018)*

## Innate immune memory in the brain shapes neurological disease hallmarks

Ann-Christin Wendeln<sup>1,2,3\*</sup>, Karoline Degenhardt<sup>1,2,3\*</sup>, Lalit Kaurani<sup>4,5</sup>, Michael Gertig<sup>4,5</sup>, Thomas Ulas<sup>6</sup>, Gaurav Jain<sup>4,5</sup>, Jessica Wagner<sup>1,2,3</sup>, Lisa M. Häslér<sup>1,2</sup>, Katleen Wild<sup>1,2</sup>, Angelos Skodras<sup>1,2</sup>, Thomas Blank<sup>8</sup>, Ori Staszewski<sup>8</sup>, Moumita Datta<sup>8</sup>, Tonatiuh Pena Centeno<sup>5</sup>, Vincenzo Capece<sup>5</sup>, Md. Rezaul Islam<sup>5</sup>, Cemil Kerimoglu<sup>5</sup>, Matthias Staufenbiel<sup>1,2</sup>, Joachim L. Schultze<sup>6,7</sup>, Marc Beyer<sup>9</sup>, Marco Prinz<sup>8,10</sup>, Mathias Jucker<sup>1,2</sup>, André Fischer<sup>4,5</sup> and Jonas J. Neher<sup>1,2#</sup>

<sup>1</sup>German Center for Neurodegenerative Diseases (DZNE), Otfried-Müller-Str. 23, 72076 Tübingen, Germany

<sup>2</sup>Department of Cellular Neurology, Hertie Institute for Clinical Brain Research, University of Tübingen, Tübingen, Germany

<sup>3</sup>Graduate School of Cellular and Molecular Neuroscience, University of Tübingen, Tübingen, Germany

<sup>4</sup>Department of Psychiatry and Psychotherapy, University Medical Center Göttingen, Grisebachstr. 5, 37077 Göttingen, Germany

<sup>5</sup>Department for Systems Medicine and Epigenetics in Neurodegenerative Diseases, German Center for Neurodegenerative Diseases (DZNE) Göttingen, Von-Siebold-Str. 3a, D-37075 Göttingen

<sup>6</sup>Genomics and Immunoregulation, LIMES-Institute, University of Bonn, 53115, Bonn, Germany

<sup>7</sup>Platform for Single Cell Genomics and Epigenomics at the University of Bonn and the German Center for Neurodegenerative Diseases, Bonn, Germany

<sup>8</sup>Institute of Neuropathology, Faculty of Medicine, University of Freiburg, Freiburg, Germany

<sup>9</sup>Molecular Immunology in Neurodegeneration, German Center for Neurodegenerative Diseases (DZNE), Bonn, Germany

<sup>10</sup>BIOSS Centre for Biological Signalling Studies, University of Freiburg, Freiburg, Germany

\* *contributed equally*

# *corresponding author*

### Abstract

‘Innate immune memory’ is a vital mechanism of myeloid cell plasticity that occurs in response to environmental stimuli and alters subsequent immune responses. Two types of immunological imprinting can be distinguished, *training* and *tolerance*, which are epigenetically mediated and enhance or suppress subsequent inflammation, respectively. Whether immune memory occurs in tissue-resident macrophages *in vivo* and how it may affect pathology remains largely unknown. Here we demonstrate that peripherally applied inflammatory stimuli induce acute immune training and tolerance in the brain and lead to differential epigenetic reprogramming of brain-resident

macrophages, microglia, that persists for at least six months. Strikingly, in a mouse model of Alzheimer's pathology, immune training exacerbates cerebral  $\beta$ -amyloidosis while tolerance alleviates it; similarly, peripheral immune stimulation modifies pathological features after stroke. Our results identify immune memory in the brain as an important modifier of neuropathology.

### **Main text**

Contrary to the long-held assumption that immunological memory exists only in cells of the adaptive immune system, recent evidence indicates that myeloid cells also display memory effects<sup>1,2</sup>. For example, certain immune stimuli 'train' blood monocytes to generate enhanced immune responses to subsequent immune insults<sup>3,4</sup>. In contrast, other stimuli induce immune tolerance, i.e. suppression of inflammatory responses to subsequent stimuli<sup>3,5</sup>. Innate immune memory lasts for several days *in vitro* and for up to three months in circulating monocytes *in vivo* and is mediated by epigenetic reprogramming in cultured cells, with chromatin changes also apparent *in vivo*<sup>3,6,7</sup>. However, whether immune memory occurs in long-lived tissue-resident macrophages and whether it alters tissue-specific pathology remains unknown.

Microglia, the brain-resident macrophages, were recently shown to be very long-lived cells<sup>8,9</sup>. This makes them particularly interesting for studying immune memory, as virtually permanent modification of their molecular profile appears possible. As microglia are also known to significantly affect many neurological diseases<sup>10-12</sup>, we investigated whether immune memory occurs in microglia *in vivo* and how it affects neuropathology.

### **Acute immune memory in the brain**

It is well-established that inflammation in the periphery can prompt immune responses in the brain<sup>13</sup>. To evaluate whether immune memory is inducible in the brain by peripheral stimulation, mice received daily intraperitoneal injections of low-dose lipopolysaccharides (LPS) on four consecutive days, leading to mild sickness behaviour and temporary weight loss (Fig.1a and Extended Data Fig.1a). Three hours after application, the first LPS injection (1xLPS) led to a pronounced increase of blood cytokine levels, but only modest increases in brain cytokines. Upon the second injection (2xLPS), the blood levels of the pro-inflammatory cytokines IL-1 $\beta$ , TNF- $\alpha$ , IL-6, IL-12 and IFN- $\gamma$  were diminished compared to 1xLPS while IL-10 release



occurred at similar levels, indicating peripheral immune tolerance. In sharp contrast, brain cytokines were dramatically increased with 2xLPS injections, indicating a brain-specific training effect induced by the first LPS stimulus (Figs.1b/c and Extended Data Fig.2). Accordingly, a conspicuous morphological change in microglia occurred after 2xLPS, while activated (GFAP+) astrocytes only increased after 3xLPS (Extended Data Figs.1b-d). Importantly, 4xLPS virtually abolished TNF- $\alpha$ , IL-1 $\beta$  and IL-6 release in the brain while IL-10 remained elevated, indicating immune tolerance. Next, we examined the contribution of microglia to immune memory in the brain using inducible CX3CR1-CreER (Cre) mice crossed with mouse lines carrying loxP-flanked genes, where tamoxifen-induced Cre expression results in persistent recombination in long-lived microglia but not in short-lived myeloid cells, including blood monocytes<sup>14</sup>. We induced microglial knockout of either ‘transforming growth factor- $\beta$ -activated kinase 1’ (*Tak1*), which results in inhibition of NF- $\kappa$ B, JNK and ERK1/2 pathways<sup>14</sup>, or histone deacetylases-1 and -2 (*Hdac1/2*), two major regulators of epigenetic reprogramming and macrophage inflammatory responses<sup>15,16</sup>. As expected, tamoxifen-induced knockout of either *Tak1* or *Hdac1/2* did not alter the peripheral inflammatory response. Furthermore, brain cytokine levels were indistinguishable after 1xLPS, but the training effect following 2xLPS injections was virtually abolished in Cre+ animals. Notably, the cytokines showing the most pronounced training and tolerance effects (IL-1 $\beta$ , TNF- $\alpha$ , IL-6) were also most affected by microglial gene knockout (Figs.1b/c and Extended Data Fig.2), indicating that immune memory in the brain is predominantly microglia-mediated. Moreover, after 1xLPS, Cre+ and Cre- mice showed indistinguishable weight loss (Extended Data Fig.1a) and sickness behaviour (not shown); however, in animals with microglial *Tak1* knockout, sickness behaviour after 2xLPS was noticeably alleviated (Supplementary Movie 1).

After intraperitoneal injections, LPS was found in the blood but not in the brain, indicating that neither significant entry of LPS into the brain nor opening of the blood-brain barrier occurred, corresponding with previous reports<sup>17</sup>. The latter was confirmed by the absence of blood iron in the brain parenchyma. Also, using ‘type 2 CC chemokine receptor’ (CCR2) reporter mice<sup>18</sup>, no extravasation of circulating monocytes was found (Extended Data Figs.1e-g), confirming that immune memory was mediated by brain-resident macrophages alone.

### **Immune memory shapes neuropathology**

Next, we analysed whether the training- and tolerance-inducing stimuli 1xLPS and 4xLPS, respectively, could lead to long-term alterations of brain immune responses and thereby modify disease pathogenesis. APP23 mice are a model of Alzheimer's disease (AD) pathology, where plaques of insoluble amyloid- $\beta$  develop from 6 months of age. Amyloid plaques lead to activation of microglia<sup>19</sup>, thereby providing a stimulus that should reveal microglial immune memory. We injected 3-month-old APP23 mice with 1x/4xLPS, then analysed pathology 6 months later (Fig.2a). Strikingly, 1xLPS significantly increased while 4xLPS significantly decreased both plaque load and total amyloid- $\beta$  levels compared to control animals (Fig.2b), with plaque-associated neuritic damage correlating directly with plaque size in all treatment groups (Extended Data Figs.3a-c). Also, the protein levels of amyloid- $\beta$  precursor protein (APP) and its cleavage products were indistinguishable amongst groups, indicating equivalent amyloid- $\beta$  generation (Extended Data Fig.3d). Furthermore, neither the total number of microglia nor the number of microglia clustering around plaques was altered by LPS treatments (Fig.2c), while the number of activated (GFAP+) astrocytes decreased slightly both with 1x and 4xLPS treatment (Extended Data Fig.3e). However, the brain levels of IL-1 $\beta$ , IL-6 and IL-12 were reduced in 4xLPS-treated APP animals, while in 1xLPS-treated APP mice IL-10 was reduced. In contrast, brain cytokine levels were not altered in wildtype littermate controls and baseline blood cytokine levels were unchanged in wildtype and APP animals. Furthermore, an additional LPS injection at 9 months of age caused indistinguishable peripheral cytokine responses (Fig.2d and Extended Data Figs.4a-c). Thus, peripheral immune stimuli cause long-term alterations in the brain immune response and differentially affect AD pathology.

To test for immune memory effects in a second disease model, we injected wildtype animals with 1x/4xLPS and induced focal brain ischemia one month later. One day post-ischemia, neuronal damage and microglial numbers were indistinguishable amongst treatment groups (Fig.3a), indicating that the initial ischemic insult was unaffected by 1x/4xLPS. However, the acute inflammatory response, which is driven by brain-resident cells early after ischemia<sup>12</sup>, differed, showing increased levels of IL-1 $\beta$  in 1xLPS- and decreased levels in 4xLPS-treated animals. In contrast, the release of IL-10 was significantly suppressed by 1xLPS only (Fig.3b), reminiscent of results in APP animals (Fig.2d). Other brain cytokines and blood cytokine levels were

indistinguishable amongst groups (Extended Data Fig.5). Importantly, seven days after brain ischemia, the volume of neuronal damage and microglial activation was strongly reduced by 4xLPS but unaffected by 1xLPS (Figs.3c/d). These results confirm long-term modulation of brain immune responses and suggest persistent modification of stroke pathology following a tolerizing but not a training stimulus, possibly due to the severity of the insult preventing its further exacerbation through amplification of the immune response.

### **Microglial molecular profiles**

*In vitro*, immune memory in macrophages results from epigenetically-mediated alterations in the enhancer repertoire, leading to transcriptional changes<sup>3,20,21</sup>. Since our data indicated that acute immune memory in the brain is mediated predominantly by microglia, we isolated microglia by cell sorting (Extended Data Fig.6) from 9-month-old animals stimulated with 1x/4xLPS at 3 months of age and performed chromatin immunoprecipitation for mono-methylation at lysine 4 of histone 3 (H3K4me1) and acetylation at lysine 27 of histone 3 (H3K27ac), which define active enhancers<sup>20,21</sup>. Thus, we identified 20,241 putative active enhancers across all conditions.

First, we focussed on H3K4me1 marks, which should mark all enhancers activated in response to the first and/or second immune stimulus (as enhancers may lose H3K27ac after cessation of inflammation but retain H3K4me1 marks)<sup>20,21</sup>. Strikingly, H3K4me1 levels differed significantly between control and LPS treatment groups both in wildtype and APP animals but also between 1x- and 4xLPS-treated mice (Extended Data Fig.7b; Supplementary Table1). For example, enhancers with increased H3K4me1 levels in microglia from 1xLPS versus 4xLPS wildtype animals showed enrichment for the ‘thyroid hormone signalling pathway’, including a putative enhancer for hypoxia inducible factor-1 $\alpha$  (HIF-1 $\alpha$ ). Similarly, enhancers with higher H3K4me1 levels in 1xLPS versus 4xLPS-treated APP mice were enriched for the ‘HIF-1 signalling pathway’. On the other hand, 4xLPS-treated APP animals showed increased H3K4me1 levels in putative enhancers related to phagocytic function (Fig.4a). Importantly, no pathway enrichment was found when comparing H3K4me1 levels in microglia from APP and wildtype controls (Fig.4a), indicating that H3K4me1 levels were altered predominantly in response to LPS stimulation.

Next, we analysed enhancer activation by determining differential regulation of H3K27ac levels. In line with the requirement of an acute stimulus for H3K27ac deposition<sup>20</sup>, differential enhancer activation was more pronounced in APP animals (where amyloid plaques activate microglia) than in wildtype groups (190±18 in APP, 69±5 in wildtype groups; Extended Data Fig.7e; Supplementary Table2). For example, differentially regulated H3K27ac levels in microglia from 1xLPS-treated versus control APP animals were enriched for the ‘HIF-1 signalling pathway’, with enhancer regions also being enriched for HIF-1α binding motifs (Fig.4b and Extended Data Fig.8), in line with changes in H3K4me1 levels (Fig.4a) and the reported key role of HIF-1α in trained immunity and macrophage inflammatory responses<sup>4,22</sup>.

Active enhancers in microglia from 4xLPS-treated versus control APP animals only showed enrichment for the ‘Rap1 signalling pathway’, a pathway implicated in phagocytosis of opsonized targets<sup>23,24</sup>, again matching changes in H3K4me1 levels (Figs.4a/b). Strikingly, the comparison of microglia from APP animals that received the training- (1xLPS) and tolerance-inducing (4xLPS) stimuli, showed no pathway enrichment for active enhancers in 4xLPS-treated animals while enhancers in 1xLPS-treated animals were enriched for a large number of inflammation-related pathways, highlighting the differential effects of the two immune memory states. Finally, the comparison of microglia from vehicle-treated wildtype and APP animals demonstrated a small number of differentially activated enhancers with enrichment for the ‘thyroid hormone signalling pathway’ (including a putative active enhancer for *Hif1a*) as well as the ‘mTOR signalling pathway’ (Fig.4b), indicating that microglia are also epigenetically reprogrammed in response to brain pathology alone.

We next examined microglial mRNA levels under the same conditions to determine whether epigenetic alterations were reflected in gene expression levels (Supplementary Table3). First, we determined the concordance between 772 enhancers with significantly increased/decreased H3K27ac levels (Supplementary Table2) and the direction of change in the expression of their nearest gene. Indeed, there was a significant (albeit modest) concordance between alterations in H3K27ac levels and gene expression (median concordance of pairwise comparisons =58%, P=0.03). This suggested that gene expression is directly affected by the microglial active enhancer repertoire. Accordingly, weighted gene correlation network analysis (WGCNA<sup>25</sup>) revealed striking parallels to epigenetic changes (Figs.5a-c and Supplementary Table4). For example, the red module (MEred) contained the *Hif1a*

gene, showed enrichment for the ‘HIF-1 signalling pathway’ and correlated strongly with the 1xLPS-treated APP group. Furthermore, gene expression in MEred was significantly upregulated in APP versus wildtype control animals and further increased by 1xLPS but downregulated by 4xLPS treatment.

HIF-1 $\alpha$  activation in inflammatory-stimulated macrophages can occur downstream of mitochondrial hyperpolarization; enhanced HIF-1 $\alpha$  signalling in turn promotes glycolysis, measurable as lactate release<sup>26</sup>. Accordingly, the green module (MEgreen), which correlated positively with control and 1xLPS-treated APP groups but negatively with control and 4xLPS-treated wildtype groups, was found to be enriched in genes of the ‘glycolysis’ pathway. Microglial gene expression in MEgreen was upregulated in APP versus wildtype control animals and again further increased in APP animals by 1xLPS but decreased by 4xLPS treatment. Therefore, we analysed mitochondrial membrane potential and lactate release in microglia. Strikingly, microglia from 1xLPS-treated APP animals showed strongly increased mitochondrial membrane potential, which correlated positively with the release of lactate (Fig.5d), functionally corroborating the epigenetic and transcriptional alterations in trained microglia. Additionally, immunostaining confirmed higher protein levels of HIF-1 $\alpha$  in plaque-associated microglia, which were further increased in 1xLPS-treated APP animals (Figs.5e/f). Thus, HIF-1 $\alpha$  signalling and a metabolic switch to glycolysis are activated in response to cerebral  $\beta$ -amyloid deposition, and are enhanced by immune training but reduced by immune tolerance in microglia.

In contrast to MEred/green, MEgrey correlated positively with the control wildtype but negatively with control and 1xLPS-treated APP groups. Compared to wildtype controls, microglial gene expression in MEgrey was downregulated in APP control animals and further decreased by 1xLPS stimulation, but showed unchanged levels in 4xLPS-treated APP animals (Figs.5a-c). Importantly, MEgrey was enriched for phagocytosis-related pathways, including the ‘Rap1 signalling pathway’ (Figs.5a-c), again reflecting epigenetic changes (Fig.4). We therefore tested whether phagocytosis of A $\beta$  was enhanced in 4xLPS-treated APP animals. Indeed, microglial A $\beta$  content was increased ~1.75-fold in 4xLPS-treated compared to APP control animals (Fig.5g), providing further functional validation of the microglial enhancer repertoire and gene expression profiles.

Recent data indicate that context-specific microglial phenotypes exist, e.g. ‘disease-associated microglia’ (DAM<sup>27</sup>) and the ‘microglial neurodegenerative phenotype’

(MGnD<sup>28</sup>). Interestingly, the brown module (MEbrown), which was significantly upregulated by both LPS treatments in wildtype as well as in all APP groups, contained a number of homeostatic microglial genes (e.g. *Hexb*, *Cx3cr1*, *Csf1r*) but also all of the ‘stage 1 DAM’ core-genes except *ApoE*, as well as 4 of 12 ‘stage 2’ core-genes<sup>27</sup> (Fig.5c). Of note, the gene encoding ApoE, which may be crucial for promoting a detrimental microglial phenotype<sup>28,29</sup> was found in the same module as *Hif1a* (MEred). MEred also contained other genes genetically linked to AD risk, namely *Cd33* and *Inpp5d*<sup>30</sup>, suggesting that HIF-1 $\alpha$  may also be a detrimental modulator of AD pathology.

The epigenetic landscape of microglia has only been described under homeostatic conditions<sup>31-33</sup>. Our data now demonstrate epigenetic modifications in microglia in response to peripheral immune stimulation but also as a result of cerebral  $\beta$ -amyloidosis, including activation of the HIF-1 $\alpha$  and mTOR pathways, and leading to transcriptional and functional alterations. While the global epigenetic and transcriptional changes were relatively modest, they were likely driven by a small number of microglia that received the required secondary immune stimulation, as evidenced for example by increased levels of HIF-1 $\alpha$  in plaque-associated microglia (Fig.5). mTOR activation is a well-known event in early AD<sup>34</sup> and was recently shown in microglia, where it activated HIF-1 $\alpha$  and glycolysis to sustain microglial energy demand in AD models<sup>35</sup>. Our data now indicate that mTOR activation may be mediated by epigenetic microglial reprogramming in response to cerebral  $\beta$ -amyloidosis and that HIF-1 $\alpha$  signalling downstream of mTOR could be a detrimental event, because augmentation or suppression of HIF-1 $\alpha$  signalling occurred concomitantly with aggravated or alleviated A $\beta$  deposition, respectively.

We here provide evidence of both immune training and tolerance in microglia and demonstrate their impact on neuropathology for the first time. While we cannot completely exclude that other cell-types contribute to immune memory and modulation of pathology in the brain, microglial-specific gene knockout of *Tak1* or *Hdac1/2* virtually abolished immune training (Fig.1), indicating that microglia are likely the major effectors of immune memory. Importantly, in our experiments, immune memory effects mostly became apparent following a secondary inflammatory stimulus, corroborating the concept of innate immune memory<sup>1,3</sup>. However, while in the periphery training may be beneficial due to enhanced pathogen elimination<sup>7,36,37</sup>,

and tolerance may be detrimental due to higher rates of infection resulting from immune suppression<sup>5</sup>, we found that training promotes while tolerance alleviates neuropathology. This is consistent with the beneficial effects of preventing microglial pro-inflammatory responses in models of AD pathology and stroke<sup>12,38</sup> and the worsening of cerebral  $\beta$ -amyloidosis in response to pro-inflammatory peripheral stimuli in animal models<sup>39</sup>. Similarly, immune training has recently been described in epithelial stem cells, where it promotes wound healing but may also underlie autoimmune disorders<sup>40</sup>. Thus, immune memory in the brain could conceivably affect the severity of any neurological disease that presents with an inflammatory component, but this will need to be studied for each individual condition.

Our data provide proof-of-principle for innate immune memory in microglia, and while our different LPS injection paradigms may not necessarily model physiological stimuli, we found that individual cytokines applied peripherally may also elicit immune memory effects in the brain (Extended Data Fig.9). These results suggest that a wide variety of immune challenges may induce microglial immune memory and provide a possible mechanism for LPS-induced immune memory in the brain. It will be crucial to determine which other stimuli may lead to long-term modulation of microglial responses and thereby contribute to the severity of many neurological diseases.

## References

1. Netea, M. G., Latz, E., Mills, K. H. G. & O'Neill, L. A. J. Innate immune memory: a paradigm shift in understanding host defense. *Nature Immunology* 16, 675–679 (2015).
2. Netea, M. G. et al. Trained immunity: A program of innate immune memory in health and disease. *Science* 352, aaf1098 (2016).
3. Saeed, S. et al. Epigenetic programming of monocyte-to-macrophage differentiation and trained innate immunity. *Science* 345, 1251086 (2014).
4. Cheng, S. C. et al. mTOR- and HIF-1 -mediated aerobic glycolysis as metabolic basis for trained immunity. *Science* 345, 1250684–1250684 (2014).
5. Biswas, S. K. & Lopez-Collazo, E. Endotoxin tolerance: new mechanisms, molecules and clinical significance. *Trends in Immunology* 30, 475–487 (2009).
6. Novakovic, B. et al. b-Glucan Reverses the Epigenetic State of LPS- Induced Immunological Tolerance. *Cell* 167, 1354–1368.e14 (2016).
7. Kleinnijenhuis, J. et al. Bacille Calmette-Guerin induces NOD2-dependent nonspecific protection from reinfection via epigenetic reprogramming of monocytes. *Proceedings of the National Academy of Sciences of the United States of America* 109, 17537–17542 (2012).
8. Tay, T. L. et al. A new fate mapping system reveals context-dependent random or clonal expansion of microglia. *Nature Neuroscience* (2017). doi:10.1038/nn.4547
9. Füger, P. et al. Microglia turnover with aging and in an Alzheimer's model via long-term in vivo single-cell imaging. *Nature Neuroscience* 20, 1371–1376 (2017).
10. Prinz, M. & Priller, J. Microglia and brain macrophages in the molecular age: from origin to neuropsychiatric disease. *Nat Rev Neurosci* 15, 300–312 (2014).
11. Heneka, M. T., Kummer, M. P. & Latz, E. Innate immune activation in neurodegenerative disease. *Nat Rev Immunol* 14, 463–477 (2014).
12. Iadecola, C. & Anrather, J. The immunology of stroke: from mechanisms to translation. *Nature Medicine* 17, 796–808 (2011).
13. Perry, V. H., Cunningham, C. & Holmes, C. Systemic infections and inflammation affect chronic neurodegeneration. *Nat Rev Immunol* 7, 161–167 (2007).
14. Goldmann, T. et al. A new type of microglia gene targeting shows TAK1 to be pivotal in CNS autoimmune inflammation. *Nature Neuroscience* 16, 1618–1626 (2013).
15. Jacob, C. et al. HDAC1 and HDAC2 control the transcriptional program of myelination and the survival of Schwann cells. *Nature Neuroscience* 14, 429–436 (2011).
16. Datta M, et al. HDAC1/2 are required for microglia identity during development, homeostasis and neurodegeneration in a context-dependent manner, *Immunity* 2018 (in press).



17. Banks, W. A. & Robinson, S. M. Minimal penetration of lipopolysaccharide across the murine blood-brain barrier. *Brain, Behavior, and Immunity* 24, 102–109 (2010).
18. Saederup, N. et al. Selective chemokine receptor usage by central nervous system myeloid cells in CCR2-red fluorescent protein knock-in mice. *PLoS ONE* 5, e13693 (2010).
19. Sturchler-Pierrat, C. et al. Two amyloid precursor protein transgenic mouse models with Alzheimer disease-like pathology. *Proceedings of the National Academy of Sciences of the United States of America* 94, 13287–13292 (1997).
20. Ostuni, R. et al. Latent Enhancers Activated by Stimulation in Differentiated Cells. *Cell* 152, 157–171 (2013).
21. Kaikkonen, M. U. et al. Remodeling of the Enhancer Landscape during Macrophage Activation Is Coupled to Enhancer Transcription. *Molecular Cell* 51, 310–325 (2013).
22. Cramer, T. et al. HIF-1alpha is essential for myeloid cell-mediated inflammation. *Cell* 112, 645–657 (2003).
23. Caron, E., Self, A. J. & Hall, A. The GTPase Rap1 controls functional activation of macrophage integrin alphaMbeta2 by LPS and other inflammatory mediators. *Curr. Biol.* 10, 974–978 (2000).
24. Li, Y. et al. Rap1a null mice have altered myeloid cell functions suggesting distinct roles for the closely related Rap1a and 1b proteins. *J. Immunol.* 179, 8322–8331 (2007).
25. Langfelder, P. & Horvath, S. WGCNA: an R package for weighted correlation network analysis. *BMC Bioinformatics* 9, 559 (2008).
26. Mills, E. L. et al. Succinate Dehydrogenase Supports Metabolic Repurposing of Mitochondria to Drive Inflammatory Macrophages. *Cell* 167, 457–461.e14 (2016).
27. Keren-Shaul, H. et al. A Unique Microglia Type Associated with Restricting Development of Alzheimer's Disease. *Cell* 1–33 (2017). doi:10.1016/j.cell.2017.05.018
28. Krasemann, S. et al. The TREM2-APOE Pathway Drives the Transcriptional Phenotype of Dysfunctional Microglia in Neurodegenerative Diseases. *Immunity* 47, 566–581.e9 (2017).
29. Shi, Y. et al. ApoE4 markedly exacerbates tau-mediated neurodegeneration in a mouse model of tauopathy. *Nature* 1–20 (2017). doi:10.1038/nature24016
30. Lambert, J. C. et al. Meta-analysis of 74,046 individuals identifies 11 new susceptibility loci for Alzheimer's disease. *Nature Genetics* 45, 1452–1458 (2013).
31. Gosselin, D. et al. Environment drives selection and function of enhancers controlling tissue-specific macrophage identities. *Cell* 159, 1327–1340 (2014).
32. Lavin, Y. et al. Tissue-resident macrophage enhancer landscapes are shaped by the local microenvironment. *Cell* 159, 1312–1326 (2014).

33. Gosselin, D. et al. An environment-dependent transcriptional network specifies human microglia identity. *Science* 1617, eaal3222 (2017).
34. Wang, C. et al. Targeting the mTOR signaling network for Alzheimer's disease therapy. *Mol. Neurobiol.* 49, 120–135 (2014).
35. Ulland, T. K. et al. TREM2 Maintains Microglial Metabolic Fitness in Alzheimer's Disease. *Cell* 170, 649–656.e13 (2017).
36. Kaufmann, E. et al. BCG Educates Hematopoietic Stem Cells to Generate Protective Innate Immunity against Tuberculosis. *Cell* 172, 176–190.e19 (2018).
37. Arts, R. J. W. et al. BCG Vaccination Protects against Experimental Viral Infection in Humans through the Induction of Cytokines Associated with Trained Immunity. *Cell Host Microbe* 23, 89–100.e5 (2018).
38. Heneka, M. T., Golenbock, D. T. & Latz, E. Innate immunity in Alzheimer's disease. *Nature Immunology* 16, 229–236 (2015).
39. O'Banion, M. K. Does peripheral inflammation contribute to Alzheimer disease? Evidence from animal models. *Neurology* 83, 480–481 (2014).
40. Naik, S. et al. Inflammatory memory sensitizes skin epithelial stem cells to tissue damage. *Nature* 550, 475–480 (2017).
41. Liu, F., Yuan, R., Benashski, S. E. & McCullough, L. D. Changes in experimental stroke outcome across the life span. *Journal of Cerebral Blood Flow & Metabolism* 29, 792–802 (2009).
42. Sturchler-Pierrat, C. & Staufienbiel, M. Pathogenic mechanisms of Alzheimer's disease analyzed in the APP23 transgenic mouse model. *Annals of the New York Academy of Sciences* 920, 134–139 (2000).
43. Neher, J. J. et al. Phagocytosis executes delayed neuronal death after focal brain ischemia. *Proceedings of the National Academy of Sciences* 110, E4098–107 (2013).
44. Hefendehl, J. K. et al. Repeatable target localization for long-term in vivo imaging of mice with 2-photon microscopy. *Journal of Neuroscience Methods* 205, 357–363 (2012).
45. Eisele, Y. S. et al. Peripherally Applied A $\beta$ -Containing Inoculates Induce Cerebral  $\beta$ -Amyloidosis. *Science* 330, 980–982 (2010).
46. Varvel, N. H. et al. Replacement of brain-resident myeloid cells does not alter cerebral amyloid- $\beta$  deposition in mouse models of Alzheimer's disease. *Journal of Experimental Medicine* 212, 1803–1809 (2015).
47. Rottenberg, H. & Wu, S. Quantitative assay by flow cytometry of the mitochondrial membrane potential in intact cells. *Biochim. Biophys. Acta* 1404, 393–404 (1998).
48. Picelli, S. et al. Full-length RNA-seq from single cells using Smart-seq2. *Nature Protocols* 9, 171–181 (2014).

49. Leek, J. T., Johnson, W. E., Parker, H. S., Jaffe, A. E. & Storey, J. D. The sva package for removing batch effects and other unwanted variation in high-throughput experiments. *Bioinformatics* 28, 882–883 (2012).
50. Ritchie, M. E. et al. limma powers differential expression analyses for RNA-sequencing and microarray studies. *Nucleic Acids Res* 43, e47 (2015).
51. Halder, R. et al. DNA methylation changes in plasticity genes accompany the formation and maintenance of memory. *Nature Neuroscience* 19, 102–110 (2016).
52. Quinlan, A. R. BEDTools: The Swiss-Army Tool for Genome Feature Analysis. *Curr Protoc Bioinformatics* 47, 11.12.1–34 (2014).

### **Acknowledgements**

We thank Richard Ransohoff (Boston) and Patrick Matthias (FMI, Basel) for providing CCR2-RFP and Hdac1/2 fl/fl mice, respectively; Patrizia Rizzu (DZNE Tuebingen) for experimental advice, Lary Walker (Emory University) for manuscript comments and Donna Bryce (Univ. Tuebingen) for statistical advice. This study was supported by a PhD fellowship of the Studienstiftung des Deutschen Volkes (A.C.W.), a Roman Herzog Fellowship of the Hertie Foundation (J.J.N.), and grants from the network ‘Neuroinflammation in Neurodegeneration’ (State of Baden-Wuerttemberg, Germany; M.J. and M.P.), the Sobek-Stiftung (M.P.), the DFG (SFB992, Reinhart-Koselleck-Grant to M.P., SFB704 to J.L.S.), the European Research Council (A.F.) the Fortüne Program (Med. Faculty, Univ. Tuebingen; 2075-1-0; J.J.N.), the Fritz Thyssen Foundation (Cologne, Germany; J.J.N.) and the Paul G. Allen Family Foundation (Seattle, USA; J.J.N.). M.B. and J.L.S are members of the Excellence Cluster ImmunoSensation.

### **Author Contributions:**

K.D., A.C.W., J.W., P.R., L.M.H., K.W., A.S., T.B, O.S., M.D., J.J.N. performed microglial isolation, *in vivo* and *ex vivo* experiments and histological/biochemical analyses. M.G., L.K., G.J., T.P., V.C., R.I., C.K., A.F., M.B., T.U., J.L.S. and J.J.N. performed ChIP-Seq/RNA-Seq analyses. J.J.N conceived the study and coordinated the experiments together with M.J., A.F., M.P., M.B., J.L.S. and M.S.; J.J.N. wrote the manuscript, with contributions from all authors.

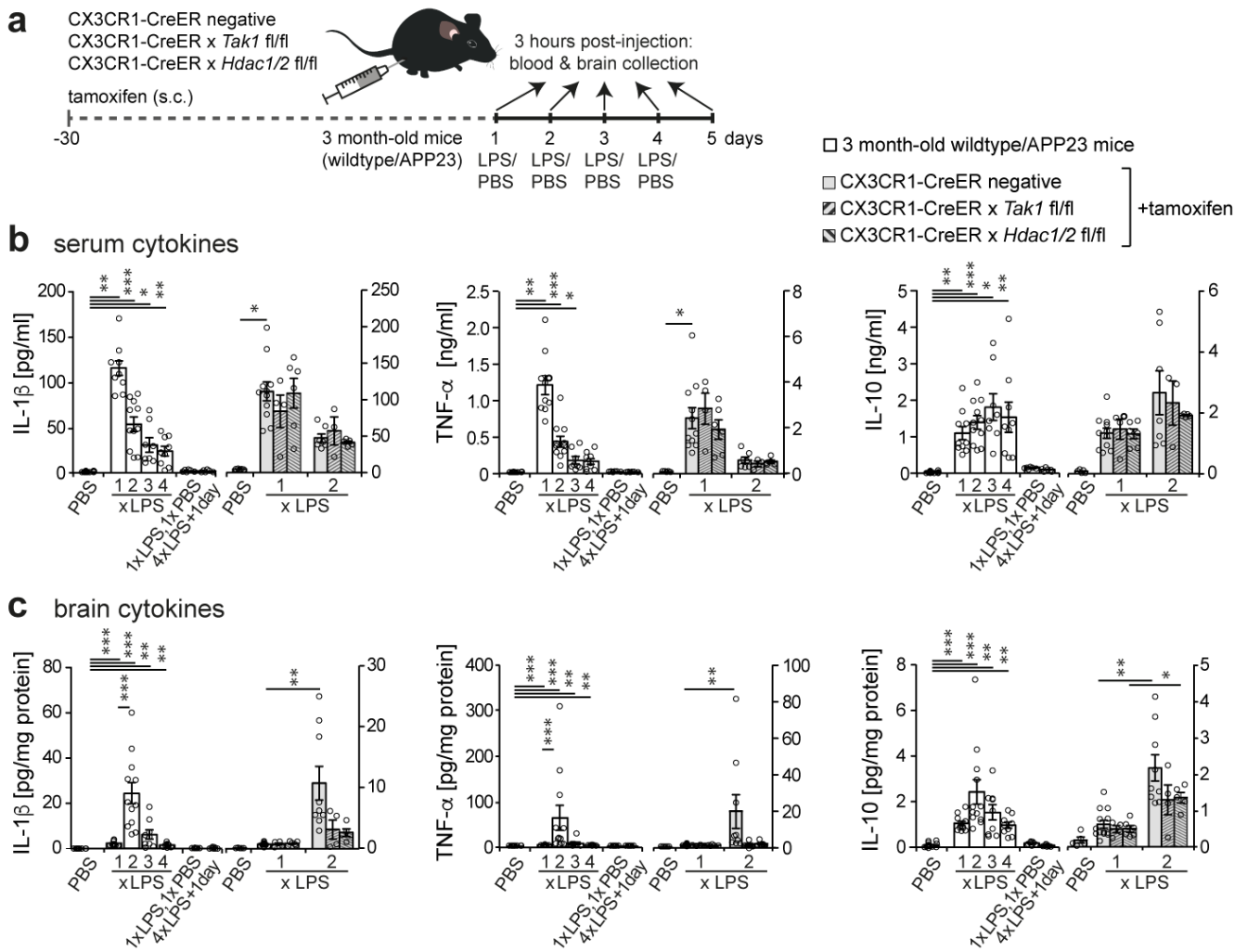


**Figure 1: Peripheral immune stimulation evokes immune memory in microglia.**

**a**, Experimental approach. **b**, *White bars*: Peripheral cytokine levels in wildtype/APP23 animals following lipopolysaccharide (LPS) injections. Note that tolerance is induced with repeated injections. **c**, Brain cytokine levels: 2xLPS amplifies IL-1 $\beta$ /TNF- $\alpha$  release, demonstrating immune training; tolerance occurs with 3x/4xLPS. Cytokines return to baseline within 24h (1xLPS,1xPBS/4xLPS+1day). *Grey bars*: Microglia-specific knockout of *Tak1* or *Hdac1/2* selectively prevents immune training in the brain. In (b/c) n=16,11,12,9,9,7,7 | 5,13,4,6,9,4,5 from left to right. \*/\*\*/\*\*\*\* $P$ <0.05/0.01/0.001 for independent-samples median test with correction for multiple comparisons. Data are means $\pm$ s.e.m.

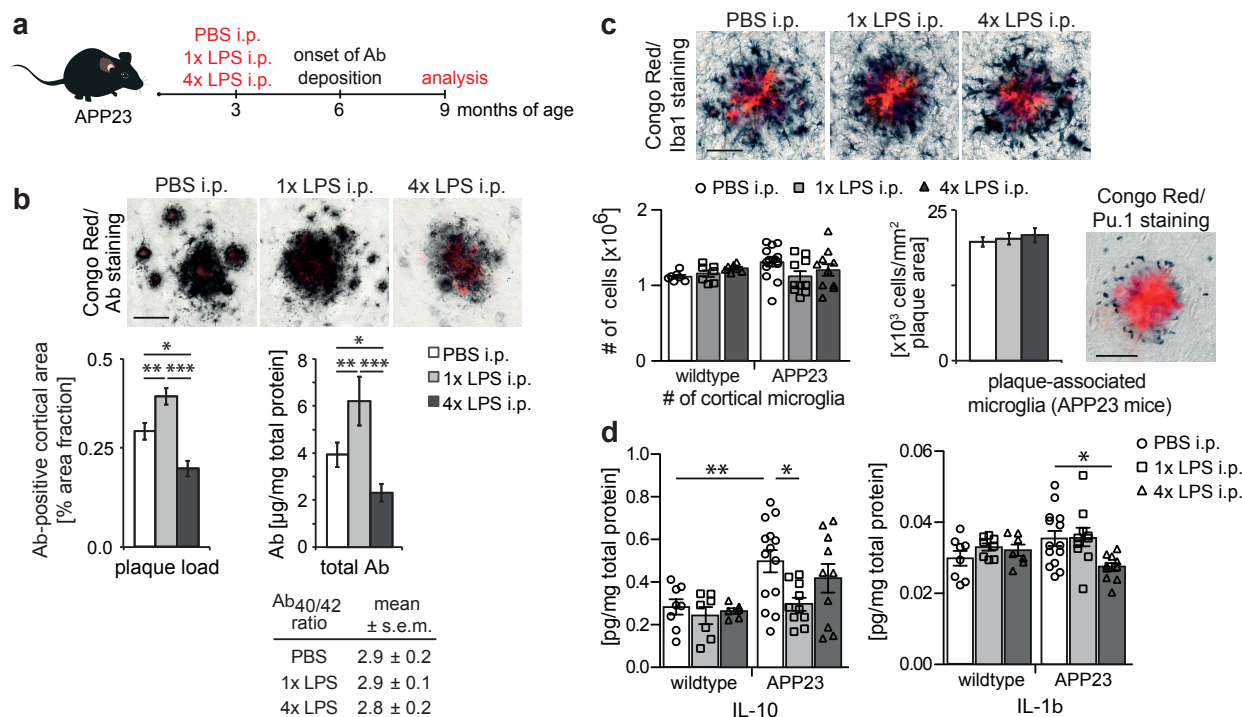


**Figure 2: Cerebral  $\beta$ -amyloidosis is altered after peripheral immune stimulation.**

**a**, Experimental design. **b**, Analysis of cortical amyloid- $\beta$  plaque load ( $n=22,10,10$  animals) and protein levels ( $n=14,10,10$  animals). **c**, Analysis of total cortical and plaque-associated microglia ( $n=7,7,7,14,10,10$  animals) and **d**, cytokine levels of IL-10 and IL-1 $\beta$  in wildtype and APP23 mice ( $n=8,8,7$  and  $n=14,10,10$  animals). Scale bar: 50  $\mu$ m.  $*/**/**P < 0.05/0.01/0.001$  for one-way (b) and two-way ANOVA (c/d) with Tukey correction. Data are means  $\pm$  s.e.m.

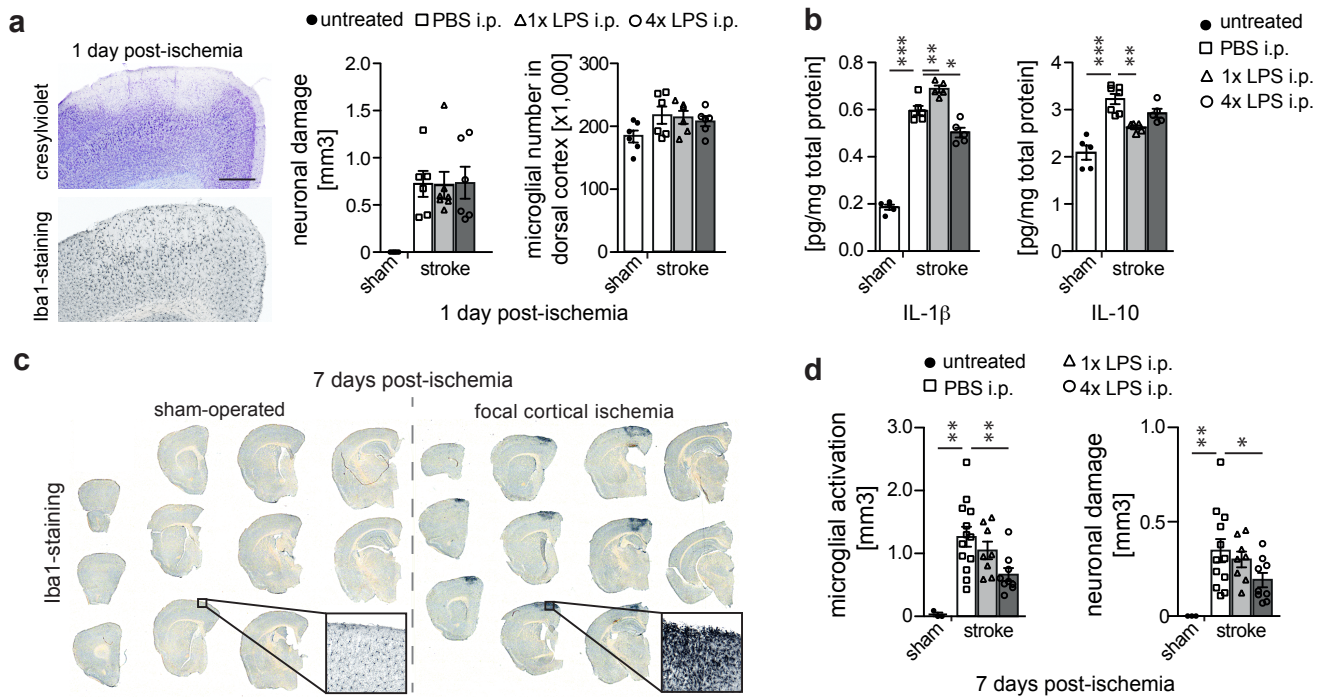


**Figure 3: Stroke pathology is altered after peripheral immune stimulation.**

Pathological features of brain ischemia induced one month after intraperitoneal injection with 1x or 4xLPS. **a**, Neuronal damage (cresylviolet, n=6,6,7,6 animals), microglial numbers (Iba1-positive, n=6,6,6 animals) and **b**, cytokine profiles one day post-ischemia (n=5,7,5,5 animals). **c**, Overview of microglial activation in the infarct and **d**, quantification of neuronal damage and microglial activation seven days post-ischemia (n=3,13,8,9 animals). Scale bar: 500  $\mu$ m. \*/\*\*/\*\* P < 0.05/0.01/ 0.001 for one-way ANOVA with Tukey correction. Data are means  $\pm$  s.e.m.

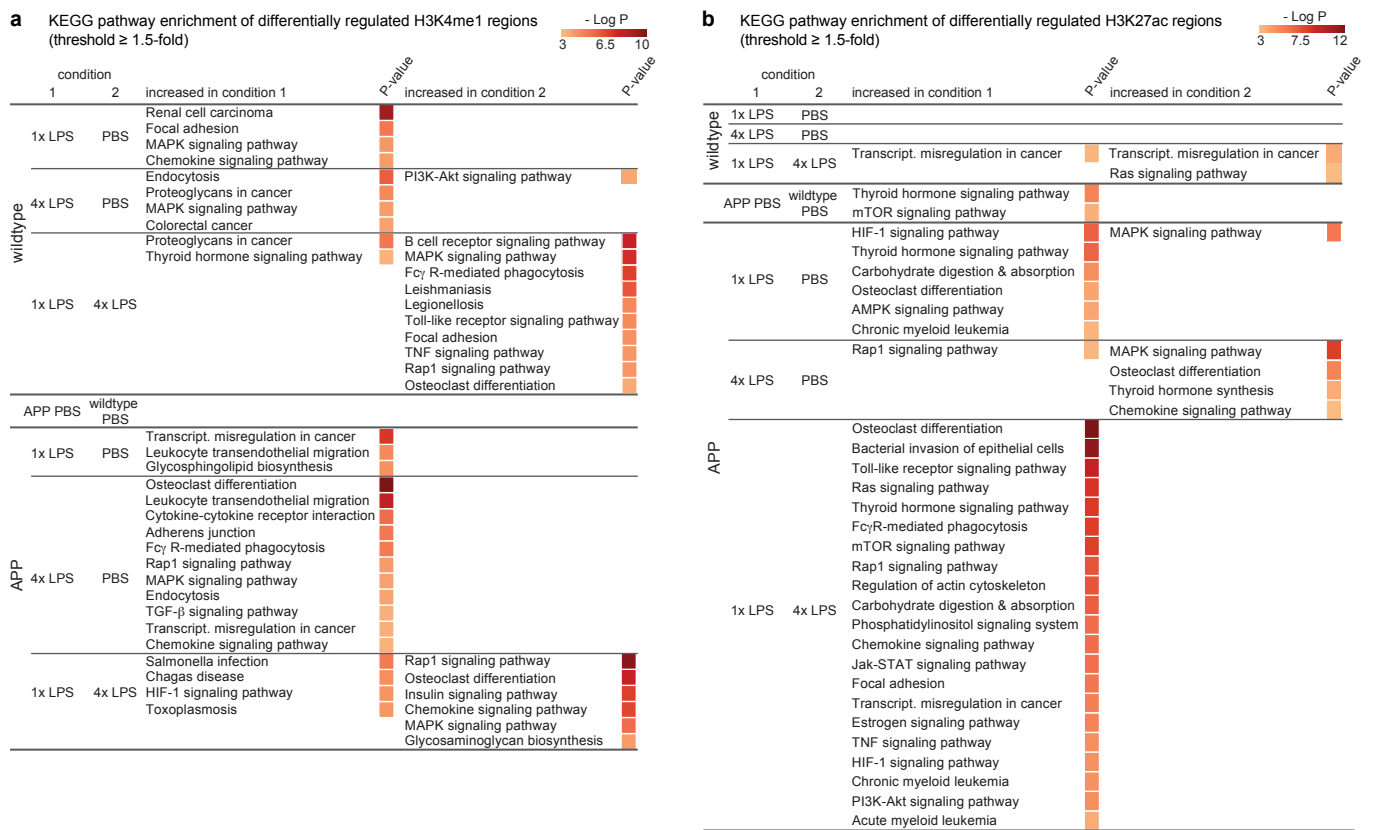


**Figure 4: The microglial enhancer repertoire 6 months after immune stimulation.**

Pathway enrichment of enhancers (with Benjamini-Hochberg correction) with differentially regulated H3K4me1 (a) and H3K27ac (b) levels (based on nearest gene; cumulative Poisson P-value  $< 0.0001$ ). n=2 replicates (8-10 animals/replicate).

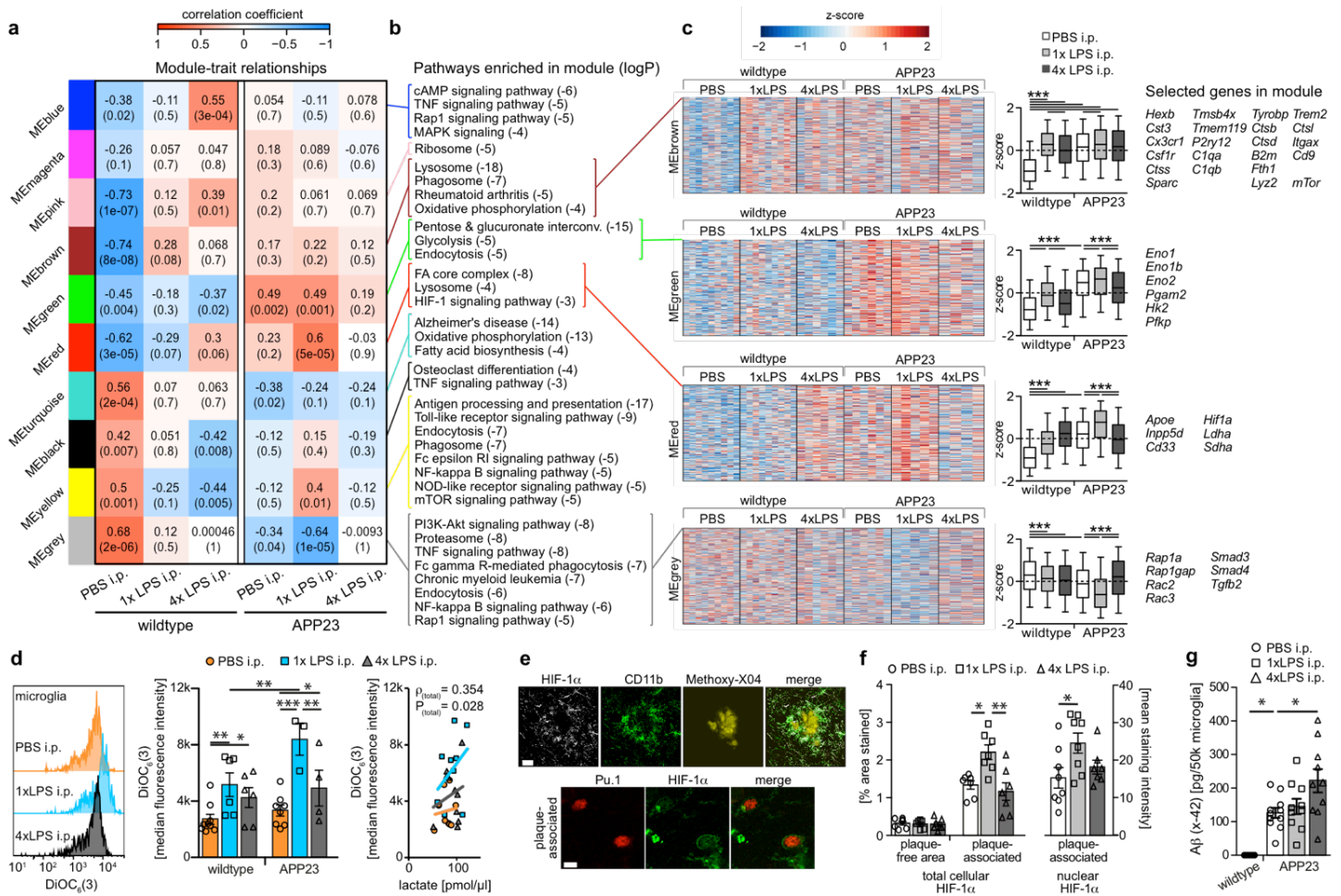


**Figure 5: Microglial gene expression and function 6 months after immune stimulation.**

**a**, Weighted gene correlation network analysis (top: correlation coefficient; bottom: P-value;  $n=9,9,6,6,5,4$  animals). **b**, Selected KEGG pathways enriched in modules. **c**, Heatmaps of genes within modules, z-scores (boxplot whiskers: 5-95<sup>th</sup> percentile;  $n=1601,990,949,3543$  genes in modules) and selected genes. **d**, Microglial mitochondrial membrane potential (left/middle;  $n=9,6,6,8,3,4$  animals) and Pearson's correlation with lactate release (right;  $n=11,10,10$  animals). **e**, Staining for *top*: HIF-1 $\alpha$ , microglia (CD11b) and amyloid plaques (Methoxy-X04) and *bottom*: HIF-1 $\alpha$  and microglial nuclei (Pu.1; single confocal plane) in brain sections from 9-month-old animals. Scale bars: 20/5  $\mu\text{m}$  (top/bottom). **f**, Total cellular ( $n=7,7,7$  animals) and nuclear ( $n=8,8,7$  animals) HIF-1 $\alpha$  staining intensity. **g**, Microglial A $\beta$  content ( $n=5,11,10,10$  animals). \*/\*\*/\* P<0.05/0.01/0.001 for one-way ANOVA with Tukey correction. Data are means $\pm$  s.e.m.



## Materials and Methods

### Animals

For all experiments, 3 month-old hemizygous APP23 transgenic (C57BL/6J-Tg(Thy1-APP<sub>K670N;M671L</sub>)23), APP23 transgene-negative littermates or C57BL/6J (wildtype) mice (Jackson Laboratory) were used.

For experiments analysing immune responses after acute LPS and cytokine stimulation (see below), both male and female mice were used. For microglia-specific gene knockouts, CX3CR1-CreER animals were crossed with *Tak1* fl/fl animals and Cre recombinase expression was induced by subcutaneous tamoxifen injections as previously described<sup>14</sup>. Similarly, microglial-specific knockout of *Hdac1/2* was achieved after crossing CX3CR1-CreER animals with a *Hdac1/2* fl/fl line<sup>15</sup>. Both *Tak1* fl/fl and *Hdac1/2* fl/fl were injected at 2-3 months of age and were incubated for four weeks without further treatment. Tamoxifen-injected CX3CR1-Cre negative littermates were used as controls (because responses in CX3CR1-Cre negative animals were indistinguishable in *Hdac1/2* fl/fl and *Tak1* fl/fl lines, pooled data are shown in Fig. 1).

As there is a significant gender effect on the pathology of both brain ischemia and cerebral  $\beta$ -amyloidosis,<sup>41,42</sup> only female mice were used for the analyses of brain pathology. APP23 mice express a transgene consisting of human amyloid- $\beta$  precursor protein (APP) with the KM670/671NL mutation under the Thy-1 promoter, and have been backcrossed with C57BL/6J mice for >20 generations. Female mice develop cerebral  $\beta$ -amyloid lesions in the neocortex around 6 months of age<sup>19</sup>.

Animals were maintained under specific pathogen-free conditions. All experiments were performed in accordance with the veterinary office regulations of Baden-Württemberg (Germany) and were approved by the Ethical Commission for animal experimentation of Tübingen and Freiburg, Germany.

### Peripheral immune stimulation

3-month-old mice were randomly assigned to treatment groups and were injected intraperitoneally (i.p.) with bacterial lipopolysaccharides (LPS from *Salmonella enterica* serotype typhimurium, Sigma) at a daily dose of 500  $\mu$ g/kg bodyweight. Animals received either four LPS injections on four consecutive days (4xLPS), a single LPS injection followed by three vehicle injections on the following three days

(1xLPS) or four vehicle injections (PBS). Acute stimulation showed indistinguishable cytokine responses in wildtype and APP23 transgenic animals; Figure 1 shows the pooled data from both genotypes (see Extended Data Fig. 2 for data separated by genotype). Furthermore, as cytokine responses were indistinguishable in animals treated with 1/2/3/4xPBS, pooled data from all time points are shown.

For peripheral cytokine treatments, recombinant murine cytokines (TNF- $\alpha$ , IL-10; PeproTech) were aliquoted as by the manufacturer's instructions and stored at -80°C until use. To determine whether a long-term change in the brain's immune response (training or tolerance) occurred after peripheral cytokine injection, mice were treated on four consecutive days with 0.1  $\mu\text{g/g}$  bodyweight IL-10 or once with 0.1/0.2  $\mu\text{g/g}$  bodyweight TNF-  $\alpha$ . Control mice received four vehicle injections (PBS). Four weeks later, cytokine- and control-treated mice received LPS (1  $\mu\text{g/g}$  bodyweight) or PBS, and were prepared 3 hours after the injection.

At the specified time-points, animals were deeply anaesthetised using sedaxylan/ketamine (64 mg/kg//472 mg/kg), blood was collected from the right ventricle of the heart and animals were transcardially perfused with ice-cold PBS through the left ventricle. The brain was removed and sagittally separated into the two hemispheres, which were either fixed in 4% paraformaldehyde (PFA) or fresh-frozen on dry ice. Fresh-frozen hemispheres were homogenised using a Precellys<sup>®</sup> lysing kit and machine at 10 or 20% (w/v) in homogenisation buffer (50 mM Tris pH 8, 150 mM NaCl, 5 mM EDTA) containing phosphatase and protease inhibitors (Pierce). Fixed hemispheres were kept in 4% PFA for 24h, followed by cryoprotection in 30% sucrose in PBS, subsequently frozen in 2-methylbutane and coronally sectioned at 25  $\mu\text{m}$  using a freezing-sliding microtome (Leica).

### **Focal brain ischemia**

For the induction of a focal cortical stroke, we modified existing models of endothelin-1 (ET-1)-induced brain ischemia<sup>43</sup> to avoid traumatic injury to the brain. Under anaesthesia and analgesia (Fentanyl, Midazolam, Medetomidin: 0.05//5//0.5 mg/kg bodyweight), 3-month-old animals were fixed in a stereotactic frame and a circular piece of skull was removed (5 mm diameter, centred on Bregma; as described in<sup>44</sup>). The dura mater was carefully removed with the help of a microhook (Fine Science Tools) and 5  $\mu\text{l}$  of ET-1 (Bachem; 64  $\mu\text{M}$ ) in Hanks Buffered Salt Solution (Invitrogen) or vehicle solution was topically applied to the cortex and incubated for

10 min. The craniotomy was then covered with a 5 mm glass coverslip, which was fixed in place with dental cement (Hybond), the skin was sutured, then the mice received antidote (Flumazenil, Atipamezol: 0.5//2.5mg/kg bodyweight) and were health-monitored. Control mice underwent the same surgical procedure with application of vehicle solution to the cortex. After 4 weeks, animals were deeply anesthetized and prepared as described above.

### **Western Blotting analysis**

For Western Blotting, total brain homogenates were sonicated 3x5 seconds (LabSonic, B. Braun Biotech), protein levels of the brain homogenates were quantified with a microplate bicinchoninic acid (BCA) assay (Pierce) and adjusted accordingly. Samples were then analysed on NuPage Bis-Tris gels (Invitrogen) using standard procedures. Proteins were transferred to nitrocellulose membranes, blocking was performed with 5% milk in PBS containing 0.05% Tween (PBST) for 1h and blots were incubated with mouse anti-A $\beta$  (6E10; 1:1000, Covance) in PBST overnight at 4°C. Membranes were then probed with the secondary HRP-labelled antibodies (1:20,000, Jackson ImmunoLaboratories). Protein bands were detected using chemiluminescent peroxidase substrate (ECL prime, GE Healthcare). Densitometric values of the protein band intensities were analysed with the software package Aida v.4.27 and normalised to GAPDH intensities.

### **Immunostaining**

Immunohistochemical staining was performed on free-floating sections using either Vectastain Elite ABC kits (Vector laboratories) or fluorescent secondary antibodies (Jackson Immunolaboratories). Unless otherwise noted, brain sections were blocked for 1h with 5% normal serum of the secondary antibody species, followed by primary antibody incubation overnight at 4°C. Primary antibodies used were: rabbit anti-Pu.1 (1:1000, Cell Signalling), rabbit anti-Iba1 (1:1,000; Wako; catalogue no. 019-19741), rabbit anti-GFAP (1:500, Biozol; catalogue no. Z0334), rabbit anti-A $\beta$  (CN3; 1:2,000<sup>45</sup>), mouse anti-HIF-1 $\alpha$  (1:500; Novus Biologicals, catalogue no. NB100-105, clone H1alpha67), rat anti-CD11b (1:2000; Millipore, catalogue no. MAB1387Z), rabbit anti-APP (antibody 5313 to the ectodomain of APP, 1:750; kind gift of Prof. Christian Haas, Munich). Sections were then washed and incubated with secondary antibodies. Cresylviolet and Congo Red staining was conducted according to standard

procedures. Fluorescent plaque staining was achieved using Methoxy-X04 (4% vol of 10 mg/ml methoxy-X04 in DMSO, and 7.7% vol CremophorEL in 88.3% vol PBS) for 20 min, RT.

Images were acquired on an Axioplan 2 microscope with Axioplan MRm and AxioVision 4.7 software (Carl Zeiss). Fluorescent images were acquired using a LSM 510 META (Axiovert 200M) confocal microscope with an oil immersion 63X/1.4NA objective and LSM software 4.2 (Carl Zeiss), using sequential excitation of fluorophores. Maximum-intensity projections were generated using IMARIS 8.3.1 software (Bitmap).

For quantitative comparisons, sections from all groups were stained in parallel and analysed with the same microscope settings by an observer blinded to the treatment groups. To quantify the intensity of total microglial HIF-1 $\alpha$  staining, high-resolution bright field images were acquired using fixed camera exposure time and lamp intensity and subsequently analysed with Fiji software. Colour channels were split and a fixed intensity threshold was applied to the red channel. On each image, the thresholded area over the total image area was calculated. Area fractions were measured on images of at least 9 plaques and 15 plaque-free regions per animal. To exclude an influence of plaque-size on microglial HIF-1 $\alpha$  levels, plaques of similar size were selected for analysis of HIF-1 $\alpha$  levels in the different treatment groups (average plaque size: PBS i.p.: 1.73 $\pm$ 0.15, 1xLPS i.p.: 1.84 $\pm$ 0.19, 4xLPS i.p. 2.27 $\pm$ 0.39% Congo red area fraction).

For nuclear HIF-1 $\alpha$  staining, a modified staining protocol was used. Briefly, sections were blocked with mouse Ig blocking reagent (Vector laboratories) for 1h, RT, followed by blocking with normal donkey serum for 1h, RT. Sections were then incubated overnight with mouse anti-HIF1 $\alpha$  (clone mgc3, 1:50; Thermo Fisher Scientific, catalogue no. MA1-516) and rabbit anti-Pu.1 (1:250; New England Biolabs, catalogue no. 2258S. Clone 9G7), 4°C. To quantify the intensity of nuclear HIF-1 $\alpha$  staining, z-stacks from 3 plaques and plaque-free regions per animal were acquired with the same microscope settings and subsequently analysed with IMARIS 8.3.1 software. Using the surfaces tool, a mask based on microglial nuclei was created using staining for Pu.1. A filter for area was applied to exclude background staining. The created surface was used to mask the HIF-1 $\alpha$  channel. The mean masked HIF-1 $\alpha$  intensity was then determined.

To quantify neuronal dystrophy, fluorescent images from 5-10 plaques per animal were acquired with the same microscope settings and subsequently analysed with Fiji software. Maximum intensity projections were generated to choose the region of interest consisting of APP-staining and the plaque. Fluorescence channels were split and intensity thresholds were applied to each channel. For every plaque, the thresholded area within the region of interest was calculated as a measure of plaque size and dystrophic area.

### **Stereological and morphological quantification**

Stereological quantification was performed by a blinded observer on random sets of every 12<sup>th</sup> systematically sampled 25 µm thick sections throughout the neocortex. Analysis was conducted using the Stereologer software (Stereo Investigator 6; MBF Bioscience) and a motorized x-y-z stage coupled to a video microscopy system (Optronics). For quantification of total Pu.1- and GFAP-positive cells, the optical fractionator technique was used with three-dimensional dissectors as previously described<sup>46</sup>. For the quantification of plaque-associated cells, plaques were identified based on Congo Red staining and cells in their immediate vicinity were counted. Plaque load was determined by analysing the cortical area covered by Congo Red and/or anti-A $\beta$  staining using the area fraction fractionator technique<sup>46</sup>. The volume of neuronal damage and microglial activation after brain ischemia was determined using the Cavalieri estimator technique.

For analysing microglial morphology, three images from three non-consecutive brain sections per animal were acquired from Iba-1 immunostained sections using identical camera acquisition settings, at 20X/0.5NA magnification. In order to perform the filament tracing in IMARIS (v.8.3.1), images were pre-processed in Fiji to optimise their contrast for reconstruction. The image background was subtracted using the in-built Fiji plugin to obtain an evenly distributed intensity and enhance contrast to the cells; subsequently the images were sharpened and their intensity was adjusted to the respective minimum and maximum histogram values. Filaments were then traced in IMARIS using the in-built Autopath algorithm. Reconstruction parameters were kept constant among all images; each cell was reconstructed as a 'filament' element in IMARIS, associated with a total length and volume.

## **ELISA**

For quantification of A $\beta$  by ELISA (Meso Scale Discovery) in brain homogenates or by SIMOA (Single Molecule Array, Quanterix) in isolated microglial cells, samples were pre-treated with formic acid (Sigma-Aldrich, final concentration: 70% vol/vol), sonicated for 35 seconds on ice, and centrifuged at 25,000g for 1 hour at 4°C. Neutralization buffer (1 M Tris base, 0.5 M Na<sub>2</sub>HPO<sub>4</sub>, 0.05% NaN<sub>3</sub> (wt/vol)) was then added at a 1:20 ratio. A $\beta$  was measured by an observer blinded to the treatment groups using human (6E10) A $\beta$  triplex assay (Meso Scale Discovery, MSD) in brain homogenates or Simoa Human Abeta 42 2.0 Kit (Quanterix) in isolated microglia according to the manufacturer's instructions.

Soluble APP $\beta$  containing the Swedish mutations (as present in the APP23 transgene) was measured using the sw soluble APP $\beta$ kit (Mesoscale Discovery) following the manufacturer's instructions after extraction with 1% Triton-X 100 and ultracentrifugation for 1h, 135,000g, 4 °C.

For cytokine measurements, brain homogenates were centrifuged at 25,000g for 30 minutes at 4°C. Supernatants were analysed using the mouse pro-inflammatory panel 1 V-plex plate (Mesoscale Discovery) according to the manufacturer's instructions. To determine blood cytokines, serum was obtained by coagulation of whole blood in Vacuettes (Greiner Bio-One) for 10 min, RT, and centrifugation for 10 min, 2,000g. Serum samples were diluted 1:2 before measurements. The investigator was blinded to the treatment groups.

Measurements were performed on a Mesoscale Sector Imager 6000 or a Simoa HD-1 Analyzer. For analyses of brain homogenates, protein levels were normalised against total protein amount as measured by BCA protein assay (Pierce).

To determine levels of LPS in blood and brain homogenates, the Limulus Amebocyte Lysate assay was used according to the manufacturer's instructions (Pierce LAL Chromogenic Endotoxin Quantitation Kit). Standards were prepared either in serum or brain homogenate from non-injected control animals. Serum samples were diluted 1:100 and brain homogenates 1:5 to eliminate matrix effects.

## **Isolation of microglia and fluorescence-activated cell sorting (FACS) analysis**

Fluorescence-activated cell sorting of microglia was performed based on CD11b<sup>high</sup> and CD45<sup>low</sup> as previously described<sup>9</sup> (see also Extended Data Fig.6).

### **Assessment of microglial mitochondrial membrane potential and lactate release**

To assess the microglial mitochondrial membrane potential, 10k microglia were sorted into 70  $\mu$ l PBS. Cells were incubated at 37°C with 3,3'-Dihexyloxycarbocyanine Iodide, DiOC<sub>6</sub>(3) (Thermo Fisher Scientific) at a final concentration of 0.2 nM for 20 minutes. At this concentration, mitochondrial dye accumulation is largely dependent on the mitochondrial membrane potential, with only minor contributions of the plasma membrane potential<sup>47</sup>. After incubation, the cell suspension was diluted with ice-cold PBS and DiOC<sub>6</sub>(3) fluorescence was immediately acquired with a Sony SH800 instrument.

For the assessment of microglial lactate release, 50k microglia from the same animals as used for DiOC<sub>6</sub>(3) staining were plated in 96-well plates with 125  $\mu$ l of macrophage serum-free medium (Thermo Fisher Scientific) and incubated for 24h at 37°C, 5% CO<sub>2</sub>. Lactate concentration in the media was determined using a Lactate Assay Kit (BioVision) following the manufacturer's instructions and was correlated to DiOC<sub>6</sub>(3) fluorescence values from cells of the same animal using IBM SPSS Statistics 22 software.

### **RNA-sequencing**

For RNA sequencing, 10k microglia were directly sorted into RNase-free PCR strips containing 30  $\mu$ l of H<sub>2</sub>O with 0.2% Triton-X and 0.8 U/ $\mu$ l RNase inhibitor (Clontech) and samples were immediately frozen on dry ice. RNA was isolated using NucleoSpin RNA XS kit (Macherey-Nagel) according to the manufacturer's instructions. 3 ng total RNA was used as input material for cDNA synthesis. cDNA synthesis and enrichment was performed following the Smart-seq2 v4 protocol as described by the manufacturer (Clontech). Sequencing Libraries were prepared with 1 ng of cDNA using the Nextera XT library preparation kit (Illumina) as described<sup>48</sup>. Multiplexing of samples was achieved using three different index-primers in each lane. For sequencing, samples from each group (APP and WILDTYPE) were pooled to rule out amplification and sequencing biases. Libraries were quality-controlled and quantified using a Qubit 2.0 Fluorometer (Life Technologies) and Agilent 2100 Bioanalyzer (Agilent Technologies). Final library concentration of 2 nM was used for sequencing. Sequencing was performed using a 50 bp single read setup on the Illumina HiSeq 2000 platform. Base calling from raw images and file conversion to fastq files were achieved by Illumina standard pipeline scripts (bcl2fastq v.2.18.0).

Quality control was then performed using FASTQC (v.2.18.0) program (<http://www.bioinformatics.babraham.ac.uk/projects/fastqc/>), eliminating one sample which had less than 20 million reads. Reads were trimmed off for sequencing adaptor and were mapped to mouse reference transcriptome (mm10) using STAR aligner 2.5.2b with non-default parameters. Unique read counts were obtained for each sample using HOMER v.4.8 software (<http://homer.salk.edu/homer/>) and ‘maketagdirectory -tbp 1’ command, followed by ‘analyzeRepeats.pl rna mm10 -count exons -noadj -condenseGenes’. Raw read counts were imported into R (v.3.2) and normalized using the Bioconductor (v.3.2) DESeq2 package (v.1.10.1) using default parameter. After normalization, all transcripts having a maximum overall group mean lower than 10 were removed. Unwanted or hidden sources of variation, such as batch and preparation date, were removed using the sva package<sup>49</sup>. The normalized rlog transformed expression values were adjusted according to the surrogate variables identified by sva using the function removeBatchEffect from the limma package<sup>50</sup>. To determine gene clusters associated with wildtype or APP23 animals following i.p. injections of 1x or 4xLPS at 3 months of age, we then used the 13,627 present genes and applied the R implementation of the Weighted Gene Correlation Network Analysis (WGCNA). We then performed WGCNA clustering using the ‘1-TOMsimilarityFromExpr’ function with the network type "signed hybrid", a power parameter of 7 (as established by scale free topology network criteria), and a minimum module size of 50 dissecting the data into 10 modules. Finally, pathway enrichment analysis of genes within modules was performed using the ‘findmotifs.pl’ function of HOMER. Correction for multiple comparisons for KEGG pathway analyses was performed using the STATS package of R and applying Benjamini-Hochberg correction. To focus on the most important molecular pathways, only pathways with  $\log P \leq -3$  and at least 5 genes were considered.

### **Chromatin Immunoprecipitation, library preparation and analysis**

For microglia isolation for chromatin purification, 1 mM sodium butyrate, an inhibitor of histone deacetylases<sup>31</sup>, was added to the dissection medium and FACS buffers. After staining, microglia were fixed in 1% PFA for 10 minutes at room temperature, followed by addition of glycine (final concentration: 125 mM) for 5 minutes and washing in HBSS. Microglia were then sorted into homogenisation buffer (0.32 M sucrose, 5 mM CaCl<sub>2</sub>, 5 mM MgAc<sub>2</sub>, 50 mM HEPES, 0.1 mM EDTA, 1 mM DTT,



0.1% vol/vol Triton-X-100) and centrifuged at 950 g for 5 minutes at 4 °C. The pellet was resuspended in 100 µl Nelson buffer (50 mM Tris, 150 mM NaCl, 20 mM EDTA, 1% vol/vol Triton-X-100, 0.5% vol/vol NP-40) and frozen on dry ice.

ChIP-sequencing was performed as previously described<sup>51</sup>, with slight modifications. In brief, two biological replicates were analysed for each condition and targeted histone modification. Cell lysates from 8-10 mice were pooled giving a total cell number of approximately 0.8-1 million cells per replicate. The cross-linked chromatin was sheared for 3x7 cycles (30 sec. On/Off) in a BioruptorPlus (Diagenode) to achieve an average fragment size of 350 bps. Proper shearing and chromatin concentration was validated by DNA isolation and quantification using a small amount of each sample individually. Samples were split in half and 1 µg of ChIP-grade antibody (H3K4me1: Abcam ab8895 or H3K27ac: Abcam ab4729) was added and incubated overnight at 4°C. From each sample, 1% of the total volume was taken as input control prior to antibody binding. Immunoprecipitation was performed by incubating samples with 30 µl BSA-blocked protein A magnetic beads (Dynabeads, Invitrogen) for 1h at 4°C. After purifying the precipitated chromatin and isolating the DNA, DNA libraries were generated using the Next Ultra DNA Library Prep Kit for Illumina and the Q5 polymerase (New England Biolabs). Multiplexing of samples was done using 6 different index-primers from the Library Prep Kit. For each replicate, samples from each condition (genotype and treatment) were pooled to rule out amplification and sequencing biases within the final data. Input samples were pooled and processed accordingly. The ideal number of amplification cycles was estimated via RealTime PCR to avoid over-amplification. Accordingly, samples were amplified for 13-15 cycles and the DNA was isolated afterwards. Individual libraries were pooled whereby each pool represented one whole batch of samples for each condition and targeted histone modification and was set to a final DNA concentration of 2 nM before sequencing (50 bp) on a HiSeq 2000 (Illumina) according to the manufacturer's instructions.

Base calling from raw images and file conversion to fastq files was achieved by standard Illumina pipeline scripts. Sequencing reads were then mapped to mouse reference genome (mm10) using rna-STAR aligner v2.3.0 with non-default parameters. Data were further processed using HOMER software (<http://homer.salk.edu/homer/>), following two recently published analyses on microglial epigenetic profiles<sup>31,32</sup>. Tag directories were created from bam files using

'makeTagDirectory' for individual samples and inputs, and peak calling was performed using 'findpeaks -style histone' with 4-fold enrichment over background and input, a Poisson p-value of 0.0001, and a peak width of 500 bp for H3K4me1 and 250 bp for H3K27ac. Peaks common to both replicates were determined using 'mergepeaks' (-prefix) function. To focus analysis on enhancers, peaks within  $\pm 2.5$  kb of known TSS were filtered out. Union peak files for H3K4me1 and H3K27ac marks were then created for group-wise comparisons using 'mergepeaks' function. Active enhancers, i.e. genomic regions containing both H3K4me1 and H3K27ac peaks, were identified using the 'window' function of bedtools2 [52], requiring peaks of both marks to be located within a genomic region of 4 kb. Union peak files of active enhancers were then used for comparisons amongst groups for both H3K4me1 and H3K27ac marks using the 'getDifferentialPeaks' function (using a fold-change cut-off of 1.5 and a cumulative Poisson p-value of 0.0001). Finally, differential peaks were annotated using the 'annotatepeaks.pl' function, including gene ontology analysis. Correction for multiple comparisons for KEGG pathway analyses was performed using the STATS package of R and applying Benjamini-Hochberg correction. To focus on the most important molecular pathways, only pathways with  $\log P \leq -3$  and at least three genes were considered.

For the generation of UCSC browser files, the 'makeUCSCfile' function was used, including normalisation to respective input and library size, with a resolution of 10 bp. Files for heatmaps of 24 kb genomic regions and with a resolution of 250 bp were generated using the 'annotatePeaks.pl' function; clustering was then performed using Gene Cluster 3.0 and visualised using JavaTreeView.

To identify transcription factors involved in the differential activation of enhancers, the 'findMotifsGenome.pl' command was used to analyse a region of 500 bp around enhancer peaks (-size 500), as this resulted in more robust identification of motifs for known microglial lineage-determining transcription factors when determining motifs of all identified microglial enhancers (Extended Data Fig.8). For all active enhancers, motif analysis was performed using the union H3K27ac peak file and standard background (i.e. random genomic sequence created by HOMER). In the case of pairwise comparisons amongst conditions, the first condition's specific H3K27ac peak file was used as input and the second condition's peak file as background. Because motif enrichment was often relatively low, we focussed on the most relevant

results by determining transcription factor (families), whose motifs occurred at least twice in ‘known’ and ‘de-novo’ motifs.

### **Comparison between enhancer activation and gene expression**

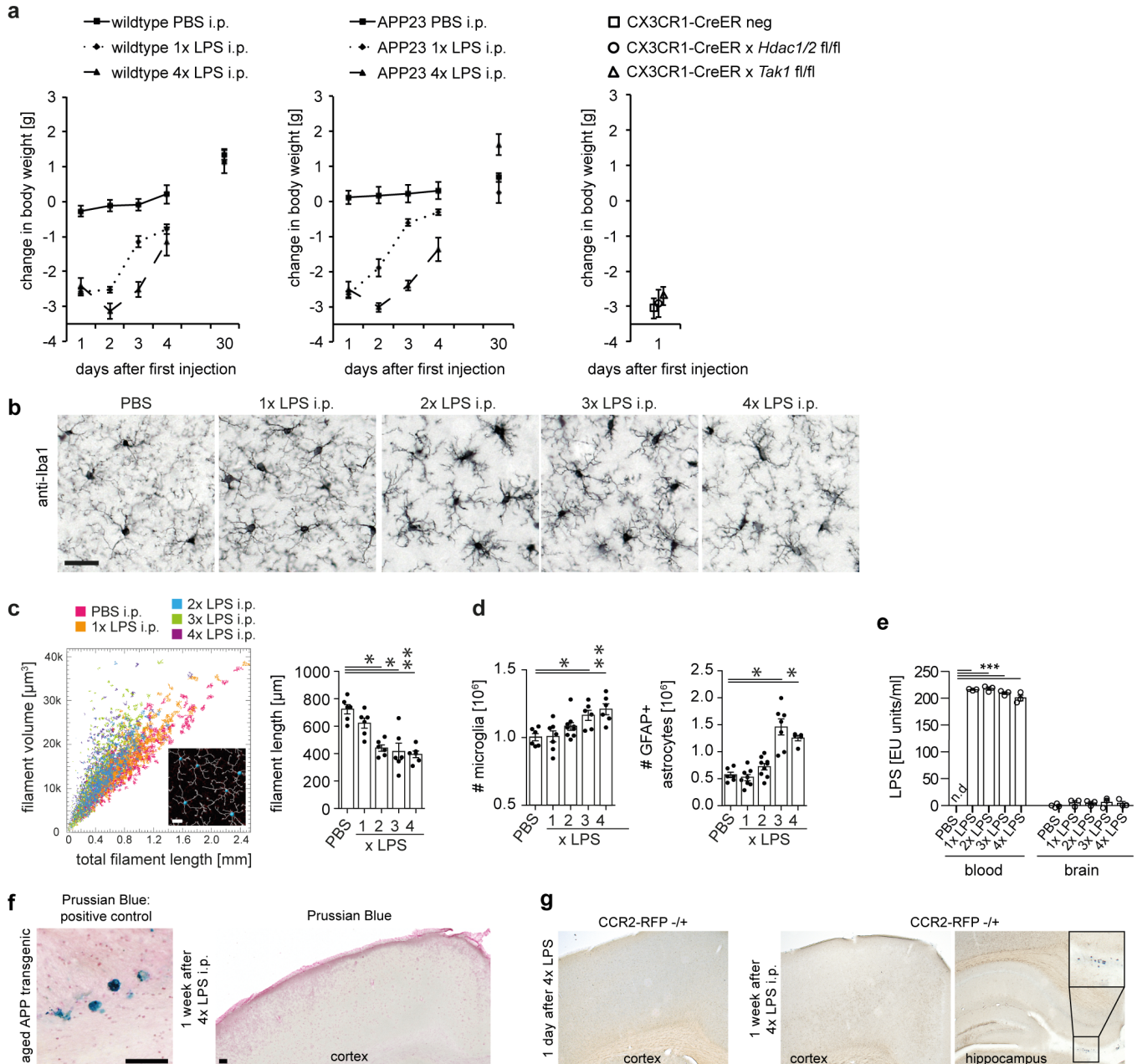
From our 14 pairwise comparisons (Fig.4, Extended Data Fig.7 and Supplementary Table 2), we analysed 772 differentially activated enhancers and compared increased/decreased H3K27ac levels with the direction of change in the expression of the nearest gene (difference in z-scores between the groups used for pairwise comparisons). The 14 concordance values were then statistically compared to chance level (50%) using a two-tailed Wilcoxon signed rank test.

### **Statistics and Reproducibility**

Statistical analyses were performed using IBM SPSS Statistics 22 or Prism 5 software. Data were assessed for normal distribution (Shapiro-Wilk test) and statistical outliers using the ‘explore’ function. If the normality criterion was met, data were analysed using a one-way ANOVA (for experiments on single genotypes), followed by pairwise comparison (if  $P < 0.05$ ) with post-hoc Tukey correction (for samples with non-significant homogeneity of variance Levene’s test) or Dunnett test (if homogeneity of variances not given). For comparisons across treatments and genotypes (e.g. cytokine analyses in Fig.2), a two-way ANOVA was performed, followed by posthoc testing with Tukey correction for significant main effects ( $P < 0.05$ ). As the cytokine data for acute LPS stimulation (Fig.1) showed inequality of variance as well as skewedness, a non-parametric independent-samples median test was performed followed by pairwise comparison with correction for multiple comparison.

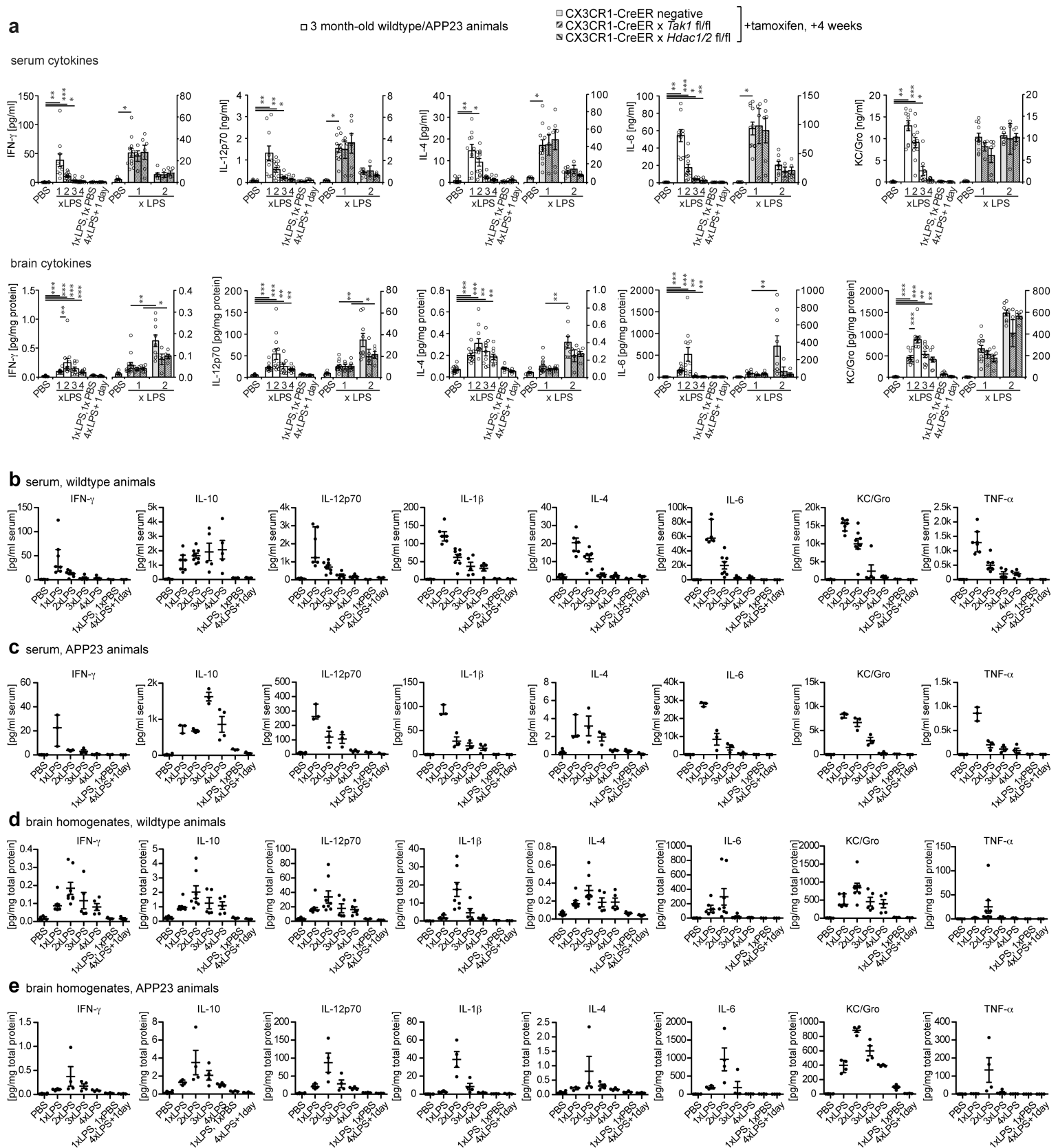
All experiments were performed at least twice and in independent batches of animals for key findings (figures show the pooled data). Due to batch-related variation in some dependent variables, ‘batch’ was added as a random variable to analyses where a significant batch effect was observed. For data sets with small sample size (e.g. Western Blotting analyses), the Kruskal-Wallis test was performed, followed by pairwise comparisons if  $P < 0.05$ . In the figure legends ‘n’ denotes the number of animals per treatment group. Minimum sample sizes were determined a priori using power analyses or as dictated by the methodology (e.g. ChIP-Seq).

Raw and processed data are provided in the Gene Expression Omnibus (accession number GSE82170; subseries GSE82168 for ChIP-Seq and GSE104630 for RNA-Seq datasets). Other data that support the findings of this study are available from the corresponding author upon reasonable request.



### Extended Data Figure 1: Acute responses to LPS injections.

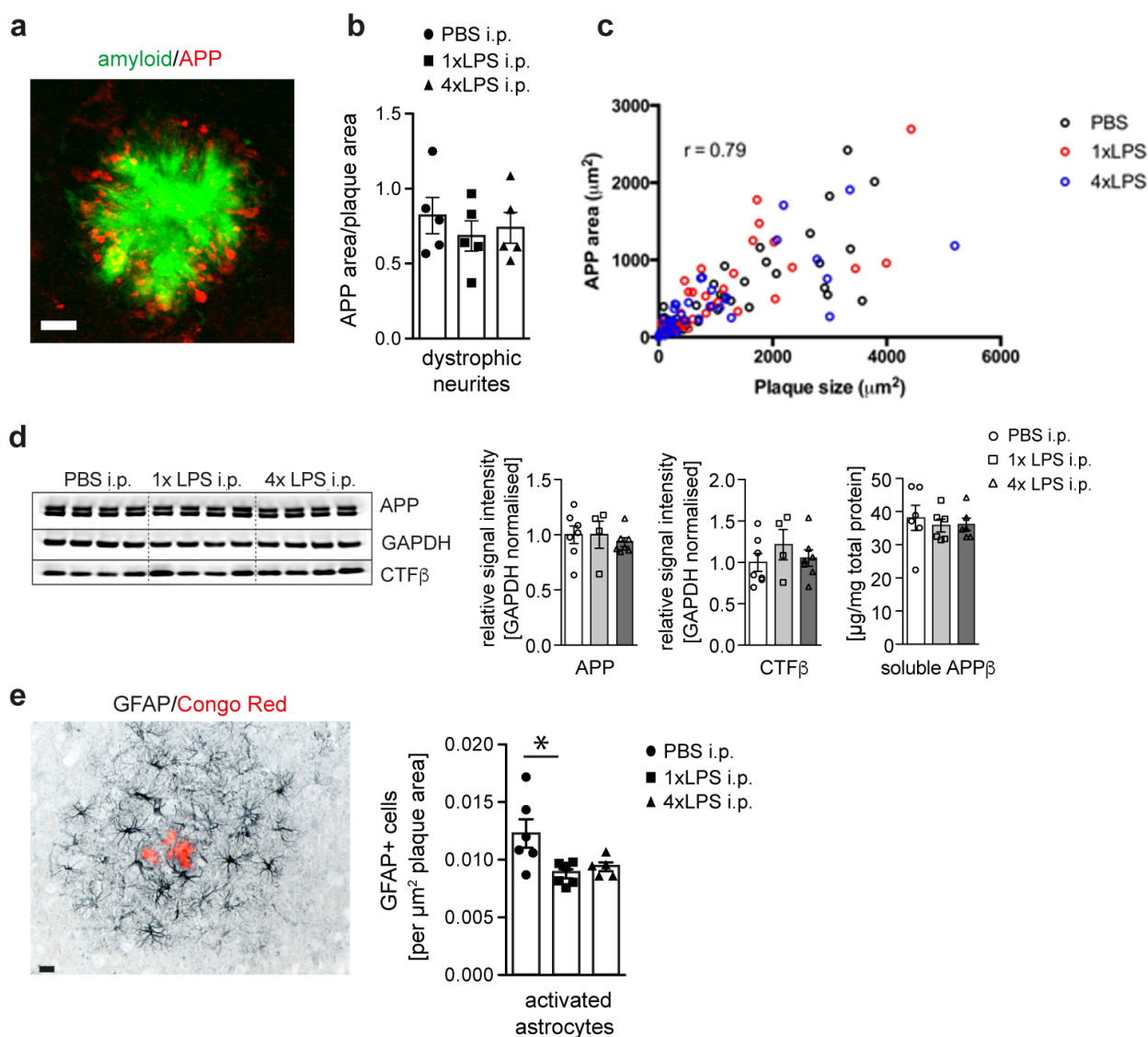
**a**, Weight changes after injection of lipopolysaccharides (LPS) (wildtype animals: n=11,11,11,11,4 for PBS, n=9,9,9,8,7 for 1xLPS, n=10,10,10,10,7 for 4xLPS; APP animals: n=14,14,14,14,7 for PBS, n=8,8,8,5,5 for 1xLPS; n=10,10,10,10,10 for 4xLPS; Cre animals n=5,5,4). **b/c**, Morphological changes in microglia (n=6,6,6,6 animals). Scale bar: 50  $\mu\text{m}$ . **d**, Numbers of microglia and activated (GFAP<sup>+</sup>) astrocytes (microglia n=6,7,8,6,6 animals, astrocytes n=6,8,9,7,5 animals). **e**, Blood and brain levels of LPS after daily injections with 500  $\mu\text{g}/\text{kg}$  bodyweight (n=4,3,3,3,3 animals). **f**, Assessment of iron entry from the blood (detected by Prussian Blue staining) shows positive staining in an aged (>25 months) APP transgenic animal, but not after repeated intraperitoneal LPS injections (n=3 mice analysed). **g**, In mice expressing red fluorescent protein (RFP) under the 'type 2 CC chemokine receptor' (*Ccr2*) promoter, no entry of CCR2-expressing blood monocytes is detected after repeated LPS injection (staining for RFP; insert shows RFP-positive monocytes in the choroid plexus; n=3 mice analysed). Scale bar: 100  $\mu\text{m}$ . Data are means  $\pm$  s.e.m. \*/\*\*/\*\* P < 0.05/0.01/0.001 for one-way ANOVA with Tukey correction.



## Extended Data Figure 2: Cytokine response after acute LPS injections.

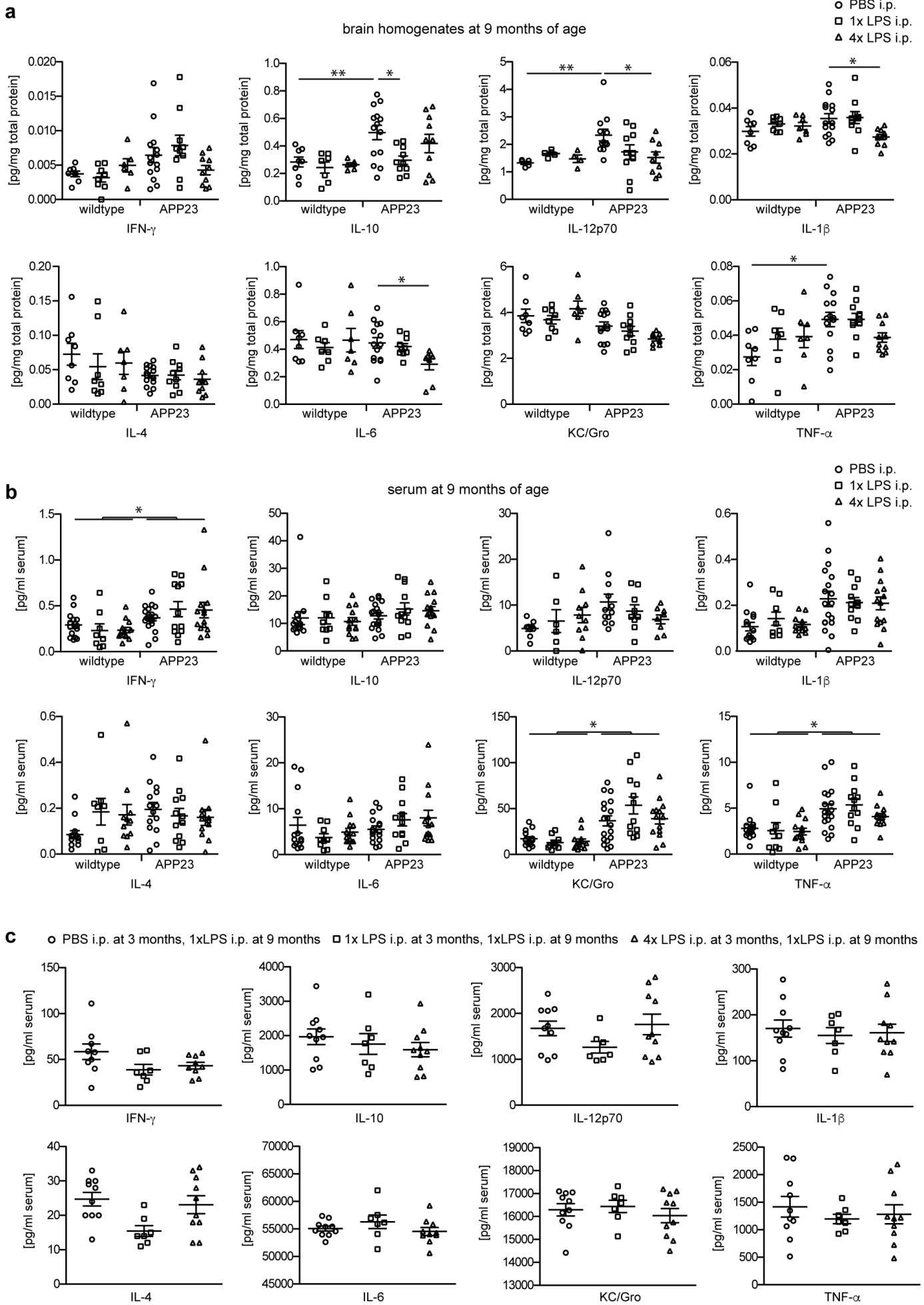
**a**, Additional cytokines (cp. Fig.1) analysed in the serum (top) and brain (bottom) 3h after each daily intraperitoneal lipopolysaccharide (LPS) injection on four consecutive days in 3-month-old mice (control animals received PBS injections; n=16,11,12,9,9,7,7 | 5,13,4,6,9,4,5 mice for groups from left to right). **b/c**, Cytokine response in the blood only in wildtype (b, n=6,7,8,5,5,3,3 animals)

or APP23 (c, n=10,3,3,3,4,3,3 animals) mice. **d/e**, Cytokine response in the brain only in wildtype (d, n=6,7,8,5,5,3,3 animals) or APP23 (e, n=10,4,4,4,4,4 animals) mice. Data are means± s.e.m. \*/\*\*/\*\*  $P < 0.05/0.01/0.001$  for independent-samples median test with correction for multiple comparisons.



### Extended Data Figure 3: APP levels and processing, neuritic dystrophy and astrocyte activation in 9-month-old APP23 animals.

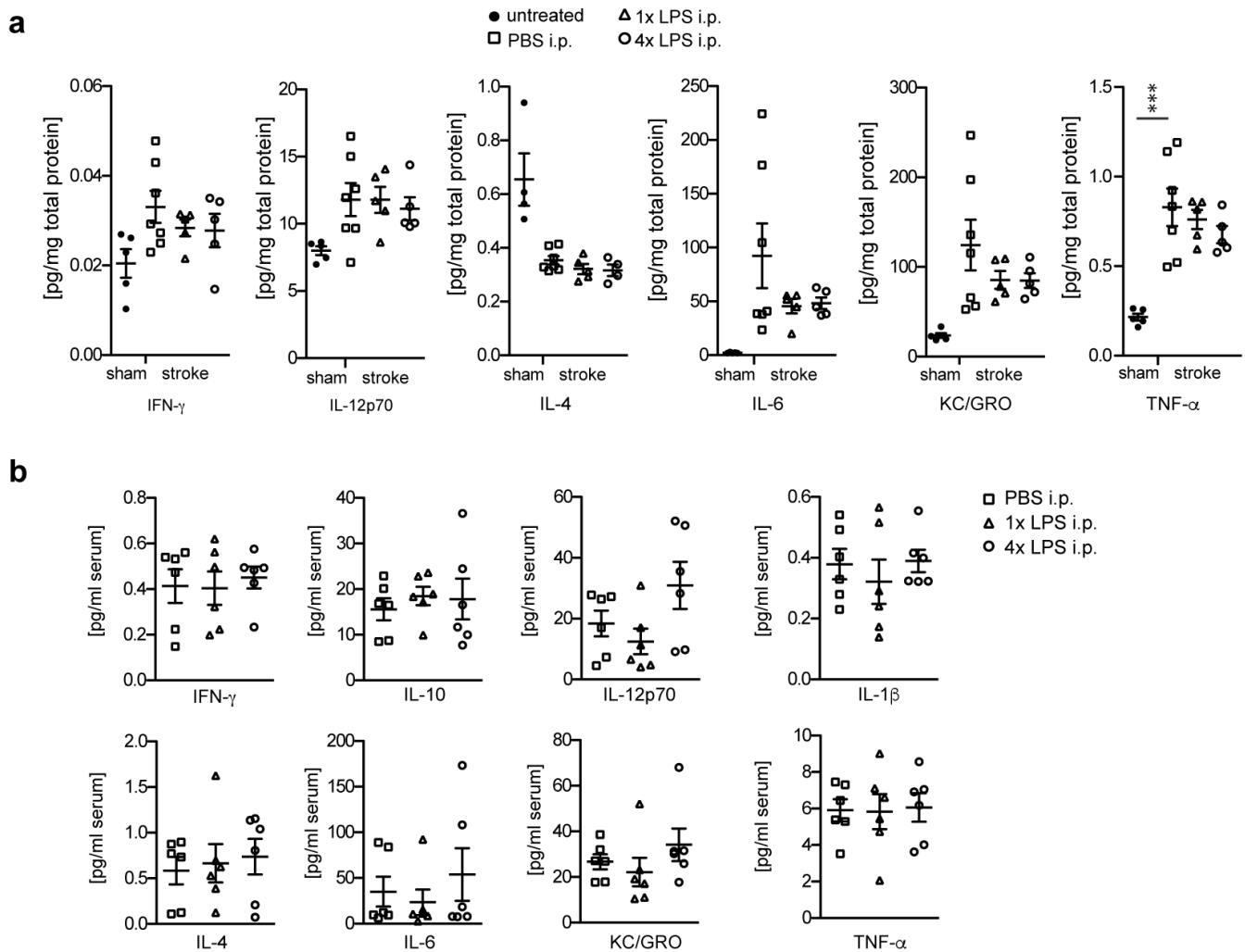
**a/b**, Micrograph of fluorescent staining for amyloid plaque (Methoxy-X04; green) and amyloid precursor protein (APP; red) shows neuritic dystrophy surrounding the amyloid deposit, which is unchanged by LPS treatments (b; n=5,5,5 animals). **c**, Overall Pearson's correlation of plaque size with neuritic dystrophy ('APP area'; n=49,39,42 plaques for PBS/1xLPS/4xLPS groups). **d**, Western Blotting analysis (for gel source data, see Supplementary Figure 1) of brain homogenates for amyloid precursor protein (APP) and C-terminal fragment- $\beta$  (CTF $\beta$ ; n=7,4,7 animals), and soluble APP $\beta$  ELISA (n=6,6,6 animals). **e**, Micrograph of activated astrocytes (glial fibrillar acidic protein: GFAP) surrounding an amyloid plaque (Congo Red) and quantification of the number of plaque-associated GFAP-positive astrocytes (n=6,6,5 animals). Scale bar: 10  $\mu\text{m}$  in (a), 20  $\mu\text{m}$  in (e). Data are means±s.e.m. \*  $P < 0.05$  for one-way ANOVA with Tukey correction.





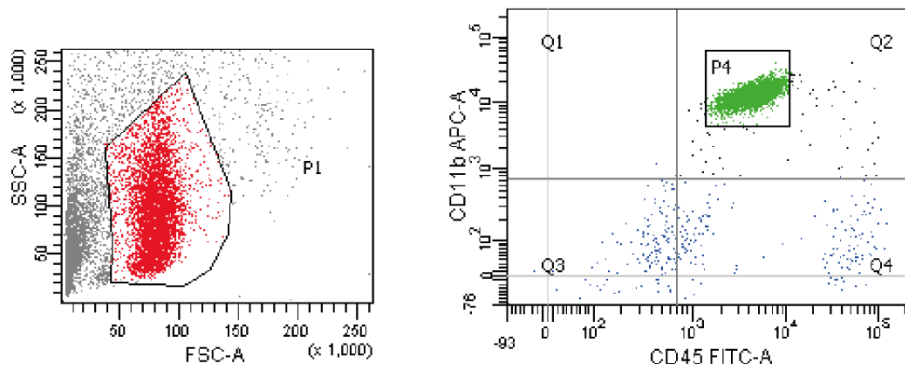
### Extended Data Figure 4: Cytokine levels in 9-month-old animals

**a**, Cytokine measurements in brain homogenates of 9-month-old wildtype (n=8,8,7 animals) and APP23 (n=14,10,10 animals) mice treated i.p. with 1x or 4xLPS at 3 months of age. **b**, Cytokine measurements in the serum of 9-month-old wildtype (WILDTYPE; n=14,9,13 animals) and APP23 (APP; n=18,12,14 animals) mice after i.p. stimulation with 1x or 4xLPS at 3 months of age. **c**, Cytokine measurements in the serum of wildtype animals stimulated i.p. with 1x or 4xLPS at 3 months of age and re-stimulated with an additional LPS injection (500 µg/kg) at 9 months of age (n=10,7,10 animals). Data are means±s.e.m. \*/\*\*  $P < 0.05/0.01$  for two-way ANOVA with Tukey correction. In (b) a significant main effect for genotype is indicated by bars spanning all conditions of the same genotype.



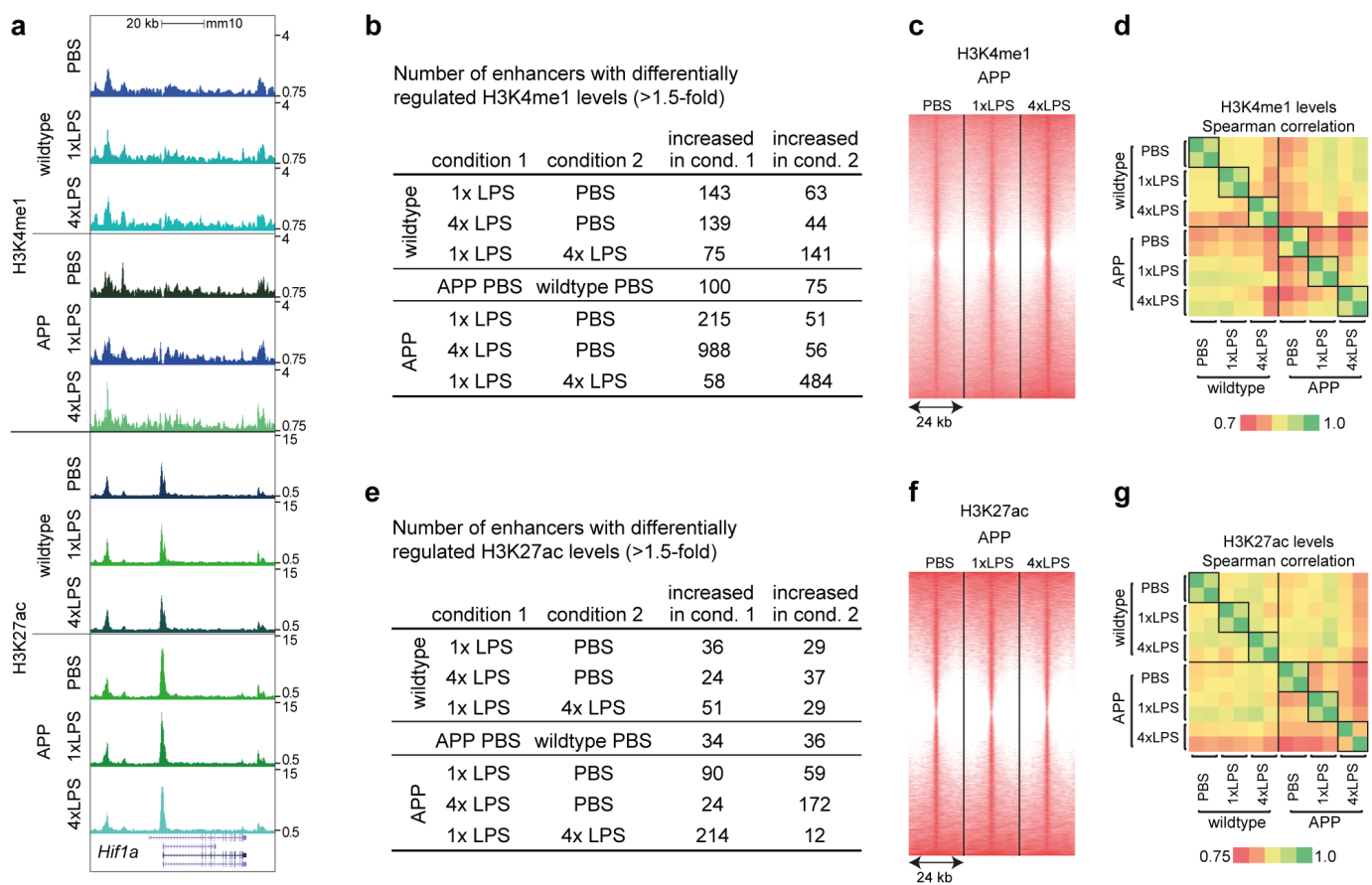
### Extended Data Figure 5: Cytokine levels after brain ischemia and in blood of 4-month-old animals.

Three-month-old animals were i.p. injected with 1x or 4xLPS and incubated for 4 weeks before receiving a stroke. **a**, Cytokine measurements in brain homogenates 24h after stroke (n=5,7,5,5 animals). **b**, Cytokine measurements in the serum (n=6,6,6 animals). Data are means±s.e.m. \*\*\*  $P < 0.001$  for one-way ANOVA with Tukey correction.



### Extended Data Figure 6: Microglial sorting strategy.

Microglia were sorted as CD11b<sup>high</sup> and CD45<sup>low</sup> cells (population P4) from 9-month-old APP23 animals or wildtype littermates following i.p. injections of 1x or 4xLPS at 3 months of age.



### Extended Data Figure 7: Analysis of microglial enhancers.

Microglial enhancers were analysed in 9-month-old wildtype and APP23 (APP) mice treated intraperitoneally with 1x or 4xLPS at 3 months of age. **a**, Exemplary UCSC browser images of genomic region around the *Hif1a* gene (normalised to input and library dimension). **b**, Numbers of regions with differentially regulated H3K4me1 levels. **c**, Heatmaps of H3K4me1 regions (centred on H3K27ac peaks). **d**, Pairwise correlations between the two replicates of H3K4me1 read densities in differentially regulated regions. **e-g**, Analyses of H3K27ac levels analogous to (b-d) for H3K4me1. n=2 replicates (8-10 animals/replicate); differential enhancers showed a cumulative Poisson P-value <0.0001; Benjamini-Hochberg correction was applied for pathway enrichment.

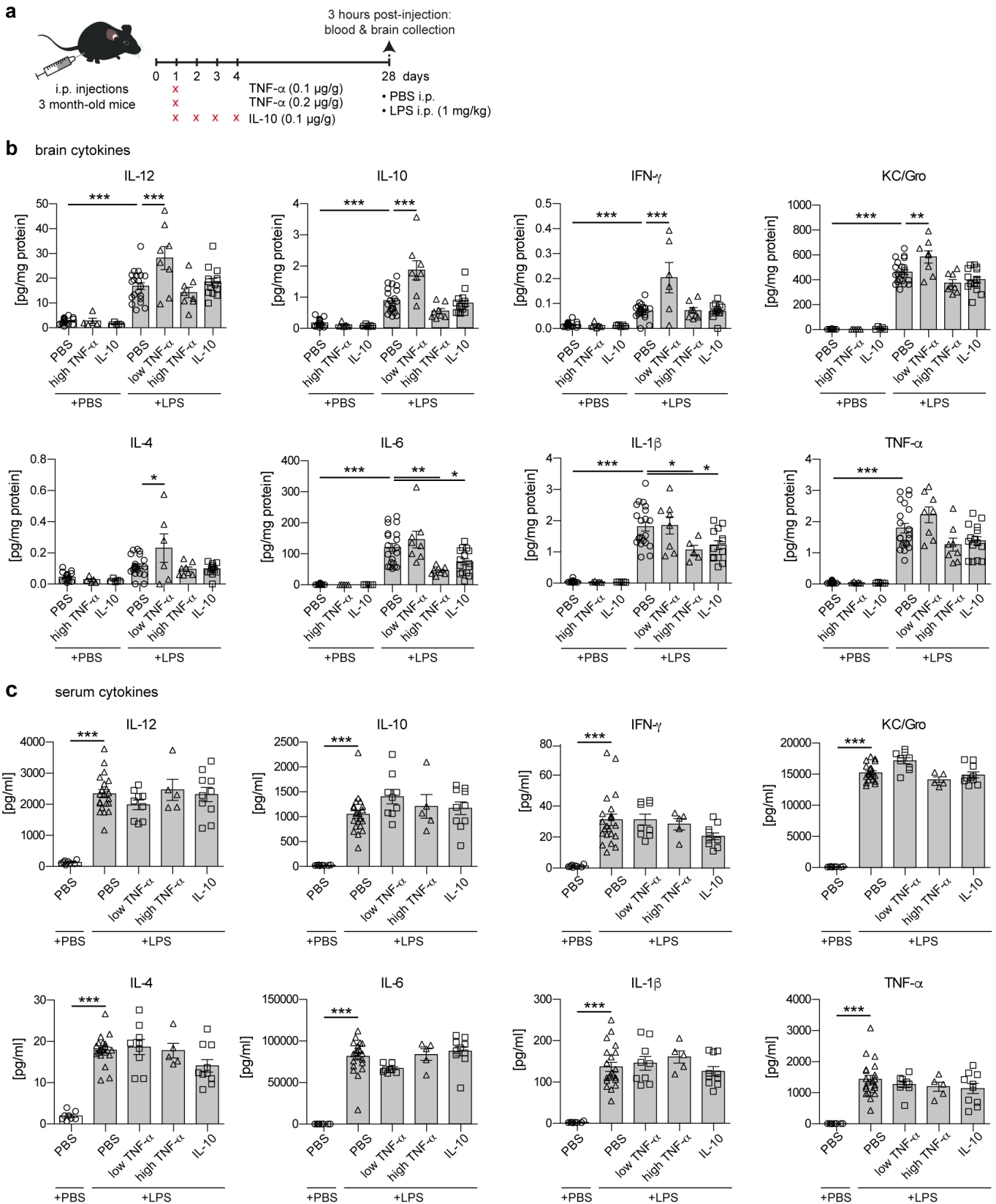
a		motifs enriched in all active enhancers (random background):		Known motifs				De novo motifs			
				Best Match	P-value	Targets	% Sequences with Motif Background	Best Match	P-value	Targets	% Sequences with Motif Background
		PU.1(ETS)	1e-624	26.58%	12.58%	Sfp1	1e-946	39.65%	19.51%		
		ELF5(ETS)	1e-549	32.44%	17.80%	PU.1:IRF8	1e-101	48.30%	40.82%		
		SpiB(ETS)	1e-511	14.65%	5.42%	Mef2a	1e-91	10.79%	6.90%		
		ETS1(ETS)	1e-492	39.47%	24.34%	RUNX2	1e-78	41.54%	35.16%		
		ETV1(ETS)	1e-471	47.55%	31.83%	Foxo1	1e-70	29.13%	23.68%		

b		comparison condition 1 2		known and de novo motifs enriched in enhancers of condition 1					known and de novo motifs enriched in enhancers of condition 2				
				Motif	Best match	P-value	Targets	% Sequences with Motif Background	Motif	Best match	P-value	Targets	% Sequences with Motif Background
APP PBS	wildtype PBS	ASATCAAAGC	TCF3	1e-06	6.80%	5.86%	TCGCASTI	TGIF2	1e-14	69.21%	65.97%		
		AGCTTTGAAC	TCF3	1e-36	0.58%	0.10%	ITGCAAT	TGIF1	1e-08	66.14%	63.66%		
		ATCACCCAT	SREBP1a	1e-03	4.69%	4.16%	AACCCGCTCTCA	TGIF2	1e-40	0.30%	0.01%		
		CACACGGAGTA	SREBP1a	1e-34	0.33%	0.04%	GTTCCGAGAT	IRF4	1e-50	0.50%	0.04%		
		ASICAAACCA	IRF4	1e-03	11.90%	10.96%	ATGAACTGC	IRF4	1e-23	0.26%	0.03%		
		GAAAAGTTTC	IRF4	1e-25	0.27%	0.04%	TCTGTCTCTT	Smad2/3	1e-29	1.03%	0.32%		
		CTAAAAATAGC	Mef2c	1e-03	12.17%	11.31%	TCAGACATCCCA	Smad3	1e-26	0.28%	0.03%		
		TCTATATG	Mef2b	1e-57	0.53%	0.05%	CGAGACAA	Smad2	1e-19	1.77%	0.92%		
							CTATCCCTCCTT	ATF1	1e-26	0.28%	0.03%		
							AGGAAATAT	ATF1	1e-25	0.27%	0.03%		
APP 1xLPS	APP 4xLPS	ATTGCGCAAC	CEBPb	1e-08	13.68%	12.23%	AGAGGAAAGTG	PU.1(ETS)	1e-10	24.57%	22.45%		
		ATGATGICAA	CEBPb	1e-02	16.62%	15.82%	CGAAATGAAAAT	PU.1:IRF8	1e-04	8.96%	8.11%		
		TCTTATCTIS	GATA2	1e-06	15.98%	14.62%	CGAAATGAAAAT	PU.1:IRF	1e-03	38.94%	37.61%		
		CAGATAAAGC	GATA1	1e-05	14.26%	13.10%	TCTCTCTCTCT	PU.1(ETS)	1e-17	0.37%	0.10%		
		CAGATAAAGC	GATA4	1e-04	24.00%	22.65%	GCTGASTCAGCA	MafK	1e-04	7.18%	6.42%		
		AGATAAAGC	GATA3	1e-04	34.99%	33.52%	TCGCAATCTT	MafF	1e-02	6.29%	5.77%		
		CCCTTATCACCA	GATA4	1e-43	0.32%	0.03%	TCGTGACTCA	MafA	1e-02	22.71%	21.88%		
		ATACGTGC	HIF-1b	1e-05	22.67%	21.23%	TTGTAAAAAA	MafB	1e-52	0.30%	0.02%		
		IACGTCC	HIF-1a	1e-02	4.20%	3.77%	GTGTGTGACCAT	MafA	1e-31	0.26%	0.03%		
		GTACGTIC	HIF-1a	1e-24	0.69%	0.23%	ASICAAACCA	IRF4	1e-03	11.89%	11.04%		
		GACGTGTA	ARNT::HIF1A	1e-17	0.27%	0.06%	CCAGAACACCT	IRF4	1e-45	0.27%	0.02%		
		CCCTGAGCCAT	AP-2gamma	1e-04	22.16%	20.85%	TCGCASTI	TGIF2	1e-02	67.78%	66.88%		
		ATCCCTGAGCC	AP-2alpha	1e-03	16.77%	15.77%	ITGCAAT	TGIF1	1e-02	64.71%	63.81%		
		CCCGTTA	MYB	1e-04	39.46%	38.06%	SCCGGAAAG	E2F	1e-02	6.96%	6.39%		
		ATATTAACIG	MYB	1e-53	0.56%	0.07%	AGCCGGGAA	E2F	1e-02	1.93%	1.65%		
		AGATCCAGCTGG	MYB	1e-53	0.30%	0.01%	ATGATCAITC	c-Jun	1e-02	6.18%	5.71%		
		CCGGAAATCF	TEAD4	1e-04	18.79%	17.65%	ATGACCTCAITC	JunD	1e-02	1.85%	1.59%		
		CGCACATTIC	TEAD4	1e-58	0.40%	0.03%							
		ACATCAAAGG	TCFL2	1e-03	2.39%	1.98%							
		GACTAFAAAG	TCFL2	1e-41	0.44%	0.06%							
CCCGTCTCC	Smad4	1e-02	42.15%	41.21%									
TAGCCCTCTG	Smad4	1e-36	0.54%	0.10%									
APP 1xLPS	APP PBS	ATACGTCC	HIF-1b	1e-14	22.67%	20.26%	ATGATGAAI	Atf4	1e-04	5.60%	4.89%		
		IACGTCC	HIF-1a	1e-03	4.20%	3.67%	GATTCGTGAG	Atf1	1e-47	0.43%	0.04%		
		TCACGTAA	HIF-1a	1e-18	0.28%	0.07%	GCTGASTCAGCA	MafK	1e-04	7.55%	6.76%		
		AGGTCAAGGICCA	RAR:RXR	1e-05	5.71%	4.97%	TCGTGACTCA	MafA	1e-03	23.32%	22.13%		
		AGGTCAAGGICCA	RARg	1e-04	3.02%	2.51%	TCGCAATCTT	MafF	1e-02	6.49%	5.92%		
		CAGATAAAGC	GATA4	1e-04	24.00%	22.76%	AGAGGAAAGTG	PU.1(ETS)	1e-02	23.81%	22.80%		
		TCTTATCTIS	GATA2	1e-03	15.98%	15.04%	CGAAATGAAAAT	PU.1:IRF8	1e-02	8.85%	8.27%		
		AGATAAAGC	GATA3	1e-03	34.99%	33.77%	CGAAATGAAAAT	PU.1:IRF	1e-02	39.43%	38.50%		
		CAGATAAAGC	GATA1	1e-02	14.26%	13.45%	CCCGGAGATATCTIS	GATA3	1e-02	2.99%	2.67%		
		ATGTACATGTCC	MYC	1e-59	0.35%	0.01%	GCAATAGCTAAG	GATA1	1e-51	0.40%	0.02%		
		GCCATGTG	MYC	1e-33	1.28%	0.50%	TATCTCAA	GATA3	1e-17	1.95%	1.12%		
		CCTCATGGGG	MYC	1e-29	0.27%	0.04%							
		AAAGCGGAAATG	SpiB	1e-15	13.15%	11.19%	CCCTGAGCCAT	AP-2gamma	1e-06	22.50%	20.82%		
		CCCTCTCTCTT	SpiB	1e-29	0.31%	0.04%	ATCCCTGAGCC	AP-2alpha	1e-05	17.06%	15.76%		
		ATGATGAAI	Atf4	1e-04	5.98%	4.83%	GACGCAAT	Atf4	1e-17	0.34%	0.08%		
ATGACCTCAITC	ATF7	1e-02	9.72%	9.05%	CTAAAAATAG	Mef2c	1e-05	12.17%	11.05%				
ATGACCTCAITC	ATF1	1e-02	13.83%	13.05%	CTAAAAATAG	Mef2a	1e-02	10.90%	10.14%				
ATGACCTCAITC	JunD	1e-04	1.85%	1.47%	ASATCAAAGGCA	Tcf4	1e-04	11.57%	10.53%				
ATGACCTCAITC	c-Jun	1e-02	6.39%	5.92%	TCAGGAGGSCA	Tcf4	1e-61	0.45%	0.03%				
					AGCTTTGAAC	Tcf3	1e-37	0.76%	0.17%				
APP 4xLPS	APP PBS	CCCTGICAAI	MEIS1	1e-02	42.34%	41.46%	ATTGCGCAAC	CEBPb	1e-03	13.80%	12.81%		
		TSACAGICAACC	MEIS1	1e-43	0.34%	0.04%	ATAGCCCA	CEBPg	1e-13	0.16%	0.02%		
							CCCGTTA	Myb	1e-02	39.82%	38.67%		
							GCAGTACAGAG	Myb	1e-68	0.39%	0.01%		
							ATTTCTATCTC	Gata5	1e-97	0.51%	0.02%		
							CTTATCCTGATA	Gata6	1e-45	0.36%	0.02%		
							CATAGTCT	Smad3	1e-27	6.22%	4.28%		
							CGTCTCAG	Smad2	1e-16	2.08%	1.25%		

### **Extended Data Figure 8: Transcription factor motif analysis of active enhancer regions.**

Motif analysis was performed for selected conditions to identify transcription factors involved in the differential activation of enhancers (using putative enhancer regions present in both replicates within 500 bp around enhancer peaks). **a**, For all active enhancers, motif analysis was performed using the union H3K27ac peak file and standard background (random genomic sequence). **b**, Pairwise comparisons between conditions, using the first condition's H3K27ac peak file as input and the second condition's peak file as background. As motif enrichment was often relatively low, the analysis was focussed on transcription factor (families), whose motifs occurred at least twice in 'known' (black) and 'de-novo' motifs (blue). Motifs are identified by HOMER software using hypergeometric testing (no adjustment for multiple comparisons was made).



### Extended Data Figure 9: Peripherally applied cytokines induce immune memory in the brain.

**a**, Experimental design. **b**, Cytokine responses in the brain, four weeks after peripheral cytokine application ( $n=17,5,5,21,8,8,15$  animals). Note that TNF- $\alpha$  dose-dependently enhances (low dose) or decreases (high dose) certain cytokines. Similar to high dose TNF- $\alpha$ , certain cytokines are also reduced by peripheral application of IL-10 four weeks earlier. **c**, Cytokine responses in the periphery are unaffected ( $n=8,21,9,5,10$  animals). Data are means $\pm$ s.e.m. \*/\*\*/\*\*  $P<0.05/0.01/0.001$  for one-way ANOVA with Tukey correction.

### **3.4 Systemic inflammation induces long-term modulation of amyloid plaque morphology and neuronal damage in a mouse model of Alzheimer's disease**

Ann-Christin Wendeln, Angelos Skodras, Natalie Beschorner, Peter Nilsson, Mathias Jucker, Jonas J. Neher

*In preparation*

## **Systemic inflammation induces long-term modulation of amyloid plaque morphology and neuronal damage in a mouse model of Alzheimer's disease**

Ann-Christin Wendeln<sup>1,2,3</sup>, Angelos Skodras<sup>1,2</sup>, Natalie Beschorner<sup>1,2,3</sup>, Peter Nilsson<sup>4</sup>, Mathias Jucker<sup>1,2</sup>, Jonas J. Neher<sup>1,2#</sup>

<sup>1</sup>German Center for Neurodegenerative Diseases (DZNE), Otfried-Müller-Str. 23, 72076 Tübingen, Germany.

<sup>2</sup>Department of Cellular Neurology, Hertie Institute for Clinical Brain Research, University of Tübingen, Tübingen, Germany.

<sup>3</sup>Graduate School of Cellular and Molecular Neuroscience, University of Tübingen, Tübingen, Germany.

<sup>4</sup>Department of Chemistry, Linköping University, Linköping, Sweden.

# *corresponding author*

### **Abstract**

Microglia, the resident parenchymal macrophages of the brain, adopt a variety of phenotypes in health and disease. Whether their role in Alzheimer's disease is beneficial or detrimental for disease progression is still under debate. A protective function of microglia in the compaction of amyloid- $\beta$  plaques has recently been described. Here, we stimulated pre-depositing APP23 mice peripherally with lipopolysaccharide (LPS), which we have previously shown to induce training (1xLPS) or tolerance (4xLPS) of the inflammatory response in the brain and differentially modulate cerebral  $\beta$ -amyloidosis. Using amyloid conformation-sensitive dyes, we herein demonstrate alterations in plaque structure 9 months after 1xLPS and 4xLPS treatment. While no other alterations in A $\beta$  pathology were detectable in 12 months old APP23 mice, number and phenotype of plaque-associated microglia were differentially modulated by peripheral immune stimulation. Both 1xLPS and 4xLPS resulted in long-term microglial barrier impairment, precipitating less compacted plaques associated with increased neuronal damage. Our study suggests a role of the individual peripheral inflammatory status in shaping amyloid plaque structure in the brain and demonstrates that systemic inflammatory events lead to long-lasting impairment in microglial barrier function associated with increased neurotoxicity.

## Introduction

It is now well accepted that many neurological diseases present with a strong immune component. For Alzheimer's disease (AD), the link between the immune system and disease pathogenesis was highlighted by the identification of risk variants in immune-related genes by large genome-wide association studies (Gagliano *et al.*, 2016; Guerreiro *et al.*, 2013; Hollingworth *et al.*, 2011; Huang *et al.*, 2017; Lambert *et al.*, 2013; Naj *et al.*, 2011; Sims *et al.*, 2017; Zhang *et al.*, 2013). Many of the disease-associated immune proteins such as Pu.1, CD33, complement receptor 1, and Trem2 are expressed in microglia, the brain's resident parenchymal macrophage population. Microglia participate in a variety of developmental and homeostatic processes in the brain and can acquire a broad spectrum of phenotypes characterized by differential transcriptional profiles (Gomez-Nicola & Perry, 2015; Keren-Shaul *et al.*, 2017; Krasemann *et al.*, 2017; Mathys *et al.*, 2017; Ransohoff & Perry, 2009). Their contribution to the onset and progression of AD has been intensely studied and resulted in many conflicting reports about the effects of immune system modulation on disease progression (Chakrabarty *et al.*, 2015; Heneka *et al.*, 2013; Jay *et al.*, 2017; Kitazawa *et al.*, 2011; Shi *et al.*, 2011; Vom Berg *et al.*, 2012), possibly due to cellular heterogeneity of immune cells in the brain. Single-cell sorting followed by transcriptional profiling has demonstrated strong heterogeneity in microglial expression profiles and identified molecular pathways activated in a subtype of microglia (termed disease-associated microglia – DAM, or microglia neurodegenerative phenotype – MgnD) under neurodegenerative disease conditions (Keren-Shaul *et al.*, 2017). In Alzheimer's disease, microglia localized in close proximity to amyloid- $\beta$  (A $\beta$ ) plaques differ in gene expression from plaque-distant microglia (Keren-Shaul *et al.*, 2017; Krasemann *et al.*, 2017). Recent studies described the compaction of amyloid plaques as a previously unappreciated function of plaque-associated microglia (Condello *et al.*, 2015; Wang *et al.*, 2016; Yuan *et al.*, 2016). Importantly, a change in the microglial activation state as a result of *CX3CRI* or *Trem2* knockout altered the structure and density of amyloid plaques. This, in turn, enhanced neurotoxicity, as evidenced by increased neuritic dystrophy and hyperphosphorylated tau around plaques.

Microglia are exceptionally long-lived cells with a median lifetime close to 24 months (equivalent to the lifespan of a mouse) in the cortex (Mai *et al.*, 2017, F $\ddot{u}$ ger *et al.*,



2017). These data indicate that at least a part of the microglial population persists for the entire lifetime of an animal. This is particularly important since microglia are sensitive to perturbations reaching the brain environment, including systemic inflammation (Cunningham, 2013; Perry *et al.*, 2007). We have recently shown that microglial stimulation results in modification of their epigenetic profile, which persists for many months, and subsequently modifies microglial responses to brain pathology, including A $\beta$  deposition (Wendeln & Degenhardt *et al.*, 2018). In particular, we found that peripheral immune stimulation of APP23 mice, a mouse model for cerebral  $\beta$ -amyloidosis (Sturchler-Pierrat *et al.*, 1997), before onset of A $\beta$  deposition differentially modulated the amount of amyloid pathology 6 months later (Wendeln & Degenhardt *et al.*, 2018).

In the present study, we further investigate whether microglial reprogramming before the onset of cerebral  $\beta$ -amyloidosis would subsequently affect the structure and neurotoxicity of amyloid plaques. To this end, we again applied single (1x) or repeated injections (4x) of lipopolysaccharide (LPS) to pre-depositing APP23 mice, which we have previously found to cause a heightened or reduced immune response to cerebral  $\beta$ -amyloidosis (also referred to as “training” and “tolerance”). Those two injection paradigms led to long-lasting alterations of the microglial epigenetic and transcriptional landscape, resulting in differential modification of plaque load upon early amyloid deposition. Here, we use the same injection paradigms to analyze whether a change in the microglial phenotype would alter amyloid plaque maturation, thereby affecting amyloid-associated neurotoxicity. Using a set of conformation-sensitive amyloid-binding dyes, the luminescent conjugated oligothiophenes (LCOs, (Klingstedt *et al.*, 2011), we show that both 1xLPS and 4xLPS injections at 3 months of age altered microglial features and thereby led to changes in plaque morphology and increased amyloid-associated neuritic dystrophy. These results confirm the protective nature of the microglial barrier function for the structural compaction of amyloid plaques and demonstrate that this function can be permanently impaired by systemic inflammation occurring much earlier in life.

## Methods

### Animals

For all experiments, 3 month-old hemizygous APP23 transgenic (C57BL/6J-Tg(Thy1-APP<sub>K670N;M671L</sub>)23) were used (Sturchler-Pierrat *et al.*, 1997). APP23 mice express human amyloid- $\beta$  precursor protein (APP) with the Swedish double mutation under the Thy-1 promoter, and have been backcrossed to C57BL/6J mice for >20 generations. Only female mice were used for experiments due to the described significant gender effect on the pathology of cerebral  $\beta$ -amyloidosis (Sturchler-Pierrat & Staufenbiel, 2000). In the neocortex, female mice develop the first amyloid plaques around 6 months of age (Sturchler-Pierrat *et al.*, 1997).

All animals were maintained under specific pathogen-free conditions and were housed in groups with enrichment. All experiments were performed in accordance with the veterinary office regulations of Baden-Württemberg (Germany) and were approved by the Ethical Commission for animal experimentation of Tübingen, Germany.

### Peripheral immune stimulation

Female APP23 mice were randomly assigned to treatment groups and were injected at the specified time points (3 months or 7 months) intraperitoneally (i.p.) with LPS (from *salmonella enterica* serotype typhimurium, Sigma) at a daily dose of 500  $\mu$ g/kg bodyweight. On four consecutive days, animals received either four LPS injections (4xLPS), or four vehicle injections (phosphate buffered saline, PBS), or a single LPS injection followed by three vehicle injections on the following three days (1xLPS).

At the specified time-points (6, 9, or 12 months of age), animals were deeply anaesthetised using sedaxylan/ketamine (64 mg/kg//472 mg/kg). Blood was collected from the right ventricle of the heart, followed by trans-cardial perfusion with ice-cold PBS through the left ventricle. The brain was removed and sagittally separated into the two hemispheres, which were either fixed in 4% paraformaldehyde (PFA) or fresh frozen on dry ice. Fresh frozen hemispheres were homogenised using a Precellys<sup>®</sup> lysing kit and machine at 20% (w/v) in homogenisation buffer (50 mM Tris pH 8, 150 mM NaCl, 5 mM EDTA) containing phosphatase and protease inhibitors (Pierce). Fixed hemispheres were kept in 4% PFA for 24 h, followed by cryoprotection in 30% sucrose in PBS, and subsequently frozen in 2-methylbutane. For histological analysis,

fixed brain hemispheres were coronally sectioned at 25  $\mu\text{m}$  using a freezing-sliding microtome (Leica).

### **Immunostaining**

Immunohistochemical stainings were performed on free-floating sections using either Vectastain Elite ABC kits (Vector laboratories) or fluorescent secondary antibodies (Jackson Immunolaboratories). If LCO costaining was desired, fluorescent secondary antibodies coupled to Alexa-647 were used for detection of the protein of interest, followed by staining with quadro-formyl thiophene acetic acid (qFTAA) and hepta-formyl thiophene acetic acid (hFTAA) (see below).

Brain sections were blocked for 1 h with 5% normal serum of the secondary antibody species, followed by primary antibody incubation overnight at 4°C. Primary antibodies used were: rabbit anti-Pu.1 (1:1,000; Cell Signaling), rabbit anti-Iba1 (1:1,000; Wako), rabbit anti-A $\beta$  (NT12; courtesy of P. Paganetti, Basel, Switzerland), rat anti-CD68 (1:1,000; Serotec), sheep anti-Trem2 (1:100; R&D systems), rabbit anti-APP (5313, 1:750; generous gift from C. Haas, Munich), and rabbit anti-GFAP (1:500, Biozol). Congo Red staining was conducted according to standard procedures. Immunohistochemical images were acquired on an Axioplan 2 microscope; colour images were captured using an Axioplan MRc camera and AxioVision 4.7 software (Carl Zeiss). Fluorescence images were acquired using an LSM 510 META (Axiovert 200M) confocal microscope with an oil immersion x40/1.3 objective and LSM software 4.2 (Carl Zeiss). Sequential excitation of fluorophores ensured no fluorescence cross-talk and best signal throughput. Maximum-intensity projections were generated using IMARIS 8.3.1 software (Bitmap) or Fiji.

### **LCO staining and spectral imaging**

Free-floating sections were stained with the LCOs qFTAA (1.5 mM in deionized water, diluted 1:500 in PBS) and hFTAA (1.5 mM in deionized water, diluted 1:1000 in PBS for double stain with qFTAA, 1:500 in PBS for single stain) for 30 minutes. After mounting, sections were dried and coverslipped with Fluorsave mounting medium (Calbiochem).

Spectra of qFTAA- and hFTAA-stained amyloid aggregates were acquired on a Zeiss LSM 510 META (Axiovert 200M) confocal microscope equipped with a spectral detector with an oil-immersion x40/1.3 objective. The dyes were excited using the

458 nm argon laser line. Emission spectra were acquired from 470 to 695 nm with steps of 10.7 nm at 3 different regions of interest (ROIs) within the middle core region from an intermediate plane of each plaque. Acquired plaques originated from at least three different sections throughout the mouse brain. The mean emission spectrum per plaque was calculated from the 3 ROIs and normalized to its respective maxima. The ratio of the intensity of emitted light at the qFTAA peak (502 nm) and the hFTAA peak (588 nm) was used as readout for spectral distinction of plaques. For 12 months old APP23 animals, the 502 / 588 nm ratio was calculated for statistical analysis from the normalized mean spectrum generated from at least 35 plaques per animal. Figure 1 shows pooled data from all PBS-injected control animals independent of injection time point.

For 9 months old APP23 animals, single staining with hFTAA was conducted and the emission spectrum of 20-30 plaques per animal was acquired and processed as described. The ratio of the intensity of emitted light at the two local emission maxima (545 nm and 588 nm) was used as readout for spectral distinction of plaques.

### **Image quantification**

For quantification of mean plaque area and Congo red positive area, mosaic images of 5 consecutive sections stained immunohistochemically for NT12 and Congo red were acquired on a Zeiss Axioplan 2 microscope with a x4/0.1 objective. Image analyses were automated using custom-written plugins in Fiji. Quantification of the mean plaque area was performed in the neocortex using the luminance channel. If needed, the gamma value was adjusted to ensure uniform contrast between staining and background. A fixed manual threshold was determined so that plaques were above threshold and was applied to all images. Staining of cerebral amyloid angiopathy and areas with high background staining were excluded from analysis. Only plaques with a minimum size of 30  $\mu\text{m}^2$  were included in the analysis. Automatic recognition of plaques was manually checked and corrected upon misclassification. The Congo red positive area was quantified by transforming the RGB image to the CIELAB colour space and subsequently thresholding the positive values of the  $a^*$  channel, which designates the purity of the red colour.

To quantify neuronal dystrophy, and microglial expression of Iba1, Trem2, and CD68, 5-10 fluorescent images per animal (APP: 7-44 plaques per animal, on average 22 plaques; Iba1: 6-55 plaques per animal, on average 22 plaques; CD68: 9-31

plaques per animal, on average 21 plaques; Trem2: 10-42 plaques per animal, on average 23 plaques) were acquired with the same microscope settings. Detection of qFTAA and hFTAA was achieved using bandpass filters encompassing their respective maximum emission wavelength. Images were subsequently semi-automatically analysed with another custom plugin written in Fiji. Maximum intensity projections were generated to choose the region of interest consisting of the plaque with the desired staining. Fluorescence channels were split and fixed intensity thresholds were applied to each channel. For every plaque, plaque size and area of the contained protein within the region of interest were determined based on thresholded areas. Plaques smaller  $100 \mu\text{m}^2$  or bigger  $2500 \mu\text{m}^2$  were excluded from analysis. The area of the protein of interest was divided by plaque size for normalization purposes.

To analyse colocalization between the protein of interest and the amyloid plaque, the same images were analysed in IMARIS. Using the 3D colocalization tool, a constant threshold was applied to the fluorescent channels for hFTAA and the protein of interest. The threshold for hFTAA was determined so that the whole amyloid plaque (i.e. including the qFTAA positive core) was included in the colocalization analysis. The percentage of colocalized plaque material in relation to total plaque material per image was used as readout for protein colocalization.

To assess the influence of plaque size and structure on neuronal dystrophy, acquired images from PBS-treated 12 months old APP23 controls were semi-automatically analyzed with a custom plugin written in Fiji. Maximum intensity projections were generated to choose the region of interest consisting of the plaque with the surrounding APP staining. For every plaque, a core region was chosen, wherein the intensity of qFTAA and hFTAA was subsequently measured. Fluorescence channels were split and fixed intensity thresholds were applied to each channel. Based on thresholded areas, plaque size and the ratio of qFTAA intensity to hFTAA intensity in its core were determined for every plaque (core qFTAA / hFTAA ratio), in addition to the area of surrounding APP staining. These data were generated for 192 plaques of 11 PBS-treated APP23 control mice and subsequently analyzed using JMP 13.0.

### **Stereological quantification**

Stereological quantification was performed by a blinded observer on random sets of every 12<sup>th</sup> systematically sampled 25  $\mu\text{m}$  thick sections throughout the neocortex. Analysis was conducted with the Stereologer software (Stereo Investigator 6; MBF

Bioscience) and a motorized x-y-z stage coupled to a video microscopy system (Optronics). For quantification of microglial numbers based on Pu.1 staining, the optical fractionator technique was used with three-dimensional dissectors as previously described (Varvel *et al.*, 2015). The number of plaque-associated GFAP- and Pu.1-positive cells was determined for at least 30 plaques per animal. Plaque load was determined using the area fraction fractionator technique (Bondolfi *et al.*, 2002) based on Congo Red and anti-A $\beta$  staining (NT12 antibody).

### **ELISA**

For quantification of A $\beta$  by ELISA, brain homogenates were pretreated with formic acid (Sigma-Aldrich, final concentration: 70% vol/vol), followed by sonication for 30 seconds on ice, and subsequent centrifugation at 25,000 g for 1 hour at 4°C. Supernatants were equilibrated in neutralization buffer (1 M Tris base, 0.5 M Na<sub>2</sub>HPO<sub>4</sub>, 0.05% NaN<sub>3</sub> (wt/vol)). A $\beta$  was measured using human (6E10) A $\beta$  triplex assay (Meso Scale Discovery, MSD) according to the manufacturer's instructions. Total A $\beta$  was calculated as the sum of the measured values for A $\beta$ <sub>1-38</sub>, A $\beta$ <sub>1-40</sub>, and A $\beta$ <sub>1-42</sub>.

For cytokine measurements, brain homogenates were centrifuged at 25,000 g for 30 minutes at 4 °C. Supernatants were analyzed with mouse pro-inflammatory panel 1 V-plex plate (MSD) according to the manufacturer's instructions. To determine blood cytokines, serum was obtained by coagulation of whole blood in Vacuettes (Greiner Bio-One) for 10 min at room temperature, followed by centrifugation for 10 min at 2,000 g. Serum samples were diluted 1:2 before cytokine measurement. The investigator was blinded to treatment groups.

Measurements were performed on a Mesoscale Sector Imager 6000 and data were analyzed using MSD discovery workbench software 2.0. For brain homogenates, cytokine levels were normalised against total protein amount as measured by microplate Pierce bicinchoninic acid (BCA) protein assay (Perbio Science).

### **Western Blotting analysis**

For Western Blotting, Urea was added at a final concentration of 5.4 M to total brain homogenates. Samples were incubated for 10 minutes at 70°C, followed by centrifugation for 1 minute at 16000 g. Pellets were discarded and protein levels of the supernatant were quantified with a microplate Pierce 660 nm protein assay (Thermo

Fischer) and adjusted to equal protein concentrations. After addition of Urea sample buffer (final concentration: 10% glycerol (vol/vol), 2% SDS (wt/vol), 0.0002% Bromophenol blue, 0.1M Tris-HCL (pH 8.6), 2%  $\beta$ -mercaptoethanol (vol/vol)) 15  $\mu$ g total protein per sample were analysed on BOLT 4-12% Bis-Tris gels (Thermo Fischer) using standard procedures. Proteins were transferred to nitrocellulose membranes, followed by boiling of the membranes for 5 minutes in a microwave. Ponceau S staining was conducted to verify equal protein transfer across samples. Blocking was performed with 5% milk in phosphate buffered saline containing 0.05% Tween (PBST) for 1h and blots were incubated with the following primary antibodies: mouse anti-A $\beta$  (6E10; 1:2500, Covance Research Products), mouse anti-GAPDH (1:10<sup>6</sup>, Acros Antibodies) in PBST overnight at 4°C. Membranes were then probed with the respective secondary HRP-labelled antibodies (1:20,000, Jackson ImmunoLaboratories). Protein bands were detected using chemiluminescent peroxidase substrate (ECL prime, GE Healthcare). Densitometric values of protein band intensities were determined in Fiji and normalised to GAPDH intensities. Samples were analysed at least three times on separate blots. The mean value of normalised intensities of all technical replicates per sample is shown and was used for statistical analysis.

### **Statistical analysis**

To assess the influence of plaque size and structure on the amount of neuritic dystrophy, a dataset comprising 192 plaques of 12 months old APP23 control mice was analysed in JMP 13.0. Plaque area and APP area were log<sub>10</sub> transformed to achieve normal distribution of data. An analysis of covariance (ANCOVA) was performed using the 'Fit model' tool with log<sub>10</sub>-transformed APP area as the dependent variable, and log<sub>10</sub>-transformed plaque area and core qFTAA / hFTAA ratio as independent variables.

All other statistical analyses were performed using Prism 6. Data were assessed for normal distribution (Shapiro-Wilk test) and statistical outliers (ROUT method, Q = 0.5%). The Brown-Forsythe test was used to check equality of variances. If the normality criterion was met and variances were not significantly different, data were analysed using a one-way ANOVA, followed by pairwise comparison (if P<0.05) with post-hoc Tukey correction. For data sets with small sample size, non-normally distributed data, or groups with unequal variances, the Kruskal-Wallis test was

performed, followed by pairwise comparisons (if  $P < 0.05$ ) with post-hoc Dunn's correction. For comparisons between two groups, two-tailed Mann Whitney test was performed. All experiments were at least performed twice or in independent batches of animals (figures show the pooled data). Data are presented as mean  $\pm$  standard error of the mean (SEM). In the figure legends, 'n' denotes the number of animals per treatment group.



## Results

Pre-depositing 3 months old APP23 mice were stimulated with either a single injection of LPS followed by three vehicle injections (1xLPS) or repeated injections of LPS on 4 consecutive days (4xLPS). We have recently shown that these stimuli induce long-lasting alterations of microglial function, with 1xLPS increasing microglial pro-inflammatory activity (e.g. enhancing glycolysis), and 4xLPS inducing a tolerant microglial state with reduced pro-inflammatory cytokine release and enhanced A $\beta$  phagocytosis (Wendeln & Degenhardt *et al.*, 2018). APP23 mice develop the first cerebral A $\beta$  deposits around 6 months of age and were analyzed at 12 months of age to determine the effect of systemic immune stimulation on plaque maturation. To this end, we employed staining with LCOs, a set of fluorescent amyloid-binding dyes that show changes in their emission spectrum upon binding of different amyloid structures (Aslund *et al.*, 2009; Klingstedt *et al.*, 2011). Costaining with two LCOs, qFTAA and hFTAA, followed by spectral imaging has previously been used to discriminate different amyloid plaque structures in human AD cases (Rasmussen *et al.*, 2017). While hFTAA stains both early prefibrillar states and mature A $\beta$  fibrils, qFTAA resembles Thioflavin S in its binding affinity for mature A $\beta$  fibrils in the dense core of plaques (Klingstedt *et al.*, 2011). Determining the ratio of emission intensities at the respective maxima of qFTAA and hFTAA (502 nm and 588 nm, respectively) in the plaque core has emerged as a useful readout for the spectral distinction of A $\beta$  plaques (Rasmussen *et al.*, 2017).

Strikingly, LCO staining revealed significant alterations of the amyloid plaque structure after 1xLPS and 4xLPS treatment. While 12 months old APP23 control mice (PBS treated) contained a heterogeneous mixture of plaque structures, LPS-treated animals predominantly demonstrated plaques with strongly reduced qFTAA staining (Figure 1a-d), indicating a shift in plaque morphology in response to peripheral immune stimulation 9 months earlier. Of note, both intra- (data not shown) and inter-individual variability in plaque structure was reduced after LPS treatment, demonstrating that systemic inflammation led to a shift from naturally occurring heterogeneity to predominance of one plaque structure (Figure 1b-d). These effects of peripheral LPS stimulation were absent in APP23 animals that were peripherally stimulated with LPS shorter before analysis (Supplementary Figure 1a-b), i.e. at

7 months of age, indicating that changes in plaque morphology require long incubation times and do not occur as an immediate result of LPS injection.

Changes in amyloid plaque structure after immune stimulation at 3 months were also detectable earlier in pathology when immature A $\beta$  fibrils predominate in APP23 mice. Prior to the age of 12 months, amyloid plaques show no binding affinity for qFTAA (Nyström *et al.*, 2013); however, hFTAA staining followed by spectral analysis can be used to assess structural differences in early immature A $\beta$  fibrils. In 9 months old APP23 animals that were treated at 3 months with 1xLPS or 4xLPS, a significant change in the emission spectrum of hFTAA, as determined by the ratio of the emission intensities at 545 nm and 588 nm, was observed in animals treated with 4xLPS only (Supplementary Figure 2a-b). Again, this effect was absent in animals stimulated with LPS at 7 months (Supplementary Figure 2c-d).

Alterations in the structure of amyloid plaques could occur as a result of differences in A $\beta$  pathology. We have previously shown that 1xLPS and 4xLPS treatment led to an increased (for 1xLPS) or decreased plaque load (for 4xLPS) in 9 months old APP23 animals. However, at 12 months of age no changes in cortical plaque load, determined as the percentage of A $\beta$  positive area in the cortex, were detectable after LPS treatment (Figure 1e), indicating that the sustained overexpression of A $\beta$  may override the effect of LPS on plaque load in later stages of pathology. Accordingly, total brain A $\beta$  levels were not significantly altered at 12 months in comparison to PBS treated control animals. Furthermore, we could not detect changes between treatment groups in the ratio of brain A $\beta_{1-42}$  to brain A $\beta_{1-40}$  (Figure 1f), excluding that different plaque structures occur as a result of altered proteolytic generation of A $\beta$  isoforms. In addition, levels of amyloid precursor protein (APP) and C-terminal fragment (CTF- $\beta$ ) were equal between treatment groups (Supplementary Figure 3a), indicating that A $\beta$  processing itself was not altered.

The amount of qFTAA binding to amyloid plaques in APP23 animals increases with age as amyloid plaques grow in size and maturation of A $\beta$  fibrils takes place (Nyström *et al.*, 2013). Therefore, we analyzed the mean size of amyloid plaques and mean Congo red positive area (Supplementary Figure 3b), but could not detect significant differences among treatment groups. Analysis of 6 months old APP23 mice that were previously stimulated with LPS at 3 months of age demonstrated equal plaque load and brain A $\beta$  levels of PBS and LPS treated animals (Supplementary Figure 3c-e). This indicates that onset of A $\beta$  pathology is not changed by LPS

stimulation, therefore excluding that structural alterations of plaques occur as a result of a different age of plaques.

Since we could not find evidence for alterations in A $\beta$  pathology other than plaque morphology by LPS stimulation, and because we have previously shown that the microglial phenotype is differentially altered after 1xLPS and 4xLPS treatment, we next examined whether alterations in plaque structure occur through a modulation of microglial responses. We therefore compared cardinal features of microglial activation among the different treatment groups. First, we analyzed the immune state in brain and periphery of 12 months old APP23 animals. While no significant alterations in serum cytokine levels were detectable (Supplementary Figure 4a), 1xLPS treated animals exhibited enhanced cytokine expression of IFN- $\gamma$ , IL-6, and IL-12 in the brain (Figure 2a), in line with previous results.

Recent studies implicate the microglial activity state and in particular Trem2 expression in the compaction of A $\beta$  plaques (Condello *et al.*, 2015; Wang *et al.*, 2016; Yuan *et al.*, 2016), therefore we analyzed microglial numbers and phenotype in LPS treated 12 months old APP23 mice. Stereological quantification revealed a significant reduction in the number of plaque-associated microglia in 4xLPS treated animals, while the overall number of microglia was not changed (Figure 2b). No alterations in the number of plaque-associated astrocytes were detectable (Supplementary Figure 4b). Analysis of Iba1 staining revealed a reduction in the amount of plaque-associated Iba1-positive microglial process area after 4xLPS treatment (Figure 2c). These data indicate that there is a specific reduction of plaque-associated microglia after 4xLPS treatment at 12 months of age, possibly due to altered migration or turnover and in line with our previous description of a sustained suppression of microglial activation (tolerance) following 4xLPS treatment. The observed reduction in the number of plaque-associated microglia leading concomitantly to less microglial processes compacting the amyloid plaque in 12 months old APP23 mice could result in impairment of the microglial barrier function and thereby to the described alterations in amyloid plaque structure. The reduction in plaque-associated microglial number observed after 4xLPS in 12 months old APP23 mice diminishes upon injection of LPS at 7 months (Supplementary Figure 1c), similar to the described effects of LPS on plaque structure.

Next, we analyzed microglial CD68 expression because we have previously observed increased A $\beta$  phagocytosis in 4xLPS treated microglia (Wendeln & Degenhardt *et al.*,

2018). CD68 marks active phagolysosomes and is activity-dependently regulated in microglia (Hendrickx *et al.*, 2017; Rabinowitz *et al.*, 1992). In 12 months old APP23 animals, quantification revealed a significant reduction of CD68 positive area around plaques in 1xLPS treated animals in comparison to 4xLPS (Figure 3a-c). Colocalization of CD68 with amyloid plaques was significantly reduced after 1xLPS treatment in comparison to controls. These results indicate a reduction in phagocytic activity of microglia by 1xLPS, but not 4xLPS treatment.

Microglial Trem2 has previously been implicated in the microglial barrier function, since Trem2<sup>-/-</sup> mice and sporadic AD cases with Trem2 R47H variant have impaired microglial migration to the plaques, resulting in a higher degree of diffuse amyloid plaques (Wang *et al.*, 2016; Yuan *et al.*, 2016). Therefore, we analyzed microglial Trem2 expression in LPS stimulated 12 months old APP23 mice. In line with previous studies, we found Trem2 to be specifically expressed in microglial processes contacting the amyloid plaque (Figure 3d). Similar to CD68, quantification of the Trem2 positive process area revealed a differential effect of 1xLPS and 4xLPS, with 1xLPS treated microglia showing decreased Trem2 positive areas. Colocalization of Trem2 with amyloid plaques was also significantly reduced in 1xLPS treated animals compared to 4xLPS (Figure 3e-f), even though less plaque-associated microglia were observed after 4xLPS. However, colocalization analysis of constitutively expressed microglial Iba1 revealed no differences between treatment groups (Figure 2c), excluding that the differences in the analyzed phenotype-dependent microglial markers occur due to an impaired microglial localization to the plaques. In summary, microglial expression of both Trem2 and CD68 was reduced in 1xLPS animals, indicating a shift in microglial activity in 1xLPS, but not 4xLPS, treated animals. These data highlight that in line with our previous work 1xLPS and 4xLPS differentially modulate the microglial response to cerebral  $\beta$ -amyloidosis, and either change in the microglial activation state is sufficient to alter plaque structure in APP23 animals.

According to the amyloid cascade hypothesis, aggregation of A $\beta$  subsequently induces inflammatory processes and neuronal tau pathology, ultimately resulting in neuronal and synaptic damage (Hardy & Selkoe, 2002; Karran *et al.*, 2011). An impairment in microglial barrier function, which leads to reduced compaction of amyloid plaques, has been shown to result in increased neurotoxic properties of plaques (Condello *et al.*, 2015; Wang *et al.*, 2016; Yuan *et al.*, 2016). Thus, we

analyzed whether plaque-associated neuronal damage was altered in LPS treated animals. Strikingly, both 1xLPS and 4xLPS treated animals showed increased amyloid-associated neuritic dystrophy, as indicated by an increased area of APP-positive dystrophic boutons around plaques (Figure 4a). Moreover, the amount of amyloid-associated neuritic dystrophy for individual plaques was significantly influenced not only by plaque size but also the qFTAA / hFTAA ratio of the plaque core (Figure 4b-c). Decreased qFTAA binding in the plaque core, corresponding to a lower grade of compactness of plaques, was associated with increased neuritic dystrophy, in line with the idea that the microglial barrier function is protective and renders plaques more inert.

## Discussion

We have herein demonstrated that following earlier systemic inflammation microglial barrier function is altered for at least 9 months in mice, leading to lasting structural changes of amyloid plaque deposits in a mouse model of AD. Our initial approach was to use two different stimuli (1xLPS and 4xLPS) whose acute and long-term effects on microglia we have recently characterized in 9 months old animals with early plaque deposition. A single injection of LPS primes microglia to respond with a trained, i.e. heightened, immune response to a secondary stimulus (e.g. the deposition of A $\beta$ ). In contrast, 4xLPS induces a long-lasting tolerant state in microglia, thereby altering their reaction to amyloid plaque deposition, resulting in increased microglial A $\beta$  uptake and decreased plaque load in 9 months old APP23 animals. At this early disease stage, plaque structure is already significantly altered in 4xLPS treated animals, possibly due to increased phagocytic activity of tolerized microglia. However, the effect of LPS on plaque structure becomes more evident at more advanced stages of cerebral  $\beta$ -amyloidosis, with similar changes being observed in the two LPS treatment groups. This is possibly due to the maturation of plaques over time, enabling the use of the qFTAA/hFTAA double stain as a more sensitive readout for spectral discrimination of plaques. At 9 months of age, A $\beta$  pathology is still in an early phase, thus a qFTAA positive core is absent in nearly all plaques. In contrast, at 12 months of age, a substantial amount of plaques stains positive for both qFTAA and hFTAA, enabling a broader range of detection for changes in plaque structure. As it was previously shown that the microglial coverage of plaques reduces as the aggregates grow (Condello *et al.*, 2015), it is also conceivable that alterations of the microglial barrier function have a larger impact at later stages of pathology. Interestingly, qFTAA binding to amyloid plaques increases with pathology as plaques mature, but is reduced again in animals over 20 months of age, indicative of less compacted plaques in aged animals (Nyström *et al.*, 2013). A recent study suggested that microglial coverage of amyloid plaques decreases in aged mice, thereby reducing plaque compactness (Condello *et al.*, 2015). It seems conceivable that, similar to other microglial functions (Hefendehl *et al.*, 2014), the microglial barrier diminishes with age, thereby contributing to age-associated increased pathology.

While both 1xLPS and 4xLPS led to similar alterations in plaque structure, this effect occurred through different microglia-mediated mechanisms. Our results indicate that

at 12 months of age 1xLPS treatment led to a change in plaque-associated microglial phenotype with reduced Trem2 and CD68 expression, while reduced plaque-associated microglial numbers were present in 4xLPS treated animals. Both mechanisms ultimately led to an impairment of microglial barrier function, thereby resulting in less compacted amyloid plaque structures. Previous reports have demonstrated alterations in the microglial barrier function as a result of *Trem2* or *CX3CR1* deficiency (Condello *et al.*, 2015; Wang *et al.*, 2016; Yuan *et al.*, 2016). Our results demonstrate that microglia mediated alterations of amyloid plaque structure are not necessarily genotype-dependent, but can also be induced by overall changes in the number of plaque-associated microglia following systemic inflammation. Despite the observed reduction of the number of plaque-associated microglia after 4xLPS, these animals had unaltered or even increased levels of microglial Trem2 and CD68, indicating that the remaining microglia may sense the loss of neighboring microglia and try to compensate for their lack in barrier function. At 9 months of age, numbers of plaque-associated microglia were not significantly altered between treatment groups (Wendeln & Degenhardt *et al.*, 2018), demonstrating that the initial microglial reaction and migration to the developing amyloid plaques is not changed. It is likely that the later observed differences in microglial numbers occur as a result of long-lasting epigenetic alterations induced by systemic LPS treatment, which could impact the turnover (proliferation or death rate) of microglia. So far, microglial turnover has only been investigated under homeostatic conditions or cerebral  $\beta$ -amyloidosis, but not in the context of systemic inflammation, which would be an interesting area to pursue.

Our results are in line with our previous description of 1xLPS and 4xLPS as stimuli exerting differential long-lasting effects on microglia. In 9 months old animals, we have previously shown these long-term alterations in microglial function to be mediated by epigenetic reprogramming in response to immune stimulation. Since differential effects of the two LPS stimuli on microglia and brain cytokine release were still present in 12 months old APP23 mice, it seems highly likely that these effects are also epigenetically mediated, indicating that microglial immune memory persists even longer than we previously described.

Through impairment of the microglial barrier function, both 1xLPS and 4xLPS treatment resulted in less compact amyloid plaques that were associated with increased neuritic dystrophy. These results are in line with previous reports

demonstrating a neuroprotective function of the microglial barrier around amyloid plaques (Condello *et al.*, 2015; Wang *et al.*, 2016; Yuan *et al.*, 2016). Similar to these previous studies, we found increased neuronal damage around plaques that were less compacted as a result of an impaired microglial barrier.

While we have demonstrated a beneficial effect of the tolerizing 4xLPS stimulus at an early stage of pathology, our present study revealed detrimental effects of both 1xLPS and 4xLPS on neuronal damage at a later stage of pathology. Similar stage-dependent effects on the pathology of cerebral  $\beta$ -amyloidosis have been described for knockout of Trem2 (Jay *et al.*, 2017).

Interestingly, our results indicate that the amount of neuritic dystrophy can be predicted as a function of plaque size and the LCO core ratio as a measure of plaque structure. Thereby, our results implicate LCO staining followed by spectral analysis as a useful indicator for the assessment of neuronal damage. Since neuronal damage is on a molecular level the best correlate for cognitive dysfunction in AD patients, our results suggest alterations in plaque structure as highly relevant for disease progression.

In summary, our results demonstrate that systemic inflammation induces long-lasting changes in the microglial response to plaques. This effect of systemic inflammation becomes evident months after the acute immune response and leads via impairment of the microglial barrier function to alterations in amyloid plaque structure that are linked to the amount of amyloid-associated neuronal damage. If these mechanisms also occur in humans, long-lasting microglial memory of systemic inflammatory events could impact the structure of much later appearing amyloid plaques and thereby represent another microglia-mediated mechanism influencing neurological disease progression.



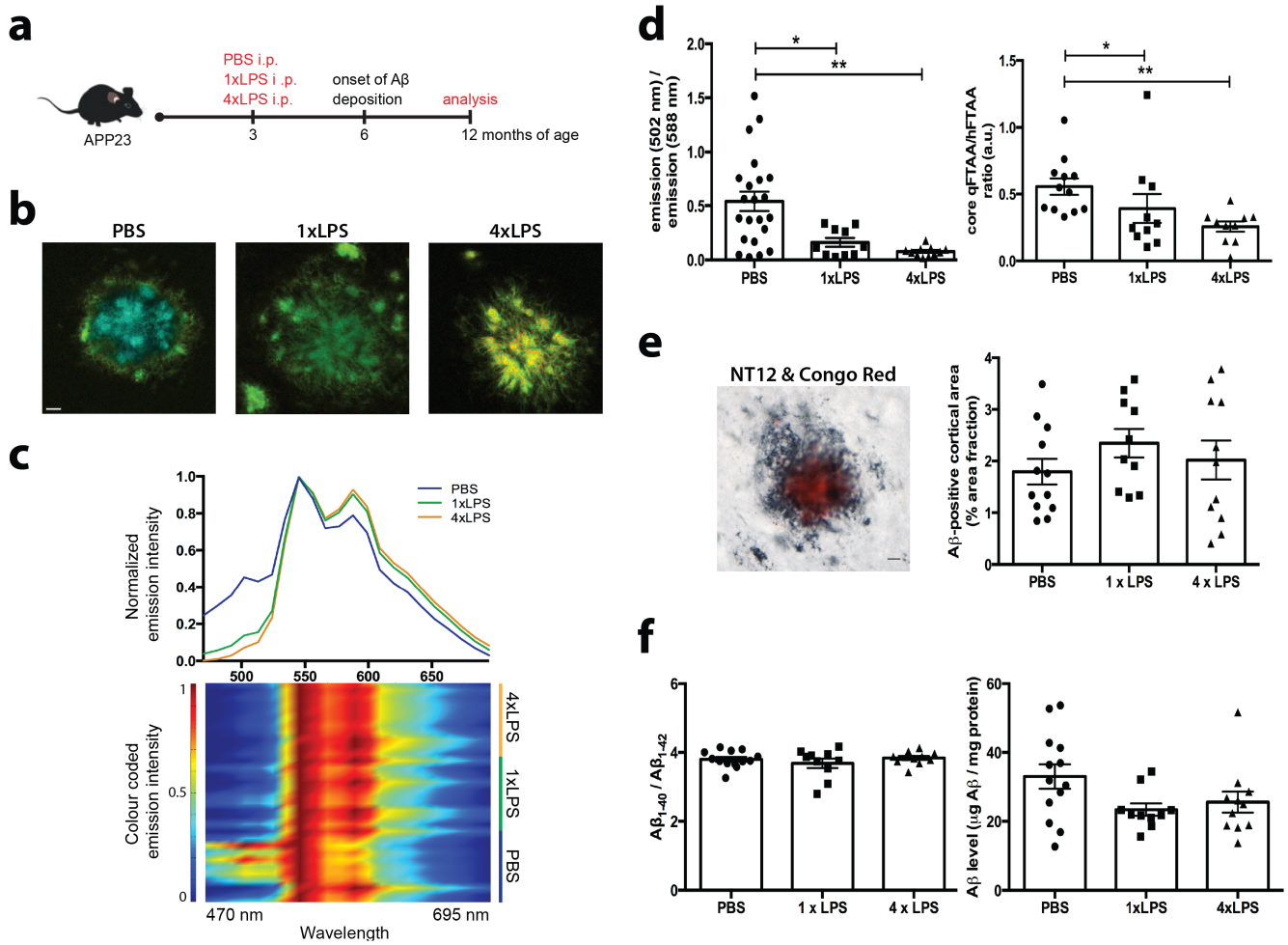


**Figure 1: Alterations in plaque morphology after peripheral immune stimulation.**

**a**, Experimental design. **b**, Micrographs depicting representative plaque morphologies in the different treatment groups after qFTAA and hFTAA staining. **c**, Normalized emission spectra per treatment group and colour coding of mean normalized emission spectra per animal. LPS treatment reduced inter-individual variability and shifted emission spectra to red wavelength. **d**, Ratio of emission intensities at 502 / 588 nm of the average spectrum per animal (n=22,10,11) and quantification of the core qFTAA/hFTAA ratio (n=12,10,10) from maximum intensity projections of acquired z-stacks revealed significant differences in plaque structure of 1xLPS and 4xLPS treated animals in comparison to controls. **e**, Micrograph and quantification of cortical A $\beta$  plaque load (n=12,10,11) per animal. **f**, ELISA measurement of total A $\beta$  levels and A $\beta_{1-40}$  to A $\beta_{1-42}$  ratio (n=13,10,11). Scale bar 10  $\mu$ m. \*/\*\*=p<0.05/0.01. Data are presented as mean  $\pm$  SEM.

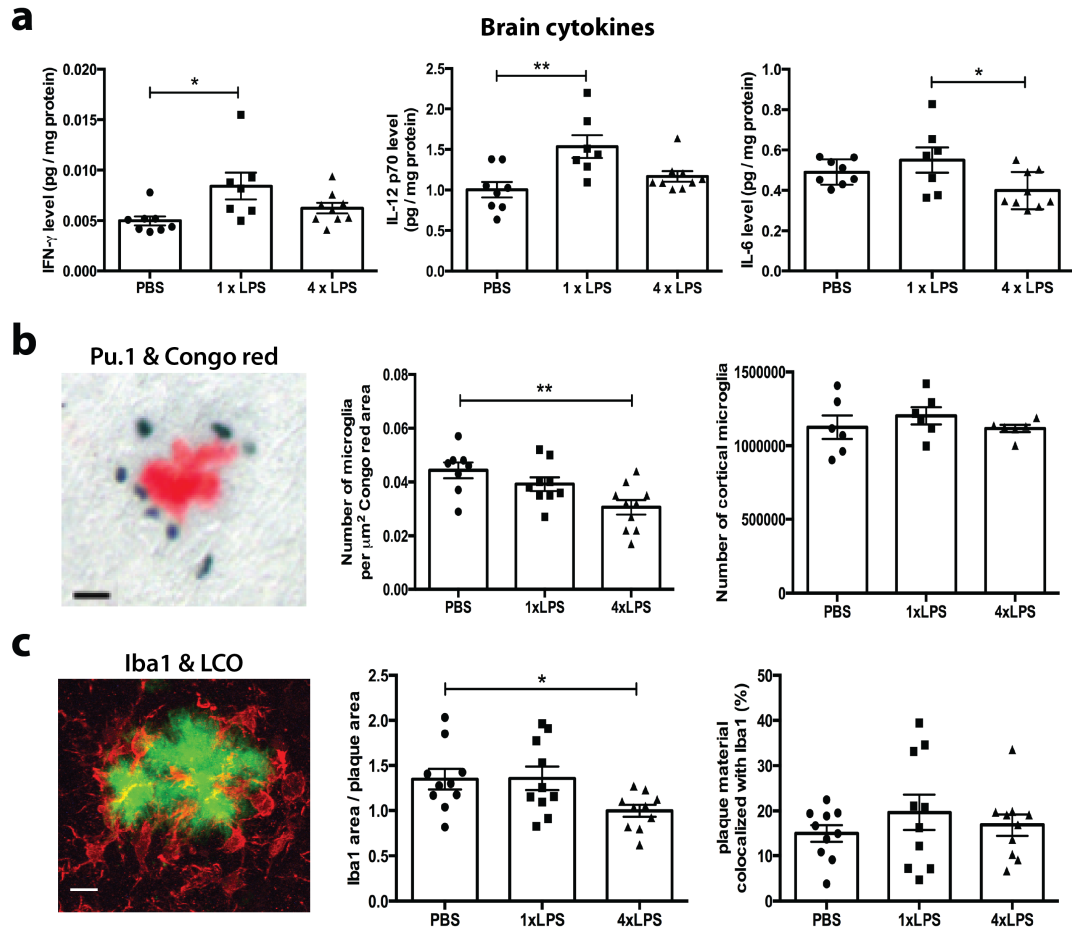


**Figure 2: Long-term changes in brain cytokine levels and number of plaque-associated microglia after peripheral immune stimulation.**

**a**, ELISA measurement of brain cytokine levels for IFN- $\gamma$ , IL-12, and IL-6 (n=8,7,9) showed increased amounts in 1xLPS treated animals. **b**, Micrograph and stereological quantification of Pu.1 stained plaque-associated (n=8,9,10 animals) and total microglia (n=6,6,6 animals). **c**, Immunofluorescent costaining for Iba1 (red) and qFTAA (blue) / hFTAA (green), quantification of normalized plaque-associated Iba1 positive area, and colocalization with plaque staining (n=10,10,10 animals with 22 plaques per animal on average). Scale bar 10  $\mu\text{m}$ . \*/\*\*=p<0.05/0.01. Data are presented as mean  $\pm$  SEM.

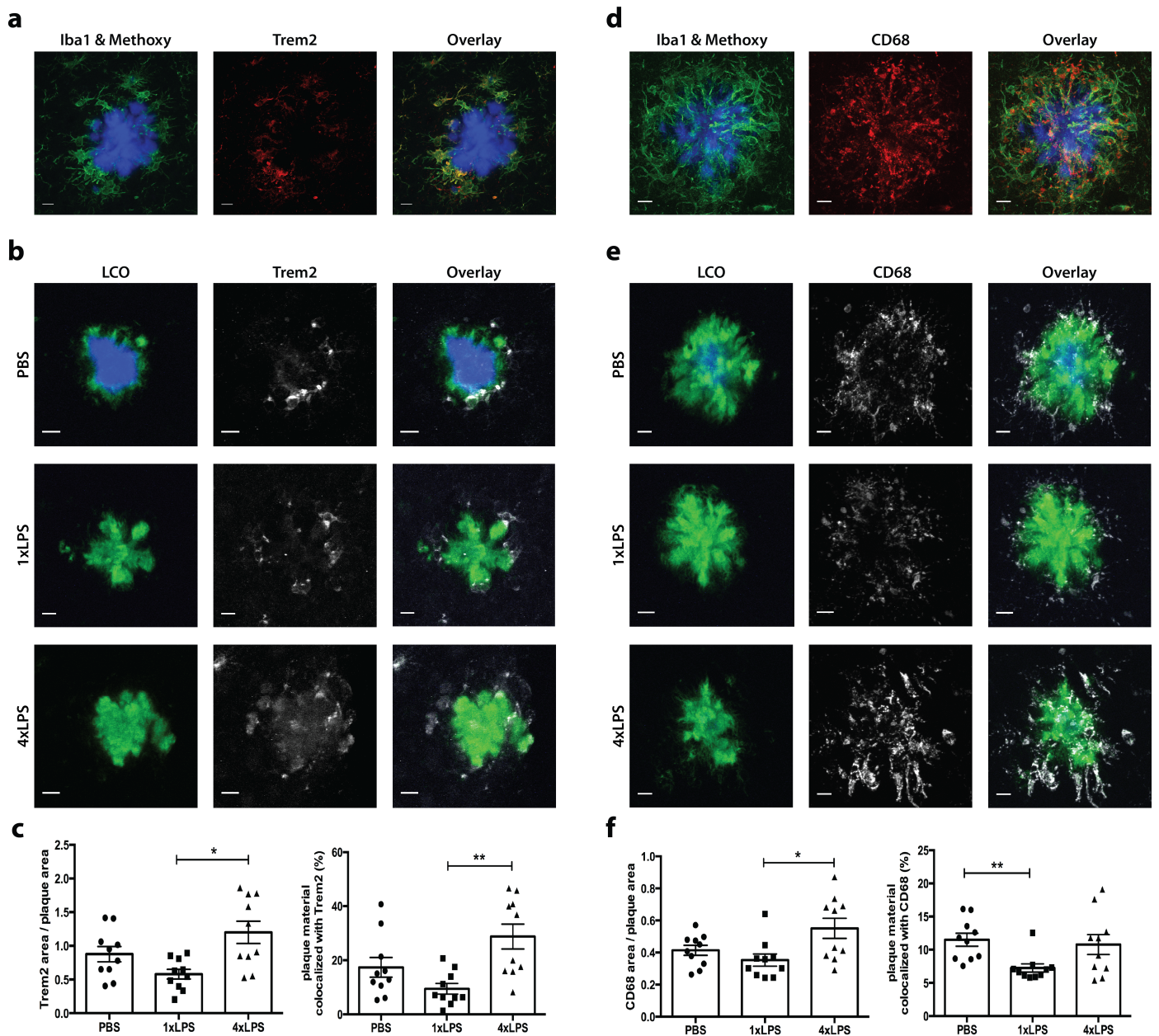


**Figure 3: Alterations in microglial Trem2 and CD68 expression after systemic inflammation.**

**a**, Immunofluorescent staining for Trem2 showing colocalization with Iba1. **b**, Representative images of Trem2 staining in different treatment groups. **c**, Quantification of normalized plaque-associated Trem2 positive area and colocalization with plaque staining (n=10,10,10 animals with 23 plaques per animal on average). **d**, Immunofluorescent staining for CD68 showing colocalization with Iba1. **e**, Representative images of CD68 staining in different treatment groups. **f**, Quantification of normalized plaque-associated CD68 positive area and colocalization with plaque staining (n=10,10,10 animals with 21 plaques per animal on average). Scale bar 10  $\mu$ m. \*/\*\*=p<0.05/0.01. Data are presented as mean  $\pm$  SEM.

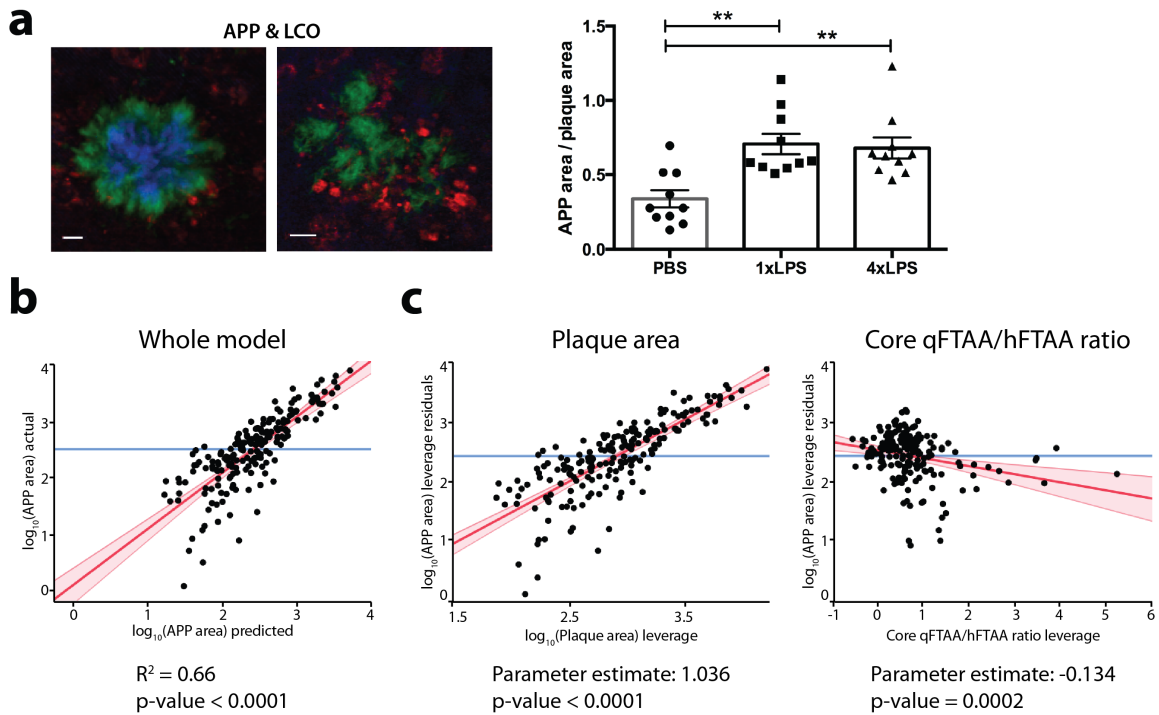
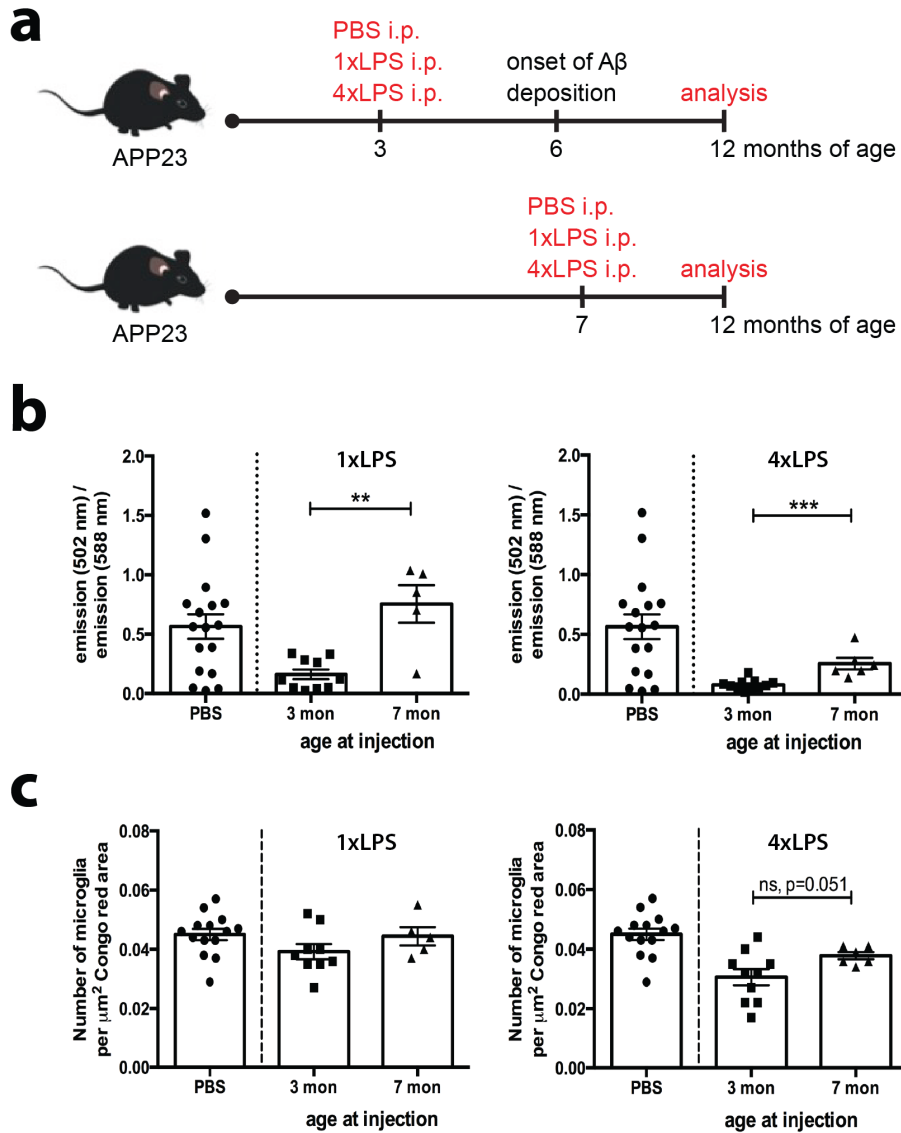


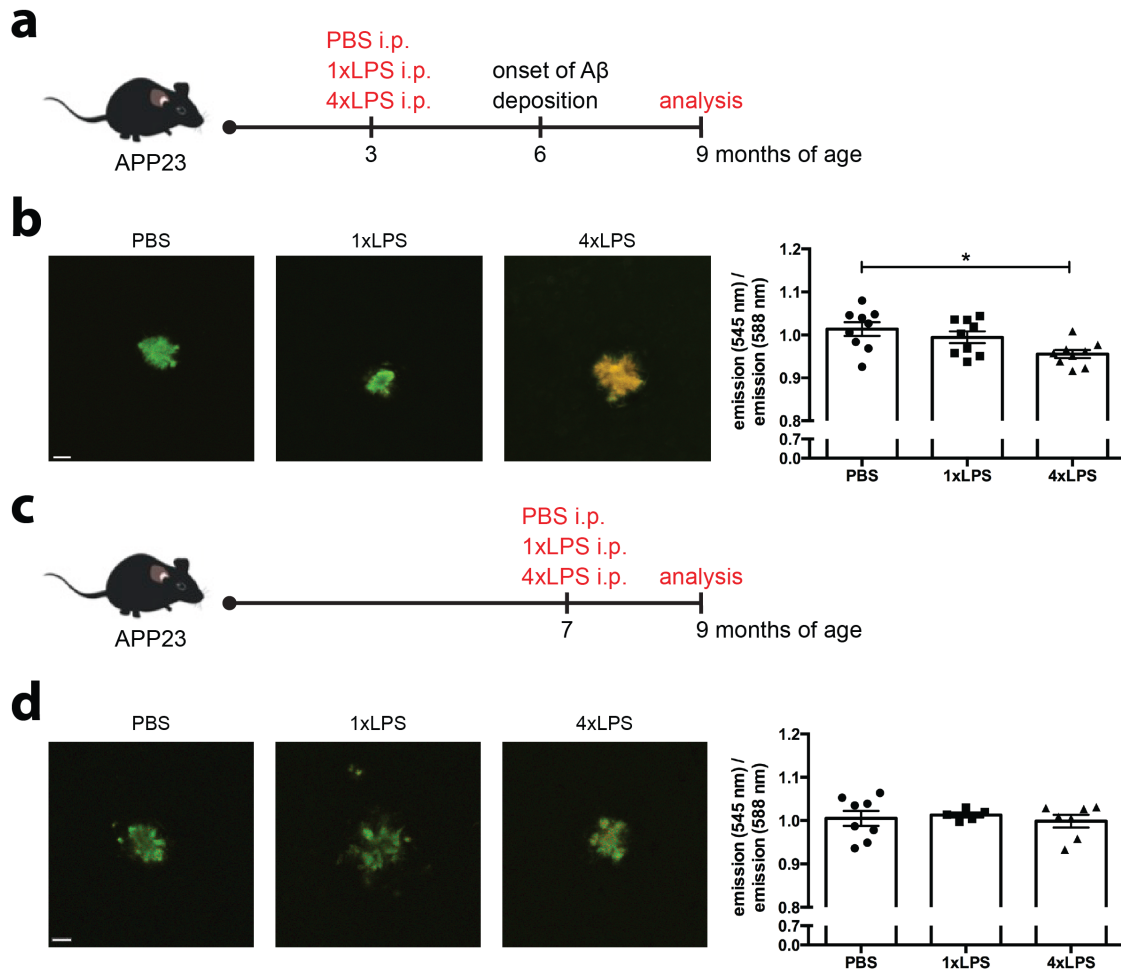
**Figure 4: Influence of plaque structure and size on amyloid-associated neuritic dystrophy.**

**a**, Immunofluorescent costaining of APP (red) with qFTAA (blue) / hFTAA (green) and quantification of normalized amyloid-associated APP positive area (n=10,10,10 mice with 22 plaques per animal on average). \*\*/=p<0.05/0.01. Scale bar 10  $\mu\text{m}$ . Data are presented as mean  $\pm$  SEM. **b**, Whole model plot depicting actual against predicted APP areas based on 192 plaques of 11 APP23 control mice at 12 months of age. **c**, Effect leverage plots and parameter estimates demonstrating the significant influence of plaque area and core qFTAA/hFTAA ratio on the amount of plaque-associated neuritic dystrophy.  $F(2,189)=184.5889$ ,  $p<0.0001$ .



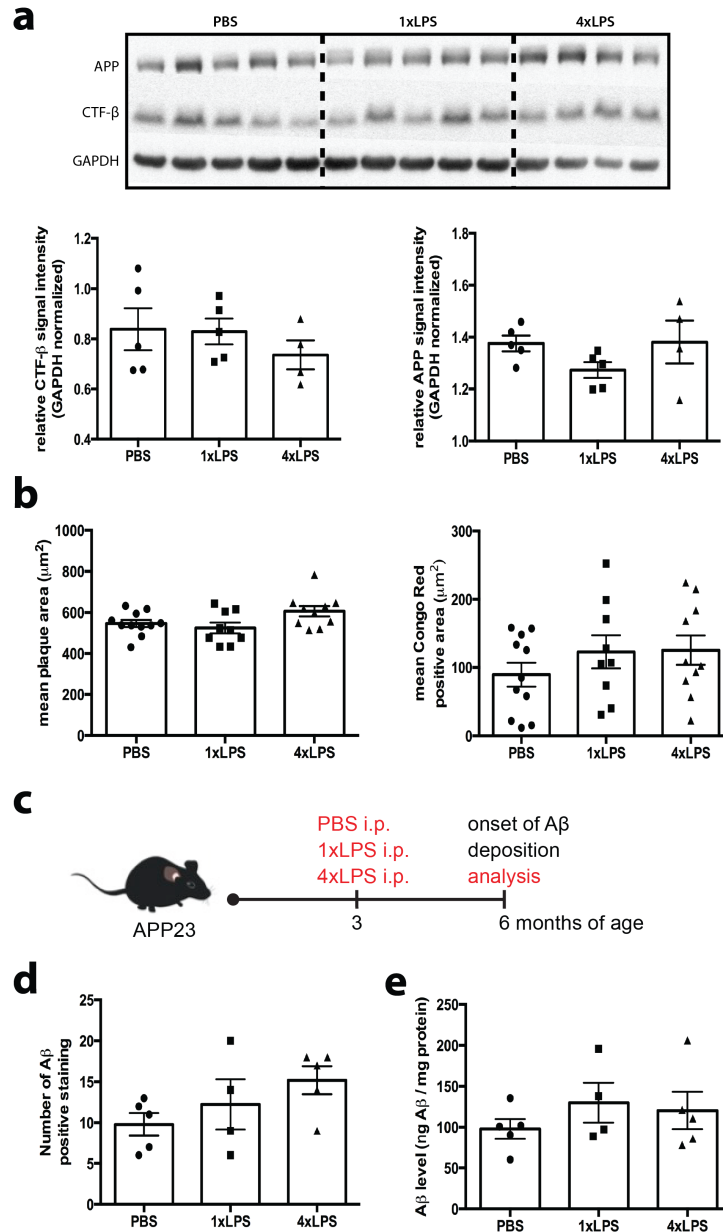
**Supplementary Figure 1: Influence of the age of peripheral immune stimulation on plaque morphology and plaque-associated microglial numbers.**

**a**, Experimental design. **b**, Emission intensities at 502 / 588 nm for PBS (n=17), 1xLPS (n=10,5), and 4xLPS (n=11,6) treated animals stimulated at 3 or 7 months of age. **c**, Stereological quantification of plaque-associated microglia for PBS (n=14), 1xLPS (n=9,5), and 4xLPS (n=10,6) treated animals stimulated at 3 or 7 months of age. \*/\*\*/\*\*=p<0.05/0.01/0.001. Data are presented as mean ± SEM.



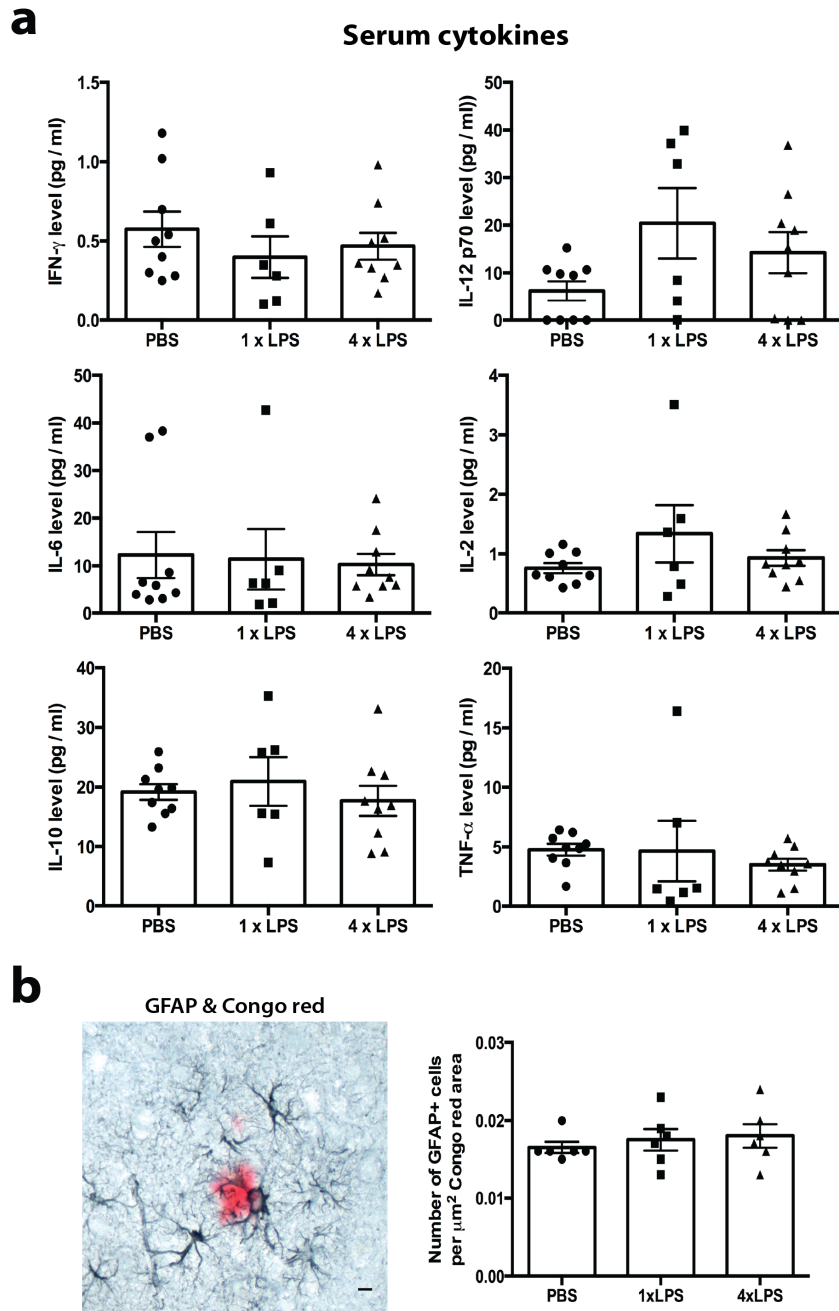
**Supplementary Figure 2: Alterations in plaque morphology in 9 months old APP23 animals after peripheral immune stimulation at 3 or 7 months**

**a**, Experimental design. **b**, Micrographs depicting representative plaque morphologies in the different treatment groups after hFTAA staining and ratio of emission intensities at 545 / 588 nm (n=9,9,9) revealed alterations in plaque structure after 4xLPS treatment. **c**, Experimental design. **d**, Micrographs depicting representative plaque morphologies in the different treatment groups after hFTAA staining and ratio of emission intensities at 545 / 588 nm (n=8,5,7) revealed no alterations in plaque structure between treatment groups. Scale bar 10  $\mu$ m. \*/\*\*=p<0.05/0.01. Data are presented as mean  $\pm$  SEM.



**Supplementary Figure 3: Absence of alterations in A $\beta$  pathology and age of onset of plaque deposition after peripheral immune stimulation.**

**a**, Western Blot and quantification of normalized signal intensities demonstrating equal levels of APP and CTF- $\beta$  between treatment groups (n=5,5,4). **b**, Quantification of mean plaque area and mean Congo red positive area in 12 months old APP23 animals (n=11,9,10). **c**, Experimental design for data in (d) and (e). **d**, Quantification of A $\beta$  positive staining in 6 months old APP23 animals (n=5,4,5). **e**, ELISA measurement of total brain A $\beta$  levels in 6 months old APP23 animals (n=5,4,5). Data are presented as mean  $\pm$  SEM.



**Supplementary Figure 4: Number of plaque-associated astrocytes and peripheral cytokine levels in 12 months old APP23 animals.**

**a**, ELISA measurement of serum cytokine levels (n=9,6,9) revealed no significant alterations between treatment groups. **b**, Micrograph and quantification of GFAP positive plaque-associated astrocytes (n=6,6,6) revealed no differences between treatment groups. Scale bar 10  $\mu$ m. \*/\*\*=p<0.05/0.01. Data are presented as mean  $\pm$  SEM.



## Acknowledgements

The authors would like to thank Katleen Wild, Lisa Häsler, and Marius Lambert for excellent technical assistance. We would like to thank Prof. Dr. Martin Eichner for advice on statistical analysis.

## Authors' contribution

A.C.W. and N.B. performed the experimental work, A.C.W. and A.S. carried out the image analysis, A.C.W. carried out the statistical analysis. P.N. developed LCOs. A.C.W., J.J.N., and M.J. designed the study, A.C.W. and J.N. prepared the manuscript with the help of all authors. The authors declare no conflict of interest.

## References

- Aslund, A., Sigurdson, C.J., Klingstedt, T., Grathwohl, S., Bolmont, T., Dickstein, D.L., ... Nilsson, K.P.R. (2009). Novel pentameric thiophene derivatives for in vitro and in vivo optical imaging of a plethora of protein aggregates in cerebral amyloidoses. *ACS chemical biology* 4(8): 673–684.
- Bondolfi, L., Calhoun, M., Ermini, F., Kuhn, H.G., Wiederhold, K.-H., Walker, L., ... Jucker, M. (2002). Amyloid-associated neuron loss and gliogenesis in the neocortex of amyloid precursor protein transgenic mice. *The Journal of Neuroscience* 22(2): 515–522.
- Cattaneo, A., Cattane, N., Galluzzi, S., Provasi, S., Lopizzo, N., Festari, C., ... INDIA-FBP Group. (2017). Association of brain amyloidosis with pro-inflammatory gut bacterial taxa and peripheral inflammation markers in cognitively impaired elderly. *Neurobiology of Aging* 49: 60–68.
- Chakrabarty, P., Li, A., Ceballos-Diaz, C., Eddy, J.A., Funk, C.C., Moore, B., ... Golde, T.E. (2015). IL-10 alters immunoproteostasis in APP mice, increasing plaque burden and worsening cognitive behavior. *Neuron* 85(3): 519–33.
- Condello, C., Yuan, P., Schain, A. & Grutzendler, J. (2015). Microglia constitute a barrier that prevents neurotoxic protofibrillar A $\beta$ 42 hotspots around plaques. *Nature communications* 6: 6176.
- Cunningham, C. (2013). Microglia and neurodegeneration: the role of systemic inflammation. *Glia* 61(1): 71–90.
- Gagliano, S.A., Pouget, J.G., Hardy, J., Knight, J., Barnes, M.R., Ryten, M. & Weale, M.E. (2016). Genomics implicates adaptive and innate immunity in Alzheimer's and Parkinson's diseases. *Annals of clinical and translational neurology* 3(12): 924–933.

- Gomez-Nicola, D. & Perry, V.H. (2015). Microglial Dynamics and Role in the Healthy and Diseased Brain. *The Neuroscientist* 21(2): 169–184.
- Guerreiro, R., Wojtas, A., Bras, J., Carrasquillo, M., Rogaevea, E., Majounie, E., ... Hardy, J. (2013). *TREM2* Variants in Alzheimer's Disease. *New England Journal of Medicine* 368(2): 117–127.
- Hardy, J. & Selkoe, D.J. (2002). The amyloid hypothesis of Alzheimer's disease: progress and problems on the road to therapeutics. *Science (New York, N.Y.)* 297(5580): 353–356.
- Hefendehl, J.K., Neher, J.J., Sühs, R.B., Kohsaka, S., Skodras, A. & Jucker, M. (2014). Homeostatic and injury-induced microglia behavior in the aging brain. *Aging Cell* 13(1): 60–69.
- Hendrickx, D.A.E., van Eden, C.G., Schuurman, K.G., Hamann, J. & Huitinga, I. (2017). Staining of HLA-DR, Iba1 and CD68 in human microglia reveals partially overlapping expression depending on cellular morphology and pathology. *Journal of Neuroimmunology* 309: 12–22.
- Heneka, M.T., Kummer, M.P., Stutz, A., Delekate, A., Schwartz, S., Vieira-Saecker, A., ... Golenbock, D.T. (2013). NLRP3 is activated in Alzheimer's disease and contributes to pathology in APP/PS1 mice. *Nature* 493(7434): 674–678.
- Hollingworth, P., Harold, D., Sims, R., Gerrish, A., Lambert, J.-C., Carrasquillo, M.M., ... Williams, J. (2011). Common variants at ABCA7, MS4A6A/MS4A4E, EPHA1, CD33 and CD2AP are associated with Alzheimer's disease. *Nature Genetics* 43(5): 429–435.
- Huang, K.-L., Marcora, E., Pimenova, A.A., Di Narzo, A.F., Kapoor, M., Jin, S.C., ... Goate, A.M. (2017). A common haplotype lowers PU.1 expression in myeloid cells and delays onset of Alzheimer's disease. *Nature Neuroscience* 20(8): 1052–1061.
- Jay, T.R., Hirsch, A.M., Broihier, M.L., Miller, C.M., Neilson, L.E., Ransohoff, R.M., ... Landreth, G.E. (2017). Disease Progression-Dependent Effects of *TREM2* Deficiency in a Mouse Model of Alzheimer's Disease. *The Journal of Neuroscience* 37(3): 637–647.
- Karran, E., Mercken, M. & Strooper, B. De. (2011). The amyloid cascade hypothesis for Alzheimer's disease: an appraisal for the development of therapeutics. *Nature Reviews Drug Discovery* 10(9): 698–712.
- Keren-Shaul, H., Spinrad, A., Weiner, A., Matcovitch-Natan, O., Dvir-Szternfeld, R., Ulland, T.K., ... Amit, I. (2017). A Unique Microglia Type Associated with Restricting Development of Alzheimer's Disease. *Cell* 169(7): 1276–1290.
- Kitazawa, M., Cheng, D., Tsukamoto, M.R., Koike, M.A., Wes, P.D., Vasilevko, V., ... LaFerla, F.M. (2011). Blocking IL-1 signaling rescues cognition, attenuates tau pathology, and restores neuronal  $\beta$ -catenin pathway function in an Alzheimer's disease model. *Journal of immunology* 187(12): 6539–49.
- Klingstedt, T., Aslund, A., Simon, R.A., Johansson, L.B.G., Mason, J.J., Nyström, S.,

- ... Nilsson, K.P.R. (2011). Synthesis of a library of oligothiophenes and their utilization as fluorescent ligands for spectral assignment of protein aggregates. *Organic & biomolecular chemistry* 9(24): 8356–8370.
- Krasemann, S., Madore, C., Cialic, R., Baufeld, C., Calcagno, N., El Fatimy, R., ... Butovsky, O. (2017). The TREM2-APOE Pathway Drives the Transcriptional Phenotype of Dysfunctional Microglia in Neurodegenerative Diseases. *Immunity* 47(3): 566–581.
- Lambert, J.C., Ibrahim-Verbaas, C.A., Harold, D., Naj, A.C., Sims, R., Bellenguez, C., ... Amouyel, P. (2013). Meta-analysis of 74,046 individuals identifies 11 new susceptibility loci for Alzheimer's disease. *Nature Genetics* 45(12): 1452–1458.
- Mai, D., Dautzenberg, J., Fern, F., Lin, G., Datta, M., Drougard, A., ... Prinz, M. (2017). A new fate mapping system reveals context-dependent random or clonal expansion of microglia. *Nature Neuroscience* 20(6): 793-803.
- Mathys, H., Adaikkan, C., Gao, F., Young, J.Z., Manet, E., Hemberg, M., ... Tsai, L.-H. (2017). Temporal Tracking of Microglia Activation in Neurodegeneration at Single-Cell Resolution. *Cell Reports* 21(2): 366–380.
- Naj, A.C., Jun, G., Beecham, G.W., Wang, L.-S., Vardarajan, B.N., Buross, J., ... Schellenberg, G.D. (2011). Common variants at MS4A4/MS4A6E, CD2AP, CD33 and EPHA1 are associated with late-onset Alzheimer's disease. *Nature Genetics* 43(5): 436–441.
- Nyström, S., Psonka-Antonczyk, K.M., Ellingsen, P.G., Johansson, L.B.G., Reitan, N., Handrick, S., ... Nilsson, K.P.R. (2013). Evidence for Age-Dependent in Vivo Conformational Rearrangement within A $\beta$  Amyloid Deposits. *ACS Chemical Biology* 8(6): 1128–1133.
- Perry, V.H., Cunningham, C. & Holmes, C. (2007). Systemic infections and inflammation affect chronic neurodegeneration. *Nature Reviews Immunology* 7(2): 161–167.
- Rabinowitz, S., Horstmann, H., Gordon, S. & Griffiths, G. (1992). Immunocytochemical characterization of the endocytic and phagolysosomal compartments in peritoneal macrophages. *The Journal of Cell Biology* 116(1): 95–112.
- Ransohoff, R.M. & Perry, V.H. (2009). Microglial physiology: unique stimuli, specialized responses. *Annual Review of Immunology* 27: 119–145.
- Rasmussen, J., Mahler, J., Beschorner, N., Kaeser, S.A., Häsler, M.L., Baumann, F., Nyström, S., Portelius, E., Blennow, K., Lashley, T., Fox, N.C., Sepulveda-Falla, D., Glatzel, M., Oblak, A.L., Ghetti, B., Nilsson, Nilsson, K.P.R., Hammarström, P., Staufenbiel, M., Walker, L.C., Jucker, M. (2017). Amyloid polymorphisms constitute distinct clouds of conformational variants in different etiological subtypes of Alzheimer's disease. *Proceedings of the National Academy of Sciences of the United States of America* 114(49): 13018-13023.

- Shi, J.-Q., Shen, W., Chen, J., Wang, B.-R., Zhong, L.-L., Zhu, Y.-W., ... Xu, J. (2011). Anti-TNF- $\alpha$  reduces amyloid plaques and tau phosphorylation and induces CD11c-positive dendritic-like cell in the APP/PS1 transgenic mouse brains. *Brain Research* 1368: 239–47.
- Sims, R., van der Lee, S.J., Naj, A.C., Bellenguez, C., Badarinarayan, N., Jakobsdottir, J., ... Schellenberg, G.D. (2017). Rare coding variants in PLCG2, ABI3, and TREM2 implicate microglial-mediated innate immunity in Alzheimer's disease. *Nature Genetics* 49(9): 1373-1384.
- Sturchler-Pierrat, C., Abramowski, D., Duke, M., Wiederhold, K.H., Mistl, C., Rothacher, S., ... Sommer, B. (1997). Two amyloid precursor protein transgenic mouse models with Alzheimer disease-like pathology. *Proceedings of the National Academy of Sciences of the United States of America* 94(24): 13287–13292.
- Sturchler-Pierrat, C. & Staufenbiel, M. (2000). Pathogenic mechanisms of Alzheimer's disease analyzed in the APP23 transgenic mouse model. *Annals of the New York Academy of Sciences* 920: 134–139.
- Varvel, N.H., Grathwohl, S.A., Degenhardt, K., Resch, C., Bosch, A., Jucker, M. & Neher, J.J. (2015). Replacement of brain-resident myeloid cells does not alter cerebral amyloid- $\beta$  deposition in mouse models of Alzheimer's disease. *Journal of Experimental Medicine* 212(11): 1803-9.
- Vom Berg, J., Prokop, S., Miller, K.R., Obst, J., Kälin, R.E., Lopategui-Cabezas, I., ... Heppner, F.L. (2012). Inhibition of IL-12/IL-23 signaling reduces Alzheimer's disease-like pathology and cognitive decline. *Nature Medicine* 18(12): 1812–1819.
- Wang, Y., Ulland, T.K., Ulrich, J.D., Song, W., Tzaferis, J.A., Hole, J.T., ... Colonna, M. (2016). TREM2-mediated early microglial response limits diffusion and toxicity of amyloid plaques. *The Journal of Experimental Medicine* 213(5): 667-675.
- Yuan, P., Condello, C., Keene, C.D., Wang, Y., Bird, T.D., Paul, S.M., ... Grutzendler, J. (2016). TREM2 Haplodeficiency in Mice and Humans Impairs the Microglia Barrier Function Leading to Decreased Amyloid Compaction and Severe Axonal Dystrophy. *Neuron* 90(4): 724–739.
- Wendeln, A.C., Degenhardt, K., Kaurani, L., Gertig, M., Ulas, T., Jain, G., ... Neher, J.J. (2018). Innate immune memory in the brain shapes neurological disease hallmarks. *Nature*. Accepted
- Zhang, B., Gaiteri, C., Bodea, L.-G., Wang, Z., McElwee, J., Podtelezhnikov, A.A., ... Emilsson, V. (2013). Integrated systems approach identifies genetic nodes and networks in late-onset Alzheimer's disease. *Cell* 153(3): 707–720.

## 4 Appendix

### 4.1 Abbreviations

A $\beta$	Amyloid beta
AD	Alzheimer's disease
APP	Amyloid precursor protein
ATP	Adenosine triphosphate
BBB	Blood-brain barrier
BCG	Bacillus Calmette-Guérin
BrdU	Bromodeoxyuridine
CTF	C-terminal fragment
DAMP	Danger-associated molecular pattern
GWAS	Genome-wide association studies
hFTAA	Hepta-formyl thiophene acetic acid
HIF	Hypoxia-inducible factor
LCO	Luminescent conjugated oligothiophene
LDTF	Lineage-determining transcription factor
LPS	Lipopolysaccharide
mTOR	Mechanistic target of rapamycin
NAD	Nicotinamide adenine dinucleotide
NFT	Neurofibrillary tangle
NSAID	Non-steroidal anti-inflammatory drug
PAMP	Pathogen-associated molecular pattern
PRR	Pattern-recognition receptor
qFTAA	quadro-formyl thiophene acetic acid
Rap	Ras-related protein
ROS	Reactive oxygen species
SDTF	Signal-dependent transcription factor
WGCNA	Weighted gene correlation network analysis

## 4.2 Bibliography

- I. Petra Füger, Jasmin K. Hefendehl, Karthik Veeraraghavalu, Ann-Christin Wendeln, Christine Schlosser, Ulrike Obermüller, Bettina M. Wegenast-Braun, Jonas J. Neher, Peter Martus, Shinichi Kohsaka, Martin Thunemann, Robert Feil, Sangram S. Sisodia, Angelos Skodras, Mathias Jucker (2017): Microglial turnover with aging and in an Alzheimer's model via long-term *in vivo* single-cell imaging. *Nature Neuroscience* 20(10): 1371-1376.
  
- II. Ann-Christin Wendeln<sup>\*</sup>, Karoline Degenhardt<sup>\*</sup>, Lalit Kaurani, Michael Gertig, Thomas Ulas, Gaurav Jain, Jessica Wagner, Lisa M. Häsler, Katleen Wild, Angelos Skodras, Thomas Blank, Ori Staszewski, Moumita Datta, Tonatiuh Pena Centeno, Vincenzo Capece, Md. Rezaul Islam, Cemil Kerimoglu, Matthias Staufenbiel, Joachim L. Schultze, Marc Beyer, Marco Prinz, Mathias Jucker, André Fischer, Jonas J. Neher: Innate immune memory in the brain shapes neurological disease hallmarks. *Nature. Accepted*  
  
\*contributed equally
  
- III. Ann-Christin Wendeln, Angelos Skodras, Natalie Beschorner, Peter Nilsson, Mathias Jucker, Jonas Neher: Systemic inflammation induces long-term modulation of amyloid plaque morphology and neuronal damage in a mouse model of Alzheimer's disease. *In preparation*